E-ISSN: 2667-5846

EXPERIMED

Volume **15** · Issue **1** · **April** 2025

https://experimed.istanbul.edu.tr/

İSTANBUL UNIVERSITY PRESS

E-ISSN: 2667-5846

EXPERIMED

Volume 15 • Issue 1 • April 2025

İSTANBUL UNIVERSITY PRESS

Indexing & Abstracting

Web of Science – Emerging Sources Citation Index
Scopus
ULAKBIM TR Index
Web of Science - Biological Abstracts
Web of Science - BIOSIS Previews
Chemical Abstracts Service (CAS)
EBSCO - Central & Eastern European Academic Source
SOBIAD
CAB Abstracts
CABI Global Health

Owner

Prof. Dr. Gunnur DENIZ

Department of Immunology, Istanbul University, Aziz Sancar Institute of Experimental Medicine, Istanbul, Turkiye

Responsible Manager

Prof. Dr. Bedia CAKMAKOGLU

Department of Molecular Medicine, Istanbul University, Aziz Sancar Institute of Experimental Medicine, Istanbul, Turkiye

Correspondence

Istanbul University, Aziz Sancar Institute of Experimental Medicine,

Vakif Gureba Avenue, 34093, Capa, Fatih, Istanbul, Turkiye

+90 (212) 414 22 29

experimed@istanbul.edu.tr

https://experimed.istanbul.edu.tr/

Publisher

Istanbul University Press

İstanbul Üniversitesi Merkez Kampüsü, 34452 Beyazıt/Fatih, İstanbul, Türkiye

+90 (212) 440 00 00

iupress@istanbul.edu.tr

https://iupress.istanbul.edu.tr/

Publication Type

Periodical

İSTANBUL UNIVERSITY PRESS

EXPERIMED

Volume: 15 • Issue: 1 • April 2025

Editorial Management

Assoc. Prof. Ali Cihan TASKIN

Department of Lab Animal Science, Istanbul University, Aziz Sancar Institute of Experimental Medicine, Istanbul, Turkiye
ataskin@istanbul.edu.tr

Assoc. Prof. Timur Hakan BARAK

Department of Pharmacognosy, Faculty of Pharmacy, Acıbadem Mehmet Ali Aydınlar University, Istanbul, Turkiye
timur.barak@acibadem.edu.tr

Language Editor

Elizabeth Mary EARL

Department of Foreign Languages, Istanbul University, Istanbul, Turkiye
elizabeth.earl@istanbul.edu.tr

Statistics Editor

Sevda OZEL YILDIZ

Department of Biostatistic, Istanbul Medical Faculty, Istanbul University, Istanbul, Türkiye
sevda@istanbul.edu.tr

İSTANBUL UNIVERSITY PRESS

EXPERIMED

Volume: 15 • Issue: 1 • April 2025

Editorial Board Members

İSTANBUL UNIVERSITY PRESS

EXPERIMED

Volume: 15 • Issue: 1 • April 2025

Suhendan EKMEKCIOGLU *MD Anderson Cancer Center, Texas University, Houston, Texas, USA*
sekmekcioglu@mdanderson.org

Yusuf BARAN *Department of Molecular Biology and Genetics, Izmir Institute of Technology, Izmir, Turkiye*
yusufbaran@iyte.edu.tr

İSTANBUL UNIVERSITY PRESS

EXPERIMED

Volume: 15 • Issue: 1 • April 2025

Table of Contents

İSTANBUL UNIVERSITY PRESS

EXPERIMED

Volume: 15 • Issue: 1 • April 2025

İSTANBUL UNIVERSITY PRESS

Experimed 2025, 15 (1): 1–14

https://doi.org/10.26650/experimed.1524088

Submitted: 30.07.2024
Revision Requested: 29.08.2024
Last Revision Received: 17.09.2024
Accepted: 08.10.2024
Published Online 12.03.2025

Experimed

Research Article

Open Access

Establishing Age-Gender Specific Reference Values of T and B Lymphocyte Subsets in Healthy Adults Using Flow Cytometry

Fatma Turgut Kaynak [1,2], Melek Yanasik [3], Suzan Cinar [1], Sevgi Kalayoglu Besisik [3,4], Gunnur Deniz [1] & Metin Yusuf Gelmez [1]

[1] Department of Immunology, Aziz Sancar Institute of Experimental Medicine, Istanbul University, Istanbul, Turkiye
[2] Institute of Graduate Studies in Health Sciences, Istanbul University, Istanbul, Turkiye
[3] Blood Transfusion Center, Istanbul Faculty of Medicine, Istanbul University, Istanbul, Turkiye
[4] Department of Internal Medicine, Division of Hematology, Istanbul Faculty of Medicine, Istanbul University, Istanbul, Turkiye

Abstract

Objective: Geographical, age and gender differences possibly affect the distribution of lymphocyte subsets. This study aimed to determine the distribution of T and B lymphocytes and their subsets by evaluating a larger healthy adult population in terms of gender and age.

Materials and Methods: Blood samples from 118 healthy adults aged 20-60 years were evaluated using flow cytometry.

Results: B cell subsets were not affected by age and gender differences; however, $CD3^+$ and $CD4^+$ T cell ratios were higher in women than in men. Gender and age differences did not affect the distribution of $CD4^+$ T cell subsets, but increased effector memory $CD45RA^+CD8^+$ T and decreased naive $CD8^+$ T were found among the group aged between 50-60 years. Additionally, regulatory T cells were found at higher levels in individuals aged between 50-60 years. Moreover, high follicular regulatory T cells in men and low follicular helper T cells in women were observed in individuals aged 50-60 years. Advanced age in females may affect the differentiation of $CD4^+$ T cells to T helper type 1.

Conclusion: Our results indicate that age and gender differences may affect cell distribution. Our findings may contribute to the clinical evaluation of lymphocyte subset distributions as diagnostic tests performed using flow cytometry for early diagnosis and appropriate treatment of patients.

Keywords T lymphocytes · B lymphocytes · Flow cytometry · Reference values of lymphocyte subsets

Citation: Turgut Kaynak, F., Yanasik, M., Cinar, S., Kalayoglu Besisik, S., Deniz, G. & Gelmez, M. Y. Establishing age-gender specific reference values of T and B lymphocyte subsets in healthy adults using flow cytometry. Experimed 2025; 15(1): 1-14. DOI: 10.26650/experimed.1524088

Corresponding author: Metin Yusuf Gelmez yusufmetin@istanbul.edu.tr

INTRODUCTION

The immune system protects the body against foreign microorganisms, such as bacteria, viruses, and tumor cells (1). Adaptive immune responses contain B and T lymphocytes that generate humoral responses by secreting the antibodies, and T lymphocytes that generate cellular responses (2). The distribution and function of B and T lymphocyte subsets are known to change in various diseases, such as primary immune deficiency (PID), autoimmunity, allergy, and cancer (3). Recent studies have shown that decreased non-switched and switched memory B and increased naive B lymphocytes were detected in common variable immunodeficiency (CVID) patients (4, 5). On the other hand, previous studies have shown that patients with various autoimmune diseases such as Hashimoto's thyroiditis, type 1 diabetes mellitus, and multiple sclerosis have a predominant $CD4^+$ T helper type 1 (Th1) response and a decline in the proportion and number of $CD8^+$ T lymphocytes with an elevated CD4/CD8 ratio (6, 7). Decreased numbers and impaired function of regulatory T cells (Treg) were observed in X-linked immune dysregulation, polyendocrinopathy, and enteropathy (IPEX) syndrome (8).

Some studies have indicated that demographic differences, such as ethnicity, geography, age, and gender, may influence lymphocyte distribution. Studies have reported that the distribution of B cell subsets changes from birth to 16-18 years of age (9, 10). Furthermore, recent studies have shown a functional relationship between immune cells and aging, with a general consensus that memory cells increase relative to naive cells as individuals age, even in healthy people (11). High levels of Tregs, effector memory T cells, switched and non-switched B cells, and natural killer (NK) cells, and low levels of $CD8^+$ T and naive T and B cells were found to be associated with aging (12-14). In addition, the differentiation of $CD4^+$ T cells into Th1 and Th2 subsets decreases, whereas Th17 proliferation increases with aging (15).

Determination of the distribution of T and B lymphocyte subsets is highly important to evaluate and diagnose the diseases like PID. Many studies have focused on the reference values of T and B lymphocyte subsets in different countries (16-19); however, the number of studies is limited in our country (9, 20, 21). Most of the reference studies from Turkiye only analyzed the distribution of $CD19^+$, $CD3^+$, $CD8^+$, and $CD4^+$ cells as well as NK cells (20, 21). One study focused on different immunologic subsets like effector memory, central memory, and effector memory RA in CD4 and CD8 T cells in adults, without data about gender and age differences (9). In this study, the effects of gender and age on the distribution of lymphocyte subsets were determined and the reference values of B and T cell subsets as well as Th1, Th2, Th17, Treg, follicular regulatory T (T_{FR}), follicular helper T (T_{FH}), and follicular cytotoxic T (T_{FC}) cells were investigated for adults in accordance with age and gender.

MATERIALS AND METHODS

Study Population

In total, 118 healthy adults, 58 females (49.15%) and 60 males (50.85%) aged 20-60 years were included. Volunteers who were not Hepatitis B carriers, had no history of allergy, autoimmunity, PID, cancer with their first-degree relatives with no such symptoms, had no tissue, organ transplantation, or blood transfusion in the previous year, were not pregnant, taking no medication, did not have infectious or chronic diseases, weighed over 50 kg, and had a body mass index (BMI) of 17-31 were included in the study after signing the informed consent form.

Venous peripheral blood samples were collected from the Istanbul University Istanbul Medical Faculty Blood Center. Ethics approval for the study was obtained from the Istanbul Medical Faculty Clinical Research Ethics Committee (21/08/2020 and numbered 19).

Volunteers were divided into four different age groups in 10-year intervals. The first age group (20-29 years) consisted of 17 females (14.40%) and 15 males (12.71%), the second age group (30-39 years) consisted of 15 females (12.71%) and 15 males (12.71%), the subsequent age group (40-49 years) consisted of 15 females (12.71%) and 16 males (13.55%), and the last age group (50-60 years) consisted of 11 females (9.32%) and 14 males (11.86%). The data on the characteristics of the volunteers are presented in Table 1.

Immunophenotyping

White blood cells (WBC) were counted using Rayto Auto Hematology Analyzer (RT-7600, China). The T and B lymphocyte subsets were determined by performing whole blood lysis using three flow cytometric panels (B cell, T cell, and Treg cell panel) which are detailed in Supplementary Table 1. The tubes containing 1 x 10^6 cells/mL were labeled for B cell panel with anti-CD19, anti-IgD, anti-CD27, anti-CD45, for T cell panel with anti-CD3, anti-CD4, anti-CD8, anti-CD45, anti-CD45RA, anti-CCR7, anti-CD31, and for Treg panel with anti-CD3, anti-CD4, anti-CD8, anti-CD45, anti-CD25, anti-CD127, anti-CXCR3, anti-CXCR5, and anti-CCR6, by cell surface staining. The cells were incubated, then, lysing solution (2mL) (BD Biosciences, San Jose, CA, USA) was added. After 15 min of incubation, the cells were washed 2 times by Flow Sheath (BD Biosciences, San Jose, CA, USA) at 1800 rpm for 5 min. The cells were acquired using a NovoCyte flow cytometer (Agilent Technologies, USA). NovoExpress software (Agilent Technologies, USA) was used to

Table 1. Demographic data of the groups

	Age Groups (years)	n	%	Age (Mean ± SD)	BMI (Mean ± SD)	WBC (Mean ± SD) (10^3/mm^3)	Lym (Mean ± SD) (10^3/mm^3)
FEMALE	20-29	17	14.40	26.23 ± 2.19	21.45 ± 2.60	6.67 ± 1.24	2.16 ± 0.48
	30-39	15	12.71	36.53 ± 2.61	21.77 ± 3.40	7.68 ± 1.23	2.35 ± 0.58
	40-49	15	13.55	43.93 ± 2.31	24.71 ± 3.01	6.90 ± 1.69	2.10 ± 0.55
	50-60	11	9.32	54.72 ± 3.63	24.42 ± 2.54	5.51 ± 1.79	1.88 ± 0.60
	Total Females	58	49.20	38.87 ± 0.53	23.00 ± 3.22	6.78 ± 1.61	2.14 ± 0.55
MALE	20-29	15	12.71	23.80 ± 3.27	24.73 ± 2.79	6.69 ± 1.57	2.45 ± 0.64
	30-39	15	12.71	33.20 ± 2.14	25.23 ± 2.18	6.94 ± 1.55	2.08 ± 0.63
	40-49	16	12.71	42.81 ± 2.25	25.22 ± 2.14	6.93 ± 1.46	2.27 ± 0.63
	50-60	14	11.86	54.85 ± 3.54	25.63 ± 4.29	7.01 ± 1.65	2.29 ± 0.49
	Total Males	60	50.80	38.44 ± 11.76	25.00 ± 2.80	6.89 ± 1.52	2.26 ± 0.61
TOTAL	20-60	118	100	38.66 ± 11.12	24.00 ± 3.23	6.83 ± 1.56	2.20 ± 0.58

BMI: Body mass index, WBC: White blood cell, Lym: Lymphocyte

analyze data by gating in the SSC/CD45 dot plot graph of at least 100,000 CD45$^+$ lymphocytes. Doublet cells were excluded from the FSC-A/FSC-H and SSC-A/SSC-H graphs.

Statistical Analyses

GraphPad Prism version 9 was used for statistical analysis. The mean, standard deviation, and 2.50%-97.50% percentile values of all parameters were calculated. The Student's t-test was used to test statistics for normally distributed groups, and the Mann–Whitney U test was used for the evaluation of variables that showed no normal distribution. Age groups and all parameters were compared and evaluated with Kruskal-Wallis and two-way ANOVA. With reference to previous studies ("Reference values for peripheral blood lymphocyte subsets in a healthy Korean population", CD3 variable), when the difference between the means was 7.8 units and the standard deviations were 6.73 and 9.97, respectively, the sample size was determined as at least n=76 to obtain 80% power at the 95% confidence level and p≤0.05 was determined as the statistical significance level.

RESULTS

Age and gender did not affect the distribution of B cell subsets

To identify age and gender differences, the ratios of CD19$^+$ (B cells), CD19$^+$CD27$^+$ (total memory B cells), CD19$^-$CD27$^+$, and CD19$^+$IgD$^+$ values in lymphocytes were analyzed. Additionally, the ratios of CD27$^+$ (total memory B), CD27$^-$IgD$^+$ (naive B), CD27$^+$IgD$^+$ (non-switched memory B), CD27$^+$IgD$^-$ (switched memory B), and CD27$^-$IgD$^-$ cells were analyzed in CD19$^+$ B lymphocytes (Supplementary Figure 1A).

The distributions of CD19$^+$, CD19$^+$CD27$^+$, and CD19$^+$IgD$^+$ in lymphocytes did not differ according to age and gender (Supplementary Figure 1 B-C). Similarly, the distributions of total memory, naive, non-switched memory, switched memory, and CD27$^-$IgD$^-$ B cells in CD19$^+$ B cell gate showed no differences in terms of age and gender. According to our data, the distribution of B cell subsets in adults in the range of 20-60 years was not affected by age or gender (Supplementary Figure 1 D-E). The age- and gender-related distributions of B cell subsets are shown for all individuals in Table 2.

CD3$^+$ and CD3$^+$CD4$^+$ T cells increased only in females

T lymphocyte subsets were analyzed in accordance with age and gender differentiation and the distribution of T cells (CD3$^+$), T helper cells (CD3$^+$CD4$^+$), cytotoxic T cells (CD3$^+$CD8$^+$), CD4$^+$CD31$^+$, CD4$^+$CD25$^+$, and CD45RA$^+$ cells were determined in lymphocyte gate. On the other hand, CD3$^+$ T cells were gated in the SSC/CD3 graph. CD4$^+$, CD8$^+$, CD4$^+$CD25$^+$, and CD45RA$^+$ (naive T) cell ratios in CD3$^+$ T lymphocytes were also analyzed Supplementary Figure 2.

The ratios of CD3$^+$, CD3$^+$CD4$^+$, CD4$^+$CD31$^+$, and CD4$^+$CD25$^+$ T cells in lymphocytes were higher in women than in men (p=0.0001, p<0.0001, p<0.0001, and p<0.0001, respectively) (Figure 1A). The CD4$^+$ T cell ratios were found higher in the age groups of 30-39, 40-49 years and total in females compared to the ratios in all men age groups (20-29, 30-39, 40-49, 50-60 years, and total) (females aged 30-39 years p<0.0001, p=0.0026, p=0.0003, p=0.0006 and p<0.0001, respectively; females aged 40-49 years p<0.0001, p=0.0021, p=0.0003, p=0.0007 and p<0.0001, respectively; total females p<0.0001, p=0.0004, p<0.0001, p=0.0001, and p<0.0001, respectively) (Figure 1B). The ratio of CD3$^+$CD8$^+$ T cells did not change according to gender or age (Figure 1C).

Table 2. B lymphocyte subset distribution in lymphocytes and CD19⁺ B cell

Age Group	20-29 Female	20-29 Male	30-39 Female	30-39 Male	40-49 Female	40-49 Male	50-60 Female	50-60 Male	Total Female	Total Male	Total Group
in Lymphocyte											
CD19⁺ (%)	9.60± 3.79 4.48-18.06	11.25 ± 2.87 7.38-16.21	10.73 ± 2.91 5.77-15.88	11.83 ± 3.51 5.45-17.09	10.55 ± 3.29 6.04-17.57	11.51 ± 3.81 5.19-19.20	10.70 ± 3.22 6.29-16.02	12.98 ± 4.20 6.35-20.62	10.35 ± 3.29 4.56-17.83	11.87 ± 3.59 5.32-20.59	**11.12 ± 3.51** **5.17-19.23**
CD19⁺CD27⁺ (%)	3.48 ± 2.11 1.06-9.68	4.05 ± 1.80 1.76-7.40	3.92 ± 1.70 1.22-7.65	4.22 ± 1.65 1.92-8.72	3.15 ± 1.27 1.30-5.98	3.62 ± 1.36 1.75-6.02	3.71 ± 1.02 2.57-5.84	4.59 ± 2.31 1.84-9.54	3.55 ± 1.62 1.13-8.76	4.09 ± 1.77 1.75-9.13	**3.83 ± 1.71** **1.29-8.78**
CD19⁺CD27⁺ (%)	67.07 ± 8.71 52.98-79.32	61.24 ± 10.59 42.99-75.64	60.02 ± 10.71 41.48-74.51	52.12 ± 12.71 30.33-70.27	62.59 ± 9.89 40.73-78.65	49.29 ± 9.48 28.24-63.96	49.38 ± 11.47 31.62-63.87	40.42 ± 15.4 7.68-61.53	60.75 ± 11.62 34.52-79.02	51.09 ± 13.85 11.50-75.04	**55.84 ± 13.63** **27.27-78.43**
CD19⁺IgD⁺ (%)	6.51 ± 3.34 1.60-12.44	7.87 ± 1.61 5.16-10.67	7.43 ± 2.79 3.40-12.91	8.87 ± 3.14 3.43-15.04	7.22 ± 2.99 2.28-14.62	8.03 ± 3.36 3.37-13.73	7.55 ± 2.64 3.77-12.06	9.01 ± 3.60 3.40-15.61	7.13 ± 2.94 1.82-3.81	8.43 ± 2.99 3.38-15.58	**7.79 ± 3.02** **2.27-15.05**
in CD19⁺ B Cells											
CD27⁺ (Total Memory B)	34.06 ± 13.47 7.64-59.09	32.38 ± 12.53 16.43-62.43	32.96 ± 14.59 17.44-66.04	34.73 ± 12.90 17.84-55.43	29.31 ± 12.01 13.04-54.14	31.75 ± 12.84 11.03-55.44	33.16 ± 7.95 17.20-44.22	32.13 ± 11.69 11.18-51.05	32.37 ± 12.34 10.07-62.91	32.75 ± 12.26 11.11-58.94	**32.56 ± 12.24** **11.17-59.34**
CD27⁻IgD⁺ (Naive B)	56.43 ± 14.55 29.72-79.46	59.24 ± 11.76 29.24-79.97	57.74 ± 13.26 28.85-72.62	59.11 ± 13.61 35.08-76.97	62.19 ± 12.82 41.19-79.45	59.79 ± 14.00 35.07-85.23	60.60 ± 9.75 47.33-74.99	60.63 ± 10.78 43.65-80.96	59.07 ± 12.85 29.24-79.46	59.66 ± 12.38 33.61-83.55	**59.37 ± 12.56** **31.96-81.03**
CD27⁺IgD⁺ (Non-switched memory B)	12.76 ± 8.98 1.75-33.29	12.94 ± 9.28 3.81-41.76	12.08 ± 9.62 2.78-40.03	17.98 ± 9.56 3.51-37.37	12.06 ± 8.39 0.46-28.96	10.77 ± 6.51 0.97-22.75	11.04 ± 6.01 2.69-23.71	14.08 ± 7.84 3.00-27.06	12.08 ± 8.30 1.04-37.00	13.89 ± 8.59 1.98-39.57	**13.00 ± 8.46** **1.69-37.57**
CD27⁺IgD⁻ (Switched memory B)	22.97 ± 8.57 5.95-38.15	20.65 ± 7.76 10.64-39.16	21.35 ± 10.17 12.20-48.89	16.99 ± 7.87 8.29-35.64	17.80 ± 5.60 6.39-26.95	20.59 ± 10.23 6.19-38.33	19.44 ± 8.05 7.23-28.88	17.29 ± 7.71 6.65-29.60	20.53 ± 8.28 6.14-44.06	18.96 ± 8.48 6.42-38.75	**19.73 ± 8.39** **6.37-38.39**
CD27⁻IgD⁻	7.82 ± 4.47 2.18-18.81	7.16 ± 3.70 1.75-13.93	8.82 ± 4.47 3.56-18.60	5.91 ± 3.25 1.87-13.49	7.95 ± 4.88 1.83-18.56	8.84 ± 4.51 2.48-16.31	8.92 ± 3.51 4.86-16.92	7.99 ± 4.13 2.15-17.58	8.31 ± 4.33 1.98-18.72	7.48 ± 3.98 1.81-16.95	**7.89 ± 4.16** **1.86-18.56**

All values are given mean ± SD and in the range of 2.50-97.50% percentile, respectively.

The proportions of T cell subsets were analyzed in the CD3⁺ T cell gate, and the ratio of CD4⁺ T cells was higher in the female group (p=0.0001), however, the ratio of CD8⁺ T cells was increased in men (p=0.0006) (Figure 1D-E, respectively). Increased CD4⁺ T cells were found in women aged 30-39 years compared with women aged 20-29 years and in all males (p<0.0001 and p=0.0009, respectively). Similarly, elevated CD4⁺ T cells were observed in women aged 40-49 years in contrast to women aged 20-29, 30-39, and 40-49 years and in all males (p<0.0001, p=0.0036, p=0.002 and p=0.0007, respectively) (Figure 1D). Increased CD8⁺ T cells were detected in men aged 20-29 years compared with the levels in men aged 30-39, 40-49 years, and in all females (p=0.0014, p=0.0022 and p=0.0002, respectively) (Figure 1E). The ratio of CD45RA⁺ cells in CD3⁺ T cells (naive T cells) showed no change with gender differences, but the ratios were lower in males aged 50-60 years compared with the levels in men aged 20-29 and 40-49 years (p=0.0052 and p=0.0029, respectively), while there was no difference among all age groups in women (Figure 1F). The analysis of the ratio of CD4⁺CD25⁺ T cells according to gender and age revealed no significant differences between the groups. The values of all cell groups evaluated within lymphocytes and CD3⁺ T cell gates are given for all age groups in Table 3.

Lower naive and higher T_{EMRA} CD8⁺ T cells are observed in individuals aged 50-60 years

Based on CD45RA and CCR7 expression, naive (CD45RA⁺CCR7⁺), T effector memory RA (T_{EMRA}) (CD45RA⁺CCR7⁻), effector memory (CD45RA⁻CCR7⁻) and central memory (CD45RA⁻CCR7⁺) T cell subsets were separately analyzed in CD4⁺ and CD8⁺ T lymphocytes. Additionally, the ratio of recent thymic emigrant cells (RTE) (CD45RA⁺CD31⁺) was evaluated in CD4⁺ T cells (Supplementary Figure 2). The values of naive, T_{EMRA}, effector memory, and central memory cells in males and females at CD4⁺ and CD8⁺ gates are given in Table 4.

The evaluation of the ratio of naive, T_{EMRA}, effector memory, and central memory CD4⁺ T lymphocytes in terms of gender and age showed no significant difference (Figure 2A). The effector and central memory CD8⁺ T cell ratios did not change according to age or gender (Figure 2B). On the other hand, the ratio of naive CD8⁺ T cells of the women aged 50-60 years was decreased compared with the ratio in women aged 20-29, 30-39, 40-49 years, and total females and with the 20-29 and 30-39 aged male groups (p<0.0001, p=0.0013, p=0.0118, p=0.0026, p=0.0006 and p=0.001, respectively) (Figure 2C). Similarly, the naive CD8⁺ T cell ratio was found lower in men aged 50-59 years compared with the ratio in men aged 20-29 years and total males (p<0.0001 and p=0.0038, respectively) and 20-29, 30-39, 40-49 aged groups and

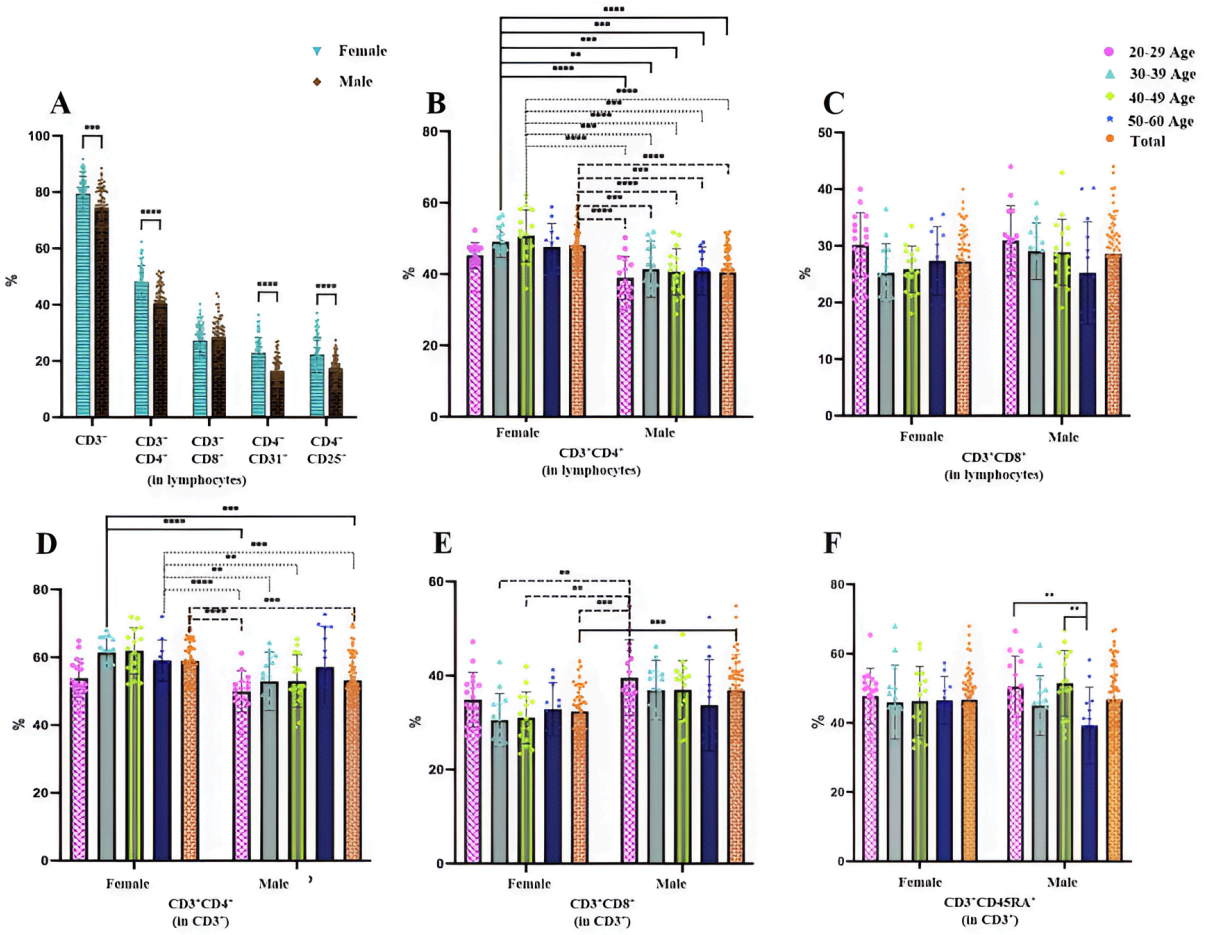

Figure 1. In lymphocytes gate **A)** Distribution of $CD3^+$, $CD3^+CD4^+$, $CD3^+CD8^+$, $CD4^+CD31^+$, and $CD4^+CD25^+$ T lymphocytes in the female and male groups **B)** Distribution of $CD4^+$ and **C)** $CD8^+$ lymphocytes according to age. In the $CD3^+$ lymphocyte gate, **D)** Distribution of $CD4^+$ and **E)** $CD8^+$ lymphocytes, **F)** $CD45RA^+$ lymphocytes according to age (**p<0.01, ***p<0.001, ****p<0.0001).

total females (p<0.0001, p<0.0001, p=0.001 and p<0.0001, respectively) (Figure 2C).

However, T_{EMRA} $CD8^+$ T cell ratios of the women aged 50-60 years increased compared with the ratios in women aged 20-29, 30-39, 40-49 years, and total females and the 20-29 and 30-39 aged group in males (p=0.0045, p=0.038, p=0.043, p=0.0039, p=0.014 and p=0.038, respectively). T_{EMRA} $CD8^+$ T cell ratios of the same age (50-60 years) men were higher compared with the ratios in the total female and youngest (20-29 years old) female group (p=0.003 and p=0.004, respectively). In addition, the TEMRA $CD8^+$ T cell ratio in the 20-29 age group was lower in females than in males in the 40-49 age group males (p=0.03) (Figure 2D).

The ratio of $CD45RA^+CD31^+$ RTE cells was higher in the total females compared with the total and 40-49 aged males (p=0.001 and p=0.0056, respectively). No difference was found in terms of age groups in the RTE of women. However, the RTE ratio was decreased in males aged 50-60 years relative to men aged 20-29 years and the total male groups and 20-29, 30-39, 40-49 aged and total female groups (p<0.0001, p=0.0044, p<0.0001, p=0.0004, p=0.0002 and p<0.0001, respectively) (Figure 2E).

The ratio of Treg and T_{FR} cells increased in elderly individuals

$CD25^{high}CD127^-$ cells in $CD4^+$ T cell population were evaluated as Treg cells. CXCR5 expressing $CD25^{high}CD127^-$ cells were selected as T_{FR}. CXCR5 expressing cells in $CD8^+$ T cells were defined as T_{FC}, and CXCR5 expressing cells within $CD4^+$ T cells were defined as T_{FH} (Supplementary Figure 2).

The ratio of Treg was found to be higher in women aged 50-60 years when compared with the ratio in women aged 20-29, 30-39, 40-49 years, and the total female groups and 20-29 and 30-39 age group in males (p<0.0001, p=0.0014, p=0.0012, p=0.0004, p=0.0002 and p=0.0004, respectively). Similarly, men aged 50-60 years had elevated Treg cells compared with the levels in the men aged 20-29, 30-39, 40-49 years and total male groups and the 20-29, 30-39, 40-49 aged and total female groups (p<0.0001, p<0.0001, p<0.0001, p<0.0001, p<0.0001, p<0.0001, p<0.0001 and p<0.0001, respectively) (Figure 3A).

Table 3. T lymphocyte subset distribution within total lymphocytes and T cell population

Age Group	20-29 Female	19-29 Male	30-39 Female	30-39 Male	40-49 Female	40-49 Male	50-60 Female	50-59 Male	Total Female	Total Male	Total Group
in Lymphocyte											
$CD3^+$ (%)	81.94 ± 6.22 72.51-91.53	76.21 ± 5.75 66.68-83.75	77.86 ± 4.29 69.97-83.57	75.55 ± 6.15 64.07-86.72	80.15 ± 6.02 67.97-88.73	74.93 ± 7.18 61.23-85.97	76.71 ± 7.10 65.01-86.44	69.58 ± 8.61 55.07-84.56	79.43 ± 6.10 65.25-90.58	74.47 ± 7.40 57.47-87.58	**76.91 ± 7.21** **61.19-88.75**
$CD3^+CD4^+$ (%)	45.21 ± 3.63 35.05-52.33	38.93 ± 6.00 30.20-50.22	49.07 ± 4.44 42.60-56.61	41.36 ± 7.85 26.37-51.94	50.75 ± 7.26 35.93-62.18	40.67 ± 6.49 28.79-51.69	47.54 ± 6.59 39.79-58.91	40.84 ± 6.73 22.97-48.96	48.08 ± 5.81 35.47-60.80	40.45 ± 6.68 24.76-51.81	**44.20 ± 7.32** **27.74-58.92**
$CD3^+CD8^+$ (%)	30.18 ± 5.64 20.56-40.01	30.91 ± 6.17 19.41-44.01	25.22 ± 5.14 17.96-36.53	29.06 ± 4.98 19.15-37.63	25.89 ± 4.06 18.03-33.48	28.89 ± 5.81 19.06-42.89	27.35 ± 6.03 19.57-35.57	25.23 ± 9.01 14.45-40.23	27.25 ± 5.47 17.99-38.93	28.59 ± 6.75 14.94-43.42	**27.93 ± 6.16** **16.40-40.30**
$CD4^+CD31^+$ (%)	22.32 ± 3.70 15.59-28.15	18.12 ± 4.94 11.01-25.61	23.31 ± 6.10 12.82-36.23	17.87 ± 4.78 12.52-27.02	24.11 ± 6.09 15.85-33.86	15.24 ± 4.53 7.50-23.25	21.51 ± 5.56 14.54-31.82	14.62 ± 4.41 6.82-21.82	22.89 ± 5.33 13.64-35.10	16.47 ± 4.81 7.17-26.85	**19.62 ± 5.99** **8.38-33.66**
$CD45RA^+$ (%)	57.69 ± 6.63 46.46-70.51	63.47 ± 8.03 47.58-73.46	56.97 ± 9.01 43.05-76.53	58.03 ± 7.31 45.52-71.36	57.62 ± 8.19 44.48-73.17	62.48 ± 8.57 48.11-79.82	57.35 ± 5.85 51.03-69.26	55.36 ± 9.37 35.55-68.45	57.42 ± 7.40 43.73-74.93	59.95 ± 8.77 37.90-77.16	**58.71 ± 8.19** **42.97-74.80**
$CD4^+CD25^+$ (%)	16.58 ± 3.43 11.86-25.05	15.05 ± 4.73 9.78-27.39	18.93 ± 6.79 3.12-29.77	16.92 ± 3.39 11.38-24.51	21.54 ± 5.16 10.04-29.12	18.77 ± 2.86 14.03-23.33	22.66 ± 6.50 12.48-31.29	19.11 ± 4.98 10.08-25.54	22.29 ± 6.12 12.24-35.65	17.46 ± 4.27 9.84-26.42	**19.83 ± 5.77** **10.08-33.95**
in $CD3^+$ T Cells											
$CD3^+CD4^+$ (%)	53.86 ± 5.66 44.02-64.88	49.88 ± 6.09 37.23-61.24	61.41 ± 4.76 50.54-68.02	52.90 ± 8.57 35.65-64.30	61.91 ± 6.84 52.13-71.86	53.01 ± 7.70 39.30-65.40	59.07 ± 6.04 50.79-72.08	57.17 ± 11.97 34.61-72.71	58.88 ± 6.64 45.22-71.98	53.17 ± 8.91 35.16-71.18	**55.98 ± 8.35** **37.19-71.87**
$CD3^+CD8^+$ (%)	34.87 ± 5.81 27.17-47.24	39.55 ± 8.05 23.30-54.87	30.51 ± 5.67 22.40-42.97	36.88 ± 6.31 22.58-46.27	31.05 ± 5.50 23.38-41.94	36.97 ± 6.24 26.00-48.77	32.86 ± 5.67 22.98-41.31	33.71 ± 9.70 18.96-52.44	32.37 ± 5.81 22.68-45.30	36.83 ± 7.72 20.86-53.59	**34.64 ± 7.18** **22.58-49.89**
$CD3^+CD45RA^+$ (%)	47.77 ± 8.03 31.48-65.36	50.48 ± 8.75 35.89-66.54	45.98 ± 10.67 27.07-67.95	44.98 ± 8.65 31.51-62.41	46.32 ± 9.94 32.70-62.93	51.48 ± 9.44 35.57-66.89	46.54 ± 6.87 31.98-57.28	39.24 ± 11.07 15.07-58.18	46.70 ± 8.89 29.16-66.72	46.75 ± 10.46 20.49-66.71	**46.72 ± 9.68** **27.03-66.55**
$CD4^+CD25^+$ (%)	23.06 ± 5.15 15.02-32.03	21.16 ± 6.29 13.38-37.97	26.94 ± 7.48 16.06-42.42	24.26 ± 4.58 15.65-32.33	28.80 ± 7.53 14.61-42.97	27.29 ± 6.36 20.36-39.14	30.10 ± 7.84 16.36-43.50	27.50 ± 7.02 15.08-39.49	26.88 ± 7.30 14.80-43.25	25.05 ± 6.51 13.86-39.31	**25.95 ± 6.94** **14.60-42.43**

All values are given mean + SD and in the range of 2.50-97.50% percentile, respectively.

Table 4. Distribution of naive ($CD45RA^+CCR7^+$), effector memory ($CD45RA^-CCR7^-$), central memory ($CD45RA^-CCR7^+$), and T_{EMRA} ($CD45RA^+CCR7^-$) lymphocyte subsets within $CD3^+CD4^+$ and $CD3^+CD8^+$ T cell populations

Age Group	20-29 Female	20-29 Male	30-39 Female	30-39 Male	40-49 Female	40-49 Male	50-60 Female	50-60 Male	Total Female	Total Male	Total Group
in $CD3^+CD4^+$ T Cells											
$CD45RA^+CCR7^+$ (%)	40.04 ± 9.05 24.23-52.77	40.23 ± 12.95 20.69-60.52	35.84 ± 12.31 16.32-55.32	32.31 ± 10.11 15.91-56.77	38.41 ± 10.80 23.38-57.44	37.03 ± 14.95 18.05-58.32	34.28 ± 9.88 17.75-43.63	25.73 ± 13.20 9.53-46.16	37.44 ± 10.53 17.00-56.43	34.01 ± 13.73 10.32-59.85	**35.70 ± 12.33** **11.47-58.34**
$CD45RA^+CCR7^-$ (%)	2.44 ± 1.22 0.41-5.12	4.38 ± 2.85 1.33-13.00	3.97 ± 2.38 0.91-10.35	4.30 ± 1.98 1.46-8.27	3.75 ± 2.18 1.04-8.10	5.77 ± 5.49 0.88-23.90	6.67 ± 3.59 2.47-13.35	4.52 ± 2.05 1.56-9.70	3.98 ± 2.71 0.64-12.61	4.76 ± 3.44 0.88-18.18	**4.38 ± 3.11** **0.88-13.01**
$CD45RA^-CCR7^-$ (%)	36.26 ± 7.74 22.88-50.37	36.89 ± 12.40 18.30-61.83	41.18 ± 11.02 25.67-57.41	43.73 ± 12.29 20.88-68.60	35.40 ± 10.03 17.87-52.49	35.52 ± 10.45 19.27-51.39	39.73 ± 9.13 30.61-59.21	47.64 ± 13.86 20.67-68.03	37.97 ± 9.58 19.84-58.36	40.74 ± 12.93 18.81-68.30	**39.38 ± 11.44** **19.25-64.00**
$CD45RA^-CCR7^+$ (%)	21.26 ± 6.84 12.62-36.89	18.49 ± 4.88 11.15-28.97	19.01 ± 6.62 11.22-30.67	19.65 ± 8.03 8.00-36.72	22.43 ± 5.53 12.36-35.05	21.67 ± 12.97 2.04-48.52	19.31 ± 6.31 10.75-31.61	22.12 ± 5.47 14.91-33.16	20.61 ± 6.36 10.97-36.04	20.48 ± 8.51 4.31-46.11	**20.54 ± 7.50** **7.96-37.07**
$CD45RA^+CD31^+$ (%)	34.91 ± 7.97 20.74-47.08	32.38 ± 9.59 20.99-50.42	30.01 ± 9.61 15.08-48.05	27.34 ± 8.01 11.59-44.12	30.88 ± 9.54 17.78-47.83	23.92 ± 8.47 9.91-38.67	27.47 ± 8.80 14.21-39.81	16.81 ± 7.77 6.93-29.37	31.19 ± 9.14 14.32-47.95	25.23 ± 10.00 6.95-48.55	**28.61 ± 10.01** **6.99-47.84**
in $CD3^+CD8^+$ T Cells											
$CD45RA^+CCR7^+$ (%)	37.48 ± 10.73 18.26-64.16	37.30 ± 14.65 18.46-62.48	32.29 ± 10.98 8.24-53.61	26.28 ± 10.65 10.78-43.24	31.83 ± 15.50 15.43-71.75	26.99 ± 14.59 10.54-54.88	17.67 ± 8.65 9.26-34.33	13.74 ± 8.84 1.65-35.65	30.92 ± 13.47 8.72-68.14	26.51 ± 14.74 3.90-60.93	**28.07 ± 14.24** **6.16-62.56**
$CD45RA^+CCR7^-$ (%)	26.56 ± 12.58 2.58-46.81	27.56 ± 10.96 13.89-44.13	30.21 ± 12.56 11.23-55.64	33.13 ± 15.28 12.20-64.81	29.45 ± 16.93 4.48-56.68	37.09 ± 15.19 17.08-58.45	41.56 ± 13.64 23.24-64.67	41.23 ± 18.54 9.66-66.70	31.10 ± 14.64 3.48-63.72	34.57 ± 15.53 10.93-65.76	**32.85 ± 15.13** **5.03-64.80**
$CD45RA^-CCR7^-$ (%)	33.84 ± 11.91 15.40-64.26	33.22 ± 9.68 20.80-55.06	34.29 ± 9.29 16.93-53.96	38.47 ± 10.86 23.97-58.76	34.91 ± 11.41 14.60-53.11	32.79 ± 9.09 20.06-54.57	38.44 ± 11.83 23.60-62.49	41.70 ± 15.56 19.95-75.15	35.11 ± 10.97 14.98-63.42	36.31 ± 11.67 20.01-66.96	**35.71 ± 11.30** **16.85-62.58**
$CD45RA^-CCR7^+$ (%)	2.11 ± 1.21 0.42-4.50	1.92 ± 1.36 0.55-5.65	3.14 ± 2.13 0.64-6.97	2.11 ± 1.58 0.44-5.32	3.85 ± 2.26 1.11-7.93	3.12 ± 3.39 0.63-13.79	2.33 ± 1.47 0.75-5.11	3.32 ± 2.22 1.07-9.11	2.87 ± 1.91 0.52-7.91	2.60 ± 2.33 0.47-11.45	**2.73 ± 2.13** **0.50-7.98**

All values are given mean + SD and in the range of 2.50-97.50% percentile, respectively.

The analysis of T_{FR} cells revealed no significant differences among women across age groups, whereas the rate of T_{FR} cells increased in males aged 50-60 compared to men aged 20-29, 40-49 years, and the overall levels in males and females aged 20-29, 30-39, 40-49, as well as total females (p=0.0063, p=0.009, p=0.01, p=0.0012, p=0.0009, p=0.0011 and p<0.0001; respectively) (Figure 3B). The ratio of T_{FH} cells was detected to have decreased in females compared with the ratio in males (p=0.0031). T_{FH} cells in females aged 20-29 years were found to be lower than the number of cells in females aged 30-39

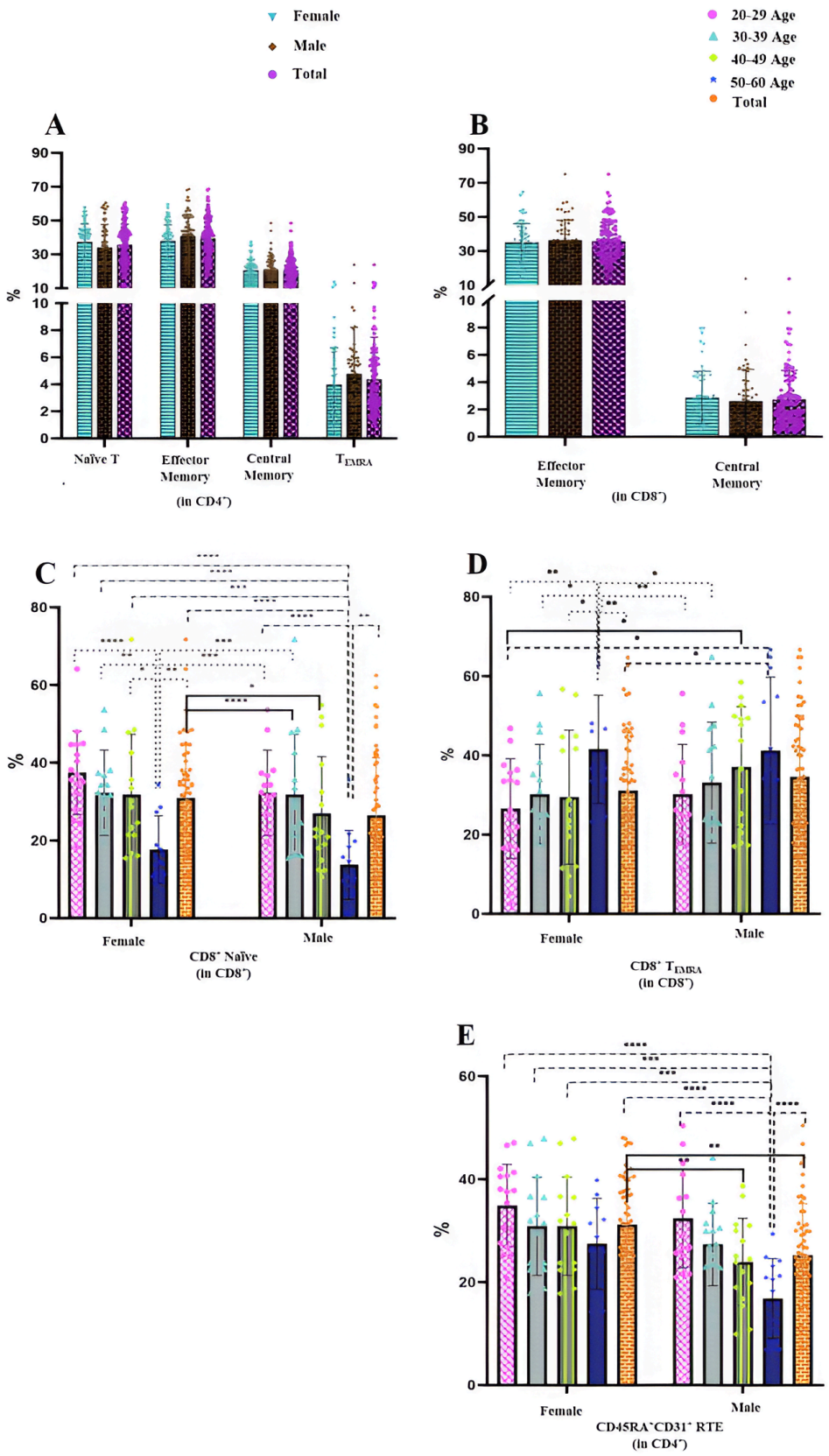

Figure 2. In the $CD4^+$ lymphocyte gate, **A)** Distribution of naive, T_{EMRA}, effector, and central memory $CD4^+$ T lymphocytes in male, female, and all individuals; **B)** Distribution of $CD45RA^+CD31^+$ RTE lymphocytes according to age. In the $CD8^+$ lymphocyte gate, **C)** Distribution of effector and central memory $CD8^+$ T lymphocytes in male, female, and total individuals; **D)** Distribution of naive $CD8^+$ cells; and **E)** distribution of T_{EMRA} $CD8^+$ lymphocytes according to age (*p<0.05, **p<0.01, ***p<0.001, ****p<0.0001).

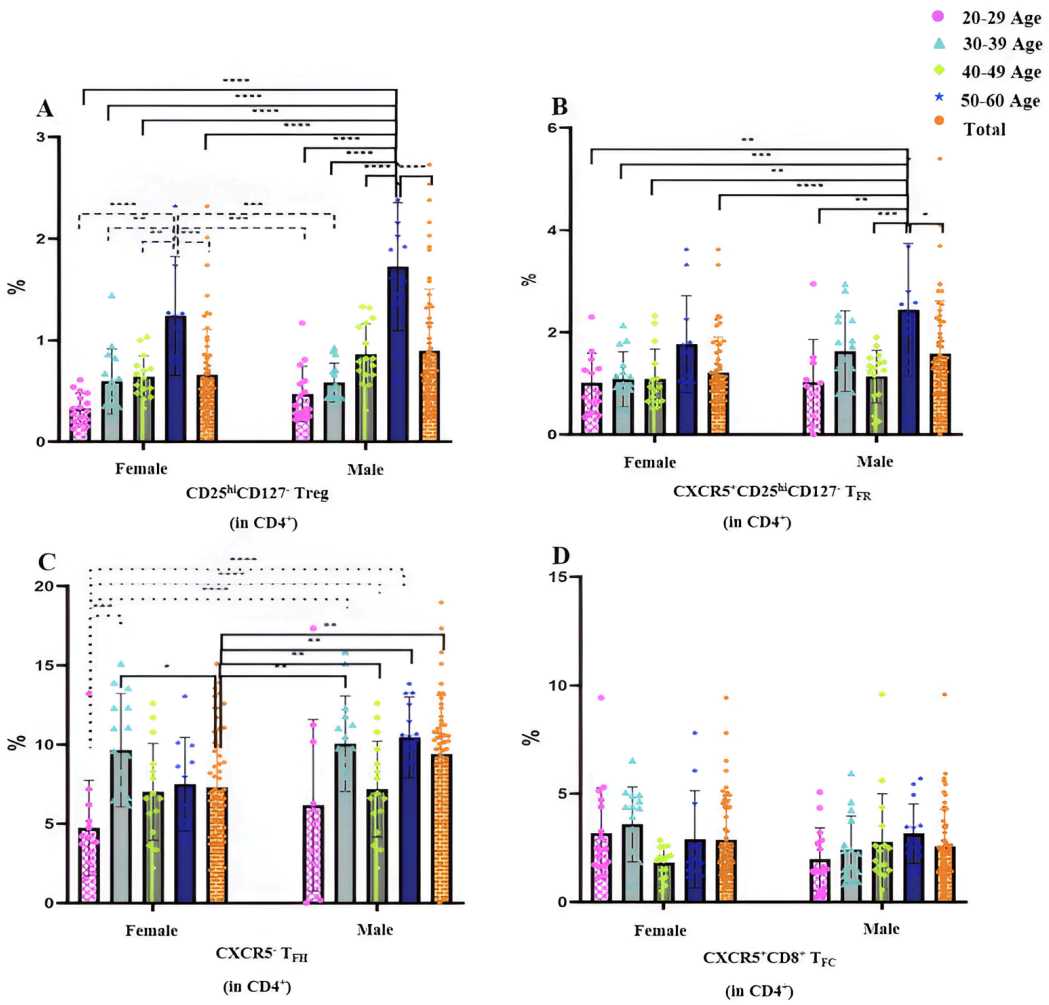

Figure 3. The distribution of $CD25^{high}CD127^{-}$ Treg **(A)**, $CXCR5^{+}CD25^{high}CD127^{-}$ T_{FR} **(B)**, $CXCR5^{+}$ T_{FH} **(C)**, and $CXCR5^{+}CD8^{+}$ T_{FC} cells **(D)** according to age.

years and males aged 30-39, 40-49, and 50-60 years (p=0.0006, p<0.0001, p<0.0001 and p<0.0001, respectively). It was also observed that the total number of the female group was lower than the 30-39 female age group and the 30-39, 40-49, 50-60, and total male groups (p=0.027, p=0.0081, p=0.0098, p=0.0028 and p=0.0031, respectively) (Figure 3C). The evaluation of the ratio of the T_{FC} cell group in terms of gender and age showed no significant differences between the groups (Figure 3D). The values for Treg, T_{FH}, and T_{FR} cells in the $CD4^{+}$ T cell gate and T_{FC} cells in the $CD8^{+}$ T cell gate for males and females by age group are presented in Table 5.

Advanced age in females may affect the differentiation of $CD4^{+}$ T cells to Th1 cells

$CD4^{+}$ T cells are divided into different subsets, such as Th1, Th2, or Th17, according to transcription factors and secreting cytokines (22). Recent studies have shown that some chemokine receptors such as CXCR3 and CCR6, can be used for the determination of Th1, Th2, and Th17 (23). Therefore, $CD4^{+}$ T lymphocytes were analyzed by CXCR3 and CCR6 surface markers as Th1 ($CXCR3^{+}$), Th2 ($CXCR3^{-}CCR6^{-}$) and Th17 ($CXCR3^{-}CCR6^{+}$) cells (Supplementary Figure 2).

Th1, Th2, and Th17 cell subsets were analyzed, and no differences were observed between genders. Th1 cells of the women aged 20-29 years were lower than those of women aged 30-39, 40-49, and 50-60 years (p<0.0001, p=0.0001, and p=0.0016, respectively) and males aged 30-39, 40-49 and 50-60 years (p=0.0001, p=0.0008 and p=0.0073, respectively). Females aged 30-39 years had higher Th1 than total females, 20-29 years, and total males (p=0.026, p=0.0044, and p=0.0044, respectively) (Figure 4A).

On the other hand, the ratio of Th2 and Th17 cells in women aged 20-29 years was increased compared with the ratio in other female age groups (Th2 cells p<0.0001, p=0.0002 and p=0.006; Th17 cells p=0.0001, p=0.0016 and p=0.0009, respectively) (Figure 4B-C). In addition, in the Th2 cell subset, females aged 20-29 years were found to be higher than males aged 30-39, 40-49 and 50-60 years (p=0.0004, p=0.0008 and p=0.0008, respectively). The number of women aged 30-39

Table 5. Distribution of Th1, Th2, Th17, Treg, T_{FH}, T_{FR}, and T_{FC} cell subsets

Age Group	20-29 Female	20-29 Male	30-39 Female	30-39 Male	40-49 Female	40-49 Male	50-60 Female	50-60 Male	Total Female	Total Male	Total Group
CXCR3$^+$ (Th1) (%)	83.63 ± 8.52 64.44-97.17	88.55 ± 8.18 73.17-98.03	95.63 ± 3.40 90.86-99.90	94.08 ± 3.89 86.62-98.57	94.15 ± 3.39 87.14-99.95	92.35 ± 3.98 86.15-99.20	93.10 ± 3.07 88.80-98.67	90.33 ± 1.73 87.05-92.75	91.25 ± 7.27 67.90-99.93	91.36 ± 5.34 73.95-98.87	**91.31 ± 6.34 72.16-99.78**
CXCR3$^-$CCR6$^-$ (Th2) (%)	12.87 ± 7.35 2.61-28.99	9.10 ± 7.33 1.67-25.22	3.43 ± 2.76 0.02-7.93	4.74 ± 3.15 1.05-11.13	4.42 ± 2.51 0.04-9.46	5.55 ± 2.83 0.72-10.31	5.88 ± 2.85 1.14-9.20	7.91 ± 4.10 1.40-17.90	6.92 ± 5.96 0.02-26.50	6.93 ± 4.61 0.89-24.28	**6.92 ± 5.30 0.08-23.78**
CXCR3$^-$CCR6$^+$ (Th17) (%)	3.51 ± 2.11 0.22-6.74	2.41 ± 2.27 0.20-7.56	0.92 ± 0.93 0.02-3.10	1.17 ± 0.86 0.24-3.08	1.41 ± 1.05 0.01-3.37	2.09 ± 1.25 0.09-3.78	1.01 ± 0.76 0.20-2.59	1.07 ± 0.73 0.35-3.15	1.82 ± 1.75 0.01-6.66	1.70 ± 1.50 0.14-6.33	**1.76 ± 1.62 0.01-6.50**
CD25^{hi}CD127$^-$ Treg (%)	0.33 ± 0.14 0.13-0.61	0.47 ± 0.27 0.22-1.17	0.59 ± 0.31 0.22-1.44	0.58 ± 0.19 0.35-0.92	0.64 ± 0.20 0.33-1.03	0.86 ± 0.29 0.31-1.33	1.23 ± 0.58 0.51-2.32	1.72 ± 0.63 0.61-2.73	0.65 ± 0.44 0.13-2.18	0.89 ± 0.60 0.22-2.63	**0.77 ± 0.54 0.16-2.38**
T_{FH} (%)	4.73 ± 3.00 1.54-13.22	6.18 ± 5.41 0.19-17.34	9.65 ± 3.57 2.07-15.10	10.06 ± 3.01 4.97-15.84	7.02 ± 3.05 2.22-12.59	9.91 ± 3.01 5.05-18.98	7.51 ± 2.98 3.77-13.05	10.46 ± 2.54 4.47-13.84	7.30 ± 3.56 1.66-14.65	9.41 ± 3.70 0.07-18.32	**8.36 ± 3.77 1.20-16.22**
T_{FR} (%)	1.00 ± 0.57 0.34-2.30	1.02 ± 0.83 0.18-2.95	1.08 ± 0.53 0.13-2.13	1.63 ± 0.78 0.28-2.94	1.08 ± 0.58 0.51-2.32	1.13 ± 0.51 0.21-1.90	1.77 ± 0.94 0.87-3.62	2.44 ± 1.30 0.29-5.40	1.20 ± 0.70 0.20-3.50	1.58 ± 1.03 0.07-4.87	**1.39 ± 0.90 0.16-3.79**
T_{FC} (%)	3.17 ± 2.09 1.14-9.43	1.97 ± 1.44 0.23-5.08	3.58 ± 1.73 0.69-6.52	2.42 ± 1.54 0.81-5.93	1.81 ± 0.71 0.51-2.86	2.78 ± 2.21 0.56-9.58	2.90 ± 2.23 1.15-7.80	3.16 ± 1.37 1.28-5.70	2.87 ± 1.85 0.59-8.65	2.58 ± 1.70 0.29-7.66	**2.72 ± 1.77 0.47-7.84**

Th1: T helper type 1, Th2: T helper type 2, Th17: T helper type 17, Treg: Regulatory T cells, T_{FH}: Follicular helper T, T_{FR}: Follicular regulatory T, T_{FC}: Follicular cytotoxic T
All values are given mean + SD and in the range of 2.50-97.50% percentile, respectively.

years was found to be lower than the number of the total female group and 20-29 years old male and total male group (p=0.031, p=0.0092, and p=0.0065, respectively). The Th2 cell subset was observed at a lower age in 30-39-years-old females compared with the total male group (p=0.046) (Figure 4B). Th1, Th2, and Th17 cell subsets of men showed no difference regarding age. The values of Th1, Th2, and Th17 lymphocyte subsets are given in Table 5.

DISCUSSION

The pathology of diseases affects the immune system, and accordingly, the distribution of T or B lymphocytes may be altered. Detecting changes in the lymphocyte subsets is important for disease diagnosis and clinical outcome. Therefore, studies focusing on the reference values of T and B lymphocyte subsets are needed. Various factors, such as gender, age, and ethnicity might affect the distribution of T and B lymphocyte subsets (9, 16, 18).

The researchers demonstrated that age and gender differences had no effect on the distribution of B lymphocyte subsets in adults in this study. Similar to our data, studies from a different country showed that B lymphocyte subset showed no change in adults (9, 16). The results of a multi-center study containing six different centers in Europe were similar regarding the distributions of total CD19$^+$, naive, non-switched, and switched memory B lymphocytes, but the range of CD27$^-$IgD$^-$ cells (2.00-6.09%) in individuals aged 20-86 years was different from the range obtained in our study (1.86-18.56%) (9). This difference may be due to the selection of age groups. Our results indicate that, apart from age and gender, ethnicity might not affect the distribution of CD19$^+$ B lymphocytes, naive, non-switched, and switched memory B lymphocytes.

The studies showed that the absolute cell counts of CD3$^+$, CD4$^+$, and CD8$^+$ T lymphocytes increased from birth until the 9th month of life and decreased at later ages (9, 24, 25). In our study, we found that age differences did not affect the ratios of CD3$^+$, CD4$^+$, and CD8$^+$ T lymphocytes in adults. CD3$^+$ and CD4$^+$ T were higher in females; however, there was no difference in CD8$^+$ T lymphocyte according to gender. It was reported that the distributions of CD3$^+$, CD4$^+$, and CD8$^+$ T lymphocytes were similar in different studies conducted in terms of gender in adult individuals (16, 20), and no difference was reported in terms of CD3$^+$ lymphocytes; the number of CD4$^+$ T lymphocytes was higher and CD8$^+$ T lymphocytes were lower in females (18). In several studies, it has been reported that sex chromosome genes and sex hormones such as estrogen, progesterone, and androgens may contribute to differences in the distribution of immune cells between women and men (26-28). In particular, estrogen has been shown to have a strong influence on NF-κB signaling, which plays a key role in a variety of inflammatory and autoimmune processes, and half of the active genes in female T cells like Treg, have estrogen response elements in their promoters (26, 27). Additionally, it is suggested that hormonal transition periods, such as menopause, may be also associated with differences in immune cell distributions in women of different age groups (26-28). A multi-cohort study identified 144 differentially expressed genes between females and males (27). According to this study, genes highly expressed in CD4$^+$ T cells of females were associated with the adaptive immune response. MicroRNAs (miRNAs) are small RNA molecules that play a role in the regulation of gene expression. Although the Y chromosome contains only 2 miRNAs, the X chromosome contains approximately 800 miRNAs. Some miRNAs encoded on the X chromosome also affect immune cells and their functions. Additionally, sex

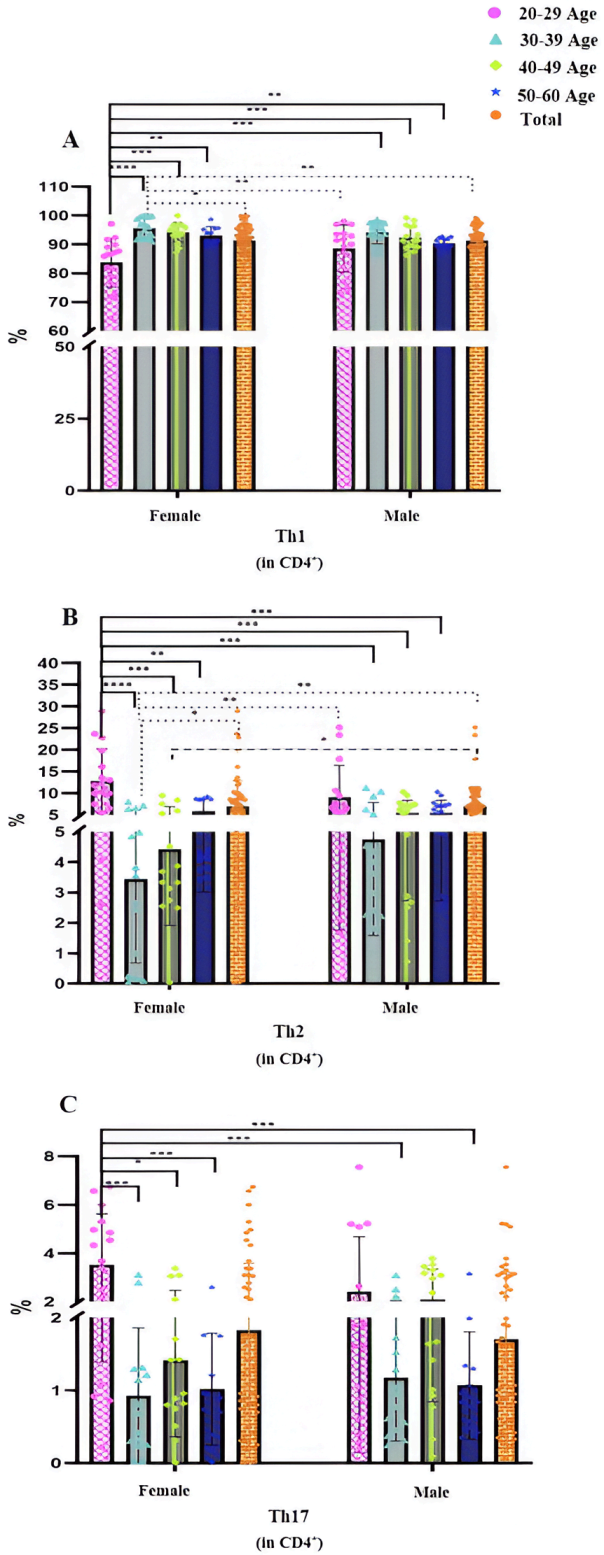

Figure 4. The distribution of CXCR3$^+$ Th1 (A), CXCR3$^-$CCR6$^-$ Th2 (B), and CXCR3$^-$CCR6$^+$ Th17 (C) in CD4$^+$ T cells according to age. (*p<0.05, **p<0.01, ***p<0.001, ****p<0.0001).

hormones also influence the expression of these miRNAs (26). In light of all the aforementioned information, it is thought that various factors, including differences in the expression profiles of sex hormones, miRNAs, and genes responsible for immune responses between males and females, may contribute to the observed differences in T cell subsets between men and women in our study. Gender and age differences were found to have not affected the effector, central memory, naive and T_{EMRA} cell distributions in CD4$^+$ T lymphocytes, whereas a decrease in naive CD8$^+$ T cell and

an increase in T_{EMRA} in $CD8^+$ T lymphocytes were found in the 50-60 age group of both genders. Some studies reported that this decrease of naive cells was a result of age-related thymic involution. However, an increase in the number of T_{EMRA} cells that develop in response to pathogens with immune aging may be among the expected results (29, 30).

Treg and T_{FR} play unique roles in autoimmune diseases, and changes in the ratio or function of these cells are associated with pathogenesis (31-33). Autoimmune diseases are rarely detected in the elderly (32, 34). In our data, Treg cell ratio was observed to increase, especially in individuals aged 50-60 years compared to the ratio in other age groups. The increase in Treg in the elderly people observed in the current literature supports the data obtained in our study. However, one study showed that Treg cell distribution differed in terms of gender, and 20-39 and 40-60 age groups compared with our data (6.00-9.00%) (18). Additionally, it was observed that T_{FR} cell ratios increased in men aged 50-60 years compared with the ratios in other age groups, while no difference was found between male and female groups. As observed for Treg cells, it might be suggested that the increase in Treg and T_{FR} cells in the elderly may have led to an increase in the protective effects against autoimmune diseases and increased susceptibility to cancer and chronic infections.

T cells play an important role in the development of autoimmune diseases, and in most diseases, a Th1 response is dominant (35). Our observations that Th1 responses are more predominant in healthy women aged 30 years and older may be related to the age at disease onset. Various factors, such as genetic predisposition, hormones, and environmental factors, are known to have possible roles in the pathogenesis of autoimmune diseases, and age- and gender-related changes in T cell subsets in healthy individuals may also be an important factor to consider.

To summarize, the T and B lymphocyte subsets were comprehensively analyzed in whole blood samples from healthy adults, and reference ranges for age and sex differences were established in the present study. The missing point of our study is that the volunteers were limited to the Istanbul region only and the total population size was low to come up with country-wide conclusions. Nevertheless, our results suggest that age and gender differences may lead to differences in cell distribution. In addition, it is suggested that the obtained data will contribute to the clinic in the evaluation of lymphocyte subset distributions in diagnostic tests performed using flow cytometry in individuals with cancer, primary immunodeficiency, or autoimmune diseases; thus, early diagnosis and correct treatment methods can be offered to patients in a short period of time.

Ethics Committee Approval: Ethics approval for the study was obtained from the Istanbul Medical Faculty Clinical Research Ethics Committee (21/08/2020 and numbered 19).
Peer Review: Externally peer-reviewed.
Author Contributions: Conception/Design of Study – F.T.K., G.D., S.C., M.Y.G.; Data Acquisition – F.T.K., M.Y.G., S.K.B., M.Y.; Data Analysis/Interpretation - F.T.K., M.Y.G.; Drafting Manuscript – F.T.K., M.Y.G.; Critical Revision of Manuscript – S.K.B., M.Y., G.D., S.C., M.Y.G.; Final Approval and Accountability – G.D., S.C., M.Y.G.
Conflict of Interest: The authors declare no conflict of interest
Financial Disclosure: This study was supported by Istanbul University Scientific Research Projects BAP Unit. Project No: 37095.

Author Details

Fatma Turgut Kaynak
[1] Department of Immunology, Aziz Sancar Institute of Experimental Medicine, Istanbul University, Istanbul, Turkiye
[2] Institute of Graduate Studies in Health Sciences, Istanbul University, Istanbul, Turkiye
0000-0003-3025-7117

Melek Yanasik
[3] Blood Transfusion Center, Istanbul Faculty of Medicine, Istanbul University, Istanbul, Turkiye
0000-0003-1164-6774

Suzan Cinar
[1] Department of Immunology, Aziz Sancar Institute of Experimental Medicine, Istanbul University, Istanbul, Turkiye
0000-0002-8330-7010

Sevgi Kalayoglu Besisik
[3] Blood Transfusion Center, Istanbul Faculty of Medicine, Istanbul University, Istanbul, Turkiye
[4] Department of Internal Medicine, Division of Hematology, Istanbul Faculty of Medicine, Istanbul University, Istanbul, Turkiye
0000-0002-9310-1278

Gunnur Deniz
[1] Department of Immunology, Aziz Sancar Institute of Experimental Medicine, Istanbul University, Istanbul, Turkiye
0000-0002-0721-6213

Metin Yusuf Gelmez
[1] Department of Immunology, Aziz Sancar Institute of Experimental Medicine, Istanbul University, Istanbul, Turkiye
0000-0002-5279-0855 yusufmetin@istanbul.edu.tr

REFERENCES

1. Marshall JS, Warrington R, Watson W, Kim HL. An introduction to immunology and immunopathology. Allergy Asthma Clin Immunol 2018; 14(Suppl 2): 49.
2. Bonilla FA, Oettgen HC. Adaptive immunity. J Allergy Clin Immunol 2010; 125(2 Suppl 2): S33-40.

3. Salzer U, Sack U, Fuchs I. Flow cytometry in the diagnosis and follow-up of human primary immunodeficiencies. EJIFCC 2019; 30(4): 407-22.
4. Vodjgani M, Aghamohammadi A, Samadi M, Moin M, Hadjati J, Mirahmadian M et al. Analysis of class-switched memory B cells in patients with common variable immunodeficiency and its clinical implications. J Investig Allergol Clin Immunol 2007; 17(5): 321-8.
5. Richardson CT, Slack MA, Dhillon G, Marcus CZ, Barnard J, Palanichamy A et al. Failure of B cell tolerance in CVID. Front Immunol 2019; 10: 2881.
6. Romagnani S. T-cell subsets (Th1 versus Th2). Ann Allergy Asthma Immunol 2000; 85(1): 9-18; 21.
7. Deng Q, Luo Y, Chang C, Wu H, Ding Y, Xiao R. The emerging epigenetic role of CD8+ T cells in autoimmune diseases: A systematic review. Front Immunol 2019; 10: 856.
8. Barzaghi F, Passerini L, Bacchetta R. Immune dysregulation, polyendocrinopathy, enteropathy, x-linked syndrome: a paradigm of immunodeficiency with autoimmunity. Front Immunol 2012; 3: 211.
9. Besci O, Baser D, Ogulur I, Berberoglu AC, Kiykim A, Besci T, et al. Reference values for T and B lymphocyte subpopulations in Turkish children and adults. Turk J Med Sci 2021; 51(4): 1814-24.
10. Duchamp M, Sterlin D, Diabate A, Uring-Lambert B, Guerin-El Khourouj V, Le Mauff B, et al. B-cell subpopulations in children: National reference values. Immun Inflamm Dis 2014; 2(3): 131-40.
11. Alam I, Goldeck D, Larbi A, Pawelec G. Aging affects the proportions of T and B cells in a group of elderly men in a developing country–a pilot study from Pakistan. Age (Dordr) 2013; 35(5): 1521-30.
12. Yan J, Greer JM, Hull R, O'Sullivan JD, Henderson RD, Read SJ, McCombe PA. The effect of ageing on human lymphocyte subsets: comparison of males and females. Immun Ageing 2010; 7: 4.
13. Qin L, Jing X, Qiu Z, Cao W, Jiao Y, Routy JP, Li T. Aging of immune system: Immune signature from peripheral blood lymphocyte subsets in 1068 healthy adults. Aging (Albany N Y) 2016; 8(5): 848-59.
14. Morbach H, Eichhorn EM, Liese JG, Girschick HJ. Reference values for B cell subpopulations from infancy to adulthood. Clin Exp Immunol 2010; 162(2): 271-9.
15. Haynes L, Maue AC. Effects of aging on T cell function. Curr Opin Immunol 2009; 21(4): 414-7.
16. Bisset LR, Lung TL, Kaelin M, Ludwig E, Dubs RW. Reference values for peripheral blood lymphocyte phenotypes applicable to the healthy adult population in Switzerland. Eur J Haematol 2004; 72(3): 203-12.
17. Lee BW, Yap HK, Chew FT, Quah TC, Prabhakaran K, Chan GS, et al. Age- and sex-related changes in lymphocyte subpopulations of healthy Asian subjects: from birth to adulthood. Cytometry 1996; 26(1): 8-15.
18. Oras A, Quirant-Sanchez B, Popadic D, Thunberg S, Winqvist O, Heck S, et al. Comprehensive flow cytometric reference intervals of leukocyte subsets from six study centers across Europe. Clin Exp Immunol 2020; 202(3): 363-78.
19. Valiathan R, Ashman M, Asthana D. Effects of ageing on the immune system: Infants to elderl. Scand J Immunol 2016; 83(4): 255-66.
20. Yaman A, Cetiner S, Kibar F, Tasova Y, Seydaoglu G, Dundar IH. Reference ranges of lymphocyte subsets of healthy adults in Turkey. Med Princ Pract 2005; 14(3): 189-93.
21. Ikinciogullari A, Kendirli T, Dogu F, Egin Y, Reisli I, Cin S, Babacan E. Peripheral blood lymphocyte subsets in healthy Turkish children. Turk J Pediatr 2004; 46(2): 125-30.
22. Luckheeram RV, Zhou R, Verma AD, Xia B. CD4(+)T cells: differentiation and functions. Clin Dev Immunol 2012; 2012: 925135.
23. Mousset CM, Hobo W, Woestenenk R, Preijers F, Dolstra H, van der Waart AB. Comprehensive phenotyping of T cells using flow cytometry. Cytometry A 2019; 95(6): 647-54.
24. Comans-Bitter WM, de Groot R, van den Beemd R, Neijens HJ, Hop WC, Groeneveld K, et al. Immunophenotyping of blood lymphocytes in childhood. Reference values for lymphocyte subpopulations. J Pediatr 1997; 130(3): 388-93.
25. Schatorje EJ, Gemen EF, Driessen GJ, Leuvenink J, van Hout RW, de Vries E. Paediatric reference values for the peripheral T cell compartment. Scand J Immunol 2012; 75(4): 436-44.
26. Klein SL, Flanagan KL. Sex differences in immune responses. Nat Rev Immunol 2016; 16(10): 626-38.
27. Shepherd R, Cheung AS, Pang K, Saffery R, Novakovic B. Sexual dimorphism in innate immunity: The role of sex hormones and epigenetics. Front Immunol 2020; 11: 604000.
28. McCombe P. JM. Sexual dimorphism in the immune system. Rose NRM, IR, editor. The autoimmune diseases. London: Academic Press; 2020.
29. Koch S, Larbi A, Derhovanessian E, Ozcelik D, Naumova E, Pawelec G. Multiparameter flow cytometric analysis of CD4 and CD8 T cell subsets in young and old people. Immun Ageing 2008; 5: 6.
30. Ponnappan S, Ponnappan U. Aging and immune function: molecular mechanisms to interventions. Antioxid Redox Signal 2011; 14(8): 1551-85.
31. Ding T, Niu H, Zhao X, Gao C, Li X, Wang C. T-follicular regulatory cells: Potential therapeutic targets in rheumatoid arthritis. Front Immunol 2019; 10: 2709.
32. Theron HD, Steyn AF, du Raan HE, Bennett JM, de Wet JI. Autonomic neuropathy and atypical myocardial infarction in a diabetic clinic population. S Afr Med J 1987; 72(4): 253-4.
33. Ribeiro F, Romao VC, Rosa S, Jesus K, Agua-Doce A, Barreira SC, et al. Different antibody-associated autoimmune diseases have distinct patterns of T follicular cell dysregulation. Sci Rep 2022; 12(1): 17638.
34. Vadasz Z, Haj T, Kessel A, Toubi E. Age-related autoimmunity. BMC Med 2013; 11: 94.
35. Romagnani S. Th1 and Th2 in human diseases. Clin Immunol Immunopathol 1996; 80(3 Pt 1): 225-35.

APPENDIX

Supplementary Table 1. Constructed panel and antibody information

	Antibody	Fluorochrome	Clone	Source/Company
T Cell Panel	CD45RA	FITC	L48	BD
	CCR7 (CD197)	PE	3D12	BD-Pharmingen
	CD31	PE.Cy7	WM59	BD-Pharmingen
	CD4	APC	OKT4	Biolegend
	CD8	APC/Cy7	SK1	BD-Pharmingen
	CD3	AlxF700	OKT3	Biolegend
	CD45	BV510	HI30	BD-Horizon
Treg Cell Panel	CXCR5 (CD185)	FITC	J252D4	Biolegend
	CD25	PE	2A3	BD
	CCR6 (CD196)	PE.Cy7	11A9	BD-Horizon
	CD4	APC	OKT4	Biolegend
	CD8	APC/Cy7	SK1	BD-Pharmingen
	CD3	AlxF700	OKT3	Biolegend
	CD127	BV421	HIL-7R-M21	BD-Horizon
	CD45	BV510	HI30	BD-Horizon
	CXCR3 (CD183)	BV711	IC6/CXCR3	BD-Horizon
B Cell Panel	IgD	FITC	IA6-2	Biolegend
	CD27	PE.Cy7	M-T271	Biolegend
	CD19	APC	SJ25C1	BD
	CD45	BV510	HI30	BD-Horizon

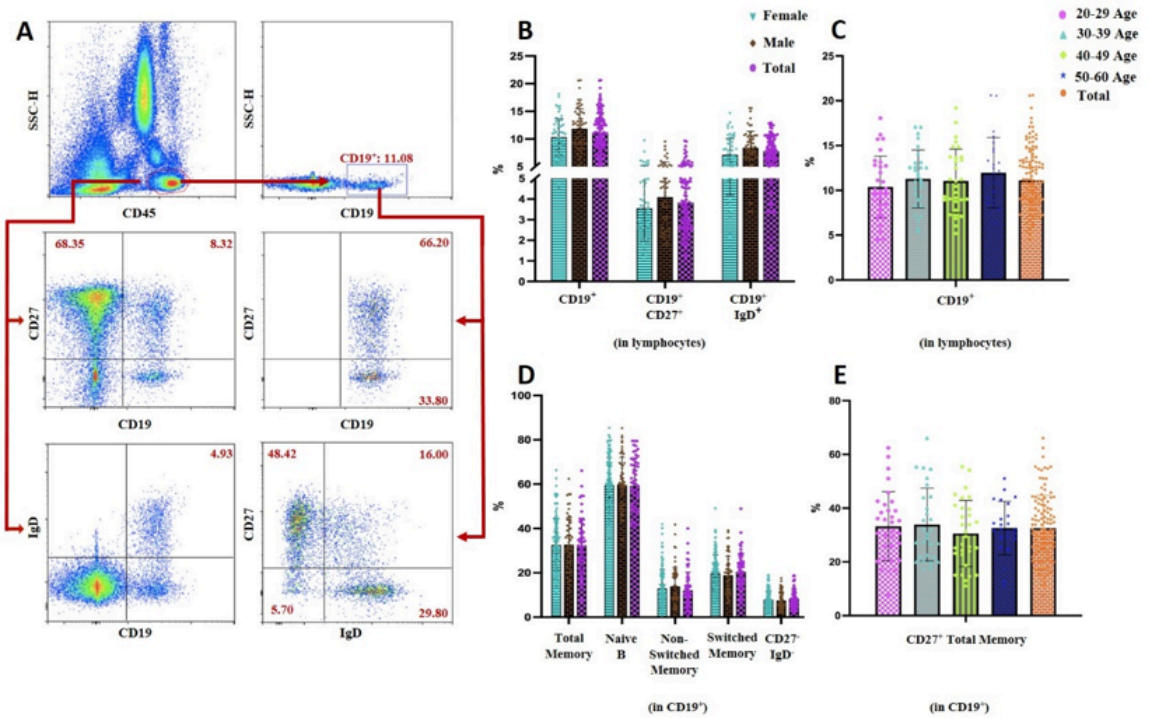

Supplementary Figure 1. A) The lymphocyte ($CD45^+$) and B cell ($CD19^+$) gating strategy for B lymphocyte subsets. **B)** The distribution of $CD19^+$, $CD19^+CD27^+$ and $CD19^+IgD^+$ lymphocytes in total individuals, according to gender, and **C)** the distribution of $CD19^+$ regarding age in lymphocytes gate. **D)** The distributions of total memory, naive, non-switched, switched memory and $CD27^-IgD^-$ B lymphocyte of total, male and female individuals in the $CD19^+$ **E)** $CD27^+$ total memory B lymphocyte distributions by age groups in the $CD19^+$ lymphocyte gate.

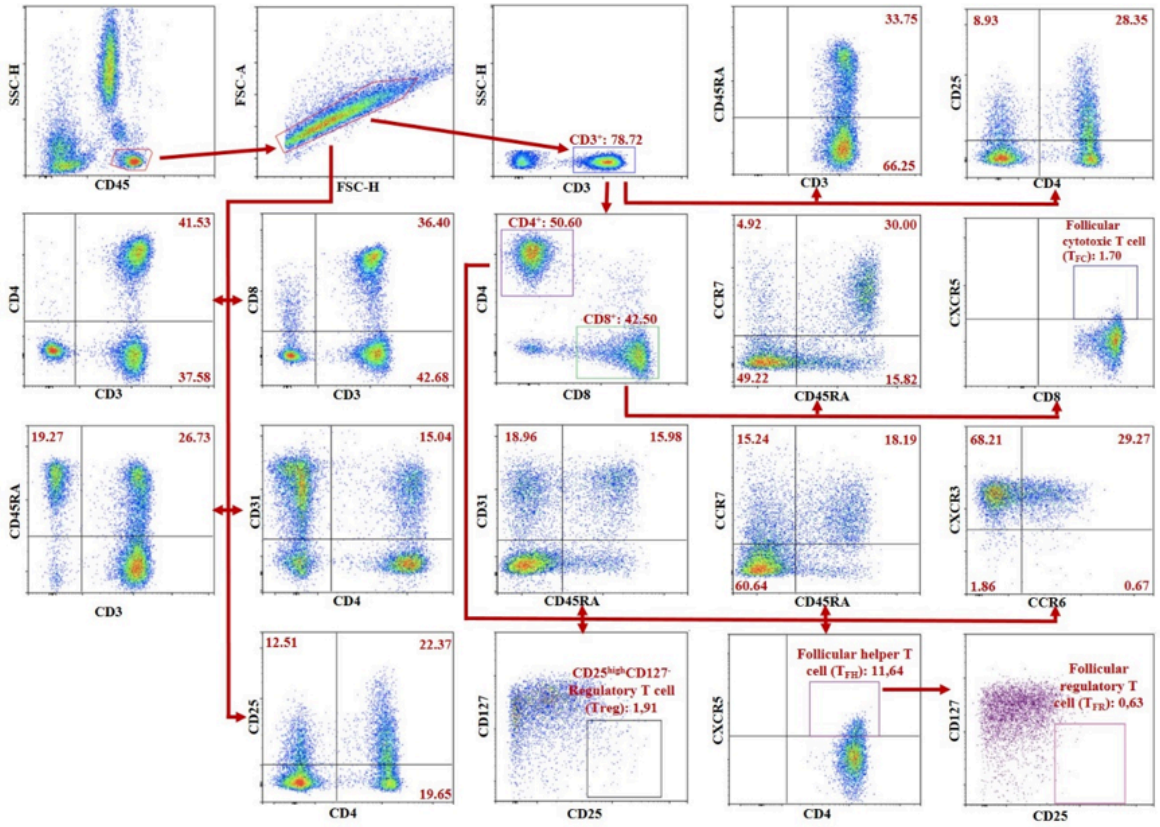

Supplementary Figure 2. The gating strategy for T lymphocytes and subsets.

İSTANBUL UNIVERSITY PRESS

Experimed 2025, 15 (1): 15–22

https://doi.org/10.26650/experimed.1529331

Submitted: 09.08.2024
Revision Requested: 06.11.2024
Last Revision Received: 19.12.2024
Accepted: 20.12.2024
Published Online 20.03.2025

Experimed

Research Article

Open Access

GWAS Analysis of Sudden Cardiac Death Cases in a Turkish Population

Gulay Ozel Cavlak [1], Mehmet Cavlak [2], Kubilay Kinoglu [3], Ayse Begum Ceviz [4], Allison Pinar Eronat [5], Isil Kobak [6], Bulent Sam [3], Mustafa Yildiz [7], Bulent Bayraktar [8], Hulya Yilmaz Aydogan [9] & Oguz Ozturk [9]

[1] Council of Forensic Medicine, Ministry of Justice, Ankara, Turkiye
[2] Department of Forensic Medicine, Faculty of Medicine, Hacettepe University, Ankara, Turkiye
[3] Council of Forensic Medicine, Ministry of Justice, Istanbul, Turkiye
[4] Department of Medical Genetics, Faculty of Medicine, Istanbul Health and Technology University, Istanbul, Turkiye
[5] Department of Molecular Biology and Genetics, Faculty of Science and Literature, Halic University, Istanbul, Turkiye
[6] Department of Data Science, Faculty of Science and Literature, Yeditepe University, Istanbul, Turkiye
[7] Cardiology Institute, Istanbul University, Istanbul, Turkiye
[8] Department of Sports Medicine, Istanbul Faculty of Medicine, Istanbul University, Istanbul, Turkiye
[9] Department of Molecular Medicine, Aziz Sancar Institute of Experimental Medicine, Istanbul University, Istanbul, Turkiye

Abstract

Objective: Sudden death is defined as death occurring within one hour of the onset of symptoms, with cardiovascular diseases being one of the leading causes. The most common genetic factors leading to sudden cardiac death are hypertrophic cardiomyopathy and arrhythmogenic right ventricular cardiomyopathy. In some cases, autopsies may reveal no evidence of long QT syndrome, short QT syndrome, catecholaminergic polymorphic ventricular tachycardia, or Brugada Syndrome.

Materials and Methods: We collected samples from sudden cardiac death cases aged 5–40 years (arrhythmia as Group 1, hypertrophy as Group 2, and ischemic heart disease as Group 3) , as well as from healthy athletes (control group as Group 4), and analyzed them using genome-wide association study (GWAS) with a DNA microchip containing 196,725 single nucleotide polymorphism (SNP) markers thought to be associated with sudden cardiac death or other cardiovascular diseases.

Results: We detected any possible genetic variations or patterns that could elucidate the mechanisms underlying sudden cardiac death in a Turkish population. In our study group, two polymorphisms; rs2971851 and rs9609516, stood out as prominent variants compared with healthy elite athletes.

Conclusion: We aimed to identify potential genetic variations or patterns that could shed light on the mechanisms underlying sudden cardiac death in the Turkish population. In our study group, two polymorphisms, rs2971851 and rs9609516, emerged as prominent variants when compared to healthy athletes.

Keywords Sudden cardiac death · Microarray analysis · GWAS · Genetics · Forensic medicine

Citation: Ozel Cavlak, G., Cavlak, M., Kinoglu, K., Ceviz, A. B., Eronat, A. P., Kobak, I., Sam, B., Yildiz, M., Bayraktar, B., Yilmaz Aydogan, H. & Ozturk, O. GWAS analysis of sudden cardiac death cases in a Turkish population. Experimed 2025; 15(1): 15-22. DOI: 10.26650/experimed.1529331

Corresponding author: Gulay Ozel Cavlak ozgulay2001@gmail.com

INTRODUCTION

In forensic medicine practices, sudden and unexpected deaths are the most frequent ones among natural death causes. It is reported that every year approximately 350,000 people in Europe and between 300,000 and 400,000 people in the USA die suddenly and unexpectedly (1). Moreover, it has been shown that most of these deaths are of cardiac origin (2). This phenomenon, known as sudden cardiac death, is defined as death occurring within one hour of the onset of cardiac symptoms—such as chest pain, palpitations, or fainting—in an otherwise healthy individual (3). While channelopathies and cardiomyopathies frequently cause sudden cardiac death in younger populations, coronary artery diseases are among the most common causes of sudden cardiac death in middle-aged individuals (4).

Sudden cardiac death is an important public health problem affecting the community and young people. Therefore, to prevent possible young deaths, it is important to understand the basic features and mechanisms of the disease. Consequently, genetic studies have gained importance in recent years. The genome-wide association study (GWAS) is a technique that has been used since 2007 to evaluate complex diseases and common diseases or population-based studies. The primary purpose of GWAS is to link potentially associated genes with a specific disease or trait. GWAS analysis is advantageous because it can include a large number of single nucleotide polymorphisms (SNPs) and can reliably analyze them in a short time with a large number of samples (5, 6).

For our study, we used a DNA chip containing 196,725 SNP markers associated with cardiovascular disease risk to identify polymorphic gene regions specific to the Turkish population and to uncover the relationships between genes and diseases.

MATERIALS AND METHODS

We selected 152 autopsies performed at the Forensic Medicine Institute between 2011 and 2013. These cases were associated with sudden cardiac death, were aged between 5 and 40 years, and had no previous cardiac complaints or family history of sudden cardiac death. Blood and tissue samples were stored at -20°C.

We divided selected cases into 3 groups according to clinical history and macroscopic and histopathological examination findings. Group 1 (n=53; 12 females and 41 males), "negative autopsy group (Group 1)" comprised cases with no structural changes in the heart and no occlusive lesions in their coronary arteries; Group 2 (n=50; 13 females and 37 males), "hypertrophic cardiomyopathy group" comprised of cases showing histopathological hypertrophic cardiomyopathy features in cardiac tissue; and Group 3 (n=49; 5 females and 44 males), "ischemic heart disease group" comprised cases showing occlusive features and histopathological ischemic features in heart tissue. Cases with a history of epilepsy, structural anomalies in the heart and/or coronary arteries (valvular malformation, coronary bridging, etc.), myocarditis, or toxicological features on chemical examination were excluded from the study. Group 4 was formed as the control group consisting of 80 healthy athletes.

The control group was selected using the following criteria to increase the scientific validity and statistical power of the results;

1) We selected individuals who did not have any heart disease in themselves or their family, have no history of sudden cardiac death in the family, have undergone echocardiogram (ECHO) and electrocardiogram (ECG) screenings, receive regular checkups, and engage in regular physical activity.
2) The samples were selected from individuals aged 16-40, as in the autopsy samples.
3) The gender distribution was adjusted to ensure a higher proportion of males in the control group, as sudden cardiac deaths are more commonly observed in males.
4) To avoid ethnic and geographical differences among individuals, the control group was selected from people living in Istanbul.

We performed total DNA isolation using an Invitrogen Mini Kit and a Qiagen Mini Blood Kit using the blood samples of the control group and tissue samples of the case groups collected during the autopsies. We measured the purity and concentration of the DNA samples by spectrophotometric method at a wavelength of 260/280 nm using a Nanodrop spectrophotometer. A minimum of 40 ng/µL concentration was needed for our purposes, and a total of 32 DNA isolates that did not reach this concentration were not included in further studies. 4-5 µL from each DNA isolate was used.

GWAS Analysis

We analyzed 196,725 SNP markers using an iScan Microarray Scanner (Illumina Inc®) and GenomeStudio®v2011.1 software (Illumina Inc®) for all preliminary analyses and quality analysis of the process.

We then compared the samples using the "Identity by Descent (IBD) Estimation" according to the alleles that they shared. The estimated proximity identification (PI) value indicates shared alleles. This value is expected to be one for monozygotic twins, 0.5 for siblings, and 0.25 for cousins. We verified the sex of the samples using the heterozygosity of the X chromosome, which was determined during the genotyping process.

The processed data were transferred from GenomeStudio to Golden Helix®SNP & Variation Suite (SVS). We started the analyses with 196,725 SNP markers, but after removing the markers on chromosome Y (due to the fact that genes on the Y chromosome are associated with very few diseases), we continued with 185,802 SNP markers.

Statistical Analyses

We applied Fisher's exact test for Hardy-Weinberg Equilibrium (HWE), and markers with p values lower than 10^{-5} and SNP markers with Linkage Disequilibrium (LD) (>0.5) were filtered out and excluded from the analysis.

We started whole genome association analysis using the markers determined during the SNP filtering process. "Additive model, (dd)>(Dd)>(DD)" and applied "Correlation/ Trend" test were selected. We used Bonferroni Adjustment and False Discovery Rate (FDR) tests as Multiple Correction tests.

We performed the statistical analyses using the SPSS 20.0 package program (IBM Corp., Armonk, NY, USA) and used p<0.05 as significance limit.

RESULTS

Group 1 consisted of 53 (12 females and 41 males, mean age=23.13), Group 2 included 50 (13 females and 37 males, mean age=28.94), and Group 3 included 49 (5 females and 44 males, mean age=35.22) cases.

Information about the activities of the cases at the time of death are given in Table 1.

Table 1. Distribution of patient groups by place of death

Activity at the Time of Death	Frequency	Percentage	Valid Percentage	Cumulative Percentage
Unknown	9	5.9	5.9	5.9
Resting	50	32.9	32.9	38.8
Driving	4	2.6	2.6	41.4
Sleeping	8	5.3	5.3	46.7
Found dead at home	22	14.5	14.5	61.2
Found dead in the bathroom	9	5.9	5.9	67.1
At workplace	9	5.9	5.9	73
During argument	2	1.3	1.3	74.3
During physical effort	34	22.4	22.4	96.7
Few days lasting chest pain	5	3.3	3.3	100
Total	152	100	100	

Evaluation of the Microarray Findings

Group 1 (arrhythmia), Group 2 (hypertrophy), and Group 3 (ischemic heart disease) were included in the analysis. Samples in Group 3 were analyzed separately as hypertrophy-coronary heart disease and hypertrophy-coronary heart disease-myocardial infarction, yet evaluated as a single group. We examined a total of 200 DNA samples, including case groups; however, in 60 samples data acquisition (call rates) were detected below 95%, and therefore these were excluded from the study. Among the 140 samples, the highest data acquisition was determined as 0.9969, and the lowest as 0.9557.

Proximity Identification (PI)

We found the estimated PI value of these 140 control samples as 0.097, and since there were no kinship between the samples, none were excluded from the analysis.

Gender Determination

We determined the sex of the samples using heterozygosity data from the X chromosome. The gender distribution of the genotyping samples was 66 male and 16 female cases. In the control group, 44 were males and 14 were females.

SNP Filtering

We began our analysis using 196,725 SNP markers across a total of 140 samples. Subsequently, we removed the markers on the Y-chromosome and continued with the remaining 185,802 markers. The number of markers with a genotyping rate below 95% was 10,596. The number of markers with minor allele frequency (MAF) below 0.01 was 60,232. Markers with a p value of less than 10^{-5} for HWE were 507, and therefore, a total of 68,688 SNP markers were excluded from the analysis (7).

Linkage Disequilibrium (LD)

A total of 57,569 SNP markers with LD (>0.5) were excluded from the analysis.

GWAS Analysis

Following SNP filtering, we analyzed 140 samples (82 cases, 58 controls) with 59,545 SNP markers. As a result of the analysis, among the SNPs with a p value below $1x10^{-4}$, the ones with the highest significance were determined as rs2971851 on the 2. chromosome (2p14, MAF=0.7342) and rs9609516 on the 22. chromosome (22q12.3, MAF=0.1273).

Evaluation of Results According to Case-Control Relationship

The Q-Q chart of the expected and observed values is shown in Figure 1. The Manhattan Plot for case groups and control group is shown in Figure 2. SNP markers with a p value below

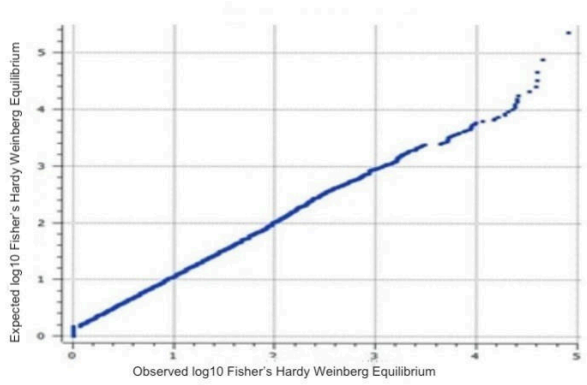

Figure 1. The Q-Q plot of the expected and observed values among the case and control groups

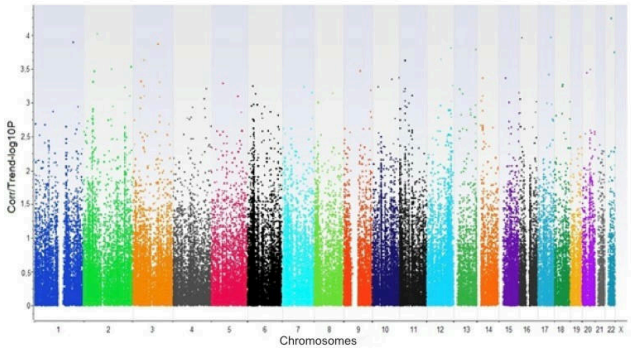

Figure 2. Manhattan Plot demonstration between case/control groups

1x10^{-4} according to the case groups-control relationship are presented in Tables 2, 3, and 4.

Table 2. SNPs associated with arrhythmia (Group 1) compared to controls (Group 4)

Marker	Chromosome	Gene	Position	Allele Change	The Minor Allele Frequency	Variant
rs2369527	1q31.2	*LINC02770*	191872334	A/G	0.1663	Intronic
rs2632594	3p22,1	*ULK4*	41480682	A/G	0.8922	Intronic
rs10213562	4q25	*MCUB*	110494732	T/G	0.2146	Intronic
rs37569	5q11.2	*PDE4D*	58839567	A/C	0.8432	Intronic
rs12209155	6p12.3	*PTCHD4*	47891704	C/T	0.1204	Intronic
rs10811461	9p21,3	*NONE*	21063183	G/A	0.1246	NONE
rs3786189	18q23	*NFATC1*	77201837	T/C	0.2533	Intronic

Table 3. SNPs associated with hypertrophic cardiomyopathy (Group 2) compared controls (Group 4)

Marker	Chromosome	Gene	Position	Allele Change	The Minor Allele Frequency	Variant
rs792232	10q23.31	*RNLS*	90147344	G/A	0.8886	Intronic
rs1172479	10q24.1	*PIK3AP1*	98481307	T/A	0.3851	Upstream
rs9609516	22q12.3	*RFPL3*	32755074	G/T	0.1273	Intronic

Table 4. SNPs associated with ischemic coronary artery disease (Group 3) compared controls (Group 4)

Marker	Chromosome	Gene	Position	Allele Change	The Minor Allele Frequency	Variant
rs7593239	2q34	LOC101927960	209605944	G/A	0.1387	Intronic
rs3856953	4p16.2	*EVC/ CRMP1*	5774747	C/A	0.9373	Intronic
rs6822202	4q32.3	*MARCHF1*	165132898	G/A	0.08282	Intronic
rs17440042	4p14	*N4BP2*	40130593	G/A	0.07490	Intronic
rs488174	5q13.2	LOC105379030	72429346	C/T	0.1095	Intronic
rs6864267	5q32	*PDE6A*	149247738	C/A	0.05700	Intronic
rs1428507	5q34	*NONE*	164791450	G/A	0.1918	NONE
rs994690	6p22,2	*NONE*	27047916	T/C	0.08668	NONE
rs6456769	6p22,1	*H2BC12*	27107865	G/A	0.08692	Intronic
rs10499295	6q25.3	LOC101928923	156223473	G/T	0.05196	Intronic
rs1107152	8q13.2	*PREX2*	68896865	A/G	0.4214	Intronic
rs10088446	8q13.2	*PREX2*	68898599	G/A	0.3783	Intronic
rs12115844	9q34.11	*FNBP1*	132720869	C/T	0.04864	Intronic
rs9424135	10p15,1	*ASB13*	5700843	G/T	0.09645	Intronic
rs2094248	13q13.3	*DCLK1*	36483466	A/G	0.09936	Intronic
rs9919897	14q11.2	LOC105370401	22862876	T/C	0.7667	Intronic
rs1034377	14q11.2	LOC105370401	22865841	A/G	0.8001	Intronic
rs2014778	14q11.2	LOC105370401	22876816	G/T	0.7081	Intronic
rs760017	14q11.2	LOC105370401	22882590	A/C	0.7063	Intronic
rs226785	16q13.12	*MRTFB*	14313728	G/A	0.05145	Intronic
rs4782921	16q24.1	*WFDC1*	84360361	C/A	0.1796	Intronic
rs1641788	16p13.13	*NUBP1/ TVP23A*	10861110	C/T	0.1796	Intronic /3'UTR
rs1468753	17q22	*AKAP1*	55162325	T/G	0.9023	Upstream
rs8111989	19q13.32	*CKM*	45809208	T/C	0.3532	Downstream
rs9619601	22q12.3	*MYH9*	36700175	A/G	0.05311	Synonym

In our study, we selected 13 polymorphisms that have been shown to be associated with the cardiac diseases and that were observed in at least one and at most 3 patients in the same group. These polymorphisms are shown in Table 5.

DISCUSSION

In our study on the prevalence of sudden cardiac deaths in the population, the results were consistent with the literature, indicating that the death rate among male is higher than that among female. This difference is considered to be due to the protective effects of the estrogen hormone on blood vessels (8).

In our study, the location of death in autopsy cases was significant in terms of its relevance to the existing literature. In this classification, since fatal symptoms were reported to occur in the bed, bathroom, and toilet, the classification was

Table 5. Candidate variations for cases (Group 1-3)

Marker	Chromosome	Gene	Coordinate	Allele Change	The Minor Allele Frequency	Changes in Amino Acid Levels	Pathogenicity	Variant
rs78121716	11p11.2	*NDUFS3*	47605891	G/A	0.00003976	p.Arg218Gln	VUS	Missense
rs61742331	2p24.1	*APOB*	21229679	G/C	0.0008392	p.Ala3354Gly	CIP	Missense
rs72653074	2p24.1	*APOB*	21239423	C/T	0.00002121	p.Gly1074Arg	VUS	Missense
rs61742990	2p24.1	*APOB*	21255262	C/T	0.00003541	p.Arg439Gln	VUS	Missense
rs72653102	2p24.1	*APOB*	21230334	G/A	0.00004782	p.Arg3136Cys	VUS	Missense
rs59827137	1q24.2	*NME7*	169138708	G/T	0.002091	p.Leu359Met		Missense
rs76757832	6p22.2	*TRIM38*	25969631	C/G	0.000004042	p.Arg164Gly		Missense
rs183414771	3q27.2	*IGF2BP2*	185393659	C/G	0.0001592	p.Leu285Phe		Missense
rs141107387	3p22.2	*SCN5A*	38592107	C/T	0.000008024	p.Arg1918His	VUS	Missense
rs35310697	9p21.3	*DMRTA1*	22451581	G/T	0.001811	p.Ala396Thr		Missense
rs3782886	12q24.12	*BRAP*	112110489	T/C	0.01867	p.Glu4Gly		Missense
rs11575933	9q34.2	*ADAMTS13*	136302063	C/T	0.005366	p.Pro475Ser	CIP	Missense
rs1800562	6p22.2	*HFE*	26093141	G/A	0.03377	p.Cys282Tyr	Pathogenic	Missense

VUS: Variant of Uncertain Significance; CIP: Conflicting Interpretations of Pathogenicity

made as death at home, death in the bed, and death in the bathroom (9).

Since the autopsy materials in our study were selected from cases sent to the Istanbul Morgue Department of the Council of Forensic Medicine, it was not possible to clearly reflect the regional distribution of sudden cardiac deaths. Therefore, a regional evaluation was not conducted.

In addition to many family studies, population-based studies have been carried out in relation to sudden cardiac deaths. Studies on the genetic background of diseases such as cardiovascular disease and cancer have been conducted with GWAS since 2007. The advantage of GWAS is that it allows a large number of samples to be run quickly on microchips with a large number of SNPs (6).

In our study, we found the SNPs rs2971851 and rs2971851 to be associated with the sudden cardiac death; however, no association with the cardiac diseases has been reported in either polymorphism.

When the cases were grouped according to their histopathological findings, the polymorphisms rs2369527, rs2632594, rs10213562, rs37569, rs12209155, rs10811461, and rs3786189 in the arrhythmia group were significantly associated with sudden cardiac death compared with the control group. None of these polymorphisms were previously associated with cardiac patients. However, mutations in the *NFATc1* gene with rs3786189 were associated with congenital cardiac diseases (10); mutations in the *ULK4* gene with rs2632594 were associated with hypertension (11) and acute aortic dissection (12); mutations in the *MCUB* gene with rs10213562 (12, 13) with ischemic heart disease; and mutations in the *PDE4D* gene with rs37569 were associated with arrhythmogenic cardiac diseases (14, 15).

A significant correlation was found between rs792232, rs1172479, and rs9609516 and sudden cardiac death in the hypertrophic cardiomyopathy group. Previously, none of these polymorphisms were associated with the cardiac events. However, mutations in the *RNLS* gene with rs792232 polymorphism have been associated with hypertension (16) and type 1 Diabetes Mellitus (17).

A significant correlation was observed with sudden cardiac death and rs7593239, rs3856953, rs6822202, rs17440042, rs488174, rs6864267, rs1428507, rs994690, rs6456769, rs6456769, rs10499295, rs1107152, rs10088446, rs12115844, rs9424135, rs2094248, rs9919897, rs1034377, rs2014778, rs760017, rs226785, rs478292, rs1641788, rs1468753, and rs8111989 in the coronary artery group. However, none of these polymorphisms had been reported in the literature to be associated with the cardiac diseases. Among these, rs6864267 has been stated as a benign variant in the ClinVar database. On the other hand, there are no mutations associated with cardiovascular diseases reported in the *PDE6A* gene, in which it is found. The *MRTFB* gene, in which the rs226785 polymorphism is found, is called Myocardin Related Transcription Factor B and is known to play an active role in heart development (18).

It has been reported that the *AKAP1* gene, in which rs1468753 is found, plays a role in the development of cardiac hypertrophy, hypoxia-induced myocardial infarction, and endothelial cell dysfunction (19, 20).

In our study, we selected 13 polymorphisms that have been associated with the cardiac diseases and observed in at least

one and at most 3 patients in the same group. Among these variants, it has been reported that the rs1801278 (p.Gly971Arg) variant in the *IRS1* gene may be a risk factor for coronary artery disease, especially with the history of diabetes (21, 22).

Although there is no literature on rs72653074 (p.Gly1074Arg), 724742990 (p.Arg439Gln), and rs72653102 (p.Arg3136Cys) in the *APOB* gene, all of them were detected among different patients in Group 3, and their clinical importance in the ClinVar database is stated as conflicting classifications of pathogenicity (CIP) for familial hypercholesterolemia patients (23). Although there is no literature on rs141107387 (p.Arg1918His) in the *SCN5A* gene, which was detected in 3 different patients in Group 1, they were reported as CIP for clinically important hereditary arrhythmic diseases in the ClinVar database (23).

The rs61742331 (p.Ala3354Gly) variant of the *APOB* gene, which was found in only one patient in Group 3, has been reported in the ClinVar database as CIP for clinically important familial hypercholesterolemia disease (23, 24). The rs11575933 (p.Pro475Ser) variant of the *ADAMTS13* gene, found in only one patient in Group 3, has been proposed as a pathogenic variant for hereditary thrombotic thrombocytopenic purpura by Kokame et al. and Akiyma et al.(25, 26).

The rs1800562 (p.Cys282Tyr) variant of the *HFE* gene, found in only one patient in Group 2, has been suggested to be a pathogenic variant of cardiomyopathy (23) and Familial Hemochromatosis Syndrome (27-31). In addition, it has been reported that the same variant is a risk factor for microvascular complications in Type II Diabetes patients (32, 33). Furthermore, the same variant was suggested as a possible pathogenic variant for Cardiomyopathy in the Clinvar database (23).

In addition to all these, variants of rs74522665 (p.Gly1386Arg) of *NOTCH2* found in only 1 case in Group 1, that is known to play a role in cardiac development, rs59827137 (p.Leu359Met) of *NME7* found in 1 case in Group 2, rs76757832 (p.Arg164Gly) on *TRIM38* found in 1 case in Group 1, rs183414771 (p.Leu285Phe) of *IGF2BP2* found in 1 case in Group 1, rs8176721 (p.Asn105Lys) of *APOB* found in 1 case in Group 1, rs35310697 (p.Ala396Thr) of *DMRTA1* found in one case each of Group 1, 2 and 3, rs115553210 (p.Trp195Ter) of *REXO4* found in one case in Group 1, rs3782886 (p.Glu4Gly) of *BRAP* found in one case in Group 1, rs114104180 (p.Glu1218Asp) of *HECTD4* found in one case each in Group 1 and 2, rs117505183 (p.Arg2511Trp) of *HECTD4* found in one case in Group 1, rs188294925 (p.Arg528Gly) of *GNL3* found in one case in Group 1 should be further evaluated in terms of sudden cardiac death.

CONCLUSION

The development of new strategies for the early diagnosis and prevention of sudden cardiac death is important for public health. Understanding the molecular mechanisms underlying sudden cardiac death represents a crucial step in this process. The results of the GWAS of our study suggest new and possibly complementary biological pathways that may be involved in sudden cardiac death. Furthermore, our study is the first autopsy-based research to investigate variants observed in the Turkish population in cases of sudden cardiac death. In future studies, sequencing analyses of these candidate genes should be performed to look for possible mutations. By determining the sudden cardiac death gene profile specific to Turkish population, it will be possible to determine the people who inherit the disease and the people who develop it spontaneously; and to take the necessary precautions in terms of the risk of sudden cardiac death.

Ethics Committee Approval	This study was approved by the Local Ethics Committee of Istanbul Faculty of Medicine (28.07.2011-805).
Peer Review	Externally peer-reviewed.
Conception/Design of Study	G.O.C., K.K.; Data Acquisition: G.O.C., M.C., K.K., A.B.C., A.P.E., I.K., B.S., M.Y., B.B., H.Y.A., O.O.; Data Analysis/Interpretation: G.O.C., M.C., K.K., A.B.C., A.P.E., I.K., B.S., M.Y., B.B., H.Y.A., O.O.; Drafting Manuscript: G.O.C., K.K., A.P.E.; Critical Revision of Manuscript: G.O.C., M.C., K.K., A.B.C., A.P.E., I.K., B.S., M.Y., B.B., H.Y.A., O.O.; Final Approval and Accountability: G.O.C., M.C., K.K., A.B.C., A.P.E., I.K., B.S., M.Y., B.B., H.Y.A., O.O.
Conflict of Interest	The authors declare no conflict of interest.
Financial Disclosure	This work was financially supported by the Research Fund of Istanbul University (Project No.20852).

Author Details

Gulay Ozel Cavlak
[1] Council of Forensic Medicine, Ministry of Justice, Ankara, Turkiye
0000-0003-4301-1319 ozgulay2001@gmail.com

Mehmet Cavlak
[2] Department of Forensic Medicine, Faculty of Medicine, Hacettepe University, Ankara, Turkiye
0000-0003-3059-3372

Kubilay Kinoglu
[3] Council of Forensic Medicine, Ministry of Justice, Istanbul, Turkiye
0000-0002-3972-559X

Ayse Begum Ceviz
[4] Department of Medical Genetics, Faculty of Medicine, Istanbul Health and Technology University, Istanbul, Turkiye
0000-0002-3635-8421

Allison Pinar Eronat
[5] Department of Molecular Biology and Genetics, Faculty of Science and Literature, Halic University, Istanbul, Turkiye
0000-0002-8095-1759

Isil Kobak
[6] Department of Data Science, Faculty of Science and Literature, Yeditepe University, Istanbul, Turkiye
0000-0002-5410-6914

Bulent Sam
[3] Council of Forensic Medicine, Ministry of Justice, Istanbul, Turkiye
0000-0003-2650-9131

Mustafa Yildiz
[7] Cardiology Institute, Istanbul University, Istanbul, Turkiye
0000-0003-3502-4785

Bulent Bayraktar
[8] Department of Sports Medicine, Istanbul Faculty of Medicine, Istanbul University, Istanbul, Turkiye
0000-0001-8102-4896

Hulya Yilmaz Aydogan
[9] Department of Molecular Medicine, Aziz Sancar Institute of Experimental Medicine, Istanbul University, Istanbul, Turkiye
0000-0002-8837-6664

Oguz Ozturk
[9] Department of Molecular Medicine, Aziz Sancar Institute of Experimental Medicine, Istanbul University, Istanbul, Turkiye
0000-0002-2439-9269

REFERENCES

1. Markwerth P, Bajanowski T, Tzimas I, Dettmeyer R. Sudden cardiac death-update. Int J Legal Med 2021 ;135(2): 483-95.
2. Benjamin EJ, Blaha MJ, Chiuve SE, Cushman M, Das SR, Deo R, et al. Heart disease and stroke statistics-2017 update: A report from the American Heart Association. Circulation 2017; 135(10): e146-e603.
3. Priori SG, Wilde AA, Horie M, Cho Y, Behr ER, Berul C, et al. HRS/EHRA/APHRS expert consensus statement on the diagnosis and management of patients with inherited primary arrhythmia syndromes: document endorsed by HRS, EHRA, and APHRS in May 2013 and by ACCF, AHA, PACES, and AEPC in June 2013. Heart Rhythm 2013; 10(12): 1932-63.
4. Eckart RE, Shry EA, Burke AP, McNear JA, Appel DA, Castillo-Rojas LM, et al. Sudden death in young adults: an autopsy-based series of a population undergoing active surveillance. J Am Coll Cardiol 2011; 58(12): 1254-61.
5. Bush WS, Moore JH. Chapter 11: Genome-wide association studies. PLoS Comput Biol 2012; 8(12): e1002822.
6. Ndiaye NC, Azimi Nehzad M, El Shamieh S, Stathopoulou MG, Visvikis-Siest S. Cardiovascular diseases and genome-wide association studies. Clin Chim Acta 2011; 412(19-20): 1697-701.
7. Roshyara NR, Kirsten H, Horn K, Ahnert P, Scholz M. Impact of pre-imputation SNP-filtering on genotype imputation results. BMC Genet 2014; 15: 88.
8. Butters A, Arnott C, Sweeting J, Winkel BG, Semsarian C, Ingles J. Sex disparities in sudden cardiac death. Circ Arrhythm Electrophysiol 2021; 14(8): e009834.
9. Matoba R, Shikata I, Iwai K, Onishi S, Fujitani N, Yoshida K, et al. An epidemiologic and histopathological study of sudden cardiac death in Osaka Medical Examiner's Office. Jpn Circ J 1989; 53(12): 1581-8.
10. Burger NB, Bekker MN, de Groot CJ, Christoffels VM, Haak MC. Why increased nuchal translucency is associated with congenital heart disease: a systematic review on genetic mechanisms. Prenat Diagn 2015; 35(6): 517-28.
11. Lu X, Wang L, Lin X, Huang J, Charles Gu C, He M, et al. Genome-wide association study in Chinese identifies novel loci for blood pressure and hypertension. Hum Mol Genet 2015; 24(3): 865-74.
12. Guo DC, Grove ML, Prakash SK, Eriksson P, Hostetler EM, LeMaire SA, et al. Genetic variants in LRP1 and ULK4 are associated with acute aortic dissections. Am J Hum Genet 2016; 99(3): 762-9.
13. Kaludercic N, Scorrano L. MCUB hearts mitochondria in sickness, less in health. Circulation 2019; 140(21): 1734-6.
14. Perera RK, Fischer TH, Wagner M, Dewenter M, Vettel C, Bork NI, et al. Atropine augments cardiac contractility by inhibiting cAMP-specific phosphodiesterase type 4. Sci Rep 2017; 7(1): 15222.
15. Mika D, Bobin P, Lindner M, Boet A, Hodzic A, Lefebvre F, et al. Synergic PDE3 and PDE4 control intracellular cAMP and cardiac excitation-contraction coupling in a porcine model. J Mol Cell Cardiol 2019; 133: 57-66.
16. Wang Y, Chu C, Ren J, Mu JJ, Wang D, Liu FQ, et al. Genetic variants in renalase and blood pressure responses to dietary salt and potassium interventions: a family-based association study. Kidney Blood Press Res 2014; 39(5): 497-506.
17. Buraczynska M, Gwiazda-Tyndel K, Drop B, Zaluska W. Renalase gene Glu37Asp polymorphism affects susceptibility to diabetic retinopathy in type 2 diabetes mellitus. Acta Diabetol 2021; 58(12): 1595-602.
18. Parmacek MS. Myocardin-related transcription factors: critical coactivators regulating cardiovascular development and adaptation. Circ Res 2007; 100(5): 633-44.
19. Baldwin TA, Dessauer CW. Function of Adenylyl cyclase in heart: the AKAP connection. J Cardiovasc Dev Dis 2018; 5(1): 2.
20. Marin W. A-kinase anchoring protein 1 (AKAP1) and its role in some cardiovascular diseases. J Mol Cell Cardiol 2020; 138: 99-109.
21. Baroni MG, D'Andrea MP, Montali A, Pannitteri G, Barillà F, Campagna F, et al. A common mutation of the insulin receptor substrate-1 gene is a risk factor for coronary artery disease. Arterioscler Thromb Vasc Biol 1999; 19(12): 2975-80.
22. Bacci S, Prudente S, Copetti M, Spoto B, Rizza S, Baratta R, et al. Joint effect of insulin signaling genes on cardiovascular events and on whole body and endothelial insulin resistance. Atherosclerosis 2013; 226(1): 140-5.
23. Landrum MJ, Chitipiralla S, Brown GR, Chen C, Gu B, Hart J, et al. ClinVar: improvements to accessing data. Nucleic Acids Res 2020; 48(D1): D835-d44.
24. Wang J, Dron JS, Ban MR, Robinson JF, McIntyre AD, Alazzam M, et al. Polygenic versus monogenic causes of hypercholesterolemia ascertained clinically. Arterioscler Thromb Vasc Biol 2016; 36(12): 2439-45.
25. Kokame K, Matsumoto M, Soejima K, Yagi H, Ishizashi H, Funato M, et al. Mutations and common polymorphisms in ADAMTS13 gene responsible for von Willebrand factor-cleaving protease activity. Proc Natl Acad Sci U S A 2002; 99(18): 11902-7.
26. Akiyama M, Nakayama D, Takeda S, Kokame K, Takagi J, Miyata T. Crystal structure and enzymatic activity of an ADAMTS-13 mutant with the East Asian-specific P475S polymorphism. J Thromb Haemost 2013; 11(7): 1399-406.
27. Beutler E, Felitti VJ, Koziol JA, Ho NJ, Gelbart T. Penetrance of 845G–> A (C282Y) HFE hereditary haemochromatosis mutation in the USA. Lancet 2002; 359(9302): 211-8.
28. Ellervik C, Tybjaerg-Hansen A, Appleyard M, Sillesen H, Boysen G, Nordestgaard BG. Hereditary hemochromatosis genotypes and risk of ischemic stroke. Neurology 2007; 68(13): 1025-31.
29. Yönal O, Hatirnaz O, Akyüz F, Köroğlu G, Ozbek U, Cefle K, et al. Definition of C282Y mutation in a hereditary hemochromatosis family from Turkey. Turk J Gastroenterol 2007; 18(1): 53-7.
30. van Gammeren A, de Baar E, Schrauwen L, van Wijngaarden P. Compound heterozygous C282Y/Q283P and Q283P/H63D mutations in haemochromatosis. Br J Haematol 2015; 171(4): 650-1.
31. Davis TM, Beilby J, Davis WA, Olynyk JK, Jeffrey GP, Rossi E, et al. Prevalence, characteristics, and prognostic significance of HFE gene mutations in type 2 diabetes: the Fremantle Diabetes Study. Diabetes Care 2008; 31(9): 1795-801.

32. Oliva R, Novials A, Sánchez M, Villa M, Ingelmo M, Recasens M, et al. The HFE gene is associated to an earlier age of onset and to the presence of diabetic nephropathy in diabetes mellitus type 2. Endocrine 2004; 24(2): 111-4.

33. Yang Q, Wu F, Mi Y, Wang F, Cai K, Yang X, et al. Aberrant expression of miR-29b-3p influences heart development and cardiomyocyte proliferation by targeting NOTCH2. Cell Prolif 2020; 53(3): e12764.

İSTANBUL UNIVERSITY PRESS

Experimed 2025, 15 (1): 23–30

https://doi.org/10.26650/experimed.1536826

Submitted: 23.08.2024
Revision Requested: 11.11.2024
Last Revision Received: 18.11.2024
Accepted: 06.01.2025
Published Online 10.03.2025

Experimed

Research Article

Open Access

Overexpression of SIK2 Inhibits FGF2-dependent Müller Glial Reprogramming

Asli Ugurlu Bayarslan [1,2] & Kuyas Bugra [1,3]

[1] Department of Molecular Biology and Genetics, Bogazici University, Istanbul, Turkiye
[2] Department of Biology, Kastamonu University, Kastamonu, Turkiye
[3] Life Sciences Center, Bogazici University, Istanbul, Turkiye

Abstract

Objective: Upon injury, Müller cells re-enter the cell cycle, acquire progenitor properties, and produce new retinal neurons in zebrafish. Proliferation is an essential step in retinal regeneration. The strict regulation of Müller cell proliferation limits mammalian retinal regeneration. Growth factors such as fibroblast growth factor 2 (FGF2) can promote the proliferation of Müller glia in mammals; however, the regeneration capacity is restricted. In this study, we investigated the possible contribution of salt-inducible kinase 2 (SIK2) to Müller reprogramming through FGF2 signaling.

Materials and Methods: MIO-M1 cells were used as the model system. Modulations in cell proliferation, extracellular signal-regulated kinase (ERK)1/2 activity, and SIK2 expression during 7 days of FGF2 treatment were documented. Overexpression studies were conducted to provide clues for the potential contribution of SIK2 to MIO-M1 reprogramming.

Results: Our findings demonstrate that the expansion of Müller cells that de-differentiate into progenitors requires ERK activation. A significant reduction in the SIK2 protein level is necessary for Müller cells to proliferate. SIK2 overexpression inhibited ERK activity, cell proliferation, and reprogramming.

Conclusion: We propose that SIK2 is involved in Müller reprogramming by suppressing ERK activation.

Keywords SIK2 · FGF2 · ERK · Reprogramming · Müller glia

Citation: Ugurlu Bayarslan, A. & Bugra, K. Overexpression of SIK2 Inhibits FGF2-dependent Müller Glial Reprogramming. Experimed 2025; 15(1): 23-30. DOI: 10.26650/experimed.1536826

Corresponding author: Asli Ugurlu Bayarslan a.z.ugurlu@gmail.com

INTRODUCTION

The description of Müller cells dates back to 1851 by Heinrich Müller, and they were later identified as the principal glial cells in the retina (1). They span the width of the retina and contact all retinal neurons (2). The major role of Müller glia is to maintain retinal homeostasis and support the survival and function of neurons. In response to damage, Müller cells undergo a series of changes including upregulated production of neuroprotective factors, such as fibroblast growth factor 2 (FGF2) (3, 4). Consistent with the upregulation of neuroprotective factors, extracellular signal-regulated kinase (ERK) activation has been detected in experimental models of various retinopathies (5, 6). ERK activation is proposed to mediate cell cycle re-entry in activated Müller cells (7).

In zebrafish, Müller glia undergo a proliferative response upon injury, gain progenitor properties, and produce all retinal cell types (8). Most of the cells produced by proliferating Müller glia remain as progenitors, whereas a few differentiate into specific neurons in chick retia (9). Müller glia can become activated in mammals, but few proliferate in response to injury and do not replenish lost neurons (10). The limited Müller cell proliferation in mammals upon injury may be due to inhibitory mechanisms or limited mitogens. Characterization of the mechanisms that limit the proliferation of mammalian Müller cells may provide clues to unlocking the dormant regenerative potential of mammals (11). Müller glia may proliferate after retinal injury in humans, but there is no evidence of neuron regeneration in the human retina. Human Müller cells (the MIO lines), isolated from different post-mortem retinas (12), express Müller and progenitor markers. Growth factors stimulate these cells to express post-mitotic neuronal markers (13, 14). FGF2 is one of the factors involved in Müller proliferation and reprogramming (13, 15). Without any damage, FGF2 and insulin stimulate Müller glia, as observed after neurotoxic damage in chicks (15). FGF2 selectively activates the Ras/MAPK/ERK signaling pathway, which regulates Müller proliferation (16).

Salt inducible kinase 2 (SIK2) was first identified in the adipose tissue of mice and has a well-defined role in regulating metabolism (17, 18). SIK2 was shown to have a role in insulin release from β-islet cells in the pancreas (19). Furthermore, SIK2 activity in cancer progression was also implicated (20, 21). In cortical neurons, oxygen-glucose deprivation causes SIK2 degradation, which activates cyclic AMP-responsive element-binding protein (CREB) and its downstream genes and promotes neuronal survival (22). By controlling Akt phosphorylation, SIK2 blocks insulin-mediated Müller cell survival in normal and chronic hyperglycaemic conditions (23).

SIK2 is expressed in Müller cells and neurons in the inner nuclear layer of the retina (23). Recently, we identified a novel regulatory role of SIK2 downstream of FGF2 signaling, induced by ERK activation (24). In this context, we provide evidence showing that SIK2 is a factor that restrain Müller proliferation and impede reprogramming.

MATERIALS AND METHODS

Cell Culture

MIO-M1 cells were provided by Prof. Astrid Limb (University College London, Institute of Ophthalmology) and grown in Dulbecco's Modified Eagle Medium (DMEM) (Thermo Scientific, USA) supplemented with 10% fetal bovine serum (FBS) (Thermo Scientific, USA) and 0.1% penicillin/streptomycin (Thermo Scientific, USA) at 37°C and under 5% CO_2. For FGF2 treatment, 500 MIO-M1 cells per cm^2 were cultured on matrigel-coated plates and serum-starved overnight. Subsequently, the cells were stimulated with 40 ng/mL FGF2 (R&D Systems, USA) for 7 days (13). The FGF2-containing medium was replenished every 2 days.

RNA Isolation and Reverse Transcription-Quantitative Polymerase Chain Reaction (RT-qPCR)

Total RNA isolation was performed using the Ouick-RNA MiniPrep Kit (Zymo Research, USA) according to the manufacturer's instructions. RNA samples were treated with DNase I on a column for 30 minutes at 37°C. Total RNA was reverse-transcribed using the RevertAid First Strand cDNA synthesis kit (Thermo Scientific, USA). RT-qPCR amplifications were performed on a Piko Real 96 Real-time Thermal Cycler (Thermo Scientific, USA) in a reaction mixture containing SYBR Green (Takara, Japan) and the primer pairs listed in Table 1. Glyceraldehyde-3-phosphate dehydrogenase (GAPDH) was used as a normalisation standard. The amplification reactions were started with initial denaturation at 95°C for 5 min. This was followed by 40 cycles of denaturation at 95°C for 10 s, annealing of primers for 10 s, and extension at 72°C for 10 s. Relative transcript levels were calculated using the ΔΔCT method.

Lysate Preparation and Western Blotting

Cell pellets were resuspended in ice-cold lysis buffer containing 20 mM Tris-HCl (pH 7.5), 150 mM NaCl, 1 mM EDTA, 1% Triton X-100 supplemented with protease and phosphatase inhibitor cocktails and lysed using ceramic beads (Roche, Germany) with MagnaLyser homogenizer (Roche, Germany) at 6500 rpm for 30 s. Centrifugation for 20 min at 13,200 rpm at 4°C removed cell debris.

Table 1. List of primers used in qPCR

Gene ID	Forward primer	Reverse primer
GAPDH	5'-GGAAGGTGAAGGTCGGAGTC-3'	5'-AACATGTAAACCATGTAGTTGAGGT-3'
Pax6	5'-CCGAGATTTCAGAGCCCCAT-3'	5'-AGACACCACCGAGCTGATTC-3'
Vimentin	5'-CGGGAGAAATTGCAGGAGGA-3'	5'-AAGGTCAAGACGTGCCAGAG-3'
Calretinin	5'-ATCCTGCCAACCGAAGAGAAC-3'	5'-GCAGGAAGTTTTCCTGGACAG-3'
Chx10	5'-AGTGTCATGGCGGAGTATGG-3'	5'-TTTTGTGCATCCCCAGTAGCC-3'
Hesr2	5'-GAGAGCGACATGGACGAGAC-3'	5'-CGACGCCTTTTCTCTATAATCCCT-3'
Prox1	5'-TGACTTTGAGGTTCCAGAGAGAT-3'	5'-AGGCAGTTCGGGGATTTGAA-3'

Total protein extracts or immunoprecipitated samples were separated on a polyacrylamide gel, electroblotted on a polyvinylidene fluoride (PVDF) membrane (Roche, Germany), blocked by either 1% skimmed milk powder or 5% bovine serum albümin (BSA) in 150 mM NaCl, 20 mM Tris-HCl (pH 8.0), 0.1% Tween 20 and probed with primary antibodies overnight at 4°C. Anti-SIK2 (Cell Signaling, 1/1000), anti-phospho-extracellular signal-regulated kinase (pERK) (Cell Signaling, 1/1000), anti-ERK (Santa Cruz, 1/1000), anti-β-actin (Santa Cruz, 1/5000) antibodies were used. The membranes were then washed and incubated with horseradish peroxidase (HRP)-tagged secondary antibodies. The antibody-antigen interactions were visualized by ImmunoCruz luminol reagent (Santa Cruz, USA) using the Stella imaging system (Raytest, Germany).

Cell Proliferation Assay

Proliferating cells were detected using an *in situ* cell proliferation kit, FLUOS (Roche, Germany). Briefly, 10 µM bromodeoxyuridine (BrdU) was added to the culture medium 5 h before fixation of the cells with 70% ethanol and 30% glycine (50 mM, pH 2). Cellular DNA was denatured with 4M HCl. The samples were incubated with the fluorescein-conjugated anti-BrdU antibody for 45 min at 37°C in the dark. 4′,6-diamidino-2-phenylindole (DAPI) was used to stain the nuclei. Samples were analysed using Zeiss Axio Observer Z1 Inverted fluorescence microscope (Zeiss, USA). For each image, 200 cells were counted from distinct areas. For SIK2 overexpressed MIO-M1 cells, anti-BrdU antibody (Roche, Germany) and Alexa Fluor 555-conjugated secondary antibody were used.

SIK2 Overexpression in MIO-M1 Cells

MIO-M1 cells were transfected with the enhanced green fluorescent protein-salt inducible kinase 2 plasmid (pEGFP-SIK2) using X-treme Gene HP DNA transfection reagent (Roche, Germany) at a 3:1 ratio as instructed by the manufacturer. An empty pEGFP vector was used as the control. After 24 h, the culture medium was replenished. To select stable clones, cells were grown in 500 µg/mL neomycin (Sigma, USA) containing medium for 2 weeks, and the medium was replenished every 3 days. Neomycin-resistant colonies were collected using cloning cylinders. Western blotting analysis verified SIK2 overexpression in neomycin-resistant colonies.

Statistical Analyses

Differences between the untreated cells and FGF2-treated cells, and mock-transfected cells and pEGFP-SIK2 transfected cells were analysed with Student's t-test using Graphpad Prism 7. $p<0.05$ was considered as significant.

RESULTS

FGF2 Stimulates Müller Proliferation Through Early ERK Activation

Müller reprogramming consists of multiple stages, including the cell cycle re-entry of Müller cells, their conversion into progenitors, progenitor amplification, and differentiation (25). The ERK pathway plays a major role in FGF2-dependent MIO-M1 proliferation (26). Hence, we analysed the effect of FGF2 on the cell proliferation and ERK activity profiles of MIO-M1 cells. The proliferation assays indicated that 25% of the cells were BrdU positive in the untreated culture. This percentage increased up to 42% after 4 h of FGF2 treatment and stayed there for 24 h (Figure 1A). A second proliferation peak with 37% of the cells expressing BrdU was observed after 6 days of FGF2 stimulation (Figure 1A).

Parallel with cell proliferation, a 1.4-fold increase in ERK activity was detected after 4 h and 12 h of FGF2 stimulation (Figure 1B). In the remaining time points, the active ERK levels were near basal.

SIK2 Protein Expression is Diminished Upon FGF2 Induction

SIK2 plays a role in the negative regulation of FGF2-dependent ERK activation and proliferation in Müller glia (24). Based on the central role of SIK2 in Müller proliferation, we investigated the possible role of SIK2 in Müller reprogramming. Western blot analysis revealed that SIK2 levels decreased by

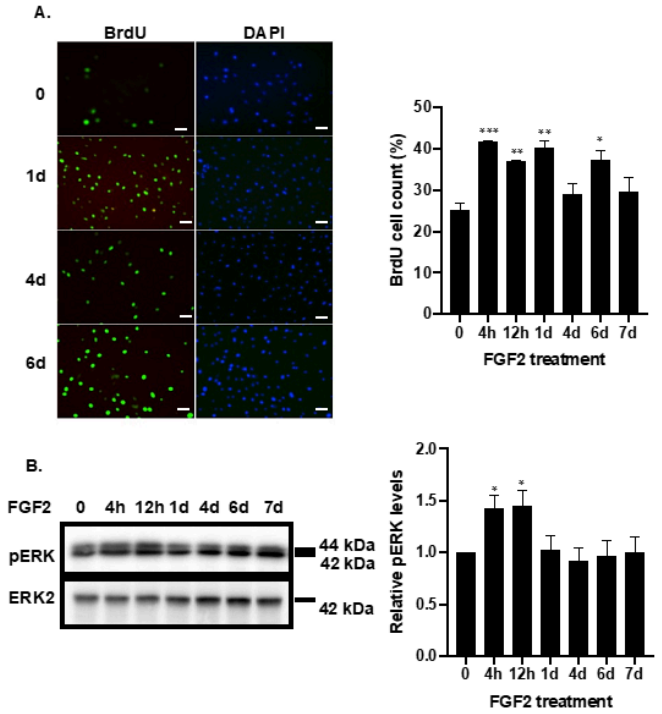

Figure 1. FGF2-dependent cell proliferation and ERK activity profile. MIO-M1 cells were treated with FGF2 for 7 days and the untreated cells were used as control group (0). A. BrdU incorporation was performed to detect proliferating cells, and DAPI staining was used to label the nuclei. The number of BrdU-positive cells was normalised to the number of DAPI-stained nuclei in the same samples. B. ERK activity was analysed by western blotting. The band intensities of pERK were normalised to that of ERK. Data are the means ± standard error; n=3. FGF2 treated cells were compared to the control group; *p<0.05, **p<0.01, ***p<0.001. Scale bar: 50 µm. BrdU: Bromodeoxyuridine; DAPI: 4′,6-diamidino-2-phenylindole; ERK2: Extracellular signal-regulated kinase 2; pERK: Phospho-extracellular signal-regulated kinase; FGF2: Fibroblast growth factor 2; h: hours, d: days.

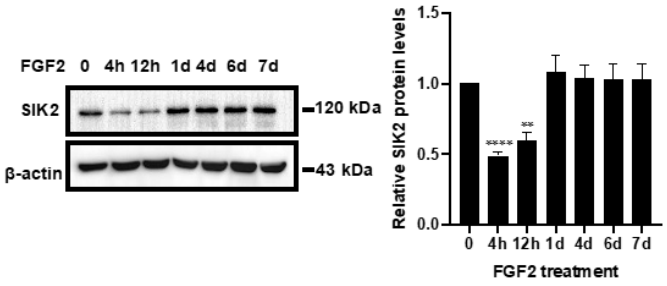

Figure 2. FGF2-dependent modulations in SIK2 expression. MIO-M1 cells were treated with FGF2 for 7 days and the untreated cells were used as control group (0). The SIK2 protein level was analysed with western blotting. Data are the means ± standard error; n=3. FGF2 treated cells were compared to the control group; ** p<0.01, ****p<0.0001. FGF2: Fibroblast growth factor 2; SIK2: Salt-inducible kinase 2; h: hours; d: days.

approximately 50% at 4 h and 12 h of FGF2 stimulation, recovered to basal levels after 24 h of FGF2 stimulation, and did not change at later time points (Figure 2).

SIK2 Overexpression Blocks FGF2-Dependent Cell Proliferation by Inhibiting ERK Activity

Because we observed a significant decrease in its protein level, we decided to focus on the expression level of SIK2 to modulate ERK activity and FGF2-dependent proliferative response in Müller cells. The pEGFP-SIK2 vector was used to transfect MIO-M1 cells for SIK2 overexpression. The presence of both the 120-kDa endogenous SIK2 band and the 150-kDa GFP-SIK2 band confirmed the SIK2 overexpression (Figure 3A). Only the endogenous SIK2 band was detected in the control cells.

We examined the effect of SIK2 overexpression on proliferation and ERK activation to test whether SIK2 inhibits proliferation through ERK in MIO-M1 cells. As in the wild-type cells, an increase in cell proliferation and ERK activity was observed at 4 h and 12 h in the mock-transfected cells. When SIK2 was overexpressed, the percentage of BrdU-positive cells was lower than the baseline at all times and strikingly near

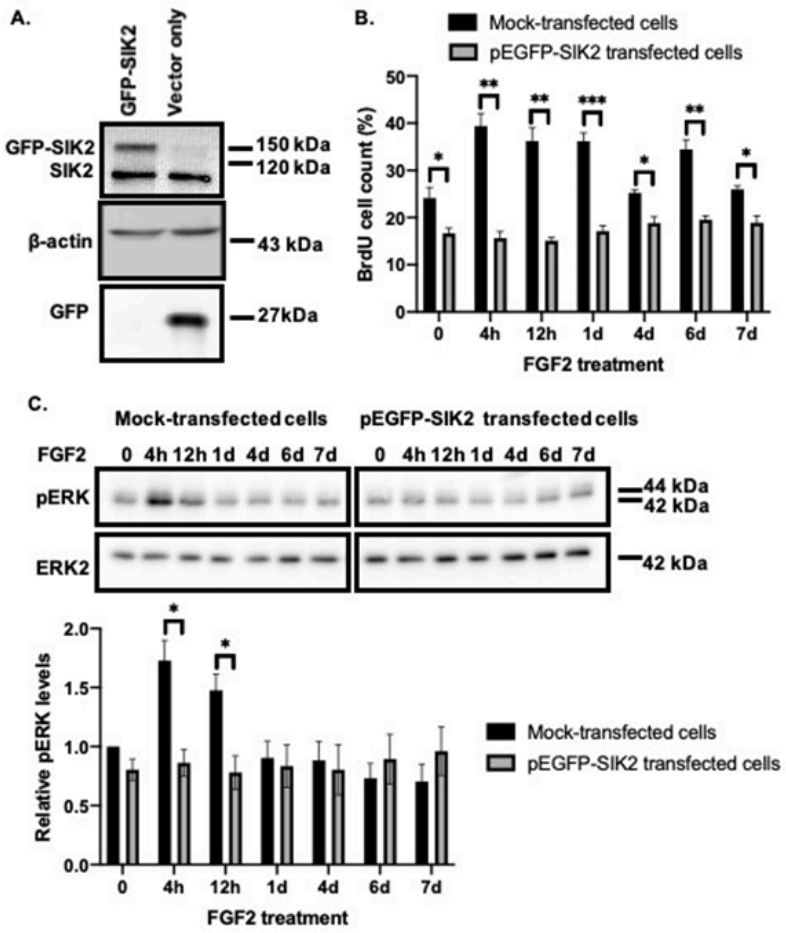

Figure 3. SIK2 overexpression in MIO-M1 cells. A. MIO-M1 cells were transfected with pEGFP-SIK2 for SIK2 overexpression and with pEGFP for mock transfection. The SIK2 protein level was analysed by western blotting. B. pEGFP-SIK2 transfected and mock-transfected MIO-M1 cells were treated with FGF2 for 7 days and the untreated cells were used as control group (0). The effect of SIK2 overexpression on cell proliferation was analysed by BrdU incorporation C. The effect of SIK2 overexpression on ERK activation was analysed by western blotting. Data are the means ± standard error; n=3. pEGFP-transfected cells were compared to mock-transfected cells; *p<0.05, **p<0.01, ***p<0.001. GFP: Green fluorescent protein; SIK2: Salt inducible kinase 2; FGF2: Fibroblast growth factor 2; pEGFP: Enhanced green fluorescent protein plasmid; pERK: Phospho-extracellular signal-regulated kinase; BrdU: Bromodeoxyuridine; ERK2: Extracellular signal-regulated kinase 2; h: hours; d: days.

half in the early days (Figure 3B). There was no significant increase in active ERK levels in the SIK2-overexpressed MIO-M1 cells, and SIK2 overexpression alone blocked the early activation of ERK2 in 4 h and 12 h (Figure 3C). These results show that during the early phases of FGF2 exposure, SIK2 overexpression inhibits cell proliferation through ERK activity, and blocking cell proliferation might hamper the reprogramming.

SIK2 Overexpression Alters FGF2-Dependent Transcriptional Activity

RT-qPCR experiments were performed to determine the FGF2-dependent transcriptional changes.

We observed an increase in the levels of the progenitor markers *paired box 6 (Pax6)* and *visual system homeobox 2 (Chx10)* that peaked at 12 h and 1 day of FGF2 treatment in mock-transfected MIO-M1 cells (Figure 4A, 4B). The simultaneous rise in the *Pax6* and *Chx10* levels shows that FGF2 stimulation induces progenitor features in MIO-M1 cells. The transcript levels of the Müller marker *vimentin* decreased after 4 days of FGF2 treatment in mock-transfected cells (Figure 4C). In the retina, Hes related family bHLH transcription factor with YRPW motif 2) Hesr2 promotes Müller development. The *Hesr2* transcript level was detectable in MIO-M1 cells as expected; however, we could not observe any significant change in the *Hesr2* level upon FGF2 treatment in mock-transfected cells (Figure 4D). After 6 days of FGF2 treatment, the expression of the neuronal marker *calretinin* increased in the mock-transfected cells (Figure 4E). We detected *Prospero homeobox 1 (Prox1)* expression, the regulator of horizontal cell development, in the mock-transfected cells. *Prox1* transcript levels were increased after 4 days of FGF2 treatment and remained high at subsequent

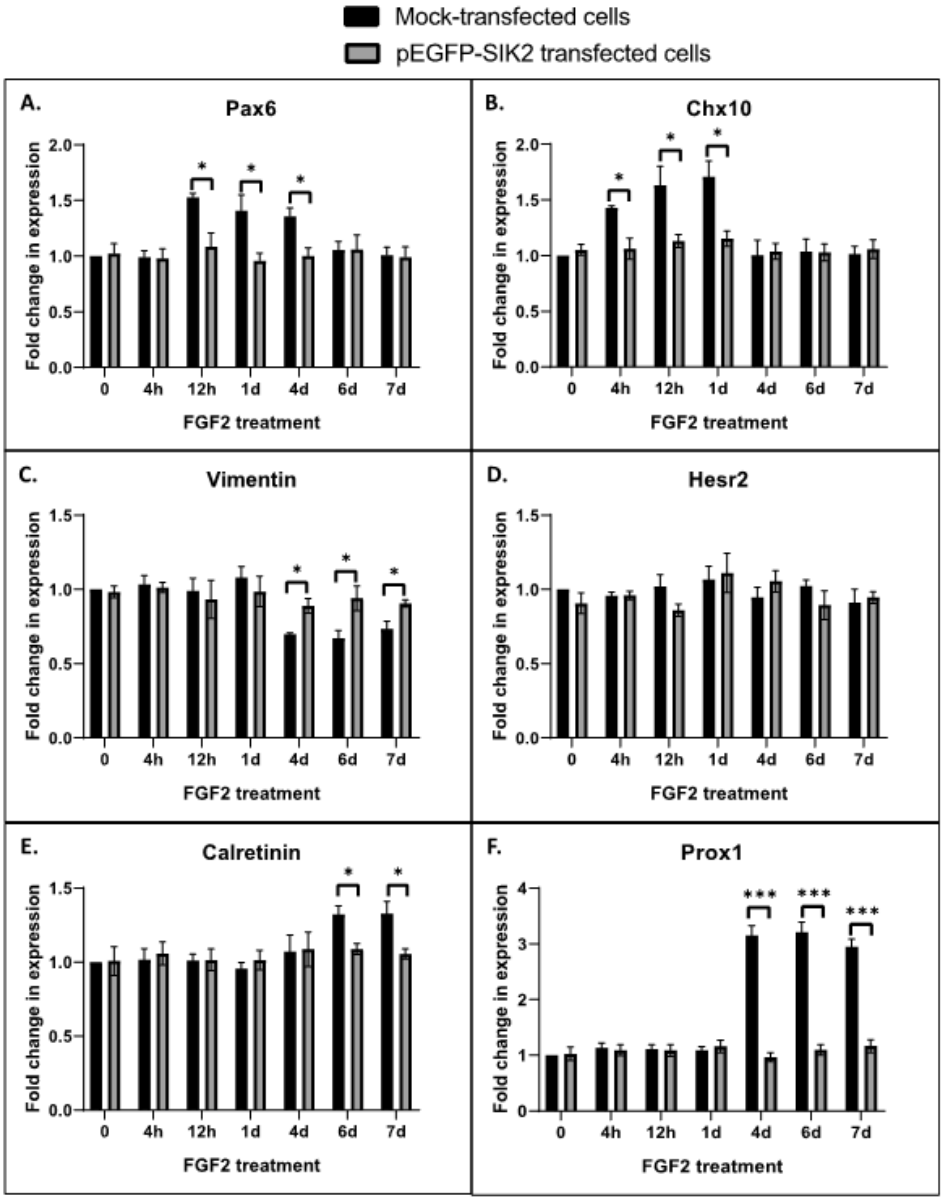

Figure 4. Effect of SIK2 overexpression on marker gene expression. pEGFP-SIK2 transfected and mock-transfected MIO-M1 cells were treated with FGF2 for 7 days and the untreated cells were used as control group (0). Relative mRNA expression levels were assessed by qPCR. The Ct of target gene/the Ct of reference gene (*GAPDH*) ratio for the untreated mock-transfected sample was set as a baseline value to which all time points were normalised. Data are the means ± SE; n=3. pEGFP transfected cells were compared to mock-transfected cells; *p<0.05, ***p<0.001. A. Pax6, B. Chx10, C. Vimentin, D. Hesr2, E. Calretinin, F. Prox1. SIK2: Salt inducible kinase 2; FGF2: Fibroblast growth factor 2; pEGFP: Enhanced green fluorescent protein plasmid; Pax6: Paired box 6; Chx10: Visual system homeobox 2; Hesr2: Hes related family bHLH transcription factor with YRPW motif 2; Prox1: Prospero homeobox 1; h: hours; d: days.

times (Figure 4F). Although MIO-M1 cells acquire certain neuronal features, as indicated by an increase in *calretinin*, our data highlight a considerable tendency towards horizontal cell fate.

In SIK2-overexpressing MIO-M1 cells, the expression of *Pax6*, *Chx10*, *vimentin*, *calretinin*, and *Prox1* remained at a basal level compared with the mock-transfected cells (Figure 4). These results support the hypothesis that SIK2 overexpression inhibits the cell cycle re-entry and reprogramming of MIO-M1 cells.

DISCUSSION

In zebrafish, Müller cells respond to injury by reprogramming, which results in the repair of the damaged retina. Mammalian Müller cells become activated, but their regeneration ability is highly restricted. Cell cycle re-entry is necessary for the functional regenerative response. The limited Müller proliferation is considered a barrier to retinal regeneration in mammals. FGF2 is one of the factors that stimulate Müller reprogramming through ERK activation (13, 15, 16). SIK2 negatively regulates FGF2-dependent Müller proliferation by

inhibiting ERK activity in MIO-M1 cells (24). Therefore, we hypothesised that SIK2 might be a crucial factor that regulates Müller proliferation and block reprogramming.

Initially, we investigated the temporal profile of proliferation and ERK activation during reprogramming. The number of BrdU-positive MIO-M1 cells was significantly increased between 4 h and 24 h of FGF2 stimulation; a second proliferation peak was detected after 6 days of FGF2 treatment. The parallel increase in ERK activity at 4-12 hours of FGF2 treatment demonstrated that enhanced proliferation at 4-12 hours involves the ERK pathway. In addition, SIK2 protein levels were nearly halved after 4 h and 12 h of FGF2 treatment and returned to basal levels after 24 h. SIK2 might regulate ERK activation during the early stages of reprogramming, as evidenced by the correlation between the rise in active ERK and the reduction in SIK2 protein levels. Consistent with this scenario, pERK levels in SIK2-overexpressing MIO-M1 cells remained at a basal level, and we could not detect any increase in the number of proliferating cells upon FGF2 treatment. In addition, the expression levels of the progenitor markers *Pax6* and *Chx10*, as well as the neuronal markers *calretinin* and *Prox1* did not increase in response to FGF2 in SIK2-overexpressing MIO-M1 cells.

Based on these results, we found that in the absence of FGF2, high levels of SIK2 prevent proliferation and reprogramming. After FGF2 stimulation, the reduction in SIK2 protein levels allows ERK activation at an early phase, and Müller cells proliferate and de-differentiate into progenitor cells, possibly through Notch, pCREB, and early growth response 1 (EGR1) (16).

De-differentiated MIO-M1 cells proliferate and enrich the progenitor pool, and a different signaling pathway may regulate this enrichment. At later stages, Notch, which functions downstream of forkhead box N4 (Foxn4), might promote horizontal cell formation (27).

Müller de-differentiation has recently been associated with changes in miRNA expression profiles (28). It has also been demonstrated that miRNAs targeting SIK2 expression, including miR143 and miR125, are involved in both de-differentiation and differentiation events (29, 30). miR-125 regulates retinal progenitor cells during development (30), and miR143 is differentially regulated in Müller glia during de-differentiation (29). It is likely that higher levels of these miRNAs result in decreased SIK2 expression in the early phase of the MIO-M1 reprogramming.

CONCLUSION

Our study provided evidence for the first time that SIK2 is involved in FGF2-induced MIO-M1 reprogramming. Increased SIK2 levels prevent cell cycle re-entry and reprogramming in the absence of FGF2. Following FGF2 treatment, the significant reduction in SIK2 levels allowed ERK activity, Müller cells re-enter the cell cycle, de-differentiate into progenitors, and differentiate into horizontal cells.

Acknowledgements: The authors would like to thank Dr. Gamze Kuser-Abali (Monash University, Australia) and Dr. Yeliz Yilmaz (İzmir Biomedicine and Genome Centre, Turkiye) for their feedback and critical reading of the manuscript during its preparation.

Ethics Committee Approval: Not applicable.

Peer Review: Externally peer-reviewed.

Author Contributions: Conception/Design of Study – A.U.B., K.B.; Data Acquisition – A.U.B., K.B.; Data Analysis/Interpretation – A.U.B., K.B.; Drafting Manuscript – A.U.B., K.B.; Critical Revision of Manuscript – A.U.B., K.B.; Final Approval and Accountability – A.U.B., K.B.

Conflict of Interest: The authors declare no conflict of interest.

Financial Disclosure: This study was supported by funding from the Bogazici University Research Projects (8921); TÜBİTAK (113Z108); and ÖYP (2012K120490).

Author Details

Asli Ugurlu Bayarslan

[1] Department of Molecular Biology and Genetics, Bogazici University, Istanbul, Turkiye

[2] Department of Biology, Kastamonu University, Kastamonu, Turkiye

0000-0003-2131-2823 a.z.ugurlu@gmail.com

Kuyas Bugra

[1] Department of Molecular Biology and Genetics, Bogazici University, Istanbul, Turkiye

[3] Life Sciences Center, Bogazici University, Istanbul, Turkiye

0000-0003-1327-5938

REFERENCES

1. Vecino E, Rodriguez FD, Ruzafa N, Pereiro X, Sharma SC. Glia–neuron interactions in the mammalian retina. Prog Retin Eye Res 2016; 51: 1–40.
2. Bringmann A, Pannicke T, Grosche J, Francke M, Wiedemann P, Skatchkov S, et al. Müller cells in the healthy and diseased retina. Prog Retin Eye Res 2006; 25(4): 397–424.
3. Frasson M, Picaud S, Léveillard T, Simonutti M, Mohand-Said S, Dreyfus H, et al. Glial cell line-derived neurotrophic factor induces histologic and functional protection of rod photoreceptors in the rd/rd mouse. Invest Ophthalmol Vis Sci 1999; 40(11): 2724–34.
4. Honjo M, Tanihara H, Kido N, Inatani M, Okazaki K, Honda Y. Expression of ciliary neurotrophic factor activated by retinal Müller cells in eyes with NMDA- and kainic acid-induced neuronal death. Invest Ophthalmol Vis Sci 2000; 41(2): 552–60.
5. Takeda M, Takamiya A, Yoshida A, Kiyama H. Extracellular signal-regulated kinase activation predominantly in Müller cells of retina with endotoxin-induced uveitis. Invest Ophthalmol Vis Sci 2002; 43(4): 907–11.

6. Tezel G, Chauhan BC, LeBlanc RP, Wax MB. Immunohistochemical assessment of the glial mitogen-activated protein kinase activation in glaucoma. Invest Ophthalmol Vis Sci 2003; 44(7): 3025-33.
7. Dyer MA, Cepko CL. Control of Müller glial cell proliferation and activation following retinal injury. Nat Neurosci 2000; 3(9): 873–80.
8. Bernardos RL, Barthel LK, Meyers JR, Raymond PA. Late-stage neuronal progenitors in the retina are radial Müller glia that function as retinal stem cells. J Neurosci 2007; 27(26): 7028–40.
9. Fischer AJ, Reh TA. Müller glia are a potential source of neural regeneration in the postnatal chicken retina. Nat Neurosci 2001; 4(3): 247–52.
10. Karl MO, Reh TA. Regenerative medicine for retinal diseases: activating endogenous repair mechanisms. Trends Mol Med 2010; 16(4): 193–202.
11. Hamon A, Roger JE, Yang XJ, Perron M. Müller glial cell-dependent regeneration of the neural retina: An overview across vertebrate model systems. Dev Dyn 2016; 245(7): 727–38.
12. Limb GA, Salt TE, Munro PMG, Moss SE, Khaw PT. In vitro characterization of a spontaneously immortalized human Müller cell line (MIO-M1). Invest Ophthalmol Vis Sci 2002; 43(3): 864–9.
13. Lawrence JM, Singhal S, Bhatia B, Keegan DJ, Reh TA, Luthert PJ, et al. MIO-M1 cells and similar muller glial cell lines derived from adult human retina exhibit neural stem cell characteristics. Stem Cells 2007; 25(8): 2033–43.
14. Bhatia B, Jayaram H, Singhal S, Jones MF, Limb GA. Differences between the neurogenic and proliferative abilities of Müller glia with stem cell characteristics and the ciliary epithelium from the adult human eye. Exp Eye Res 2011; 93(6): 852–61.
15. Fischer AJ, McGuire CR, Dierks BD, Reh TA. Insulin and fibroblast growth factor 2 activate a neurogenic program in Müller glia of the chicken retina. J Neurosci 2002; 22(21): 9387–98.
16. Fischer AJ, Scott MA, Tuten W. Mitogen-activated protein kinase-signaling stimulates Müller glia to proliferate in acutely damaged chicken retina. Glia 2009; 57(2): 166–81.
17. Horike N, Takemori H, Katoh Y, Doi J, Min L, Asano T, et al. Adipose-specific expression, phosphorylation of Ser794 in insulin receptor substrate-1, and activation in diabetic animals of salt-inducible kinase-2. J Biol Chem 2003; 278(20): 18440–7.
18. Zhang ZN, Gong L, Lv S, Li J, Tai X, Cao W, et al. SIK2 regulates fasting-induced PPARα activity and ketogenesis through p300. Sci Rep 2016; 6(1): 23317.
19. Sakamaki JI, Fu A, Reeks C, Baird S, Depatie C, Al Azzabi M, et al. Role of the SIK2–p35–PJA2 complex in pancreatic β-cell functional compensation. Nat Cell Biol 2014; 16(3): 234–44.
20. Zohrap N, Saatci Ö, Ozes B, Coban I, Atay HM, Battaloglu E, et al. SIK2 attenuates proliferation and survival of breast cancer cells with simultaneous perturbation of MAPK and PI3K/Akt pathways. Oncotarget 2018; 9(31): 21876–92.
21. Miranda F, Mannion D, Liu S, Zheng Y, Mangala LS, Redondo C, et al. Salt-inducible kinase 2 couples ovarian cancer cell metabolism with survival at the adipocyte-rich metastatic niche. Cancer Cell 2016; 30(2): 273–89.
22. Sasaki T, Takemori H, Yagita Y, Terasaki Y, Uebi T, Horike N, et al. SIK2 is a key regulator for neuronal survival after ischemia via TORC1-CREB. Neuron 2011; 69(1): 106–19.
23. Küser-Abali G, Ozcan F, Ugurlu A, Uysal A, Fuss SH, Bugra-Bilge K. SIK2 is involved in the negative modulation of insulin-dependent Müller cell survival and implicated in hyperglycemia-induced cell death. Invest Ophthalmol Vis Sci 2013; 54(5): 3526.
24. Kuser-Abali G, Ugurlu-Bayarslan A, Yilmaz Y, Ozcan F, Karaer F, Bugra K. SIK2: A novel negative feedback regulator of FGF signaling. Adv Biology 2024; 8(11): 240003.
25. Goldman D. Müller glial cell reprogramming and retina regeneration. Nat Rev Neurosci 2014; 15(7): 431–42.
26. Hollborn M, Jahn K, Limb GA, Kohen L, Wiedemann P, Bringmann A. Characterization of the basic fibroblast growth factor-evoked proliferation of the human Müller cell line, MIO-M1. Graefes Arch Clin Exp Ophthalmol 2004; 242(5): 414–22.
27. Luo H, Jin K, Xie Z, Qiu F, Li S, Zou M, et al. Forkhead box N4 (Foxn4) activates Dll4-Notch signaling to suppress photoreceptor cell fates of early retinal progenitors. Proc Natl Acad Sci U S A 2012; 109(9): E553-62.
28. Quintero H, Gómez-Montalvo AI, Lamas M. MicroRNA changes through Müller glia dedifferentiation and early/late rod photoreceptor differentiation. Neurosci 2016; 316: 109–21.
29. Katsman D, Stackpole EJ, Domin DR, Farber DB. Embryonic stem cell-derived microvesicles induce gene expression changes in Müller cells of the retina. PLoS One 2012; 7(11): e50417.
30. Tao Z, Zhao C, Jian Q, Gillies M, Xu H, Yin ZQ. Lin28B promotes Müller glial cell de-differentiation and proliferation in the regenerative rat retinas. Oncotarget 2016; 7(31): 49368–83.

İSTANBUL UNIVERSITY PRESS

Experimed 2025, 15 (1): 31–40

https://doi.org/10.26650/experimed.1562959

Submitted: 08.10.2024
Revision Requested: 08.12.2024
Last Revision Received: 28.01.2025
Accepted: 04.02.2025
Published Online 13.03.2025

Experimed

Research Article

Open Access

Contributing to the Functional Classification of Missense Variants in RAG1 Protein from Structural Perspective

Asli Kutlu [1], Begum Isikgil [1] & Sinem Firtina [2]

[1] Department of Molecular Biology and Genetics, Faculty of Engineering and Natural Science, Istinye University, Istanbul, Turkiye
[2] Department of Medical Genetics, Cerrahpasa Medical Faculty, Istanbul University-Cerrahpasa, Istanbul, Turkiye

Abstract

Objective: Primary immune deficiencies (PIDs) are syndromic diseases characterized by severe clinical findings in early childhood. The diagnosis and treatment of PID are challenging due to its genetic and clinical heterogeneity. Severe combined immune deficiency (SCID) is one of its most severe and fatal forms and is characterized by the absence of T lymphocytes and either the presence of B and/or natural killer (NK) cells. The failures in variable, diversity, joining (V(D)J) recombination, which are also controlled by the recombination activating gene (RAG) 1/2 complex, result in the deficiency of B- and T-cells, and these failures are associated with SCID or its alternative forms. Due to complete defect in RAG1 function, the SCID phenotype occurs, but OMENN syndrome (OS) and atypic SCID (AS) occur if defects in RAG1 function are partially tolerated.

Materials and Methods: By using *in-silico* computational tools, the structural differences are revealed and then variants are prioritized according to how degree the existing structural alterations are tolerated or not.

Results: These promising ones are Arg474Cys, Arg778Gln & Arg975Trp in AS, Arg396His, Arg396Leu, Arg624Cys, Trp552Cys, Val433Met & Met435Val in OS, and Arg474His and Glu722Lys in SCID.

Conclusion: The utilization of *in-silico* computational tools provides a great advantage to gain insight about variant specific molecular mechanisms of diseases to boost existing knowledge about RAG1/2 failures.

Keywords Primer immune deficiency · Severe combined immunodeficiency · Omenn syndrome · Atypical SCID · RAG1 gene · Structural alterations

Citation: Kutlu, A., Isikgil, B. & Firtina, S. Contributing to the Functional Classification of Missense Variants in RAG1 Protein from Structural Perspective . Experimed 2025; 15(1): 31-40. DOI: 10.26650/experimed.1562959

Corresponding author: Asli Kutlu asli.kutlu@istinye.edu.tr

INTRODUCTION

Hematopoietic stem cells are the source of B and T cell development, and their maturation and differentiation depend on the proper activity of essential enzymes that are common to both cell types. The process of lymphocyte development is orchestrated by the number of genes that play specific roles at different stages of B or T cell differentiation. DNA recombinase, also known as the recombination activating gene (RAGs) complex, provides instructions for the rearrangement and diversification of B and T cell antigen receptors to participate in immune cell maturation (1).

During the maturation of B- and T-cells, variable, diversity, joining (V(D)J) recombination occurs collectively (2). By recognizing recombination signal sequences (RSS), V, D, and J gene segments are flanked, and they direct the assembly of functionally relevant gene segments. There are two types of RSSs: 12 (12-RSS) or 23 (23-RSS) base pairs (bp) existing between conserved heptamer (5'-CACAGTG-3') and nonamer (5'-ACAAAAACC-3') motifs. Two types of RSS are required for recombination, and RAG complex proteins participate in recombination by forming double-chain breaks from these regions. The RSS must be split (V to J or V to D to J) specifically for the V(D)J gene segments to assemble in the correct order (3, 4). V(D)J recombination, rearranged by the RAG complex, facilitates the generation of B and T cell repertoire diversity against different pathogens. Mutations in the RAG complex, composed of *RAG1* and *RAG2* genes (chromosome 11p13), have resulted in defective B and T cell formation or inhibited B- and T-cell development (5). Although RAG1 and RAG2 protein structures act together within this complex system, RAG2 protein cannot bind to DNA; therefore, RAG1 is required for mediating V(D)J recombination. Unlike the RAG2 protein, the RAG1 protein has a DNA-binding domain to which it can bind by recognizing the RSS nonamer in its homeodomain structure. This interaction model has also been supported by RAG1-DNA & RAG2-DNA binding affinity studies (Figure 1) (6).

The *RAG1* gene is polymorphic, and the mutations are associated with severe combined immune deficiency (SCID). SCID is one of the most severe forms of primary immune deficiency (PID), appearing in early childhood as a genetically heterogeneous course (7). It is defined as a genetically heterogeneous group of diseases characterized by the absence or dysfunction of T cells as well as the presence or absence of B and/or natural killer (NK) cells (7, 8), and its phenotype is reflected in early childhood with severe symptoms, e.g. recurrent and severe infections, T lymphocyte-mediated immune response defects, and lymphopenia. The different forms of RAG deficiencies exist as Omenn Syndrome (OS) and atypical SCID (AS), also known as granulomas and cancer (8). In general, the complete defect in the RAG1 protein molecule is referred to as the SCID phenotype. In contrast, other variants may result in OS or AS forms indicating the existence of defective but functional RAG1 (8).

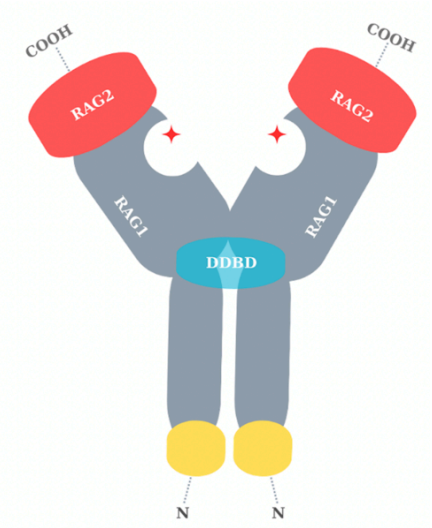

Figure 1. RAG1/2 synaptic diagram. The two monomers of RAG2 represent red, the nonamer-binding region of RAG1 in yellow, and the active region as red stars. DDBD: dimerization and DNA-binding domain, RAG: Recombination activating gene; N: RAG1 N-termini, COOH: RAG2 C-terminus.

The RAG1 protein consists of 1043 amino acids and has two basic regions: core and non-core. The non-nuclear region of RAG1 contains the zinc-binding dimerization domain (ZDD; residues 265-380) that includes the RING and zing fingers (ZF) domains. The core region (residues 387-1011) includes the nonamer-binding domain (NBD; residues 394-460), dimerization and DNA-binding domain (DDBD; residues 461-517), zinc-binding domain (ZBD; residues 722-965), and the carboxy-terminal domain (CTD; residues 966–1008), which performs the catalytic functions of the protein (9). The ZBD plays a crucial role in the multiple functions of V(D)J recombinase, including nicking and hairpin formation. The role of the NBD domain is to mediate specific binding from the nonamer and heptamer motifs of RSSs. The RAG complex creates a hairpin structure by forming a nick (the '12–23 rule') between the heptamer and the neighboring coding sequence and causes a double-strand break in DNA. When cleaving double-stranded DNA, sequences from the V, D, and J gene segments are selected in the correct order (first D-J and then V-DJ). The RAG complex binds to form 12-RSS and 23-RSS synapses. The broken ends must join properly for recombination to occur. The non-homologous end joining (NHEJ) repair mechanism and broken ends of other proteins (DNA-dependent protein kinase (DNA-PKcs), Ku70/80, Artemis, and DNA ligase IV) are then joined (10, 11). Upon the presence

of missense variants on RAG1, the different phenotypes are reported as pathogenic, which is related to either the disruption of the VDJ complex or the RAG1/RAG2 complex interaction.

In this study, we aimed to provide a detailed understanding of the impact of missense variants on RAG1 from a structural perspective. To achieve this, we used *in-silico* bioinformatics tools to assess structural changes in RAG1 from the perspective of intramolecular interactions and cavity changes. Based on the principal relationship between the structure and function of RAG1, we aimed to prioritize RAG1-associated variants that cause SCID or its alternative forms. Here, we harness the power of structural bioinformatics tools to describe promising variants in RAG1 that could be further investigated to capture SCID or its alternative forms based on unique molecular mechanisms to promote or accelerate ongoing research in orphan drug design.

MATERIALS AND METHODS

Variant Selection

RAG1-associated missense mutations were retrieved from the literature via a text-mining approach from PubMed and classified according to clinical outputs as either SCID, OS, or atypic SCID. These clinical outputs were also confirmed in the UniProt database with P15918, the UniProt ID (https://www.uniprot.org/uniprot/P15918). The OMIM (https://www.omim.org/) and GeneCards (https://www.genecards.org/) databases were used for RAG1 gene information. Selected variants were reviewed in the clinical and literature using the ClinVar (https://www.ncbi.nlm.nih.gov/clinvar/), dbSNP (https://www.ncbi.nlm.nih.gov/snp/), and PubMed (https://pubmed.ncbi.nlm.nih.gov/) databases. In addition, several web-based bioinformatics tools were used to retrieve all related information about RAG1-associated missense variants (Table 1).

Structural Interpretation Using Web-Based Tools

AlphaFold model of the RAG1 protein model (AP-P15918-F1) was used to elucidate structural and functional changes induced by the presence of missense variants in RAG1. We used the Visual Molecular Dynamics (VMD) tool to visualize mutant protein conformations, to identify changes in intramolecular interactions, to measure distances between residues, and so on (12). More details regarding structural changes in the RAG1 protein were also assessed using the Missense 3D, Stride Database, and Disulfide by Design 2 (DbD2) tools (13, 14). The location of the variants in the protein domains was determined using the Mutation Mapper tool (Figure 2) (15).

RESULTS

The first step was to identify RAG1-associated missense variants and categorize them according to their clinical outputs (SCID, AS, and OS). A schematic of the RAG1/2 complex is presented in Figure 2, and the distribution of the domain-based variants is presented in Table 1. At first sight, two things are important; (1) no domain-specific clinics associated with RAG1 and (2) multiple variants at the same position that lead to varied clinical outputs. For (2), it implies the presence of unique molecular mechanisms of SCID, AS, and OS by referring to replacements at Arg396, Arg474, Arg561, and Arg624 in RAG1. Depending on the clinical output, structural alterations in RAG1 are described below.

Structural Alterations of RAG1 Caused by SCID-associated Missense Variants

We first describe structural changes in RAG1 caused by SCID-associated missense variants. According to Table 1, the 12 SCID-causing variants that were most interesting at first sight were Arg396Leu, Arg396His, Arg561Cys, and Arg624His. The presence of variants at positions 396 (loop), 561 (alpha helix), and 624 (beta sheet) causes either SCID or OS (Table 1). This information makes these positions critical in terms of tolerating structural changes at different levels if we consider the fact that the Arg residue is involved in advanced molecular interactions (salt bridge, ionic interactions, etc.). Among these critical Arg residues, neither Arg396/Arg624 in the native structure nor His replacement in mutant RAG1 structures are involved in salt bridge interactions. Only Arg561 is involved in salt-bridge interactions by partnering with Asp563 at 3.31 Å, but it is disrupted by the SCID-induced Arg561Cys substitution, which also does not lead to newly formed disulfide bond interactions. We also checked the relative surface area (RSA) values of these residues, and increased RSA values were reported for all residues excluding Arg561Cys. Here we have summarized the RSA results such that 93.4% in Arg396His, 87.8% in Arg396Leu, and 82.8% in native, 2.1% in Arg624His and 1.6% in native, 9.2% in Arg474His, 8.8% in Arg474Cys, and 3.2% in native were associated with the conformational shift to “exposed” upon His replacement but remained “buried” upon Cys replacement (Figure 3). Finally, the presence of significant cavity expansions of 81.4 Å in Arg474Cys and 52.9 Å in Arg474His, respectively, is crucial for Arg474His and Arg474Cys (Figure 4). It is also important to note that the Arg474Cys substitution leads to the formation of new disulfide bonds such as Cys474-Cys481 with 5.57 Å.

In the Glu722Lys substitution, we observed the preservation of the salt-bridge interaction with the same strength (2.6 Å), but with a changed interacting partner from Asp711 to Lys722.

Structural studies show that these two interacting partners are localized in different parts of RAG1, e.g. Asp711 is in the core region but Asp766 is on the surface; therefore, their contributions to the local stability of RAG1 are likely to be different even if the same distance is maintained. The RSA measurement of Lys722 also supports this finding by showing that the RSA value for Glu722Lys increases from 20.1% in the native state to 26.3%, which is associated with a change in the conformational state from exposed to buried. For the Arg776Trp and Arg841Trp substitutions, the most striking changes in the RSA value are reported together with the loss of salt-bridge interaction, e.g., an increase from 29.0% to 45.3% for Arg776Trp and from 47.9% to 68.7% for Arg841Trp. There is no information on changes in intramolecular interactions caused by Ala444Val, Phe972Ser, and Gln981Pro; therefore, we only report changes in cavity measurements. Among these three substitutions, the Phe927Ser substitution results in a 75.8 Å^3 cavity expansion in RAG1, which is considered significant for altering the local stability of RAG1.

Structural Alterations of RAG1 Caused by Atypical SCID (AS)-associated Missense Variants

Based on Table 1, we present six AS-associated variants of RAG1. In terms of changes in intramolecular interactions, Arg314Trp (3.1 Å), Arg778Gln (2.9 Å) and Arg975Trp (4.1 Å) involve salt bridge interactions that are disrupted by Trp or Gln substitutions. Consistent with the loss of intramolecular interactions, we report increased patterns in RSA values, e.g., from 23.7% to 54.6% for Arg314Trp, 42.3% to 57.5% for Arg778Gln, and 7.6% to 10.5% for Arg975Trp. For Arg975Trp, only a conformational shift from buried to exposed is reported. His375Asp substitution preserved the existing salt bridge interaction in RAG1 but caused a shift in the interaction partner from Glu365 to His388 in RAG1. Arg699Trp was not involved in any salt bridge interaction in native or mutant RAG1, and there was no change in the RSA value (0.8% in both). For Leu454Gln, no structural change was observed in RAG1. Of the six AS-associated variants, only Arg314Trp and Arg778Gln were reported to be pathogenic, whereas the others were probably pathogenic.

Structural Alterations of RAG1 Caused by OS-associated Missense Variants

According to Table 1, the remaining 17 variants in RAG2 are OS-associated. Because these positions were mutated more than once, we first focused on the changes in the intramolecular interactions present in the 396th, 561st, and 624th positions of RAG1. After Cys substitutions at the 396th and 624th positions, salt-bridge interactions are lost in mutant RAG1, but Arg624Cys is associated with the formation of a possible new disulfide bond as Cys624-Cys655 with 6.85 Å, which seems insignificant at first sight but has the potential to alter the local dynamics within RAG1. The RSA results support these changes in intramolecular interactions, such as an increase in Arg396Cys from 82.8% in native to 85.9% and in Arg624Cys from 1.6% in native to 4.4%. For the RSA results of Arg561His, we report a decrease from 27% in native to 20.6%. According to the literature, Arg396Cys and Arg561His are pathogenic, whereas Arg624Cys is probably pathogenic.

Among the remaining variants, we first checked whether the presence of Gly392Glu, Ser401Pro, Asp429Gly, and Glu669Gly in RAG1 leads to any change in secondary structures or not by referring to Gly and Pro residues as structural breakers. Based on the close structural examination of native and mutant RAG1, there was no alteration in secondary structures in which replacements existed, e.g., Gly392Glu in coil, Ser401Pro in turn, Asp429Gly in turn, and Glu669Gly in the helix for both. Even after preserving the same secondary structures, the presence or existence of Gly or Pro resulted in changes in RSA values, e.g., 72.6% to 94.7% in Gly392Glu, 58.2% to 34.5% in Asp429Gly, 59.2% to 52.3% in Glu669Gly, and 60.7% to 65.4% in Ser401Pro in native and mutant RAG1s. In terms of advanced molecular interactions within RAG1, Gly392Gly, Asp429Gly, and Glu669Gly made no contribution.

Even though Arg737His and Arg507Trp seem to involve a salt-bridge interaction and to disrupt existing ones, respectively, they do not contribute to intramolecular interactions. For Arg507Trp replacement, there exists a conformational shift from being buried to exposed according to RSA measurement. For Arg559Ser and His753Leu, we report the loss of strong salt-bridge interactions in RAG1 as Glu861-Arg559 in 4.4 Å, and Glu719-His753 in 3.5 Å that are significant to alter local dynamics in mutant RAG1s. The remaining Cys328Tyr, Trp552Cys, and Tyr912Cys replacements in RAG1 were evaluated based on their potential in disulfide bond formation. Our VMD measurements did not detect any disulfide bond formation with the involvement of Cys328. Upon Cys replacements at the 552nd and 912nd positions, we also detected no newly formed disulfide bond formations in mutant RAG1s, and the limited increases in RSA values support this finding, e.g., from 9.2% to 14% in Trp552Cys and 0.9% to 14% in Tyr912Cys. For Trp552Cys replacement, we report 79.3 Å^3 cavity alteration in RAG1 as a striking structural change that alters local protein dynamics.

The remaining Val433Met and Met435Val variants in RAG1 appear at first sight to be neutral because they replace more likely amino acids in terms of physicochemical properties. This was also suggested by the RSA results, which reported changes in the range of 2%-4% between native and mutant

RAG1. The closer structural examination of the RAG1 protein suggests that these are parts of the alpha-helices in the hydrophobic pocket, and the dynamic changes that exist around this region could be critical in terms of clinical outcome(s), as shown in Figure 1. These findings may help explain OS associations.

DISCUSSION

The overall structure of RAG1 protein is composed of several domains in core and non-core regions with specified functions, e.g., ZBD in the non-core region, nonamer-binding domain, carboxy-terminal domains (C-ter; CTD) in the core region, etc. The literature findings suggest that there is no direct relationship between the presence of domain-specific missense variants and their associated clinics. As shown in

Table 1. RAG1-associated missense mutations with clinical outputs

Variant No	cDNA	Protein	dbSNP	Pathogenicity	Clinics
1	c.940C>T	p. Arg314Trp	rs121918568	P	AS
2	c.983G>A	p. Cys328Tyr	rs121918571	P	OS
3	c.1123C>G	p. His375Asp	rs773272902	LP	AS
4	c.1175G>A	p. Gly392Glu	-	LP	OS
5	c.1186C>T	p. Arg396Cys	rs104894289	P	OS
6	c.1187G>T	p. Arg396Leu	rs104894291	P	SCID
7	c.1187G>A	p. Arg396His	rs104894291	P	SCID
8	c.1201T>C	p. Ser401Pro	rs199474682	P	OS
9	c.1229G>A	p. Arg410Gln	rs199474684	P	OS
10	c.1286A>G	p. Asp429Gly	rs104894292	LP	OS
11	c.1297G>A	p. Val433Met	rs199474679	LP	OS
12	c.1303A>G	p. Met435Val	rs141524540	P	OS
13	c.1331C>T	p. Ala444Val	rs199474685	P	SCID
14	c.1361T>A	p. Leu454Gln	rs199474677	LP	AS
15	c.1420C>T	p. Arg474Cys	rs199474678	P	SCID
16	c.1421G>A	p. Arg474His	rs199474686	P	SCID
17	c.1519C>T	p. Arg507Trp	rs104894298	P	OS
18	c.1566G>T	p. Trp522Cys	rs193922461	P	OS
19	c.1677G>C, c.1677G>T	p. Arg559Ser, p. Arg559Ser	rs199474681	LP	OS
20	c.1682G>A	p. Arg561His	rs104894284	P	OS
21	c.1681C>T	p. Arg561Cys	rs104894285	P	SCID
22	c.1870C>T	p. Arg624Cys	rs199474688	LP	OS
23	c.1871G>A	p. Arg624His	rs199474680	P	SCID
24	c.2006A>G	p. Glu669Gly	rs199474689	LP	OS
25	c.2095C>T	p. Arg699Trp	rs199474676	LP	AS
26	c.2164G>A	p. Glu722Lys	rs28933392	P	SCID
27	c.2210G>A	p. Arg737His	rs104894286	P	OS
28	c.2258A>T	p. His753Leu	rs199474687	P	OS
29	c.2326C>T	p. Arg776Trp	rs121918572	P	SCID
30	c.2333G>A	p. Arg778Gln	rs121918569	P	AS
31	c.2521C>T	p. Arg841Trp	rs104894287	P	SCID
32	c.2735A>G	p. Tyr912Cys	rs104894290	P	OS
33	c.2780 T >C	p. Phe927Ser:	rs1249862287	P	SCID
34	c.2923C>T	p. Arg975Trp	rs121918570	LP	AS
35	c.2942A>C	p. Gln981Pro	rs104894288	P	SCID

SCID: Severe combined immune deficiency; AS: Atypical SCID, OS: Omenn's Syndrome; LP: Likely pathogenic; P: Pathogenic.

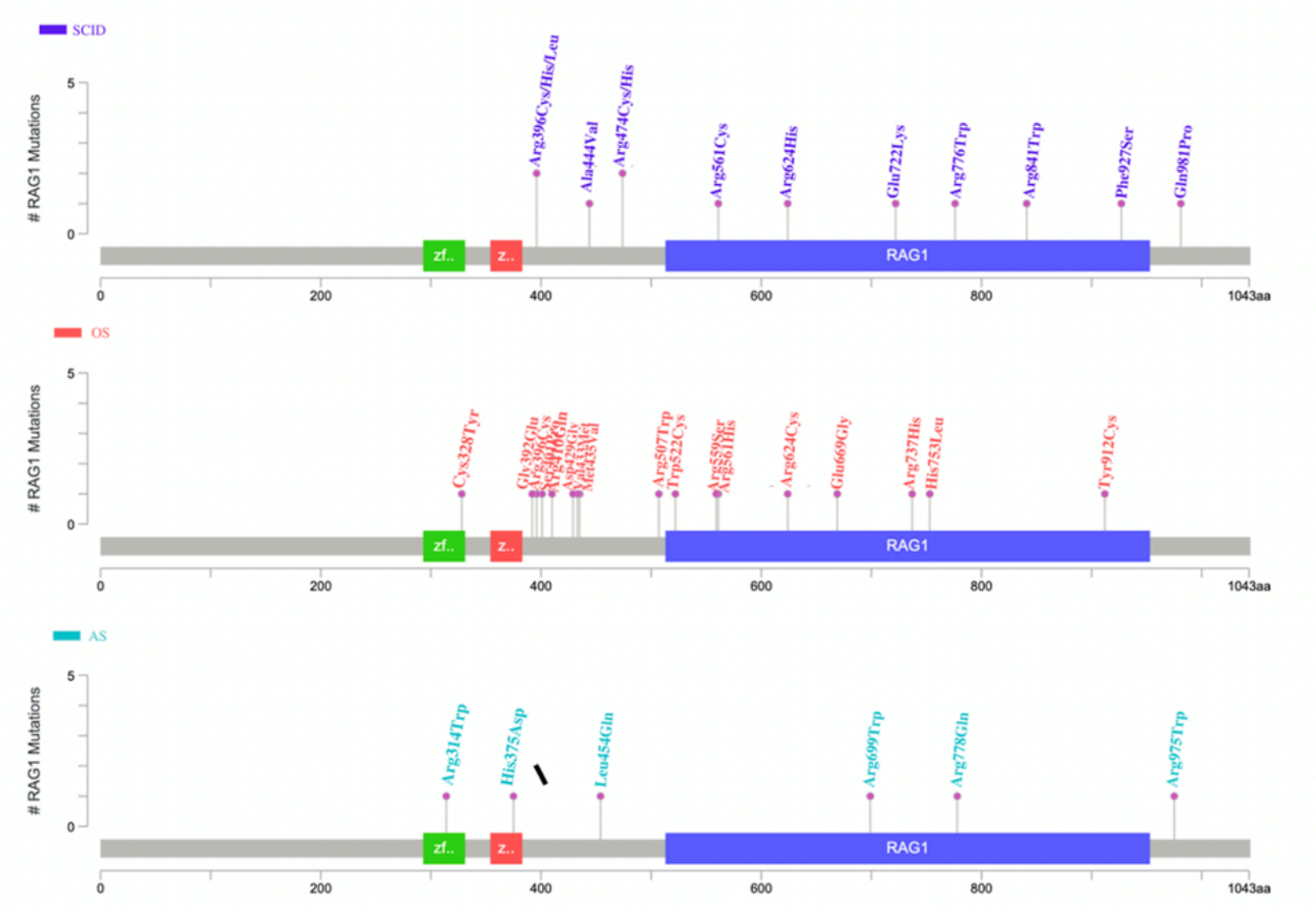

Figure 2. RAG1-associated missense variants in SCID, OS, and AS clinics (Color coding: Purple-SCID, Red-OS, and Light Blue-AS). RAG: Recombination activating gene; SCID: Severe combined immune deficiency; OS: OMENN syndrome; AS: Atypic SCID.

Figure 2 and Table 1, the missense variants existing in the same domains are associated with different clinical outputs that highlight the importance of the variant-specific etiology of RAG1. However, in terms of their significance, the role of the core region has been emphasized more than the N-terminal region by referring to the fact that the recombination activity of RAG1 is preserved even in both N-terminal knockdown and highly mutated model(s) (10). Another study finding suggested that the variable phenotypes (CID, SCID, or OS) are reported within a study cohort composed of 22 patients upon the interruption of the same N-terminal region of RAG1, and this leads to the conclusion that the clinical penetrance of RAG deficiency is uncertain (16).

Within the non-core region ZBD of RAG1, we assessed the impact of three missense variants (Arg314Trp, Cys328Tyr & His375Asp), and only His375Asp appeared to be significant in terms of the conformational change caused by the His to Asp substitution, resulting in a shift in the interacting partner of the salt bridge interaction. The role of this domain has been defined as regulating the catalytic activity of RAG1 by contributing to the maintenance of genomic stability (34). Here, the presence of AS clinics can be explained by their negative contribution to AS stability.

In the core region, there is also the ZBD domain (residues 722-965), and its role is defined as interacting with the catalytic region of the RAG1 protein by playing a role in conjugation with the catalytic center, the RAG2 protein, and the DNA sequence. Here, RAG1 exists as a 'Y' shaped dimer with RAG2 binding to each arm to form the RAG1/RAG2 complex. Specifically, the NBD dimer of RAG1 forms the body, while the center of RAG1 and the CTD are shifted to form the DNA-binding surface, as shown in Figure 1. Both polar and hydrophobic residues play a crucial role in maintaining this Y-shaped shape. In particular, RAG2 interacts with Glu607 and Val615 and Glu719 and Val724 of RAG1 (17).

Upon the presence of missense mutations within the borders of the core-ZBD region, destabilization is introduced by breaking down the crucial interactions; hence, the binding of RAG2 to RSS is adversely affected. Within this region, we report the impacts of 8 variants (Glu722Lys, Arg737His, His753Leu,

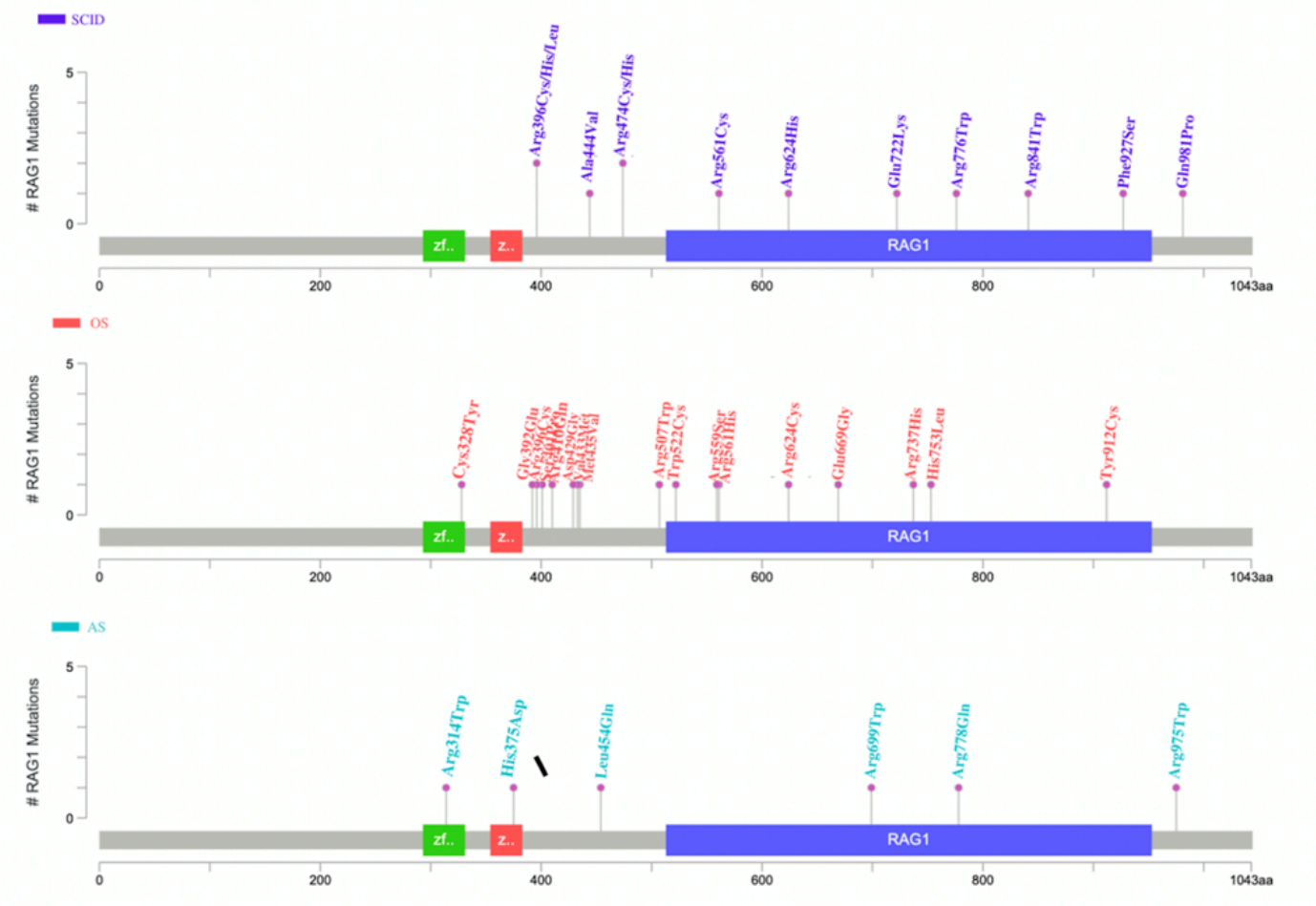

Figure 3. Conformational changes in RAG1 protein structures in the presence of multiple variants at position 396, 474, 561, and 624. RAG: Recombination activating gene; SCID: Severe combined immune deficiency; OS: OMENN syndrome; AS: Atypic SCID.

Arg776Trp, Arg778Gln, Arg841Trp, Tyr912Cys, Phe927Ser) associated with different clinical outputs (Figure 2). Among them, we report Glu722Lys (SCID) and Arg778Gln (AS) as significant in terms of leading structural alterations beyond the tolerable limits of RAG1 and promising ones for further evaluation. Specifically, in Glu722Lys replacement, we detect the shift in interacting partner from Asp711 in native to Asp766 in mutant as a salt bridge partner. Even though the length of the salt-bridge interaction is almost the same for these two interacting partners, the localization of the interacting partner for the 722nd residue is shifted from the core (Asp711) to the surface (Asp766), and this shift leads to different contributions to the local stability of RAG1. In terms of local stability contributions, salt bridges existing on the surface contribute to the local stability of protein molecules with less than 1 kcal/mol, whereas it is more than 4 kcal/mol if existing in a hydrophobic core (18, 19). Similarly, five more missense variants existing in the core ZBD domain of RAG1 (Cys730Phe, Leu732Phe, Trp893Arg, Tyr909Cys, and Ile953Arg) were reported by indicating their associations as a cause of PID due to bringing destabilization in this region. These five missense variants were excluded from our missense variant lists (see Table 1) because they were not listed in UniProt (20, 21).

In line with literature findings on PID associations in the core ZBD domain, our results also pointed out the local destabilization in RAG1 caused by the presence of His753Leu (OS) and Phe927Ser (SCID) missense variants located near the ZBD of RAG1 protein in the core region. Within the ZBD of RAG1 in the core region, there is also a DDE motif composed of three acidic residues (Asp603, Asp711, and Glu965) that plays a role in nicking and hairpin formation immediately after RSS binding to the RAG1/RAG2 complex. Due to the presence of closely located mutations around this region, the catalytic activity of the RAG1 protein together with its DNA binding ability has been altered, and hence, these mutations are associated with SCID and OS phenotypes. Moreover, this highly conserved motif is crucial for controlling the coordination of Mg^{2+} divalent ions. The importance of the DDE motif and its close association with SCID and OS phenotypes would help us further explain the association between missense variants and clinics (Figure 2).

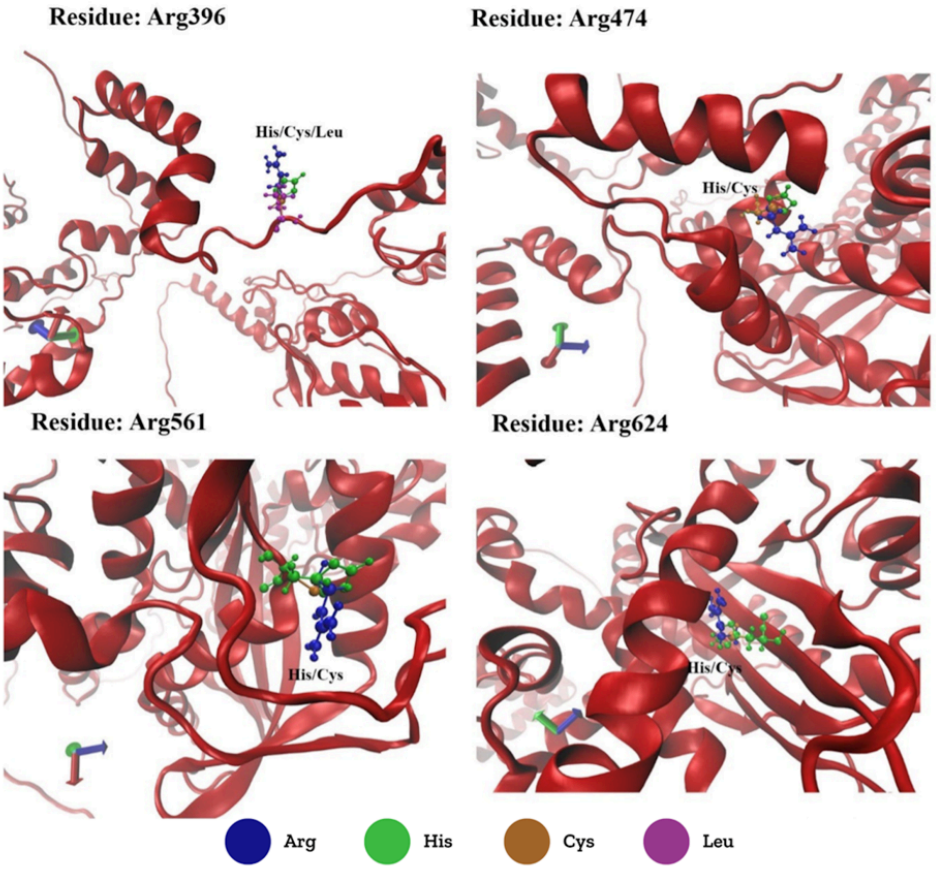

Figure 4. Changes in protein surfaces in the presence of Arg474His (SCID), Arg474Cys (AS), and Trp552Cys (OS). SCID: Severe combined immune deficiency; OS: OMENN syndrome; AS: Atypic SCID.

Within the core NBD of RAG1, we highlight four variants as promising for further investigations, e.g. Arg396His, Arg396Leu, Val433Met, and Met435Val. For Arg396His and Arg396Leu replacements, it is crucial to identify their contributions to the local stability of RAG1 compared with other Arg396 replacements. Since differences in local stability contributions result in the presence of different clinical outputs (SCID vs. OS) for Arg396 cases, it would be possible to capture clinic-specific molecular mechanism pattern(s) if exist. For Ala444Val replacement, it is reported as pathogenic in the literature with SCID clinics by indicating the role of the hydrophobic pocket composed of Ala444, Val433, and Met435 (10) even though we detect no crucial change in intramolecular interactions or conformation changes within RAG1. A closer look at the RAG1 molecule suggests that Ala444Val, Val433Met, and Met435Val are located on the same α-helices, and more attention is required for further structural investigation.

Within the core DDBD of RAG1, we detect 2 variants that are promising for further study: Arg474His (SCID) and Arg474Cys (AS). We report a significant degree of cavity expansion for both mutations and the presence of a new disulfide bond in RAG1 resulting from the Arg474Cys substitution. Since the conformational asymmetry of the RAG1 and RAG2 dimer, together with the off-center NBD, is very important for modulating 12- and 23-RSS DNA binding (11), the presence of these missense variants would result in destabilization of the DDBD of RAG1 by altering the required structural conformation for effective binding of 12- and 23-RSS. The experimental finding of Arg474Cys has also supported this by concluding that this substitution does not alter the protein expression level but leads to a failure in DNA binding (11). Further investigation, including molecular dynamics studies together with docking studies, may reveal the potential uniqueness of the molecular disease mechanisms of Arg474His and Arg474Cys leading to different clinics, SCID and AS, respectively.

Finally, Arg975Trp (AS), located in the CTD of RAG1, is a promising variant for further investigation because it results in the loss of a strong salt-bridge interaction. The role of the CTD in RAG1 is defined as the coordination of divalent zinc atoms (Zn^{2+}) required for effective DNA recombination. The effective coordination of these zinc atoms is well organized by the presence of CC and HH regions, composed of C902 and C907 and H942, respectively. According to the literature, there

is a close association between the HH zinc coordination site and the DDE active site, in which Glu962 plays a key role in coordinating this association either directly or indirectly (9). A close examination of the RAG1 structure revealed that Arg975 and Glu962 are in the same alpha-helix structure with their ends and beginnings, respectively. The loss of the strong salt-bridge interaction would probably cause local destabilization around here, and adversely affect the Zn^{2+} coordination through the HH region in RAG1. From a structural point of view, the Arg975Trp substitution seems worthy of further investigation to define the degree of loss in Zn^{2+} coordination, together with its impact on the overall stability of RAG1.

The remaining RAG1 variants present in the core of RAG1 but not clearly defined in any region (ZBD, NBD, DDBD or CTD) are Arg559Ser, Arg561Cys, Arg561His, Glu669Gly and Glu669Trp. Except for the Glu669Trp substitution, all of these variants have been reported to be associated with OS. Based on the literature, OS clinics are described with reference to RAG2 protein being required for DNA cleavage, although its role in V(D)J recombination for B and T lymphocyte development has not yet been specified (22). All these residues are exposed on the surface of RAG1, and it is likely that they contribute to RAG1/2 interactions. In addition, from the perspective of RAG2, there have been several studies of missense variants in RAG2 such that they cause a decrease in interaction with the RAG and result in OS and SCID by destroying the degradation function of the RAG recombinase (23).

Until now, we have reported the possible outcomes of RAG1-associated variants from a structural perspective as the output of web-based computer tools. The use of web-based computational tools is, at first sight, a good and useful option to assess what they are likely to do to the protein structure and, of course, to its associated function, but they have suffered in describing the full changes in protein dynamics that are essential to reveal the disease mechanism. Instead of using experimental methods to understand more about functional interpretations of missense variants in the RAG1 gene, computational tools, e.g., molecular dynamics simulations, would also be preferred to evaluate the structural effects of RAG1 to gain deeper insight into disease mechanisms by using a detailed atomistic approach as a cheaper and reliable option, but these disease mechanism-related studies were out of scope for this paper.

Besides providing a limited understanding of the structure and functional associations of RAG1 via web-based prediction tools, the use of an artificial intelligence (AI)-predicted model of the RAG1 protein to provide a discussion of the effects of missense variants would be considered another limitation of this study. As the RAG1 protein molecule is a very large protein structure and is mostly found in complexes with RAG2 and other associated molecule(s), the experimentally determined structures were mostly reported as different fragments or functional domains including associated molecules rather than the whole structure, and some of these structures included point mutations that did not represent the native state. To validate the power and accuracy of AI integration into homology modeling, we used the AlphaFold model of the RAG1 protein structure to discuss the structural effects of missense variants.

CONCLUSION

Within the scope of this study, we provided a detailed discussion of the structural alterations based on SCID, AS and OS caused missense variants in RAG1. Our results suggest that there is no direct relationship between associated clinical outcomes and RAG1 domains in cases with missense variants exist. It is very clearly stated by previous studies that the clinical penetrance of RAG deficiency is so uncertain, and these also imply the presence of a unique disease mechanism behind SCID, OS, or AS. In other words, the degree of tolerance to structural alterations caused by missenses in RAG1 may lead to various clinical outputs. Basically, we used the advantage of *in-silico* computer tools to assess the potential impacts of missense variants in RAG1 by aiming to prioritize them as 'promising' variants in terms of leading to changes in protein structure, especially its stability, beyond the tolerable limit. Even all listed variants in RAG1 are significant to discuss because they lead to SCID or its alternative clinical forms, Arg396His, Arg396Leu, Arg624Cys, Trp552Cys, Val433Met, and Met435Val in OS; Arg474His and Glu722Lys in SCID; and Arg474Cys, Arg778Gln, and Arg975Trp in AS are highlighted as more crucial ones for further investigations. Understanding the molecular basis of SCID, AS, and OS could be possible if these promising variants are employed to constitute a theoretical background via molecular dynamics simulations, docking studies, and so on. Rather than employing all existing variants in RAG1 for further investigations, assessing their structural impacts via *in-silico* bioinformatics tools would provide great time and money advantages in terms of their effective usage. In particular, in the field of rare diseases, the identification of the molecular mechanism of disease plus clinic-based characteristics is important to direct and accelerate future research studies for the development of orphan drugs, which are considered the actual and immediate need of this field. Currently, hematopoietic stem cell transplantation is offered as the only option regarding SCID or its alternative forms owing to its low success rate, high complications, and so on. Any contribution to accelerating translational medicine in this field is crucial, and accelerating

research studies by performing prioritization studies with structural bioinformatics tools would be greatly served for this purpose.

Ethics Committee Approval: Since this article does not contain any studies with human or animals, ethics committee approval is not required.
Peer Review: Externally peer-reviewed.
Author Contributions: Conception/Design of Study – A.K., S.F.; Data Acquisition – B.I.; Data Analysis/Interpretation – A.K., SF, B.I.; Drafting Manuscript – A.K., B.I.; Critical Revision of Manuscript – A.K., SF, B.I.; Final Approval and Accountability – A.K., SF, B.I.
Conflict of Interest: The authors declare no conflict of interest.
Financial Disclosure: The authors declare that they received no financial support for this study.

Author Details

Asli Kutlu
[1] Department of Molecular Biology and Genetics, Faculty of Engineering and Natural Science, Istinye University, Istanbul, Turkiye
0000-0002-9169-388X asli.kutlu@istinye.edu.tr

Begum Isikgil
[1] Department of Molecular Biology and Genetics, Faculty of Engineering and Natural Science, Istinye University, Istanbul, Turkiye
0000-0002-7541-4596

Sinem Firtina
[2] Department of Medical Genetics, Cerrahpasa Medical Faculty, Istanbul University-Cerrahpasa, Istanbul, Turkiye
0000-0002-3370-8545

REFERENCES

1. Marti LC, Bacal NS, Bento LC, Correia RP, Rocha FA. Lymphoid Hematopoiesis and Lymphocytes Differentiation and Maturation. Gheorghita Isvaronu, editors. Lymphocyte Updates: Cancer, Autoimmunity and Infectious. Crotatia: Intect; Open; 2007. p: 1-32.
2. Villa A, Sobacchi C, Notarangelo LD, Bozzi F, Abinun M, Abrahamsen TG, et al. V(D)J recombination defects in lymphocytes due to RAG mutations: Severe immunodeficiency with a spectrum of clinical presentations. Blood 2001; 97(1): 81-8.
3. Lewis SM. The mechanism of V(D)J joining: Lessons from molecular, immunological, and comparative analyses. Adv Immunol 1994; 56: 27-150.
4. Kim MS, Chuenchor W, Chen X, Cui Y, Zhang X, Zhou ZH, et al. Cracking the DNA code for V(D)J recombination. Mol Cell 2018; 70(2): 358–70.
5. Gennery A. Recent advances in understanding RAG deficiencies. F1000Research 2019; 8: F1000 Faculty Rev-148.
6. Spanopoulou E, Zaitseva F, Wang FH, Santagata S, Baltimore D, Panayotou G. The homeodomain region of Rag-1 reveals the parallel mechanisms of bacterial and V(D)J recombination. Cell 1996; 87 (2): 263–76.
7. Lawless D, Lango Allen H, Thaventhiran J, NIHR BioResource–Rare Diseases Consortium, Hodel F, Anwar R, et al. Predicting the occurrence of variants in RAG1 and RAG2. J Clin Immunol 2019; 39(7): 688–701.
8. Pasic S, Djuricic S, Ristic G, Slavkovic B. Recombinase-activating gene 1 immunodeficiency: Different immunological phenotypes in three siblings. Acta Paediatr Int J Paediatr 2009; 98(6): 1062-64.
9. Notarangelo LD, Kim MS, Walter JE, Lee YN. Human RAG mutations: Biochemistry and clinical implications. Nat Rev Immunol 2016; 16: 234–46.
10. Ru H, Chambers MG, Fu TM, Tong AB, Liao M, Wu H. Molecular mechanism of V(D)J recombination from synaptic RAG1-RAG2 complex structures. Cell 2015; 163 (5): 1138–52.
11. Gellert M. V(D)J recombination: RAG proteins, repair factors, and regulation. Annu Rev Biochem 2002; 71: 101–32.
12. Humphrey W., Dalke A., Schulten K. VMD: visual molecular dynamics. J Mol Graph 1996; 14(1): 28-33.
13. Craig DB, Dombkowski AA. Disulfide by Design 2.0: A web-based tool for disulfide engineering in proteins. BMC Bioinformatics 2013; 14: 340–6.
14. Khanna T, Hanna G, Sternberg MJE, David A. Missense3D-DB web catalogue: an atom-based analysis and repository of 4M human protein-coding genetic variants. Hum Genet 2021; 140(5): 805–12.
15. Vohra S, Biggin PC. Mutationmapper: A tool to aid the mapping of protein mutation data. PLoS One 2013; 8(8): e71711.
16. IJspeert H, Driessen G J, Moorhouse M J, Hartwig NG, Wolska-Kusnierz B, Kalwak K et al. Similar recombination-activating gene (RAG) mutations result in similar immunobiological effects but in different clinical phenotypes. J Allergy Clin Immunol 2014; 133(4): 1124–33.
17. Mo X, Bailin T, Sadofsky MJ. RAG1 and RAG2 cooperate in specific binding to the recombination signal sequence in vitro. J Biol Chem 1999; 274(11): 7025–31.
18. Makhatadze GI, Loladze V V., Ermolenko DN, Chen XF, Thomas ST. Contribution of surface salt bridges to protein stability: Guidelines for protein engineering. J Mol Biol 2003; 327(5): 1135–48.
19. Anderson DE, Becktel WJ, Dahlquist FW. pH-induced denaturation of proteins: A single salt bridge contributes 3-5 kcal/mol to the free energy of folding of T4 lysozyme. Biochemistry 1990; 29(9): 2403–08.
20. Gwyn LM, Peak MM, De P, Rahman NS, Rodgers KK. A Zinc site in the C-terminal domain of RAG1 is essential for DNA cleavage activity. J Mol Biol 2009; 390: 863–78.
21. Matthews AG, Kuo AJ, Ramón-Maiques S, Han S, Champagne KS, Ivanov D, et al. RAG2 PHD finger couples histone H3 lysine 4 trimethylation with V(D)J recombination. Nature 2007; 450(7172): 1106–10.
22. Kuo TC, Schlissel MS. Mechanisms controlling expression of the RAG locus during lymphocyte development. Curr Opin Immunol 2009; 21(2): 173–8.
23. Gomez CA, Ptaszek LM, Villa A, Bozzi F, Sobacchi C, Brooks EG, et al. Mutations in conserved regions of the predicted RAG2 kelch repeats block initiation of V (D) J recombination and result in primary immunodeficiencies 2000; 20(15): 5653–64.

İSTANBUL UNIVERSITY PRESS

Experimed 2025, 15 (1): 41–48

https://doi.org/10.26650/experimed.1584823

Submitted: 13.11.2024
Revision Requested: 23.12.2024
Last Revision Received: 07.01.2025
Accepted: 13.01.2025
Published Online 19.03.2025

Experimed

Research Article

Open Access

Impact of a Missense Mutation in *TRAPPC12* in Patients with Progressive Encephalopathy, Brain Atrophy and Spasticity Phenotype without Microcephaly and Epilepsy

Beyza Goncu [1], Gozde Yesil Sayin [2], Ayca Dilruba Aslanger [2] & Emrah Yucesan [3]

[1] Department of Medical Services and Techniques, Vocational School of Health Services, Bezmialem Vakif University, Istanbul, Turkiye
[2] Department of Medical Genetics, Faculty of Medicine, Istanbul University, Istanbul, Turkiye
[3] Department of Neurogenetics, Institute of Neurological Sciences, Istanbul University-Cerrahpasa, Istanbul, Turkiye

Abstract

Objective: Various symptoms, including microcephaly, corpus callosum agenesis, cerebellar atrophy, spasticity, and epilepsy, are associated with variations in the *TRAPPC12* gene. This diversity of features contributes to a broad range of mortality and morbidity. Identifying variations with functional consequences is crucial for accurate diagnosis and appropriate counseling for affected families. This study presented the results of a functional analysis of a previously detected mutation.

Materials and Methods: Patient-derived fibroblast cells (have a c.679T>G; p. Phe227Val variation) and the CCD1079Sk cell line (as a healthy control) were used. The relative protein expression of TRAPPC12 along with morphological changes, including Golgi integrity, endoplasmic reticulum (ER) structure, and vesicle distribution for neutral lipids, were assessed using immunofluorescent staining.

Results: Protein expression analysis revealed an absence of the mature TRAPPC12 protein and the uncharacterized protein fragment (CGI-87) via mutation compared with the wild-type. Additionally, milder outcomes were observed for Golgi integrity, slight ER structure enlargement, and further vesicle distribution changes, particularly with the truncated TRAPPC12 protein.

Conclusion: Despite the variant leading to a milder clinical phenotype without microcephaly and epilepsy, as previously reported, the study showed unstable protein expression and mild effects on Golgi and ER structures along with alterations in vesicle distribution throughout the cytoplasm. Despite the lack of mature TRAPPC12 protein expression and mild organelle impairments, the vesicle trafficking persisted. We showed that a single amino acid substitution might cause a loss of mature protein expression and also cause a milder disruption of organelles. More functional analyses are necessary to confirm these outcomes.

Keywords *TRAPPC12* · TRAMM · Neutral Lipid · Vesicle Trafficking · Progressive Encephalopathy

Citation: Goncu, B., Yesil Sayin, G., Dilruba Aslanger, A. & Yucesan, E. Impact of a Missense Mutation in *TRAPPC12* in Patients with Progressive Encephalopathy, Brain Atrophy and Spasticity Phenotype without Microcephaly and Epilepsy. Experimed 2025; 15(1): 41-48. DOI: 10.26650/experimed.1584823

Corresponding author: Beyza Goncu bgoncu@bezmialem.edu.tr

INTRODUCTION

Early-onset progressive encephalopathy with brain atrophy and spasticity (PEBAS) (MIM#614139) caused by bi-allelic variations in the *TRAPPC12* gene is an autosomal recessive condition characterized by progressive central nervous system (CNS) deterioration with seizures, hypotonia, microcephaly, dystonia, and/or global developmental delay (1).

TRAPPC12 is a constituent of the transport protein particle (TRAPP) multisubunit tethering complex and plays a role in intracellular vesicle trafficking (2). Every cell engages in intracellular trafficking, facilitating interaction for the delivery and/or recognition of its contents. The intracellular trafficking process involves multiple stages, including coating the cargo, cargo movement, tethering to the target membrane, and uncoating the cargo protein (3-5). Initially conceptualized as the tethering of two membranes, the transportation mechanism is now recognized to be much more intricate and involves a diverse array of proteins (5). The tethering function of the TRAPP complex has been extensively studied. This complex is categorized into two protein families in mammals: TRAPP II and TRAPP III (3, 5). One of the primary functions of these cells is to facilitate trafficking interaction among the endoplasmic reticulum (ER), ER-Golgi intermediate compartment (ERGIC), and Golgi apparatus (3, 5, 6). Over the course of 20 years of subsequent research, TRAPP complexes have been revealed to play a crucial role in mediating interactions between ER exit sites (Coat protein complex, COP, I and II vesicles) through the Golgi apparatus (7), exhibiting guanine nucleotide exchange factor (GEF) activity (8). A recent study highlighted that the TRAPP complex undergoes various conformational changes, leading to robust GEF activity, especially with regard to its interaction with Rab1 and Rab11; TRAPP II interacts with both, while TRAPP III exhibits distinct specificity for Rab1 (8). TRAPP III complexes are also implicated in kinetochore stability, mitotic transformation, and autophagy (9-11).

A wide spectrum of human diseases is linked to the alterations observed in TRAPP subunits. Changes in TRAPP subunit proteins have been correlated with diverse clinical manifestations, including global developmental delay, intellectual disability, microcephaly, spasticity, epilepsy, and encephalopathy (6, 11-14).

In this study, we evaluated the protein expression and organelle integrity, including the Golgi, ER, and vesicle distributions of the *TRAPPC12* gene variation reported by Aslanger et al. (c.679T >G; p. Phe227Val) (12).

MATERIALS AND METHODS

Approval was obtained from the Bezmialem Vakif University Ethics Committee (approval number: 2019/2659). Written informed consent was obtained from the patient and the parents of the patients were included in this study. This study evaluated a functional analysis of the previously reported (12) homozygous missense variation (NM_016030.6:c.679T>G; p. Phe227Val) of the *TRAPPC12* gene.

Sample Retrieval

Punch biopsy samples of the patient's skin were harvested after clinical determination. The derivation of fibroblast cells was performed as described previously (15). The skin biopsy in media was dissected into 10-12 pieces using sterile forceps and then cultivated. Medium was refreshed every 2-3 days. Further assays were performed once fibroblasts were confluent. CCD1079Sk (ATCC® CRL-2097™) human skin fibroblast cell line was used as the healthy control group. Cells were grown in DMEM/F12 (Panbiotech, Aidenbach, Germany) supplemented with 10% fetal bovine serum, 0.5% non-essential amino acids (NEAA), and 1% penicillin/streptomycin. Both primary skin fibroblast and CCD1079Sk cell lines were cultivated at 37°C in 5% CO_2 and 95% relative humidity. Protein samples from cells were prepared using a 100 µL RIPA lysis buffer containing 100-mM phenylmethylsulfonyl fluoride, 100-mM sodium orthovanadate solution, and 1X protease inhibitor cocktail (Santa Cruz, Texas, USA). The lysed protein samples were frozen overnight at −80°C then centrifugation was performed at 13000 g for 10 min. The total protein concentrations were determined using the Qubit protein assay kit protocol with a Qubit Fluorometer 4.0 (Thermo Fisher Scientific MA, USA).

Western Blotting

A 75 µg protein sample with 4X Laemmli buffer (EcoTech Biotechnology, Erzurum, Turkiye) was separated on 4–12% handmade polyacrylamide gel electrophoresis**.** Proteins were transferred to 0.2 µm polyvinylidene fluoride (PVDF) membranes (EcoTech Biotechnology, Erzurum, Turkiye) via semi-dry hot transfer using 20% MeOH and a Trans-Blot Turbo Transfer System (Bio-Rad, USA). Blocking was performed for 1 h at room temperature with Tris-buffered saline containing 0.02% Tween-20 containing 5% nonfat milk. Two different primary antibodies were used for TRAPPC12. The rabbit polyclonal antibody (cat no: NBP1-84500 from Novus Biologicals, Oxfordshire, UK) recognizes 625 amino acid (a.a.) and 710 a.a. sequences of human-TRAPPC12. The second primary antibody was a mouse polyclonal antibody (cat no. H00051112-B01P from Novus Biologicals, Oxfordshire, UK),

which recognizes the full-length protein (1 a.a. - 735 a.a) of the human TRAPPC12. The secondary antibodies were anti-rabbit IgG and anti-mouse IgG (both from Cell Signaling, MA, USA), and as a reference protein, horseradish peroxidase (HRP)-conjugated rabbit monoclonal β-actin primary antibody was used (cat no. AC028, Abclonal, MA, USA). The membranes were washed five times for 5 min per wash, each between primary and secondary antibody incubations. The blots were generated using an enhanced chemiluminescence (ECL) detection kit (WesternBright ECL, Advansta, CA, USA). The ImageJ (National Institutes of Health; NIH) program (16) was used to analyze Western blot images and to measure the intensity of organelle staining.

Organelle Staining

The Golgi and ER staining were performed with BODIPY™ FL C5-Ceramide and ER-Tracker™ Red (BODIPY™ TR Glibenclamide) dyes from Thermo Fisher Scientific, respectively, according to the manufacturer's instructions. Additionally, the cytoplasmic neutral lipid droplets were stained with Nile red (Thermo Fisher Scientific) as previously described (17). Nuclei were counterstained with DAPI, and images were acquired using a laser scanning confocal microscope (Leica TCS-SPE, Leica Microsystems, Wetzlar, Germany) from the Aziz Sancar Institute of Experimental Medicine, Istanbul University, as a service purchase.

Statistical Analyses

Statistical analyses were performed for experimental values by t-tests using GraphPad (GraphPad Software v10, Inc., CA, USA). Data are presented as means with a significance level of $p \leq 0.05$.

RESULTS

Before further experiments, we checked the pathogenicity scores of the variation, which was previously reported by our team (*TRAPPC12* NM_016030.6:c.679T>G, rs1312522735) using prediction tools (12). The patient was shown to be homozygous, and the parents were determined to be obligate carriers. The variant was not found in public databases in the homozygous state. However, 2 of 237.118 alleles were found in the Gnomad exome database, indicating a very rare carrier rate (0.00000843) (18). The variant was classified as pathogenic based on the tools integrated into the Varsome platform (19). The region appeared to be highly conserved across species according to PyhloP5.680 PhastCons 1.00 scores (20). Additionally, to detect our variation's nature, we used the *in-silico* prediction tool Mutalyzer (Mutalyzer 2.0.35) and found a non-truncating variant. Variations in the *TRAPPC12* gene have been reported in the literature, and the results of this study are presented in Figure 1A.

TRAPPC12 Protein Expression

Patient fibroblasts and CCD1079Sk human skin fibroblasts were used as mutant and wild type, respectively. Prior to Western blotting, we replicated the cells using consecutive passages during cultivation for the wild-type and mutant types. The variation itself did not cause a stop gain mutation; therefore, we evaluated the protein level with two different primary antibodies, including one that recognizes between 625 a.a. - 710 a.a. region (tetratricopeptide region) and the other region recognizes the full-length of the human TRAPPC12 protein while β-actin was used as a reference control (Figure 1B). Our chemiluminescent detection was >70 pg sensitive. The Western blot analysis of TRAPPC12 showed that the primary antibody that identified the tetratricopeptide region showed no bands of the expected size (79 kDa). However, an absence of the intact protein according to the second primary antibody that recognizes the full-length TRAPPC12 resulted in only a cleaved-like pattern protein product compared with the wild-type (Figure 1B). Regarding the Western blot, highly reduced protein expression and possibly cleaved protein products were observed (Figure 1B right blot). The second primary antibody recognizes the tetratricopeptide region of the TRAPPC12 protein, and mutation occurred via a nonpolar phenyl (F) at position 227 to another nonpolar amino acid, Valine (V). This may result in unstable, cleaved, or limited target protein function. To confirm whether the primary antibodies recognize the amino acid sequence, we ran the standard protein BLAST. We then determined the sizes of the cleaved-like pattern proteins and CGI-87. In addition, we also identified wild-type CGI-87 expression at approximately 35 kDa, and the subcellular location of the CGI-87 was reported to be located in the Golgi apparatus, according to UniProt (UniProt ID: Q53S18) (Figure 1B). The CGI-87 protein is identical to the a.a. sequence from 1 to 349 a.a. of the TRAPPC12 a.a. sequence. Regarding the outcome of the two primary antibodies of the TRAPPC12 region, the mutant type failed to show a protein expression for TRAPPC12 and CGI-87 (TRAPPC12-related protein, an uncharacterized protein fragment) compared with the wild type. In addition, the cleaved-like pattern did not show any reference point from BLAST. Thus, the *TRAPPC12* NM_016030.6:c.679T>G variation also affected the mature TRAPPC12 protein and CGI-87 by changing the position at 227 a.a.

Intracellular Differences

To investigate variations that interfere with organelle structure via mutation, we performed ER and Golgi

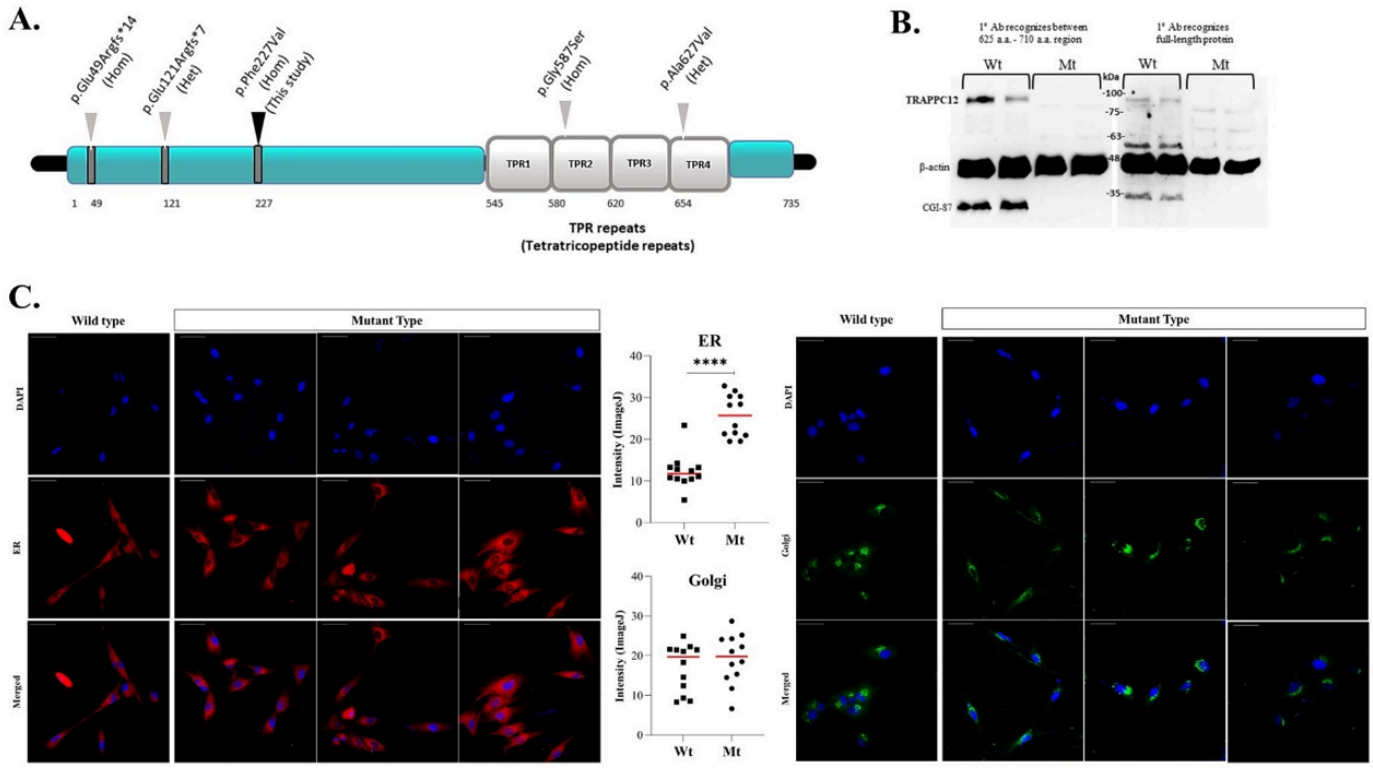

Figure 1. The variations were mapped at the protein level (NP_001308031.1). Schematic depicting aligned protein-coding sequence for the TRAPPC12. The gray arrows mark the locations of previously identified TRAPPC12 variations. A black arrow indicates the new variation. Variants are named according to GRCh37. **B.** Immunoblot images of 75µg protein samples per lane. The wild type of CCD1079Sk cells was replicated using different passages. The mutant type from patient fibroblast was replicated from passages two and three during cultivation. The left panel shows a primary antibody recognizes between 625 a.a. and 710 a.a. sequence (tetratricopeptide region) and the right panel shows a second primary antibody that recognizes a full-length protein of the human-TRAPPC12, respectively. Both primary antibodies demonstrated that the mutant type showed no visible bands or isoforms of intact TRAPPC12 which appeared to be associated with changes in the amino acid sequence. The CGI-87 bands indicate uncharacterized protein fragments and TRAPPC12-associated protein products (UniProt ID: Q53A18) from UniProt, which were detected by both primary antibodies that we used for TRAPPC12. The sequence similarity analysis of TRAPPC12 revealed 100% identity for this protein fragment. **C.** Evaluation of the Golgi and ER structures by immunostaining wild type and mutant type. The left panel shows the ER structure in red, middle panel compiles the intensity analysis between wild-type and mutant Golgi and the ER. Each dot represents a single cell. The right panel shows the Golgi structure in green. Nuclei were stained with DAPI (shown in blue) Magnification 40X. Scale bar=50µm. Intensity measurements were performed using ImageJ, and 12 cells/group were analyzed.

visualization using confocal laser scanning microscopy (Figure 1C). The Golgi staining showed corrupted integrity, and Golgi clusters expanded around the juxta nuclear region compared with the wild type. In addition, a comparison of the intensity between the wild-type and mutant types revealed no significant changes. However, the ER staining intensity analysis showed an increase in the mutant type ($p<0.0001$) (Figure 1C). Moreover, we visualized vesicles with neutral lipids to assess the vesicle trafficking process. We used Nile red staining to understand the intracellular distribution of lipid droplets. The cellular distribution of the lipid droplets did not show significant changes and only slight disruption was observed. Compared with the wild type, a wild type, heterogeneous distribution of cells their stage was observed (Supplementary Figure S1).

DISCUSSION

PEBAS is a severe disorder, and its etiopathogenesis has not been fully understood. To identify the pathogenesis of the disease, two independent groups noticed that Golgi apparatus is associated with neuronal loss, leading to the PEBAS phenotype (12, 21). According to the literature, many pathways are associated with progressive encephalopathy (22). Among these pathways, the TRAPP complex is particularly remarkable. The complex is a highly conserved modular multi-subunit protein complex that plays a role in endoplasmic reticulum-to-Golgi transport (11).

A significant number of proteins, including TRAPP complexes, regulate intracellular trafficking. Since the discovery of specific subunits of the TRAPP complexes contributed to the molecular processes between the ER-ERGIC-Golgi apparatus (23). Particularly, two different complexes exist, TRAPP II and TRAPP III, in metazoans and humans (8). One study on the

cryo-EM structure of metazoan TRAPP III demonstrated that there are two arms and one core of the complex. The one arm includes TRAPPC8 and TRAPPC11, and the other arm includes TRAPPC12 and TRAPPC13 together (24). The Ras-related protein Rab-1 (Rab1) contacts half of TRAPPC8 which is a GEF (8, 25), and provides a starting point for the completion of the TRAPP III structure. According to Galindo et al., the vertexes of the arms between subunits of the TRAPP III complex and Rab1 mediate vesicle membrane attachment (24). Additionally, among subunits of the TRAPP III complex, particularly TRAPPC12, also known as TTC15, has been reported for various cellular processes (8-10, 23). In 2015, Milev et al. reported that depletion of TRAPPC12 prohibited the migration of chromosomes to the metaphase, resulting in failed chromosome congression. In addition, TRAPPC12-depleted HeLa cells exhibited a disrupted kinetochore structure (10). Subsequent research by Milev et al. also identified a novel function of TRAPPC12 phosphorylation during mitosis, which acts as a mitotic regulator and provides Centromere-associated protein E (CENP-E) recruitment to the kinetochores (10). The distinctive features of TRAPPC12 differ from those of other TRAPP complexes; therefore, Milev et al. renamed the TRAPPC12 as TRAMM (trafficking of membranes and mitosis) (9).

The TRAPPC12 structure and its functions are being studied at the molecular level, as well as considering its relationship to the TRAPP complex, as mentioned above. Genetic studies identified a possible effect of TRAPPC12 variations, on etiopathogenesis. For instance, in 2017, Milev et al. showed that three individuals from two unrelated families (one consanguineous and one nonconsanguineous) had either a homozygous deleterious variant (c.145delG [p. Glu49Argfs*14]) or compound-heterozygous variants (c.360dupC [p. Glu121Argfs*7] and c.1880C>T [p. Ala627Val]) (1). According to their study, the clinical characteristics of the three patients were highly similar, i.e., severe disability, microcephaly, spasticity, hearing loss, visual impairment, and specific brain imaging findings such as; severe cortical atrophy, simplified gyri, and hypogenesis of the corpus callosum. In our case, the patient did not have epilepsy but presented with EEG abnormalities without seizures. In addition, Milev et al. reported that their patients had agenesis of the corpus callosum and severe cerebral atrophy, although our patient had no agenesis of the corpus callosum and only mild cerebral atrophy (1). Based on this difference, we report our case as "mild".

The importance of their study from our point of view is that they provide functional data that exhibits changes in Golgi morphology, membrane trafficking dysfunction, and mitotic delay in fibroblasts (1). In 2020, two case reports by Gass et al. and Aslanger et al. were published, respectively (12, 26). Gass et al. reported compound heterozygous variations in *TRAPPC12* in two fetuses with ventriculomegaly. The family had a previously deceased fetus with hydrocephaly, polydactyly, and interhemispheric cysts, an effect on cilia (26). Aslanger et al. reported two patients from unrelated families with homozygous *TRAPPC12* variants. The first patient was a 2-year-old boy with severe progressive cortical atrophy, moderate cerebellar atrophy, epilepsy, and microcephaly who had previously reported variations (c.1880C > T (p. Ala627Val)) in TRAPPC12. The second patient, a 9-year-old boy, was carrying novel variation (c.679T > G (p. Phe227Val) and manifested mild cortical atrophy, severe cerebellar atrophy without epilepsy, and microcephaly. The absence of cardinal manifestations like epilepsy and microcephaly, led us to investigate the pathogenic mechanism of this variation (12). The variation evaluated in this study is an extension of our previous report.

Herein, we found mature TRAPPC12 protein loss or high protein-level decrease, but contrary to the previous report by Milev et al., our variation did not have stop-gain variation (1). It is also noteworthy that CGI-87 (UniProt ID: Q53S18), a protein with 100% similarity to the TRAPPC12 a.a. sequence, was absent in the wild type. Immunostaining provided a more comprehensive outcome. Our results showed that the variation caused mild structural changes in the Golgi and made in a slight enlargement of the cell size, which was validated by the ER staining. The lack/loss of TRAPPC12 mature protein raises the possibility of COPII-associated membrane clustering to the juxta nuclear region of Golgi. Instead, our findings demonstrate that the TRAPPC12 protein is unstable and may be degraded by proteasome and has a marked effect on the architecture of the Golgi complex.

To understand whether the differences at the organelle level affected vesicle trafficking, we visualized the vesicles that carried neutral lipids (by Nile red staining). When examined using Nile red staining, we observed heterogeneous vesicle distribution depending on cell stage. In wild-type comparisons, we assumed that morphological differences were heterogeneous but homogeneous within the cell groups. However, Nile Red is a dye that dissolves in acetone, and when it is applied to cells, the cells become round, regardless of the concentration. Afterward, we became aware that it would be inappropriate to make a definitive interpretation of the possible changes in the vesicle distribution. Another limitation of the study was that the other molecules found in the core structure of TRAPPC12 could not be examined in terms of their relevance to the mutation. In addition, the vesicle traffic neither showed accumulation nor stopped

via variation (c.679T>G (p. Phe227Val). Consequently, the mild disarrangement of the Golgi and ER structure showed that the neutral lipid-carrying vesicle distribution was altered throughout the cytoplasm. Further studies are required to examine the relationship between the mutagenicity of the changes in cell morphologies caused by this mutation.

CONCLUSION

In conclusion, genetic diagnosis confirms the specific cause of the related diseases however the exact diagnosis requires more functional consequences at the protein and cellular levels. The precise pathways associated with the determined genes and their protein products play an important role in elucidating intracellular processes. Herein, the cellular impact of homozygous c.679T>G (p. Phe227Val) variation provides an understanding of the disruption of variation in cellular behavior. To prove this point, further experiments with proteasome inhibitors could help detect possible protein degradation. Further functional analysis, including high-throughput structural and functional relationships with other TRAPP molecules will underline the exact diagnosis of patients with PEBAS.

Acknowledgments: We are grateful to the patient for their participation in the study.

Ethics Committee Approval: Approval was obtained from the Bezmialem Vakif University Ethics Committee (approval number: 2019/2659). Written informed consent was obtained from the patient and the parents of the patients were included in this study.

Peer-review: Externally peer-reviewed.

Author Contributions: Conception/Design of Study – B.G., G.Y.S., A.D.A., E.Y.; Data Acquisition – B.G.; Data Analysis/Interpretation – B.G., E.Y.; Drafting Manuscript – B.G., G.Y.S.; Critical Revision of Manuscript – E.Y.; Final Approval and Accountability – B.G., G.Y.S., A.D.A., E.Y.

Conflict of Interest: The authors declare no conflict of interest.

Financial Disclosure: The Research Fund of Bezmialem Vakif University supported this study (grant number 4201919).

Author Details

Beyza Goncu
[1] Department of Medical Services and Techniques, Vocational School of Health Services, Bezmialem Vakif University, Istanbul, Turkiye
0000-0001-6026-8218 bgoncu@bezmialem.edu.tr

Gozde Yesil Sayin
[2] Department of Medical Genetics, Faculty of Medicine, Istanbul University, Istanbul, Turkiye
0000-0003-1964-6306

Ayca Dilruba Aslanger
[2] Department of Medical Genetics, Faculty of Medicine, Istanbul University, Istanbul, Turkiye
0000-0003-1770-1762

Emrah Yucesan
[3] Department of Neurogenetics, Institute of Neurological Sciences, Istanbul University-Cerrahpasa, Istanbul, Turkiye
0000-0003-4512-8764

REFERENCES

1. Milev MP, Grout ME, Saint-Dic D, Cheng YH, Glass IA, Hale CJ, et al. Mutations in TRAPPC12 manifest in progressive childhood encephalopathy and Golgi dysfunction. Am J Hum Genet. 2017; 101(2): 291-9.
2. Scrivens PJ, Noueihed B, Shahrzad N, Hul S, Brunet S, Sacher M. C4orf41 and TTC-15 are mammalian TRAPP components with a role at an early stage in ER-to-Golgi trafficking. Mol Biol Cell 2011; 22(12): 2083-93.
3. Sacher M, Kim YG, Lavie A, Oh BH, Segev N. The TRAPP complex: insights into its architecture and function. Traffic 2008; 9(12): 2032-42.
4. Whyte JR, Munro S. Vesicle tethering complexes in membrane traffic. J Cell Sci 2002; 115(Pt 13): 2627-37.
5. Sacher M, Jiang Y, Barrowman J, Scarpa A, Burston J, Zhang L, et al. TRAPP, a highly conserved novel complex on the cis-Golgi that mediates vesicle docking and fusion. EMBO J 1998; 17(9): 2494-503.
6. Kim MS, Yi MJ, Lee KH, Wagner J, Munger C, Kim YG, et al. Biochemical and crystallographic studies reveal a specific interaction between TRAPP subunits Trs33p and Bet3p. Traffic 2005; 6(12): 1183-95.
7. Cox R, Chen SH, Yoo E, Segev N. Conservation of the TRAPPII-specific subunits of a Ypt/Rab exchanger complex. BMC Evol Biol 2007; 7: 12.
8. Harris NJ, Jenkins ML, Dalwadi U, Fleming KD, Nam SE, Parson MAH, et al. Biochemical insight into novel Rab-GEF activity of the mammalian TRAPPIII complex. J Mol Biol 2021; 433(18): 167145.
9. Milev MP, Sacher M. Mitotic transformation of TRAMM/TrappC12. Oncotarget 2015; 6(20): 17853-4.
10. Milev MP, Hasaj B, Saint-Dic D, Snounou S, Zhao Q, Sacher M. TRAMM/TrappC12 plays a role in chromosome congression, kinetochore stability, and CENP-E recruitment. J Cell Biol 2015; 209(2): 221-34.
11. Kim JJ, Lipatova Z, Segev N. TRAPP complexes in secretion and autophagy. Front Cell Dev Biol 2016; 4: 20.
12. Aslanger AD, Demiral E, Sonmez-Sahin S, Guler S, Goncu B, Yucesan E, et al. Expanding clinical phenotype of TRAPPC12-related childhood encephalopathy: Two cases and review of literature. Neuropediatrics 2020; 51(6): 430-4.
13. Andresen K, Caliebe A, Spielmann M, Nagel I, Eckmann-Scholz C. Expansion of the symptoms associated with bi-allelic variants in TRAPPC12. Z Geburtshilfe Neonatol 2023; 227(S 01): P073.
14. Bhola PT, Marshall AE, Liang Y, Couse M, Wang X, Miller E, et al. RNA sequencing to support intronic variant interpretation: A case report of TRAPPC12-related disorder. Am J Med Genet A 2023; 191(6): 1664-8.
15. Vangipuram M, Ting D, Kim S, Diaz R, Schule B. Skin punch biopsy explant culture for derivation of primary human fibroblasts. J Vis Exp 2013; (77): e3779.
16. Schneider CA, Rasband WS, Eliceiri KW. NIH image to ImageJ: 25 years of image analysis. Nat Methods 2012; 9(7): 671-5.
17. Greenspan P, Mayer EP, Fowler SD. Nile red: a selective fluorescent stain for intracellular lipid droplets. J Cell Biol 1985; 100(3): 965-73.
18. Karczewski KJ, Francioli LC, Tiao G, Cummings BB, Alfoldi J, Wang Q, et al. The mutational constraint spectrum quantified from variation in 141,456 humans. Nature 2020; 581(7809): 434-43.
19. Kopanos C, Tsiolkas V, Kouris A, Chapple CE, Albarca Aguilera M, Meyer R, et al. VarSome: the human genomic variant search engine. Bioinformatics 2019; 35(11): 1978-80.

20. Pollard KS, Hubisz MJ, Rosenbloom KR, Siepel A. Detection of nonneutral substitution rates on mammalian phylogenies. Genome Res 2010; 20(1): 110-21.
21. Rabouille C, Haase G. Editorial: Golgi pathology in neurodegenerative diseases. Front Neurosci 2015; 9: 489.
22. La Cognata V, Morello G, Cavallaro S. Omics Data and Their Integrative analysis to support stratified medicine in neurodegenerative diseases. Int J Mol Sci 2021; 22(9): 4820.
23. Sacher M, Shahrzad N, Kamel H, Milev MP. TRAPPopathies: An emerging set of disorders linked to variations in the genes encoding transport protein particle (TRAPP)-associated proteins. Traffic 2019; 20(1): 5-26.
24. Galindo A, Planelles-Herrero VJ, Degliesposti G, Munro S. Cryo-EM structure of metazoan TRAPPIII, the multi-subunit complex that activates the GTPase Rab1. EMBO J 2021; 40(12): e107608.
25. Li F, Yi L, Zhao L, Itzen A, Goody RS, Wu YW. The role of the hypervariable C-terminal domain in Rab GTPases membrane targeting. Proc Natl Acad Sci U S A 2014; 111(7): 2572-7.
26. Gass JM, Head BB, Shields SM, Stevenson RE, Louie RJ. Hydrocephaly associated with compound heterozygous alterations in TRAPPC12. Birth Defects Res 2020; 112(13): 1028-34.

APPENDIX

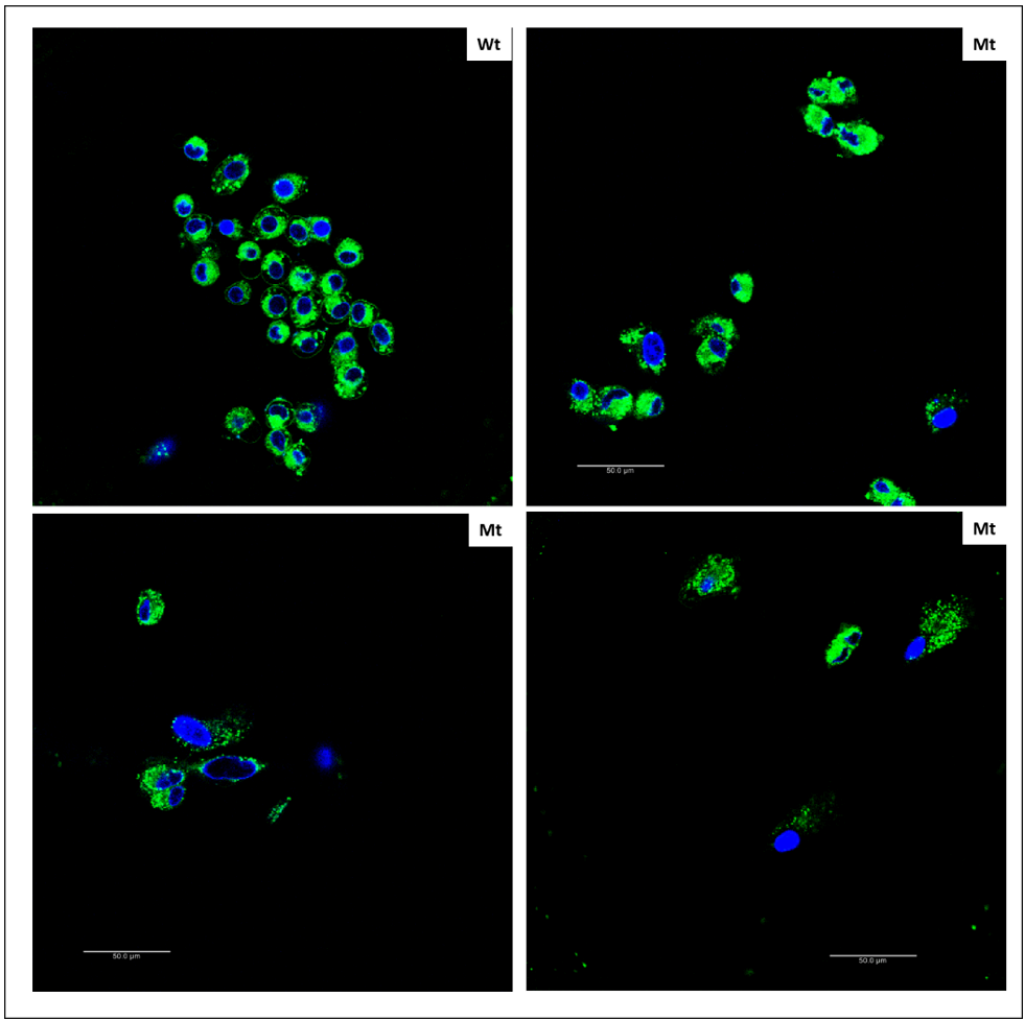

Figure S 1. Detection of neutral lipids in human skin fibroblasts from the patient (Mt) and CCD1079Sk cells (Wt) using the Nile red staining. The green fluorescence observed in the presence of Nile red indicates the presence of neutral lipid-containing vesicles. Nuclei was stained with DAPI (shown in blue). Scale bar=50µm.

İSTANBUL UNIVERSITY PRESS

Experimed 2025, 15 (1): 49–56

https://doi.org/10.26650/experimed.1527119

Submitted: 02.08.2024
Revision Requested: 17.12.2024
Last Revision Received: 15.01.2025
Accepted: 23.01.2025
Published Online 10.03.2025

Experimed

Research Article

Open Access

Assessing Serum Asprosin Levels among Iraqi Individuals Diagnosed with Acromegaly

Omar Yasir Shakir [1], Safaa Ehssan Atta [1], Karam Gharab [1], Lujain A. Ghannawi [1] & Abbas M. Rahmah [1]

[1] National Diabetes Center, Mustansiriyah University, Baghdad, Iraq

Abstract

Objective: Asprosin (ASP) is a modern adipokine produced from white adipose tissue that is linked to metabolic disorders such as obesity and diabetes. Acromegalic syndrome results from excessive pituitary growth hormone (GH) secretion, leading to increased insulin-like growth factor-1 (IGF-1) production, usually due to a pituitary adenoma. The serum ASP levels were higher in acromegaly patients (AC-PTs) than in healthy controls. The aim of the study was to explore ASP levels in AC-PTs compared with healthy controls, considering gender, diabetes status, treatment duration, and hypertension.

Materials and Methods: Fifty AC-PTs with different body mass index, sex, age, diabetes, and blood pressure were enrolled in this study. IGF-1, GH, and fasting blood glucose (FBG) levels were measured alongside 30 healthy controls. In addition, enzyme-linked immunoassay (ELISA) was used to measure ASP.

Results: There was no significant difference in ASP levels between AC-PTs and healthy controls ($p>0.05$). Moreover, the current study showed no statistically significant difference in ASP levels among the subgroups categorized according to the patient's gender, diabetes status, hypertension, and treatment course.

Conclusion: ASP levels revealed no difference between Iraqi AC-PTs and control group; ASP is not affected by hormonal changes that are typically associated with acromegaly.

Keywords Acromegaly · Adipokine · Asprosin · GH · IGF-1 · Pituitary Adenoma

Citation: Shakir, O. Y., Atta, S. E., Gharab, K., Ghannawi, L. A. & Rahmah, A. M. Assessing serum asprosin levels among Iraqi individuals diagnosed with acromegaly. Experimed 2025; 15(1): 49-56. DOI: 10.26650/experimed.1527119

Corresponding author: Lujain A. Ghannawi lujainghannawi@uomustansiriyah.edu.iq

INTRODUCTION

Acromegaly is a slowly developing disorder resulting from the raised secretion of insulin-like growth factor-I (IGF-I) and growth hormone (GH). Acromegaly patients (AC-PTs) are commonly induced by a growth hormone-secreting pituitary adenoma, which causes the extra production of IGF-1 (1). It may result in musculoskeletal, endocrine, and metabolic comorbidities. The global annual incidence is up to 13 cases per 100,000 people (2). Premature diagnosis and cure are important to relieve the extra mortality linked with AC-PTs (3, 4). Correspondingly, AC-PTs are personified by unproportioned growth of the organs, tissues, and skeleton (5, 6). In response to GH, IGF-1 is produced by the liver (7). Excess spread of IGF-I and GH levels in acromegaly includes harmful influences on various physiological processes and tissues. Patients typically share abnormal enlargements of soft tissue and bone, and have dysregulated glucose metabolism, with an increased risk of cardiovascular disease, which may influence mortality chance (8). In adipose tissue, GH action (catabolic) induces the decomposition of accumulated triglycerides into free fatty acids (FFA). GH provokes insulin action via different biomolecular pathways. Long-lasting GH secretion suppresses the anti-lipolytic effect of insulin. It raises FFA changes in the blood, thus enabling lipotoxicity and insulin resistance, which can lead to certain pathophysiological complications (9). AC-PTs have irregular glucolipid metabolism, which involves diabetes and insulin resistance; it may be linked with high GH levels, leading to adipose tissue dysfunction and the imbalances of adipocytokine production (10). Multiple research studies have investigated the serum levels of various adipokine between AC-PT and the control group. In addition, correlations between glucolipid metabolism indexes and adipokine have been reported (11). IGF-1 has been a biomarker of acromegaly since the turn of the millennium. The levels of circulating IGF-I are considered as critical biochemical means because of their prolonged half-life of 18–20 h (stability throughout the day) (12). An elevated IGF-I level and an incapability to lower GH levels <1 μg/L in an oral glucose tolerance test (OGTT) are considered influential standards for diagnosing acromegaly (13). IGF-I levels are influenced by multiple physiological characteristics, such as body mass index (BMI), sex, and age, and these should be considered during data performance (14).

Asprosin (ASP), a modern peptide recently found to be an influential regulatory adipokine, affects obesity in adult humans and animals (15, 16). Remarkably, several studies suggested that ASP as a modern fasting-induced glucogenic protein adipokine was found exalted in persons (and in rodent models) with metabolic disease (17-19). ASP is impacted by fasting and targets the liver, stimulating hepatic glucose release via the G protein cyclic adenosine monophosphate protein kinase A (cAMP-PKA) pathway (20-22). The tardy study conducted by Liu et al. (23) showed that ASP triggers agouti-related protein (AgRP) neurons, improving olfaction and facilitating appetite when attached to the central OLFR734 receptor. Recent investigations have detected that ASP levels in serum have risen in persons with metabolic disorders, such as type 2 diabetes, thyroid dysfunction, and obesity (24, 25). Other studies have suggested that ASP triggers the pathway of G-protein-linked receptor-cAMP-PKA, inducing phosphorylase activity by fast breakdown and glycogen release in the liver and increasing blood glucose (26). We know that glucose levels negatively affect GH levels, and excessive GH will raise the production of IGF-1 (27).

According to recent research, ASP plays a significant role in metabolic regulation, particularly in controlling glucose homeostasis and energy expenditure. This involvement specifically induces glucose tolerance, insulin resistance, and fasting-induced homeostasis (28). ASP is critical and essential in metabolic disorders (29).

This study is the first to evaluate serum ASP concentrations in individuals with acromegaly in Iraq. In addition, this study focuses on different subgroups, such as sex, hypertension, and diabetes mellitus (DM); thus, this work addresses a significant gap in the literature. We hypothesized that serum ASP levels are altered in AC-PT patients compared with healthy controls, and these levels may be influenced by factors such as gender, diabetes status, hypertension, and treatment duration. The findings of this study contribute to our understanding of metabolic dysregulation in acromegaly. This study provides a novel understanding of the role of ASP as a potential biomarker of acromegaly and links it to metabolic dysregulation, such as diabetes and hypertension. Thus, the present study aimed to examine serum ASP levels in Iraqi AC-PT and their correlation with elevated GH levels.

MATERIALS AND METHODS

Samples

The study enrolled individuals diagnosed with acromegaly, and healthy controls. To ensure a fair comparison, the control participants were matched with the patients based on age, gender, and BMI. Controls were selected to be within ±5 years of age and of the same gender as individuals with acromegaly.

More than 350 AC-PTs have been registered in Mustansiriyah University/National Diabetes Center (NDC) since 2003 from various provinces of Iraq; they have been regularly checked by endocrinologists clinically. Diagnosis depends on biochemical

parameters such as elevated IGF-1 levels and the absence of GH suppression after glucose management. Magnetic resonance imaging (MRI) of the pituitary in AC-PTs identifies an implied adenoma. The diagnosis and optimal administration of acromegaly comorbidities are essential for providing the best long-term outcomes for acromegaly (30). The samples of AC-PT and healthy participants were collected from September to December 2023; fifty AC-PT (female and male) with pituitary adenoma were enrolled at the NDC in Baghdad, Iraq, and considering parameters: sex, age, BMI, fasting blood glucose (FBG), hypertension, basal GH (morning), and IGF-1 levels. The age range of the AC-PT and healthy participants was 26–73 years. The patients were also administered a lanreotide injection (90 or 120 mg) intramuscularly according to their clinical status. Thus, patients were selected randomly according to their prespecified appointment. The treatment duration ranged from 1 to 10 years. Before the commencement of this trial, all patients provided written and dated consent for their participation. Furthermore, ethical approval for this study was extradited from the ethics committee of the National Diabetes Center at Mustansiriyah University in September 2023, ensuring compliance with the principles outlined in the 1964 Declaration of Helsinki and any subsequent revisions or comparable ethical standards.

Hormonal and Biochemical Assessments

Eight milliliters (mL) of peripheral blood were collected utilizing a one-use plastic needle and analyzed in a laboratory gel tube. All samples were centrifuged at 3000 rpm for 7 min to collect blood serum for laboratory examinations. The chronology of individual AC-PT and control subjects were subjected to medical estimation and physical parameters (weight, height). BMI was calculated using the following formula: BMI = weight (kg)/height² (m²). GH and IGF-1 were tested using a DiaSorin analyzer device (Elecsys hGH and IGF-1 kit-Germany), respectively. FBG levels were assayed with Gluc2 kit in a Cobas C11-1 analyzer (Roche Diagnostics, Germany).

Enzyme-Linked Immunosorbent Assay (ELISA) for ASP Levels

The ASP levels of the control and patients' serum groups were determined using an ELISA kit (Catalog no: E-EL-H0515, E-lab science, USA) following the manufacturer's instructions. We excluded any criteria linked to endocrinopathy and autoimmune diseases. In contrast, the reagents and ELISA plates were brought to room temperature before use. Serum samples were diluted according to kit instructions, and standards were prepared to create calibration curves. The assay was initiated by coating the ELISA plates with ASP and incubating them to allow binding. After that, a buffer was used to block non-specific binding. Next, serum samples and standards were added and incubated to allow ASP binding. Detection was achieved by adding a detection antibody and streptavidin- horseradish peroxidase conjugate then, a substrate solution was added to develop a colorimetric reaction. Finally, the intensity of the color was measured at 450 nm using a microplate reader. ASP levels were quantified based on the standard curve.

Statistical Analyses

In this research, statistical data were explored utilizing the Statistical Package for the Social Sciences (SPSS) version 26.0 (SPSS Inc, Chicago, IL, USA) software. The Shapiro-Wilk test was used to determine parametric or non-parametric analyses; all variables (except IGF-1) were determined to have non-parametric distributions. Thus, the Mann–Whitney U test was used to evaluate the significance level of the differences between the AC-PTs. Results are presented as median, minimum, and maximum. The Spearman test was used for correlation. A result was considered statistically significant when the p value was less than 0.05.

RESULTS

Fifty AC-PTs and 30 control subjects were included in this study. Half of the patients had DM, whereas the remaining had non-DM. The subjects were aged between 26 and 73 years, with a mean of 50.33 ± 13.59 years. The gender distribution of AC-PT was roughly distributed (Figure 1).

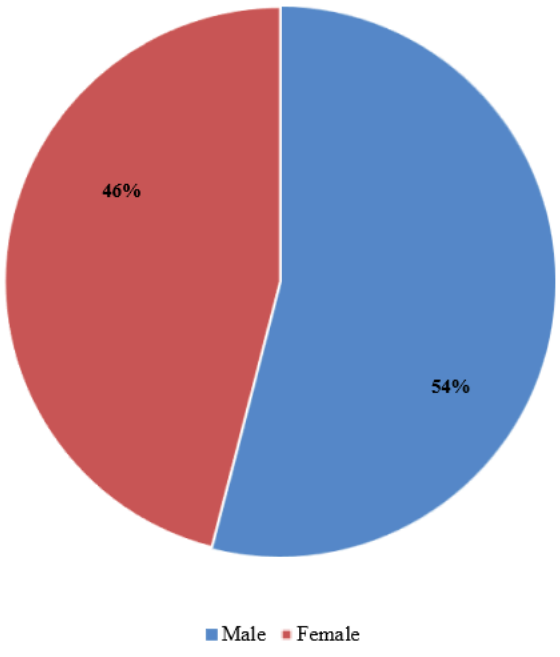

Figure 1. Gender distribution of acromegaly patients

The current study investigated the levels of ASP in AC-PT and healthy controls. Additionally, this study further explored the variations in the concentrations of ASP, GH, IGF-1, and FBG among different cohorts, categorized by gender, diabetic status, treatment course, and tension status.

When ASP levels in patients and the control group were compared, no significant differences between the patients and the controls were noted (Table 1).

Table 1. Median, minimum, maximum, and p values of study parameters between patients and control groups

Parameters	Patients Median (Min-Max)	Controls Median (Min-Max)	p value
ASP (ng/mL)	5.63 (2.88-11.67)	4.9 (3.7-6.77)	0.097
GH (ng/mL)	2.2 (0.21-54)	-	-
IGF-1 (ng/mL)	491 (105-1386)	-	-

p values calculated by Mann–Whitney U test

In this study, within AC-PT, the BMI showed no significant differences between males and females, as shown in (Table 2) and between DM and Non-DM, as shown in (Table 3).

Table 2. Median, minimum, maximum, and p values of the study parameters for male and female patients with acromegaly

Metabolites	Male Median (Min-Max)	Female Median (Min-Max)	p value
ASP (ng/mL)	5.35 (2.88-11.29)	5.93 (3.34-11.67)	0.770
GH (ng/mL)	2 (0.31-20)	3 (0.21-54)	0.247
IGF-1 (ng/mL)	450 (117-1120)	530 (105-1386)	0.403
FBG (mg/mL)	104 (60-240)	118 (60-306)	0.209
BMI (kg/m²)	27.75 (24.1-41.5)	27.9 (19.7-38.7)	0.874

p values calculated by Mann–Whitney U test.

Table 3. Median, minimum, maximum, and p values of the study parameters between patients with and without DM acromegaly

Metabolites	DM Median (Min-Max)	Non-DM Median (Min-Max)	p value
ASP (ng/mL)	5.35 (2.88-11.67)	6.04 (3.4-11.22)	0.938
GH (ng/mL)	2.6 (0.21-46.8)	2 (0.4-54)	0.884
IGF-1 (ng/mL)	480 (153-1386)	503 (105-1120)	0.923
FBG (mg/mL)	136 (60-306)	94 (60-136)	0.000*
BMI (kg/m²)	28.125 (19.7-41.5)	27.4 (24.1-39.8)	0.271

p values calculated by Mann–Whitney U test, * significant difference <0.05

The results obtained in the Mann-Whitney U test to evaluate the level of significance between male and female AC-PT showed that all the parameters had no significant values (p>0.05) (Table 2). Between the DM and non-DM AC-PTs, FBG showed a significant difference (p=0.000) while all other study parameters showed no significant differences (p>0.05) (Table 3).

A sub-group of patients with acromegaly based on their treatment duration with somatostatin analogous (Lanreotide) was conducted. Of the 50 AC-PT, 28 patients have been under treatment for >7 years and 22 patients have been under treatment for <7 years. The results revealed no significant differences in ASP, GH, and IGF-1 levels (Table 4).

Table 4. Median, minimum, maximum, and p values of the study parameters between the treatment course groups of acromegaly patients

Metabolites	<7 years Median (Min-Max)	>7 years Median (Min-Max)	p value
ASP (ng/mL)	5.81 (3.4-10.31)	5.35 (2.88-11.67)	0.377
GH (ng/mL)	3.8 (0.4-54)	1.4 (0.21-13.4)	0.014*
IGF-1 (ng/mL)	521 (105-1386)	480 (117-966)	0.491

p values calculated by Mann–Whitney U test, * significant difference <0.050

The blood pressure in AC-PTs was measured (28 with hypertension and 22 with normal tension), and the results indicated no significant differences in ASP and IGF-1 levels. Nevertheless, there was a considerable difference in GH levels (p=0.004) (Table 5).

Table 5. Median, minimum, maximum, and p values of patients with acromegaly between blood pressure groups

Metabolites	Hypertension Median (Min-Max)	Normal tension Median (Min-Max)	p value
ASP (ng/mL)	6.01 (2.88-11.67)	5.2 (3.34-10.31)	0.197
GH (ng/mL)	1.7 (0.21-7.2)	4.2 (0.6-54)	0.004
IGF-1 (ng/mL)	506.5 (117-1386)	455 (105-1120)	0.953

Positive correlations between GH and IGF-1 (p=0.000, r=0.578), FBG and BMI (p=0.016, r=0.359), weight and height (p=0.000, r=0.537), and weight and BMI (p=0.000, r=0.787), and a negative correlation between GH and weight (p=0.003, r=-0.434) were observed. Other correlation results showed no relationship between parameters. The correlation results are presented in Table 6.

In this study, linear regression analysis was performed to determine the relationship between ASP and various independent variables like GH, IGF-1, and FBG. The test showed a weak relationship between the independent variables and serum ASP levels, as indicated by an r^2 value of 0.059, meaning that only 5.9% of the variance in ASP levels could be explained by the model. The overall regression did not show a significant value (p=0.537). Between predictor variables, FBG had the highest standardized coefficient (Beta=0.235), followed by IGF-1 (Beta=0.081) and GH (Beta=-0.065); however, none of these predictors showed a statistically significant

Table 6. Correlations among all study parameters

Parameters	GH		IGF1		ASP		FBG		Weight		Height		BMI	
	r	p	r	p	r	p	r	p	r	p	r	p	r	p
GH (ng/mL)	1000	-	0.578**	**0.000**	−0.060	0.684	−0.183	0.208	−0.434**	**0.003**	−0.188	0.221	−0.030*	**0.046**
IGF1 (ng/mL)	0.578**	**0.000**	1000	-	−0.048	0.740	−0.055	0.704	−0.013	0.929	−0.060	0.693	0.110	0.472
ASP (ng/mL)	−0.060	0.684	−0.048	0.740	1.000	-	0.123	0.395	−0.104	0.490	0.034	0.824	−0.148	0.332
FBG (mg/mL)	−0.183	0.208	−0.055	0.704	0.123	0.395	1.000	-	0.202	0.179	−0.057	0.708	0.359*	**0.016**
Weight (kg)	−0.434**	**0.003**	−0.013	0.929	−0.104	0.490	0.202	0.179	1.000	-	0.537**	**0.000**	0.787**	**0.000**
Height (m)	−0.188	0.221	−0.060	0.693	0.034	0.824	−0.057	0.708	0.537**	**0.000**	1.000	-	−0.013	0.932
BMI (kg/m²)	−0.030*	**0.046**	0.110	0.472	−0.148	0.332	0.359*	**0.016**	0.787**	**0.000**	−0.013	0.932	1.000	-

r is Spearman's rho correlation coefficient. *Correlation was significant at the 0.05 level (2-tailed). **Correlation is significant at the 0.01 level (2-tailed).

association with serum ASP levels (p=0.170, p=0.663, and p=0.727, respectively).

DISCUSSION

ASP is a favorable selector share in the beginning and progress of processing endocrine or pathologic conditions, such as cancer, type 2 DM (T2DM), cardiomyopathy, polycystic ovarian syndrome, and obesity, and plays an important role in balancing energy metabolism (31).

A recent study by Lei Zhang et al. found that ASP levels were greater in adult T2DM patients than in healthy controls and might serve as a risk factor associated with the pathogenesis of T2DM; however, the researcher stated that it was not an ideal biomarker for prediction of T2DM (32). Other studies found that serum ASP levels were considerably higher in obese children than in lean and normal-weight children (33, 34). In addition, in 88 coronary artery disease patients, serum ASP were higher than that of healthy controls, suggesting a possible relation of ASP to the pathogenesis of acromegaly (35).

In 2020, Xiaoan Ke et al. revealed that ASP levels were lower in AC-PTs than in a healthy control group. Thus, we suggested the measurement of ASP levels in AC-PTs subgroups (gender, diabetes, duration of treatment course, and hypertension) (36).

The results showed no significant difference in ASP levels between AC-PTs and healthy controls. In addition, in the investigation involving 50 patients diagnosed with acromegaly, the analyses of subgroups categorized by gender, diabetes status, hypertension, and treatment course revealed no statistically significant outcomes. In the correlation study, no significant differences were found between ASP and any other parameter. In this survey, AC-PTs showed a similar gender distribution among acromegaly, analogous to that of Dal et al., 2021 which revealed a minor gender difference in the epidemiology of acromegaly.

Despite this, somatostatin (SST) drug (Lanreotide) binds to pancreatic β-cells (on SSTRs), then inhibits canals of voltage-gated calcium, leads to suppress the response of premature insulin to glucose, herewith restricting the energy transformation to adipose tissue, as we already know that ASP adipokine is a circulating hormone mainly secreted by white adipose tissue (37). The ASP in AC-PTs that course of treatment less than 7 years showed no significant difference for that in >7 years of SST treatment. This implies that the duration of treatment with SST does not directly affect ASP secretion in this research due to the regulation of ASP secretion, which includes multiple factors (38).

This study showed no correlation between disease course, FBG, GH, and IGF-1 levels, and serum ASP levels in AC-PTs. Despite past studies, ASP production is concerned with serum glucose. Nonetheless, Romere et al. presented that serum ASP levels were directly reduced with elevated serum glucose levels after feeding mice (16). After overnight fasting, the FBG was superfast, indicating that FBG plays a role in the systematization of ASP production. In addition, Wiecek et al. found that women's blood glucose levels were gradually decreased within 30 min after aerobic training, whereas serum ASP levels were gradually elevated, interpreted that reduced blood glucose might prompt increased production of ASP (39).

Our results disagree with the finding of Xiaoan Ke et al. 2020 who found lower ASP levels in AC-PTs with elevated FBG than in control individuals, although both were within the normal range (36).

This disagreement might stem from several factors, including differences in patient demographics, study designs, and methods of measuring serum ASP. It has also been suggested that the hormone ASP may not be affected by the hormonal changes typically associated with acromegaly due to genetic factors, lifestyle, or hormonal interplay mechanisms. A recent study showed that ASP is considered as an important influencer of the amelioration of metabolic disorders by

exercise and is likely to become an indispensable regulation target of exercise in forthcoming clinical practice and scientific research (40).

Another potential methodological issue is the use of measurement tools to evaluate serum ASP levels. Variability in laboratory techniques, equipment calibration, or the timing of sample collection can affect the accuracy and consistency of data. Additionally, hormonal interactions in acromegaly are complex, and ASP secretion may be modulated by multiple factors, such as insulin resistance, inflammatory cytokines, and adipokine, which were not investigated here.

Our findings might also replicate exclusive genetic or environmental characteristics of the Iraqi population, such as dietary designs or variations in GH treatment regimes, which may reduce the observed effects of acromegaly on ASP levels. These factors warrant further investigation to clarify the role of ASP in diverse populations. These suggestions may aid in clarifying ASP's role in metabolic disorders.

We studied ASP levels in diabetic and non-diabetic AC-PTs and found no notable changes in ASP levels between these groups. Because ASP possibly does not have a direct function in the diabetes of AC-PTs, indicating that metabolic conditions or hormonal changes linked with increased GH and IGF-1 could overshadow ASP secretion in diabetes or the pathophysiology of AC-PTs. This finding suggests that systemized ASP production is very complex and affected by the implicit factors of AC-PTs, not only diabetes (41). Regarding the sex group, there were no significant differences in ASP levels between males and females, possibly because the hormonal environment of AC-PTs may be a further homogenous metabolic process, where ASP secretion is regulated analogously regardless of acromegaly sex (42).

According to blood pressure in AC-PT, our results revealed no notable differences in ASP and IGF-1 levels, but there was a considerable difference in GH levels (p=0.004). This result may not be valuable because GH is normally released in pulses throughout the day and night, with peaks occurring mostly at night. As a result, it is challenging to interpret a single measure of GH in the blood, and it is not usually clinically applicable (43). The sample value may exhibit an increase when taken during a pulse and a decrease when taken between pulses.

The results of linear regression analyses displayed that FBG, GH, and IGF-1 collectively did not significantly predict serum ASP levels. Although FBG has a slightly stronger relationship with ASP than GH and IGF-1, none of these variables showed a statistical significance (p>0.05). Additionally, the model explains only 5.9% of the variance in serum ASP, indicating poor predictive power. These findings suggested that factors other than FBG, GH, and IGF-1 may play a more important role in regulating serum ASP levels. Further research is warranted to explore other potential determinants, such as adipokine, insulin resistance markers, and inflammatory cytokines.

Although our results did not reveal a significant difference in ASP levels, they provide valuable data to the literature. Further investigation of ASP as a marker of acromegaly is not necessary. Future research should focus on exploring other potential biomarkers or pathways to better understand the metabolic aspects of acromegaly and improve patient management strategies.

The limitation of this study was the relatively small sample size. However, acromegaly is a rare disease that limits the number of available patients for research. Additionally, the genetic and environmental specificity of the Iraqi population could influence the observed results, limiting their applicability to other populations. The potential influence of unaccounted factors such as diet, treatment regimens, and genetic variability may also affect these findings.

Conclusion

Levels of serum ASP have no difference between Iraqi AC-PT and the normal control group; according to this, ASP is not affected by the hormonal changes that are typically associated with acromegaly due to genetic factors, lifestyle, or patient behavior. Additionally, ASP can not be a helpful biomarker as there is no significant difference between study parameters in the DM and non-DM groups of AC-PTs. Moreover, ASP levels are not affected by long-term exposure to high GH levels and disease courses.

Acknowledgements

We would like to thank the scientific community of the National Diabetes Center and all individuals who continue to share medical knowledge with us for offering the necessary facilities for this research and for acknowledging the consent of their patients to publish this study.

Ethics Committee Approval	Ethics approval for the study was obtained from Mustansiriyah University National Diabetes Center Ethics Committee (15 Sep 2023).
Peer Review	Externally peer-reviewed.
Author Contributions:	Conception/Design of Study – O.Y.S., S.E.A., K.G., L.A., A.M.R.; Data Acquisition – O.Y.S., S.E.A., K.G., L.A., A.M.R.; Data Analysis/Interpretation - O.Y.S., S.E.A., K.G., L.A., A.M.R.; Drafting Manuscript – O.Y.S., S.E.A., K.G., L.A., A.M.R.; Critical Revision of Manuscript – O.Y.S., S.E.A., K.G., L.A., A.M.R.; Final Approval and Accountability – O.Y.S., S.E.A., K.G., L.A., A.M.R.
Conflict of Interest:	The authors declare no conflict of interest.

Financial Disclosure: The authors declare that they received no financial support for this study.

Author Details

Omar Yasir Shakir
[1] National Diabetes Center, Mustansiriyah University, Baghdad, Iraq
0009-0006-8834-5143

Safaa Ehssan Atta
[1] National Diabetes Center, Mustansiriyah University, Baghdad, Iraq
0009-0004-8252-9967

Karam Gharab
[1] National Diabetes Center, Mustansiriyah University, Baghdad, Iraq
0000-0003-4879-3671

Lujain A. Ghannawi
[1] National Diabetes Center, Mustansiriyah University, Baghdad, Iraq
0009-0009-1067-6550 lujainghannawi@uomustansiriyah.edu.iq

Abbas M. Rahmah
[1] National Diabetes Center, Mustansiriyah University, Baghdad, Iraq
0000-0003-0368-4383

REFERENCES

1. Vilar L, Vilar CF, Lyra R, Lyra R, Naves LA. Acromegaly: clinical features at diagnosis. Pituitary 2017; 20: 22-32.
2. Colao A, Pivonello C, Grasso LFS, Pirchio R. Acromegaly. In: La Rosa, S., Uccella, S. (eds) Endocrine Pathology. Encyclopedia of Pathology. Cham: Springer; 2022. p. 9-11.
3. Ershadinia N, Tritos NA. Diagnosis and treatment of acromegaly: an update. Mayo Clin Proc 2022; 97(2): 333-46.
4. Saadi MT, Mohammed NUG, Abed BA, Farhan LO, Salman IN. Validity of galactin-3 in acromegaly: comparison with traditional markers. Ir J Med Sci 2024; 193(4): 1837-41.
5. Farhan LO, Abed BA, Salman IN. Insulin like growth factor binding protein 7 as a novel diagnostic marker in sera of Iraqi patients with acromegaly. Baghdad Sci J 2023; 20(3 Suppl): 0979.
6. Chanson P, Salenave S. Acromegaly. Orphanet J Rare Dis 2008; 3: 1-17.
7. Ghannawi L, Gharab K, Hadi M, Shakir O, Rahmah A. Spexin level in growth hormone deficiency Iraqi children. Ukr Biochem J 2024; 96(4): 55-61.
8. Turki TG. The Association of growth hormone releasing hormone gene polymorphism with acromegaly in patients from Iraq. AL-Qasim Green University, Master thesis. 2023.
9. Sharma R, Kopchick JJ, Puri V, Sharma VM. Effect of growth hormone on insulin signaling. Mol Cell Endocrinol 2020; 518: 111038.
10. Olarescu NC, Bollerslev J. The impact of adipose tissue on insulin resistance in acromegaly. Trends Endocrinol Metab 2016; 27(4): 226-37.
11. Kuker AP, Shen W, Jin Z, Chen J, Bruce JN, Freda PU. Long-term outcome of body composition, ectopic lipid, and insulin resistance changes with surgical treatment of acromegaly. J Endocr Soc 2023; 7(5): bvad028.
12. Abreu A, Román-González A, Tovar H, Maestre K, Builes-Barrera CA, Nessim E, et al. Characterizing the burden of uncontrolled acromegaly–a description of real-world patient characteristics in Colombia. Rev Colomb Endocrinol Diabetes Metab 2022; 9(2): e678.
13. Bona C, Prencipe N, Berton A, Bioletto F, Parasiliti-Caprino M, Gasco V, et al. Mean GH profile is more accurate than single fasting GH in the evaluation of acromegaly disease control during somatostatin receptor ligands therapy. J Endocrinol Invest 2022; 45(10): 1955-65.
14. Peixe C, Sánchez-García M, Grossman AB, Korbonits M, Marques P. Biochemical discrepancies in the evaluation of the somatotroph axis: Elevated GH or IGF-1 levels do not always diagnose acromegaly. Growth Horm IGF Res 2022; 64: 101467.
15. Gozel N, Kilinc F. Investigation of plasma asprosin and saliva levels in newly diagnosed type 2 diabetes mellitus patients treated with metformin. Endokrynol Pol 2021; 72(1): 37-43.
16. Romere C, Duerrschmid C, Bournat J, Constable P, Jain M, Xia F, et al. Asprosin, a fasting-induced glucogenic protein hormone. Cell 2016; 165(3): 566-79.
17. Baykus Y, Yavuzkir S, Ustebay S, Ugur K, Deniz R, Aydin S. Asprosin in umbilical cord of newborns and maternal blood of gestational diabetes, preeclampsia, severe preeclampsia, intrauterine growth retardation and macrosemic fetus. Peptides 2019; 120: 170132.
18. Alan M, Gurlek B, Yilmaz A, Aksit M, Aslanipour B, Gulhan I, et al. Asprosin: a novel peptide hormone related to insulin resistance in women with polycystic ovary syndrome. Gynecol Endocrinol 2019; 35(3): 220-3.
19. Atta SE, Abed BA, Salman IN, Ghannawi LA. Review of Asprosin as new biomarker for diagnosis of different diseases. Univ Thi-Qar J Sci 2023; 10(2): 160-4.
20. Janoschek R, Hoffmann T, Morcos YAT, Sengle G, Dötsch J, Hucklenbruch-Rother E. Asprosin in pregnancy and childhood. Mol Cell Pediatr 2020; 7: 1-5.
21. Farhan LO, Salman IN. A review on the role of novel adipokine Isthmin-1 and Subfatin in human type 2 diabetes mellitus. Univ Thi-Qar J Sci 2023; 10(2): 181-6.
22. Lefta NA, Abed AY, Abed BA. Estimation of Asprosin levels in female Iraqi patients with type 2 diabetes and hypothyroidism. J Med Chem Sci 2023; 6(2): 433-9.
23. Liu Y, Long A, Chen L, Jia L, Wang Y. The Asprosin–OLFR734 module regulates appetitive behaviors. Cell Discov 2020; 6(1): 19.
24. Yuan M, Li W, Zhu Y, Yu B, Wu J. Asprosin: a novel player in metabolic diseases. Front Endocrinol 2020; 11: 64.
25. Wang CY, Lin TA, Liu KH, Liao CH, Liu YY, Wu VC, et al. Serum asprosin levels and bariatric surgery outcomes in obese adults. Int J Obes (Lond) 2019; 43(5): 1019-25.
26. Li E, Shan H, Chen L, Long A, Zhang Y, Liu Y, et al. OLFR734 mediates glucose metabolism as a receptor of asprosin. Cell Metab 2019; 30(2): 319-28.e8.
27. Nijenhuis-Noort EC, Berk KA, Neggers SJ, van der Lely AJ. The fascinating interplay between growth hormone, insulin-like growth factor-1, and insulin. Endocrinol Metab 2024; 39(1): 83.
28. Wiecek M, Szymura J, Kusmierczyk J, Lipowska M, Szygula Z. Whole-body cryotherapy improves asprosin secretion and insulin sensitivity in postmenopausal women–perspectives in the management of type 2 diabetes. Biomolecules 2023; 13(11): 1602.
29. Muthu ML, Reinhardt DP. Fibrillin-1 and fibrillin-1-derived asprosin in adipose tissue function and metabolic disorders. J Cell Commun Signal 2020; 14(2): 159-73.
30. Kim JH, Chae HW, Chin SO, Ku CR, Park KH, Lim DJ, et al. Diagnosis and treatment of growth hormone deficiency: a position statement from the Korean Endocrine Society and Korean Society of Pediatric Endocrinology. Endocrinol Metab 2020; 35(2): 272.
31. Hekim MG, Kelestemur MM, Bulmus FG, Bilgin B, Bulut F, Gokdere E, et al. Asprosin, a novel glucogenic adipokine: a potential therapeutic implication in diabetes mellitus. Arch Physiol Biochem 2023; 129(5): 1038-44.
32. Zhang L, Chen C, Zhou N, Fu Y, Cheng X. Circulating asprosin concentrations are increased in type 2 diabetes mellitus and independently associated with fasting glucose and triglyceride. Clin Chim Acta 2019; 489: 183-8.
33. Wang M, Yin C, Wang L, Liu Y, Li H, Li M, et al. Serum asprosin concentrations are increased and associated with insulin resistance in children with obesity. Ann Nutr Metab 2020; 75(4): 205-12.
34. Sunnetci Silistre E, Hatipogl HU. Increased serum circulating asprosin levels in children with obesity. Pediatr Int 2020; 62(4): 467-76.
35. Moradi N, Fouani FZ, Vatannejad A, Bakhti Arani A, Shahrzad S, Fadaei R. Serum levels of asprosin in patients diagnosed with coronary artery disease (CAD): a case-control study. Lipids Health Dis 2021; 20(1): 88.

36. Ke X, Duan L, Gong F, Zhang Y, Deng K, Yao Y, et al. Serum levels of asprosin, a novel adipokine, are significantly lowered in patients with acromegaly. Int J Endocrinol 2020: 8855996.
37. Kumar U, Singh S. Role of somatostatin in the regulation of central and peripheral factors of satiety and obesity. Int J Mol Sci 2020; 21(7): 2568.
38. Hoffmann JG, Xie W, Chopra AR. Energy regulation mechanism and therapeutic potential of asprosin. Diabetes 2020; 69(4): 559-66.
39. Wojciak G, Szymura J, Szygula Z, Gradek J, Wiecek M. The effect of repeated whole-body cryotherapy on SIRT1 and SIRT3 concentrations and oxidative status in older and young men performing different levels of physical activity. Antioxidants 2020; 10(1): 37.
40. Liu L, Liu Y, Huang M, Zhang M, Zhu C, Chen X, et al. The effects of asprosin on exercise-intervention in metabolic diseases. Front Physiol 2022; 13: 907358.
41. Challa TD. Regulation of adipogenesis and energy metabolism through the cross-talk between adipose tissue, gastrointestinal wall and the brain: Evidence from adipokines and incretin hormones. ETH Zurich, Doctoral thesis; 2014.
42. Dal J, Skov BG, Andersen M, Feldt-Rasmussen U, Feltoft CL, Karmisholt J, et al. Sex differences in acromegaly at diagnosis: a nationwide cohort study and meta-analysis of the literature. Clin Endocrinol 2021; 94(4): 625-35.
43. Wang W, Duan X, Huang Z, Pan Q, Chen C, Guo L. The GH-IGF-1 axis in circadian rhythm. Front Mol Neurosci 2021; 14: 742294.

İSTANBUL UNIVERSITY PRESS

Experimed 2025, 15 (1): 57–65

https://doi.org/10.26650/experimed.1440182

Submitted: 20.02.2024
Revision Requested: 16.06.2024
Last Revision Received: 17.02.2025
Accepted: 18.02.2025
Published Online 28.03.2025

Experimed

Research Article

Open Access

Evaluation of the Effect of Caffeine Consumption on Cognitive Functions by Electroencephalography

Fatma Ozlem [1,2], Asli Zengin Turkmen [2], Gokcer Eskikurt [3,4], Asli Ceren Macunluoglu [5], Asiye Nurten [2] & Ayfer Dayi [6]

[1] Department of Physiology, Institute of Health Sciences, Dokuz Eylul University, Izmir, Turkiye
[2] Department of Physiology, Faculty of Medicine, Istanbul Yeni Yuzyil University, Istanbul, Turkiye
[3] Department of Psychology, Faculty of Humanities and Social Sciences, Istinye University, Istanbul, Turkiye
[4] Innovative Center of Applied Neurosciences, Istinye University, Istanbul, Turkiye
[5] Institute of Health Sciences, Department of Biostatistics, Uludag University, Bursa, Turkiye
[6] Department of Physiology, Faculty of Medicine, Dokuz Eylul University, Izmir, Turkiye

Abstract

Objective: To evaluate cognitive performance and neurophysiological changes after caffeine consumption in individuals who regularly consume different amounts of caffeine.

Materials and Methods: Thirty-seven people aged 18-25 were divided into two groups according to their caffeine consumption as less than 3 mg/kg/day (low consumption group; LC) and more than 3 mg/kg/day (high-consumption group; HC). Electroencephalography (EEG) and Montreal Cognitive Assessment test (MoCA) were performed in both groups (baseline records). One week later, caffeinated (Caff) and decaffeinated (Decaff) coffee were randomly given to LC and HC. Thus, four groups were formed (LC+Caff, LC+Decaff, HC+Caff and HC+Decaff). EEG was repeated one hour after coffee, and MoCA was performed within 20 minutes.

Results: In baseline eyes-opened EEG, the power of beta2 and delta were higher in the LC group than in the HC. After coffee consumption in the eyes-opened EEG, alpha1 and alpha2 power were significantly reduced in the HC+Caff. Following coffee consumption, the MoCA score increased significantly in the HC+Decaff and LC+Caff groups compared with the baseline.

Conclusion: Our study showed that low caffeine consumers had increased brain activity and cognitive performance post consumption high amounts of caffeine. However, this effect was less in high caffeine consumers. Therefore, caffeine habituation may alter the brain's response to caffeine.

Keywords Caffeine · Cognition · Electroencephalography

Citation: Ozlem, F., Zengin Turkmen, A., Eskikurt, G., Macunluoglu, A. C., Nurten, A. & Dayi, A. Evaluation of the effect of caffeine consumption on cognitive functions by electroencephalography. Experimed 2025; 15(1): 57-65. DOI: 10.26650/experimed.1440182

Corresponding author: Fatma Ozlem fatma.ozlem@yeniyuzyil.edu.tr

INTRODUCTION

Caffeine, a psychoactive substance found in coffee, is consumed daily by 80% of the global population, making it a significant focus in cognitive and physiological research (1, 2). The European Food Safety Authority reported that a person can consume more than 200 mg or 3 mg/kg of caffeine at a time and a maximum of 400 mg of caffeine can be consumed in 24 hours (3). Caffeine's cognitive-enhancing effects are largely mediated through its antagonistic action on adenosine A1 and A2A receptors in the brain, which increases neurotransmitter release and improves attention and alertness (4).

Cognition involves various mental processes, such as memory, executive functions, and attention, which are critical for adapting to new situations (5, 6). These cognitive processes are underpinned by specific patterns of brain activity, which can be effectively studied using electroencephalography (EEG). EEG, a noninvasive technique for measuring brain electrical activity, provides valuable information about neurophysiological changes associated with cognitive processes (7). When examining the EEG frequency bands in more detail, alpha waves from EEG frequency bands are associated with attention and working memory; beta waves are most prominent during wakefulness and the performance of mental functions; delta waves are dominant during deep sleep; and theta waves occur in certain sleep stages and during emotional stress (8). Understanding how caffeine modulates these parameters can provide deeper insights into its effects on cognition (9).

The Montreal Cognitive Assessment (MoCA) is a brief cognitive assessment tool designed to identify mild cognitive impairment and it evaluates various cognitive domains, such as attention, executive function, memory, language, visuospatial ability, numerical skills, and orientation (10).

Some studies have demonstrated significant improvements in attention and memory with moderate caffeine intake, while certain studies report insignificant effects, especially among regular coffee consumers (9, 11). Additionally, EEG studies evaluating the effects of caffeine on brain activity yielded conflicting results, making it difficult to understand caffeine-induced neurophysiological changes (12).

The study hypothesis is that people with habitual high caffeine consumption exhibit higher cognitive performance after consuming caffeinated coffee, whereas this effect is less pronounced in those with habitual low caffeine consumption. The aim of this study was to examine the neurophysiological effects of caffeinated or decaffeinated coffee consumption using EEG and its effects on cognitive functions with the MoCA test in individuals with habitual consumption of low or high caffeine.

MATERIALS AND METHODS

Study Design and Participants

This was a single blended randomized controlled study. Approval was received from the Non-Interventional Clinical Research Ethics Committee of Dokuz Eylul University, with approval number 2020/28-26.

The sample size was calculated using GPower 3.1 software with a power of 90% and an α value of 0.05. The minimum required sample size was estimated to be 17 participants per group, totaling 34 participants. For possible errors, the sample size was increased by 10%, and 37 volunteers were included in the study. Thirty-seven university students (22 females, 15 males) aged 18-25 years participated in the study. Initially, participants were enlisted from a database containing their reported caffeine consumption habits. The participants' demographic characteristics, including age and gender, were documented. We were unable to exclude participants based on their smoking and alcohol consumption. However, to minimize potential confounding effects, participants were instructed to refrain from smoking for at least 12 hours and from alcohol consumption for at least 24 hours before the study.

The participants were then requested to fill out a survey specifically prepared by us to assess their average daily caffeine intake from tea, coffee, cocoa, and caffeinated soft drinks. According to the survey, the participants were categorized into two groups. The low consumption group (LC) included individuals who consumed less than 3 mg/kg/day of caffeine. The high consumption group (HC) included those who consumed more than 3 mg/kg/day caffeine (3). On the first day, EEG recordings were conducted for 5 min with participants' eyes-opened and closed, followed by the MoCA test. The data obtained on the first day were considered as baseline measurements.

Seven days later, each main group was randomly and blindly divided into two subgroups. One subgroup received caffeinated coffee containing 200 mg caffeine (Caff), while the other received decaffeinated coffee (Decaff). In this case, the study was consisted of four groups: LC+Caff, LC+Decaff, HC+Caff, and HC+Decaff. One hour after coffee consumption, EEG recordings were taken with eyes-opened and closed for 5 minutes each. After quickly removing the EEG cap, the MoCA test was performed within 20 min, and the study was terminated.

EEG recording was performed using an electrocap with 19 silver chloride electrodes (Fp1, Fp2, F7, F3, Fz, F4, F8, T3, C3, Cz, C4 T4, T5, P3, Pz, P4, T6, O1 and O2). The electrodes were placed on the cap in accordance with the International 10-20 system and gel was used to increase the conductivity. EEG data were recorded in the range of 0-30 Hz, recorded using a Mitsar-EEG-201 system (Mitsar Co. Ltd. Saint Petersburg, Russia). WinEEG program (Version 2.130.101 Mitsar Co. Ltd. St. Petersburg, Russia) compatible with the system was used as the recording program. EEG activity was recorded in the resting and sitting position.

The MoCA test, which is scored out of 30 points, considers a score of 21 or above to be normal (13). In the MoCA test repeated 1 week later, modifications were made to certain sections to minimize recall effects. Due to the complex structure of the MoCA, which includes words, pictures, and sequences, these adjustments were designed to reduce recall bias while preserving the reliability of the test. For instance, in the word recall task, words starting with different letters were used, and in the number-letter matching task, the positions of the numbers and letters were altered.

Statistical Analyses

Statistical analysis was conducted using the IBM SPSS 20.0 software package (IBM Corp., Armonk, NY, USA).

The MoCA test scores were compared using the paired samples t-test. The WinEEG program was used for the analysis of EEG data. EEG epochs with artifacts were determined in two stages, automatic and manual, and they were excluded from the evaluation. In the first step, epochs with amplitudes exceeding 100 µV were marked and automatically excluded. In the second stage, the remaining artifact epochs were reviewed in more detail and manually excluded from the evaluation. The spectral power was calculated using the fast fourier transform (FFT) method. After calculating all 19 electrodes' average spectrum power, the frequency was separated into delta (0.5-3.9 Hz), theta (4.0-7.4 Hz), alpha1 (7.5-9.9 Hz), alpha2 (10.0-13.9 Hz), beta1 (14.0-19.9 Hz), and beta2 (20.0-30.0 Hz). In the statistical evaluation, the power and frequency changes between the two measurements of the waves obtained from the EEG records of the four groups were compared using repeated measures ANOVA (RM-ANOVA). Post hoc analyses were conducted using the Bonferroni method. The baseline EEG recordings of the LC and HC groups were compared using multivariate ANOVA (MANOVA). Data obtained from EEG recordings of caffeinated and decaffeinated coffee consumers were analyzed using MANOVA. EEG results recorded with eyes open and closed were evaluated separately. The findings were assessed with a confidence level of 95%, and values for $p<0.05$ were considered statistically significant.

RESULTS

A total of 37 participants, including 22 females and 15 males, were enrolled in the study, with a mean age of 22.24 ± 0.33 years. According to the survey, 17 participants (11 females) in the LC group had a mean age of 21.88 ± 1.99, whereas 20 participants (11 females) were in the HC group with a mean age of 22.5 ± 2.06.

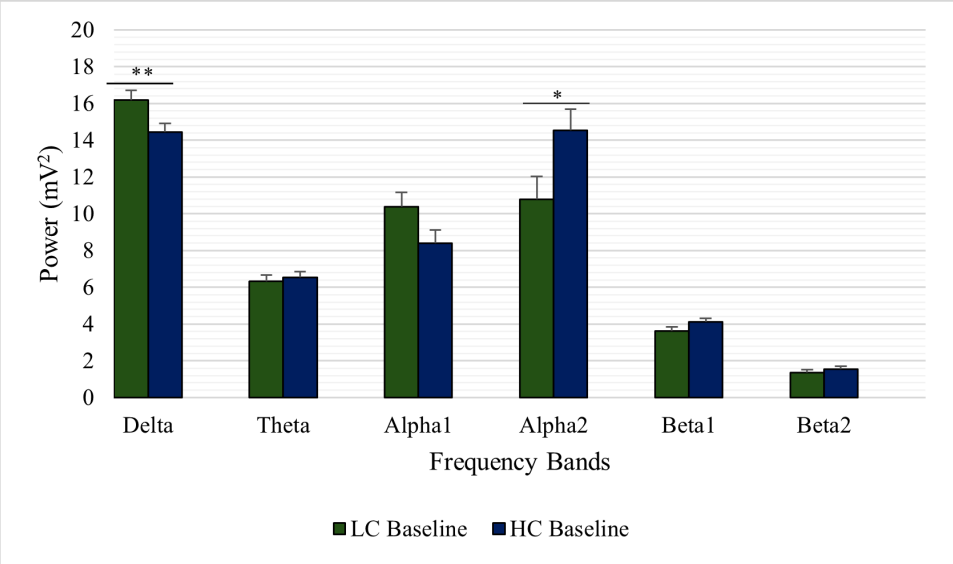

Figure 1. Baseline eyes-closed EEG findings for the LC and HC groups, MANOVA.
*the power of alpha2 was significantly higher (p=0.026),
**the power of delta was significantly lower (p=0.014) in the HC group when compared with LC group.

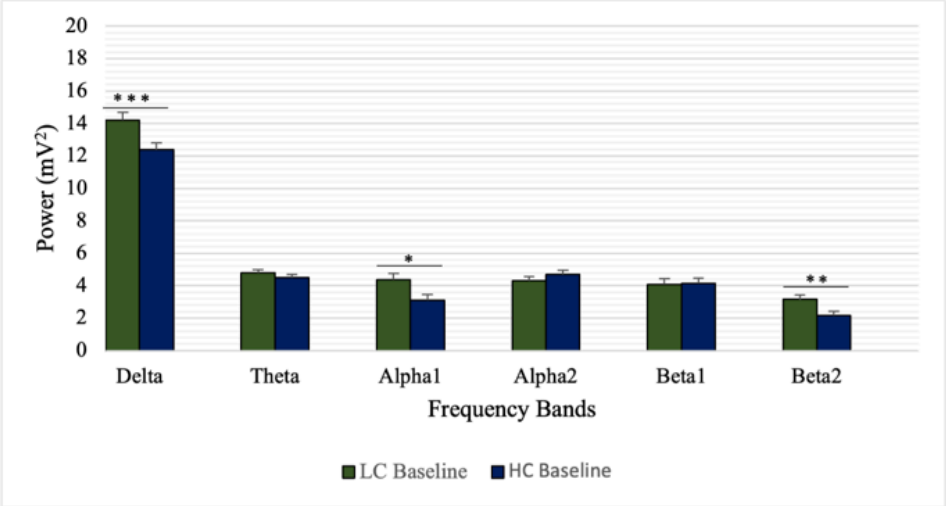

Figure 2. Baseline eyes-opened EEG findings for the LC and HC groups, MANOVA. *the power of alpha1 was significantly higher (p=0.016), **the power of beta2 was significantly higher (p=0.013), *** the power of delta was significantly higher (p=0.005) in the LC group when compared with HC group.

When divided into four groups, 9 participants (6 females) were in the LC+Caff group with a mean age of 21.77 ± 1.92, 8 participants (5 females) in the LC+Decaff group with a mean age of 22.00 ± 2.20, 10 participants (6 females) in the HC+Caff group with a mean age of 22.50 ± 2.27 and 10 participants (5 females) in the HC+Decaff group with a mean age of 22.60 ± 1.95.

EEG Results

In the baseline eyes closed EEG condition, the power of alpha2 was significantly higher in the HC group compared with the LC group ($F_{1,7}$=5.003; p=0.026), and the power of delta was significantly lower ($F_{1,7}$=6.31; p=0.014) (Figure 1). In the baseline eyes-opened condition, the power of alpha1 ($F_{1,7}$=5.885; p=0.016), beta2 ($F_{1,7}$=6.248; p=0.013), and delta ($F_{1,7}$=8.014; p=0.005) was significantly higher in the LC group than in the HC group (Figure 2).

In the eyes-closed EEG condition, the power of delta ($F_{1,3}$=19.504; p<0.0001) and theta ($F_{1,3}$=6.976; p=0.009) was significantly lower, while the power of beta2 ($F_{1,3}$=10.459; p=0.001) was significantly higher in the LC+Caff group after consuming coffee compared with the LC+Decaff group (Figure 3). In the eyes-closed condition of the HC+Decaff group, it was found that the power of alpha2 was significantly decreased compared with the HC+Decaff group's own baseline ($F_{1,9}$=9.166; p=0.014) (Figure 4). In the eyes-opened condition of the HC+Caff group, the power of alpha1 was significantly decreased compared with baseline ($F_{1,9}$=9.630; p=0.013).

In the eyes-opened condition of the LC+Caff group, the power of beta2 significantly increased compared with the LC+Caff group's own baseline ($F_{1,8}$=5.687; p=0.044). In the eyes-opened condition of the LC+Decaff group, it was found that the power of beta2 significantly decreased compared with the LC+Decaff group's own baseline ($F_{1,7}$=12.557; p=0.009) (Figure 5). In the eyes-opened after coffee intake, the power of alpha1 ($F_{1,3}$=11.310; p=0.001) and alpha2 ($F_{1,3}$=17.835; p<0.0001) were significantly lower, and the power of delta ($F_{1,3}$=9.985; p=0.002) was higher in the HC+Caff group compared with the HC+Decaff group (Figure 6). In the eyes closed condition after coffee intake, the power of alpha1 ($F_{1,3}$=6.443; p=0.012) and alpha2 ($F_{1,3}$=4.653; p=0.032) were significantly lower in the HC+Caff group compared with the HC+Decaff group.

Table 1. Difference in MoCA scores between baseline and after coffee

Groups	n	Baseline Mean ± SE	After coffee Mean ± SE
LC+Caff	9	23.5 ± 1.43	26.1 ± 0.93*
LC+Decaff	8	22.5 ± 1.25	24.9 ± 1.11
HC+Caff	10	24.9 ± 1.23	25.5 ± 0.93
HC+Decaff	10	24.5 ± 0.83	26.5 ± 1.02**

*p=0.038, **p=0.002 compared with the baseline, paired samples t-test. MoCA: Montreal Cognitive Assessment test; LC: Low caffeine consumption group; HC: High caffeine consumption group; Caff: Caffeinated coffee; Decaff: Decaffeinated coffee; SE: Standart error.

MoCA Test Results

A significant increase was observed in MOCA test scores after caffeine intake in LC+Caff (p=0.038) and HC+Decaff (p=0.002) groups compared with the baseline (Table 1).

DISCUSSION

Many studies investigating the effect of caffeine on alpha waves have indicated that caffeine reduces alpha power in humans and rats (14, 15). In our study, alpha1 and alpha2

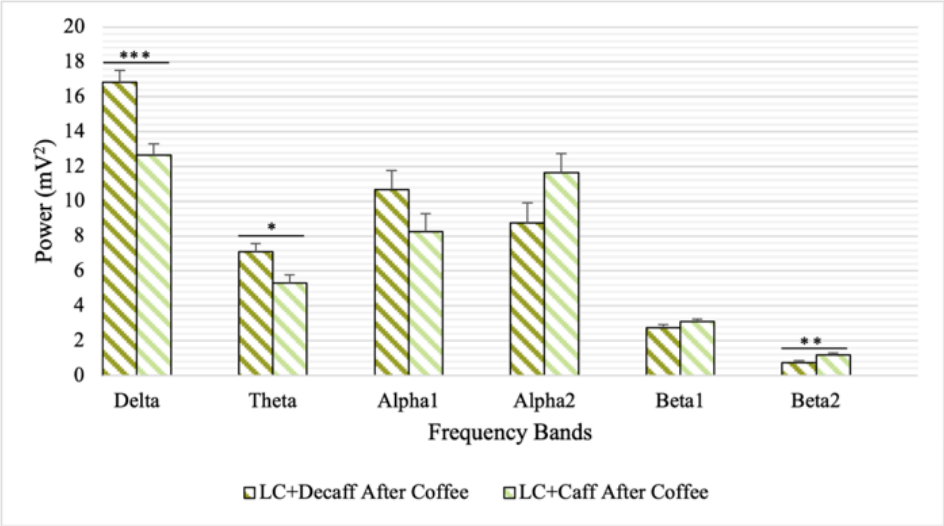

Figure 3. Eyes closed EEG after coffee consumption findings for the LC+Caff and LC+Decaff groups, MANOVA. *the power of theta was significantly lower (p=0.009), **the power of beta2 was significantly higher (p=0.001), ***the power of delta was significantly lower (p=0.000) in the LC+Caff group when compared with LC+Decaff group.

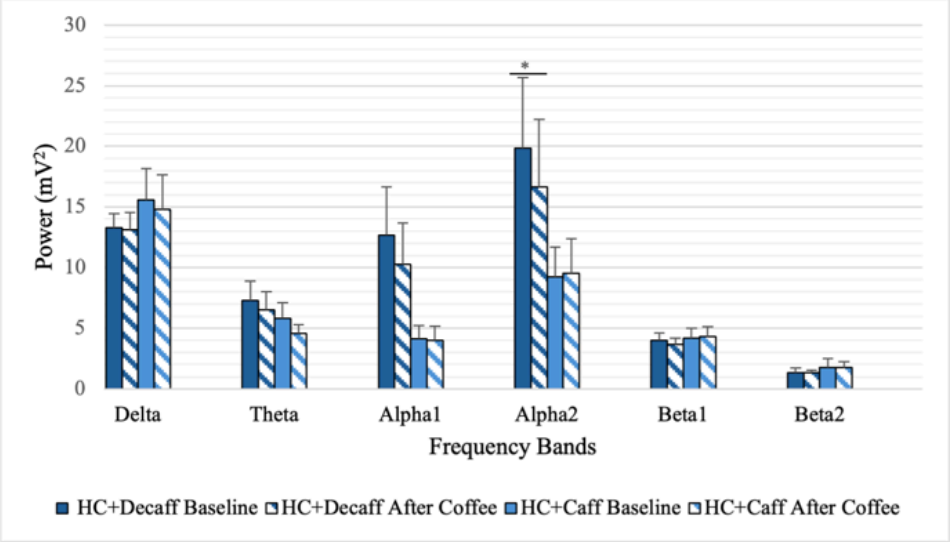

Figure 4. The comparison between the baseline and after coffee consumption in eyes-closed EEG findings for the HC+Caff and HC+Decaff groups (RM-ANOVA). *the power of alpha2 was significantly lower (p=0.014) in the HC+Decaff group when compared with baseline.

power were significantly lower in the HC+Caff group than in the HC+Decaff group in both eyes closed and opened EEG. In the eyes-opened EEG findings of the HC+Caff group, alpha1 power was significantly reduced after coffee consumption compared to the HC+Caff group's own baseline. However, in the LC+Caff group with both eyes open and closed EEG recordings, no significant decrease in alpha1 and alpha2 power were observed compared with the LC+Decaff group. Unlike our study, Foxe et al. showed that caffeine consumption (50 mg) significantly reduced alpha power in individuals consuming less than 3 mg/kg caffeine per day (16). In another study, caffeine consumption (200 mg) caused a significant decrease in alpha1 and alpha2 power in both eyes-opened and closed EEG recordings in subjects consuming 300 mg or more of caffeine daily (17). Since individuals who consume less coffee have a minimal regular intake of caffeine, their responses to the acute effects of caffeine may be less pronounced. These individuals may not have developed caffeine tolerance to the same extent as those who consume more coffee and thus may exhibit a typical neurophysiological response to caffeine without significant changes in alpha power. While both our study and previous research point to caffeine's potential impact on alpha power, the varying results may reflect differences in participant characteristics,

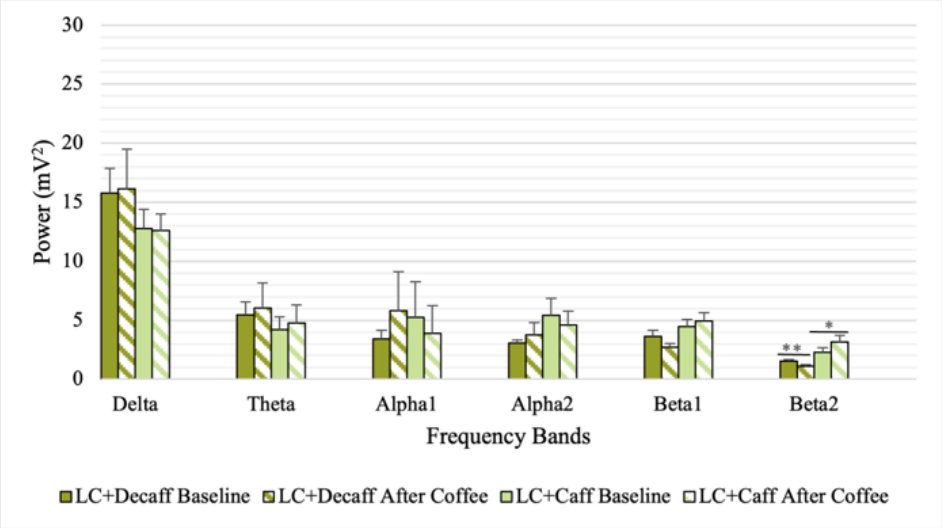

Figure 5. The comparison between the baseline and after coffee consumption in eyes-opened EEG findings for the LC+Caff and LC+Decaff groups (RM-ANOVA). *the power of beta2 was significantly higher (p=0.044) in the LC+Caff group when compared with baseline, **the power of beta2 was significantly lower (p=0.009) in the LC+Decaff group when compared with baseline.

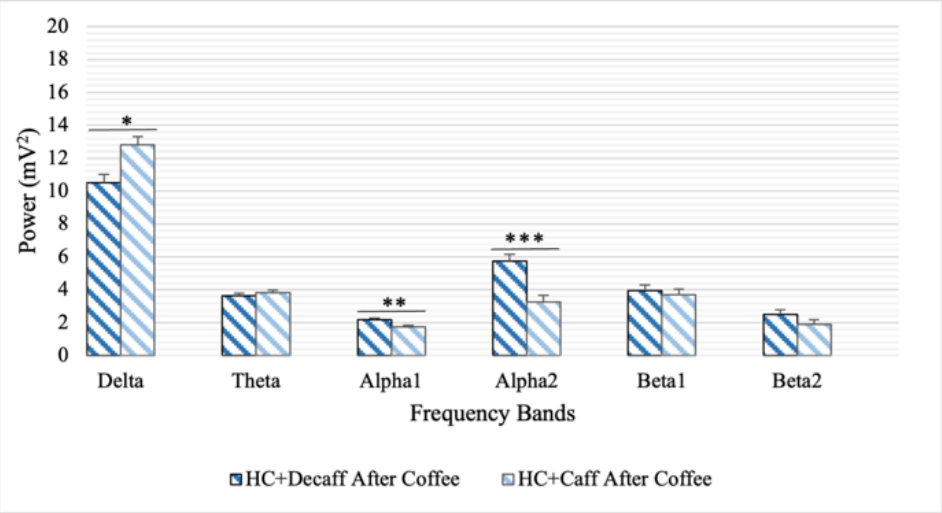

Figure 6. Eye-opened EEG after coffee consumption findings for the HC+Caff and HC+Decaff groups, MANOVA. *the power of delta was significantly higher (p=0.002), **the power of alpha1 was significantly lower (p=0.001), ***the power of alpha2 was significantly lower (p=0.000) in the HC+Caff group compared with the HC+Decaff group.

caffeine consumption levels, and the development of caffeine tolerance, all of which may modulate caffeine's effect on brain activity.

Research findings indicate that caffeine increases the power of beta, which is associated with an increase in mental activity (18). In a study conducted with women who consumed large amounts of coffee (150 mL×6.4 cups/day), EEG was recorded by giving different amounts of caffeine to the subjects. It was found that the power of the beta wave was significantly higher in groups that consumed highly caffeinated coffee (19). In our study, it was observed that in the eyes-closed EEG record of the LC+Caff group, the power of beta2 increased significantly after the intake of caffeine compared with the LC+Caff group's own baseline. In addition, in the eyes-closed EEG record, the power of beta2 was significantly higher in the LC+Caff group than in the LC+Decaff. However, no significant increase in beta power was observed in the HC+Caff group compared with the HC+Decaff group. An increase in beta power was not observed in the HC+Caff and HC+Decaff groups when compared with their own baseline. High caffeine consumption may lead to caffeine tolerance in individuals, which can attenuate the effect of caffeine on beta power.

In the findings of our study, it was observed that in the baseline recordings with both eyes-opened and closed, the

delta power was higher in the LC group than in the HC group. In the eyes-closed EEG data, the power of delta was significantly lower in the LC+Caff group than in the LC+Decaff group. Furthermore, no significant decrease in eyes-closed delta power was observed in the HC+Caff group compared with the HC+Decaff group. Siepmann et al. showed that delta power was significantly lower in those consuming 200 mg/day of caffeinated coffee (17). In another study, caffeine consumption (200-400 mg/day) significantly reduced delta wave power in EEG recordings, both with eyes open and closed (20). The observed reduction in delta power in the LC+Caff group is consistent with previous studies suggesting that caffeine has a stimulating effect, which may lead to a decrease in the power of slow-wave activity such as delta waves (21).

The lack of a significant change in delta power in the HC+Caff group indicates that high caffeine exposure may limit this effect.

Conversely, the different results of our study regarding eyes-opened EEG findings, the power of delta was significantly higher in the HC+Caff group than in the HC+Decaff group. This result is in contrast to the anticipated reduction in delta power associated with caffeine consumption. A possible explanation could be the development of tolerance in habitual high-dose caffeine consumers, leading to altered neurophysiological responses. This divergence from the expected outcomes highlights the need for further research to explore how chronic caffeine consumption modifies brainwave activity and its implications for cognitive function.

In our study, we observed a significant improvement in cognitive performance in the LC+Caff group following coffee intake, which suggests that individuals with lower habitual caffeine consumption may benefit more from its cognitive-enhancing effects. Haskell et al.'s study (22) included groups with low and high caffeine intake (less than 50 mg/day and more than 50 mg/day, respectively). Although no significant differences were observed in cognitive performance. The study highlighted the complexity of caffeine's effects, which might depend on the dosage, individual sensitivity, and baseline caffeine consumption. However, it should be noted that the low caffeine intake in Haskell's study might not have been sufficient to elicit noticeable changes in cognitive performance, which could support the differing results in our study. A separate study involving college students who consumed caffeine chronically compared cognitive performance between one half of the group, which consumed 4 mg/kg/day of caffeine, and the other half, which abstained (23). In contrast to our findings, this study did not report a notable distinction in cognitive performance between chronic caffeine consumers and non-consumers. Zhang et al. evaluated cognitive performance after administering 3, 6, or 9 mg/kg of caffeine and found that only the group consuming 3 mg/kg showed a significant improvement in cognition (24). This suggests that lower caffeine doses may be particularly effective for enhancing cognitive performance in individuals with lower baseline caffeine intake, similar to the findings of our study where significant cognitive improvement was observed in the LC+Caff group.

These contrasting results may reflect differences in study design or caffeine dosages. Notably, our results indicate that regular high caffeine consumers (HC+Caff group) might develop tolerance to caffeine's cognitive benefits, supporting the hypothesis that the effects of caffeine are more pronounced in individuals with lower baseline consumption. This tolerance mechanism could explain the absence of significant cognitive enhancement in high-consumers, as also claimed by previous literature (25). Further research is required to explore the interplay between habitual caffeine intake, tolerance development, and cognitive performance.

In our study, we observed a significant increase in cognitive performance in the HC+Decaff group, which could potentially be influenced by placebo-like effects. This finding highlights a potential interplay between expectations, caffeine consumption habits, and cognitive outcomes.

Wang et al. reported that individuals consuming 3 mg/kg of caffeine demonstrated better cognitive performance than those consuming 6 or 9 mg/kg (26). The researchers attributed this discrepancy to potential side effects associated with higher doses of caffeine, such as increased anxiety, jitteriness, or overstimulation, which may counteract its cognitive benefits. Interestingly, the placebo effect observed in our HC+Decaff group could be explained by the strong association between habitual caffeine consumption and expected cognitive benefits. In high caffeine consumers, the perception of receiving caffeine even in its absence may have triggered a performance boost through psychological or physiological mechanisms. These findings, when considered along with Zhang et al. and Wang et al.'s results, suggest that both the caffeine dose and individuals' baseline consumption levels are critical factors influencing cognitive performance (24, 26). Furthermore, the reduced effectiveness of higher caffeine doses in the aforementioned studies might reflect a ceiling effect, where excessive caffeine begins to impair rather than enhance cognitive function.

However, our findings did not support our hypothesis. Nevertheless, the findings shed light on the possibility of different mechanisms regarding how caffeine tolerance and consumption influence consumers' expected cognitive outcomes. Future research could explore how the placebo

effect interacts with different levels of habitual caffeine intake and the extent to which subjective expectation influence performance outcomes. These factors are particularly relevant in understanding the nuanced and dose-dependent effects of caffeine on cognition.

We had to perform this work during the timeline of Covid-19 pandemic. Although our sample size was sufficient, according to the power analysis, we were unable to further increase the sample size and enhance the study, as all university students were attending online classes during this period. We could not exclude participants based on smoking and alcohol use. To minimize potential confounding effects, participants were instructed to abstain from smoking for at least 12 hours and from alcohol for at least 24 hours before the study. In the future, we would like to further develop this study, further increase the number of participants (excluding smoking and alcohol use), and interpret the effects of caffeine on cognitive functions in comparison with EEG and other imaging methods.

CONCLUSION

Our findings demonstrate the differential effects of caffeine on cognitive performance and EEG activity based on habitual daily caffeine consumption. Low caffeine consumers exhibited improved cognitive performance and increased beta power, whereas high caffeine consumers showed limited changes, indicating the development of tolerance.

In our study, we found that individuals who regularly consumed low amounts of caffeine showed increased brain activity in EEG recordings and improved cognitive functions after consuming high amounts of caffeine. Individuals who regularly consumed high amounts of caffeine showed a smaller increase in brain activity and cognitive functions following caffeine administration compared with those who routinely consumed low amounts of caffeine. Therefore, cognitive performance, as assessed using the MoCA test in our study, may vary among individuals with different caffeine consumption habits, depending on their usual intake levels.

This is a pilot study investigating the effect of caffeine consumption on neurophysiological findings. Our findings will shed light on further studies with larger numbers of participants and different imaging techniques (e.g. functional magnetic resonance imaging) combined with EEG.

Acknowledgments: This research did not receive any specific grant from funding agencies in the public, commercial, or not-for-profit sectors.

Ethics Committee Approval: Permission was obtained from the Non-Interventional Clinical Research Ethics Committee of Dokuz Eylul University for the study (Approval number: 2020/28-26).

Peer Review: Externally peer-reviewed.

Author Contributions: Conception/Design of Study – F.O., A.N., A.D.; Data Acquisition – F.O., G.E.; Data Analysis/Interpretation – F.O., A.Z.T., A.C.M., A.N.; Drafting Manuscript – F.O., A.Z.T., A.N., A.D.; Critical Revision of Manuscript – F.O., A.N., A.D.; Final Approval and Accountability – F.O., A.N., A.D.

Conflict of Interest: The authors declare no conflict of interest.

Financial Disclosure: The authors declare that they received no financial support for this study.

Author Details

Fatma Ozlem
[1] Department of Physiology, Institute of Health Sciences, Dokuz Eylul University, Izmir, Turkiye
[2] Department of Physiology, Faculty of Medicine, Istanbul Yeni Yuzyil University, Istanbul, Turkiye
0000-0003-2747-4903 fatma.ozlem@yeniyuzyil.edu.tr

Asli Zengin Turkmen
[2] Department of Physiology, Faculty of Medicine, Istanbul Yeni Yuzyil University, Istanbul, Turkiye
0000-0002-8309-8431

Gokcer Eskikurt
[3] Department of Psychology, Faculty of Humanities and Social Sciences, Istinye University, Istanbul, Turkiye
[4] Innovative Center of Applied Neurosciences, Istinye University, Istanbul, Turkiye
0000-0003-4898-8639

Asli Ceren Macunluoglu
[5] Institute of Health Sciences, Department of Biostatistics, Uludag University, Bursa, Turkiye
0000-0002-6802-5998

Asiye Nurten
[2] Department of Physiology, Faculty of Medicine, Istanbul Yeni Yuzyil University, Istanbul, Turkiye
0000-0001-7847-1716

Ayfer Dayi
[6] Department of Physiology, Faculty of Medicine, Dokuz Eylul University, Izmir, Turkiye
0000-0002-4102-1399

REFERENCES

1. Heckman MA, Weil J, De Mejia EG. Caffeine (1, 3, 7-trimethylxanthine) in foods: a comprehensive review on consumption, functionality, safety and regulatory matters. J Food Sci 2010; 75(3): 77–87.
2. Lane JD. Understanding caffeine: a biobehavioral analysis. Health Education & Behavior. Sage publications INC: CA; 1999. p.141-43.
3. European Food Safety Authority. Scientific opinion on the safety of caffeine. EFSA: 2015; 13(5): 17-21.
4. Carter AJ, O'Connor WT, Carter MJ, Ungerstedi U. Caffeine enhances acetylcholine release in the hippocampus in vivo by a selective İnteraction with adenosine A1 receptors. J Pharmacol Exp Ther 1995; 273(2): 637–42.

5. Shimamura AP. The cognitive science perspective. Handbook of Neuropsychology. Springer: New York; 1989.p.35-73.
6. Singh M, Sachdeva S. Cognitive assessment techniques. Int. J Inf Technol 2014; 7(2): 108–18.
7. Dabbabi T, Bouafif L. Cherif A. A review of non invasive methods of brain activity measurements via EEG signals analysis. IEEE International Conference on Advanced Systems and Emergent Technologies. Hammamet, Tunisia; 2023. pp.01-06.
8. Jadeja NM. Frequencies and Rhythms. In: How to read an EEG. Cambridge University Press; 2021. pp. 32-9.
9. Sigmon SC, Herming RI, Better W, Cadet JL Geiffits RB. Caffeine withdrawal, acute effects, tolerance, and absence of net beneficial effects of chronic administration: cerebral blood flow velocity, quantitative EEG and subjective effects. J Clin Psychopharmacol 2009; 204(4): 573–85.
10. Nasreddine ZS, Philips NA, Bedirian V, Charbonneau S, Whitehead V, Collin I et al. The Montreal Cognitive Assessment, MoCA: a brief screening tool for mild cognitive impairment. J Am Geriatr Soc 2005; 53(4): 695–9.
11. Sherman SM, Buckley TP, Baena E, Ryan L. Caffeine enhances memory performance in young adults during their non-optimal time of day. Front Psychology 2016; 14(7): 1764.
12. Trunk A, Stefanics G, Zentai N, Bacskay I, Felinger A, Thuroczy G et al. Effects of concurrent caffeine and mobile phone exposure on local target probability processing in the human brain. Sci Rep 2015; 23(5): 1–12.
13. Güngen C, Ertan T, Eker E, Yaşar R, Engin F. Reliability and validity of the standardized Mini Mental State Examination in the diagnosis of mild dementia in Turkish population. Turk Psikiyatri Derg 2002; 13(4): 273-81.
14. Ajjimaporn A, Noppongsakit P, Ramyarangsi P, Siripornpanich V, Chaunchaiyakul R. A low-dose of caffeine suppresses EEG alpha power and improves working memory in healthy university males. Physiol Behav 2022; 256: 113955.
15. Voiculescu M, Segarceanu A, Negutu M, Ghita I, Fulga I, Coman OA. The effect of caffeine on cerebral asymmetry in rats. J Med Life 2015; 8(4): 476-82.
16. Foxe JJ, Morie KP, Laud PJ, Rowson MJ, De Bruin EA, Kelly SP. Assessing the effects of caffeine and theanine on the maintenance of vigilance during a sustained attention task. Neuropharmacology 2012; 62(7): 2320–7.
17. Siepmann M, Kirch W. Effects of caffeine on topographic quantitative EEG. Neuropsychobiology 2002; 45(1): 161–6.
18. Engel, A. K, Fries, P. Beta-band oscillations-signalling the status quo. Curr Opin Neurobiol 2010; 20(2): 156–165.
19. Hasenfratz M, Bättig K. Acute dose effect relationships of caffeine and mental performance, EEG, cardiovascular and subjective parameters. Psychopharmacol 1994; 114(2): 281–7.
20. Dimpfel W, Schober F, Spüler M. The influence of caffeine on human EEG under resting conditions and during mental loads. Clin Investig 1993; 71(3): 197-207.
21. Landolt HP, Dijk DJ, Gaus SE, Borbély AA. Caffeine reduces low-frequency delta activity in the human sleep EEG. Neuropsychopharmacology 1995; 12(3): 229-38.
22. Haskell CF, Kennedy DO, Wesnes KA Scholey AB. Cognitive and mood improvements of caffeine in habitual consumers and habitual non-consumers of caffeine. J Psychopharmacol 2005; 179(4): 813–25.
23. Shoulder RJ, Hall EE, Miller PC. The influence of exercise and caffeine on cognitive function in college students. Health 2016; 8(2): 156–62.
24. Zhang B, Liu Y, Wang X, Deng Y, Zheng X. Cognition and brain activation in response to various doses of caffeine: a near-infrared spectroscopy study. Front Psychol 2020; 11(2): 1–9.
25. Juliano LM, Griffiths RR. A critical review of caffeine withdrawal: empirical validation of symptoms and signs, incidence, severity, and associated features. Psychopharmacology 2004; 176(1): 1-29.
26. Wang C, Zhu Y, Dong C, Zhou Z, Zheng X. Effects of various doses of caffeine ingestion on intermittent exercise performance and cognition. Brain Sci 2020; 10(9): 1–12.

İSTANBUL UNIVERSITY PRESS

Experimed 2025, 15 (1): 66–76

https://doi.org/10.26650/experimed.1558871

Submitted: 30.09.2024
Revision Requested: 20.01.2025
Last Revision Received: 20.02.2025
Accepted: 21.02.2025
Published Online 28.03.2025

Experimed

Research Article

Open Access

Biological and Immunological Properties of Mesenchymal Stromal Cells Derived From Bone Marrow in Childhood Acute Myeloid Leukemia

Ilkay Piskin [1], Tuba Ozdemir Sanci [1], Yasin Koksal [2], H. Nese Yarali [3], Fatma Karaca Kara [4], Bahattin Tunc [5] & Meltem Ozguner [1]

[1] Department of Histology Embryology, Faculty of Medicine, Ankara Yildirim Beyazit University, Ankara, Turkiye
[2] Department of Pediatric Hematology Oncology, Stem Cell Processing Laboratory, Ministry of Health Ankara Bilkent City Hospital, Ankara, Turkiye
[3] Department of Pediatric Hematology, Ministry of Health Ankara Bilkent City Hospital, Ankara, Turkiye
[4] Department of Medical Biochemistry, Ministry of Health Ankara Kecioren Training and Research Hospital, Ankara, Turkiye
[5] Ankara Child Health and Diseases Hematology Oncology Training and Research Hospital, Ankara, Turkiye

Abstract

Objective: Pediatric acute myeloid leukemia (AML) is a common form of pediatric leukemia and is characterized by the accumulation of abnormal white blood cells, called blasts, in the bone marrow (BM). The aim of this study was to understand the BM microenvironment by studying the biological and immunological properties of BM-derived mesenchymal stromal cells (MSCs) and mononuclear cells (MNCs) to elucidate the potential role of phytohaemagglutinin in cell viability.

Materials and Methods: BM and peripheral blood samples were obtained from seven pediatric AML patients and seven donors. BM-MSCs and MNCs were isolated and characterized. Population doubling (PD) values, adipogenic and osteogenic differentiation capacity, cell viability, phytohemagglutinin (PHA) assay, and flow cytometry were performed.

Results: Mononucleated cells from peripheral blood of AML patients and donors and T-cell activation markers ($CD3^+CD69^+$, $CD4^+C25^+$, $CD3^+HLA\text{-}DR^+$) were measured by flow cytometry (χ^2=2.184; p=0.823). BM-MSCs were co-cultured with MNCs, and PD values for AML patients were similar to those of donors (z=1.074; p=0.394). It was statistically significant when healthy MNC and healthy MNC PHA(+) groups were compared (p=0.015). When healthy MNC PHA(+) and healthy MSC+AML MNC PHA(+) groups were compared, it was found to be statistically significant (p=0.014).

Conclusion: This interaction is also not unidirectional. This interaction serves as a marker for understanding the immunological effects of AML.

Keywords Pediatric AML · BM-MSCs · PHA · Cell viability · MNCs

Author Note A part of this study was presented in a poster session at the 15th International Congress of Histochemistry and Cytochemistry 'From Molecules to Diseases' held in Antalya, Turkiye in 2017.

Citation: Piskin, I., Ozdemir Sanci, T., Koksal, Y., Yarali, H. N., Karaca Kara, F., Tunc, B. & Ozguner, M. Biological and immunological properties of Mesenchymal stromal cells derived from bone marrow in childhood acute myeloid leukemia. Experimed 2025; 15(1): 66-76. DOI: 10.26650/experimed.1558871

Corresponding author: Ilkay Piskin ilkaycorumluoglu@aybu.edu.tr

INTRODUCTION

The formation of aberrant myeloid progenitor cells (myeloblasts) in the bone marrow (BM) is a characteristic of acute myeloid leukemia (AML), an aggressive hematologic malignancy that frequently invades extramedullary tissues like the liver and spleen as well as the bloodstream (1, 2). Although AML is very rare in children, it is associated with a disproportionately high mortality rate (3). Isolated from extramedullary tissues, mesenchymal stromal cells (MSCs) can be used in tissue regeneration cell therapies, serving as a reserve to replace damaged and senescent cells (4). The multipotent and self-renewing nature of MSCs makes them promising for use in cell treatment, tissue repair, and regenerative medicine research (5). Within the bone marrow (BM) niche, MSCs provide support for hematopoietic progenitor and stem cells (HSPCs) (6). MSCs are extremely rare in the BM and account for less than 0.01% of all mononucleated cells (7).

MSCs remain quiet under normal circumstances. They are thought to be attracted to injured sites to restore or repair damaged tissues. They are thought to be activated and to divide symmetrically or asymmetrically upon activation by biological signals, such as those resulting from tissue injuries. MSCs have been used in a growing number of clinical indications because of their strong reparative potential, particularly for bone deformities and cartilage loss (7).

By attaching itself to the T cell receptor (TCR)CD3 complex, phytohaemagglutinin (PHA) imitates every intracellular activation event caused by anti-CD3 antibodies. Red kidney beans are a source of PHA, a lectin that attaches itself to T cell membranes to promote metabolic processes and cell proliferation (8). Four hours after cell activation, the T, B, and natural killer cell surfaces show the earliest activation marker, CD69, which is linked to the transcription of tumor necrosis factor-alpha (TNF-α) and interleukin-2 (IL-2). Increased expression of the IL-2 receptor's CD25 component is observed 12 to 24 hours following cell activation. Sixty to eighty hours later, T cells initiate to express HLA-DR (9).

The aim of this study was to understand the relationship between MSCs and the BM microenvironment, as well as the viability of the cells in pediatric AML by examining the immunological characteristics of these cells derived from the BM and to shed light on potential roles in the pathogenesis of AML.

MATERIALS AND METHODS

Research Methodology and Ethics

Seven healthy donors who were matched with 7 newly diagnosed pediatric AML patients were included in this study. The Ankara Children's Health Diseases Hematology Oncology Training and Research Hospital's clinical research ethics committee approved the haematopoietic stem cell transplantation (HSCT) protocol, and all participants provided informed consent (10, 11) (ID:2014062). At the time of diagnosis, MSCs were isolated from the BM and cultivated *ex vivo* for testing.

BM Collection

BM samples from pediatric AML patients and donors were extracted, frozen, and centrifuged under general anesthesia. Plasma was collected and stored at -80°C.

Isolation, Freezing, and Thawing of Mononuclear Cells (MNCs) Derived from BM

MNC samples were diluted with phosphate buffered saline (PBS) (Biochrom, Germany) and Biocoll (1.077 g/mL) separating solution (Biochrom, Germany) (1:1), frozen in Dulbecco's Modified Eagle Medium with low glucose (DMEM-LG) (Biochrom, Germany), thawed, centrifuged, and reconstituted in DMEM-LG, FBS, and penicillin-streptomycin (Biochrom, Germany). Cells were seeded in 75 cm^2 plastic flasks, maintained in a humidified atmosphere with 5% CO_2 at 37°C, and then seeded in a Galaxy 170R incubator (Eppendorf Company, Hamburg, Germany).

Cell Culture of BM-Derived MSCs

The cell culture medium was changed every 3 days, non-adherent cells were removed after 72 h, and adherent cells (Passage 2) were trypsinized at 37°C for 5 minutes after 70%-80% confluence.

Characterization and Differentiation Capacity of MSCs

Flow cytometry was also used to examine MSC cell surface markers. CD45-Alexa Fluor® 488 (BioLegend, cat. no. 304019), CD34-FITC (BioLegend, cat. no. 343604), CD90-PE (BioLegend, cat. no. 328110), CD73-APC (BioLegend, cat. no. 344006), and CD105-PE/Cy7 (BioLegend, cat. no. 323218) were used to stain the cells. The cells were then examined using the Navios-Beckman Coulter flow cytometer and Navios Software v1.2. Positive and negative antibody staining was also performed (BD Biosciences, Piscataway, NJ, USA). Flow cytometry was used to surface phenotype MSCs.

The differentiation potential of MSCs into adipogenic and osteogenic lineages was assessed *in vitro* using osteogenic and adipogenic supplemental supplements (Stemcell Technologies, Vancouver, Canada). On day 21, the differentiation of MSCs into these cells was confirmed using alizarin red and oil red O staining.

Proliferative MSC Assay

The proliferative capacity of MSCs was assessed using trypsinization, cell growth detection, and hematoxylin and eosin staining. The number of PDs from passage P1 to P2 was calculated using $\log_{10}(N)/\log_{10}(2)$ indicating harvested/sown cells (12, 13).

Coculture and PHA Activation Tests

MNCs from peripheral blood samples were plated on T-25 flasks in DMEM supplemented with FBS and penicillin-streptomycin for 72 hours to activate lymphocytes, with a density of $3x10^5$ cells/cm² with a density of 10 mL PHA/$1x10^6$ cells in DMEM supplemented with 10% FBS and 1% penicillin-streptomycin at 37°C in a humidified environment with 5% CO_2 for 72 hours in order to activate the lymphocytes. PHA-activated MNCs-MSCs were co-cultured with allogeneic human MSCs in a study, comparing control, newly isolated MNCs, PHA-activated MNCs-MSCs, and PHA non-activated MNCs-MSCs, for immunological tests. 30,000 MNCs were added to each well at a 10:1 ratio, and the cells were centrifuged and cleaned after four days. The quantity and viability of the cells were determined.

Flow Cytometry Analysis

CD45-Alexa Fluor® 488 (BioLegend, cat. no. 304019), CD34-FITC (BioLegend, cat. no. 343604), CD90-PE (BioLegend, cat. no. 328110), CD73-APC (BioLegend, cat. no. 344006), and CD105-PE/Cy7 (BioLegend, cat. no. 323218) cell surface markers were analysed for the MSCs. CD3, CD4, CD25, CD69, and HLA-DR were analyzed by flow cytometry (Beckman Coulter, Brea, CA, USA), and MNCs were extracted using Kaluza version 1.2 software.

Statistical Analyses

Statistical significance was assessed using Student's t-test and the Mann–Whitney U test $p<0.05$ was considered statistically significant. IBM SPSS Statistics for Windows, Version 21.0 (IBM Corp., Armonk, NY, USA) was used for statistical analysis.

Table 1. Demographic features of pediatric AML patients and donors

Pediatric AML (n=7)		**Healthy Donor (n=7)**	
Age, median (range)	13 (2-17)	Age, median (range)	10 (3-51)
Gender		Gender	
Male	3	Male	5
Female	4	Female	2
AML immunophenotyping		Total number of healthy MNC donors	1
AML	5	Median age	31
M2	0	Gender	
M4	1	Male	0
MDS	1	Female	1

Abbreviations: AML: Acute myeloid leukemia; MDS: Myelodysplastic syndrome; MNC: Mononuclear cells; n=number

Table 2. BM-derived MSC expression of CD Markers

Marker	**Donor 1**	**Donor 2**	**Donor 3**
CD90	100	99.4	99.5
CD73	90.4	88.2	93.4
CD105	95.6	89.8	90.1
CD34	0.1	0.2	0.1
CD45	0.2	0.3	0.1

Abbreviations: BM: Bone marrow; MSC: Mesenchymal stromal cells. Data are presented as percentages.

RESULTS

Demographic Features of AML Patients and Donors

In this study, the demographic features of AML and donors are presented in Table 1. The median age ranged from 2-17 years in the AML group and 3–51 years in the healthy group. The AML group had 4 females and 3 males, whereas the healthy group had 5 females and 2 males (Table 1).

Proliferation and Characterization of AML-MSCs and HD-MSCs

BM-MSCs were plated, treated with trypsin-EDTA, harvested, and measured by haemogram. Population doubling (PD) values of AML patients and healthy donors were calculated using the $\log_{10}(N)/\log_{10}(2)$ formula. AML patients had similar PD2 values to healthy donors ($z=1.074$; $p=0.394$). The median values for PD1 and PD2 were similar between the groups (Figure 1). After passage 2 of the BM-MSCs, trypan blue dye was used to examine the percentages of cellular viability. Both types of MSCs were used in the tests. The immunophenotyping study revealed that both types of MSCs had been carried for $CD34^-$, $CD3^-$, $CD4^-$, $HLA\text{-}DR^-$, $CD90^+$, $CD73^+$, $CD44^+$, $CD49e^+$ and $HLA\ ABC^+$. Differentiation tests were used to verify the ability of both the study and control groups of MSCs to differentiate into

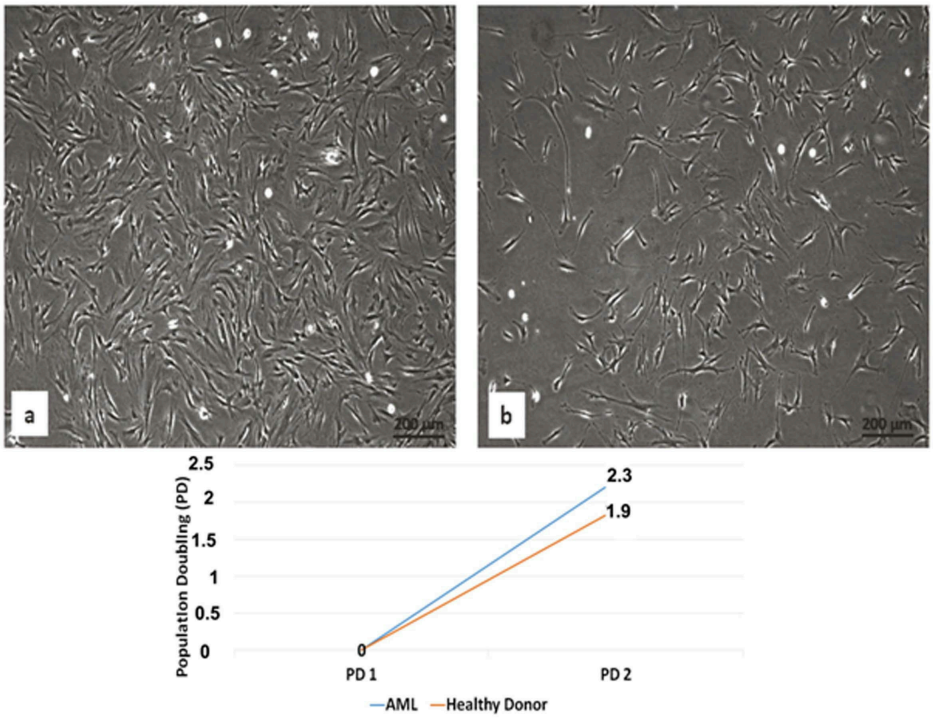

	AML		Control			
	Median (min-max)	Mean ± SD	Median (min-max)	Mean ± SD	z	p value
Population doubling value (PD)	2.0 (2.0-3.0)	2.3 ± 0.4	2.0 (1.0-3.6)	1.9 ± 0.9	1.074	0.394

Figure 1. Cell morphology images of MSCs. **a:** BM-MSCs of AML patient; **b:** BM-MSCs of donors (Olympus CKX41-40X). Logaritmic population doubling (PD) values of BM-MSCs derived from AML patients and donors. The proliferation capacity of AML-MSCs compared with HD-MSCs. Calculated cumulative PD (PDs) from P1 to P2 of MSCs isolated from HDs and from AML patients. Statistical significance is $p<0.05$.

adipogenic and osteogenic tissues (Figure 2). The expression levels of CD markers were analyzed in BM-derived MSCs (Table 2).

Cell-viability

The statistical values of the healthy donors were significantly higher than those of the AML patients (z=2.246; p=0.026). The median value; 65.70 (min=55.60; max=80.80) was determined for AML patients, while 89.05 (min=61.80; max=90.50) for healthy donors. For the other wells compared, there was no significant difference in the percentage of cell viability (p>0.05). The median value for AML patients was 73.50 (min=56.40; max=92.50), and the median value for healthy donors was 78.85 (min=76.60; max=85.40) (z=0.321; p=0.818). The percentage cellular viability values obtained from the wells in AML patients were not statistically significant (χ^2=2.184; p=0.823). The percent cellular viability values obtained from all wells were similar to those obtained from healthy subjects (χ^2=10.714; p=0.057) (Table 3).

Immunological Assays

Clonal division occurs in lymphocytes following mitogenic activation. The study examined the kinetics of lymphocyte stimulation with PHA and the impact of pediatric and normal bone marrow MSCs on activated lymphocytes using flow cytometry. We examined various lymphocyte subpopulations, particularly T cells phenotypically identified as $CD3^+CD69^+$, $CD3^+HLADR^+$, and $CD4^+CD25^+$, under various culture conditions.

MSCs of AML patients and healthy donors presented with the same morphological features, proliferation rates (z=1.074; p=0.394), and differentiation capacities. We analyzed T lymphocytes phenotypically defined as $CD3^+CD69^+$, $CD3^+HLADR^+$, and $CD4^+CD25^+$ in culture conditions by flow cytometry (Table 2 and Table 3). We observed differences between the different sets of co-cultures. We defined and compared different stages of lymphocyte activation in AML patients and healthy donors. The MNCs of healthy donors with PHA stimulation were found to be consistent with the

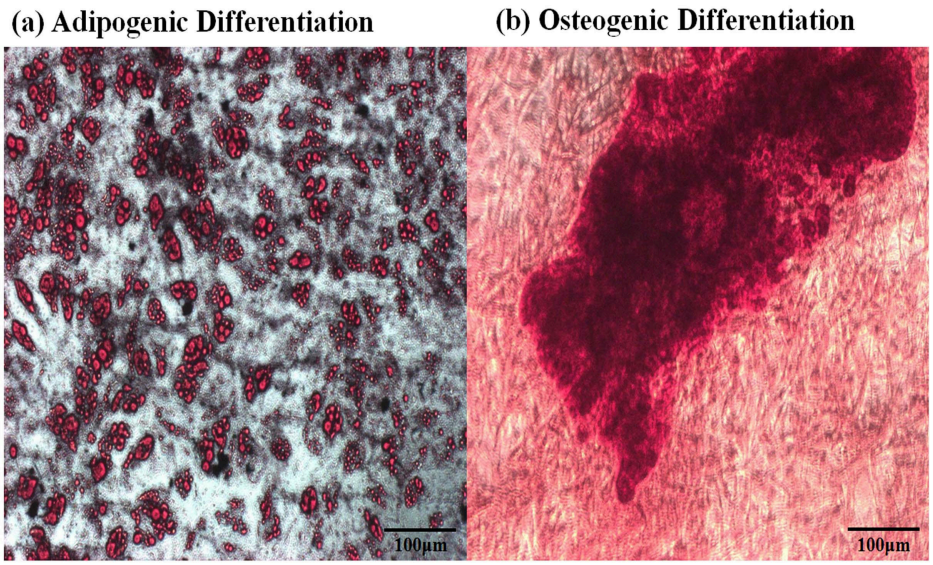

Figure 2. (a) Adipogenic differentiation of the MSCs of AML patients (stain: oil red o) (b) Osteogenic differentiation of the MSCs of AML patients (Olympus CKX41-40X)(Stain: Alizarin Red).

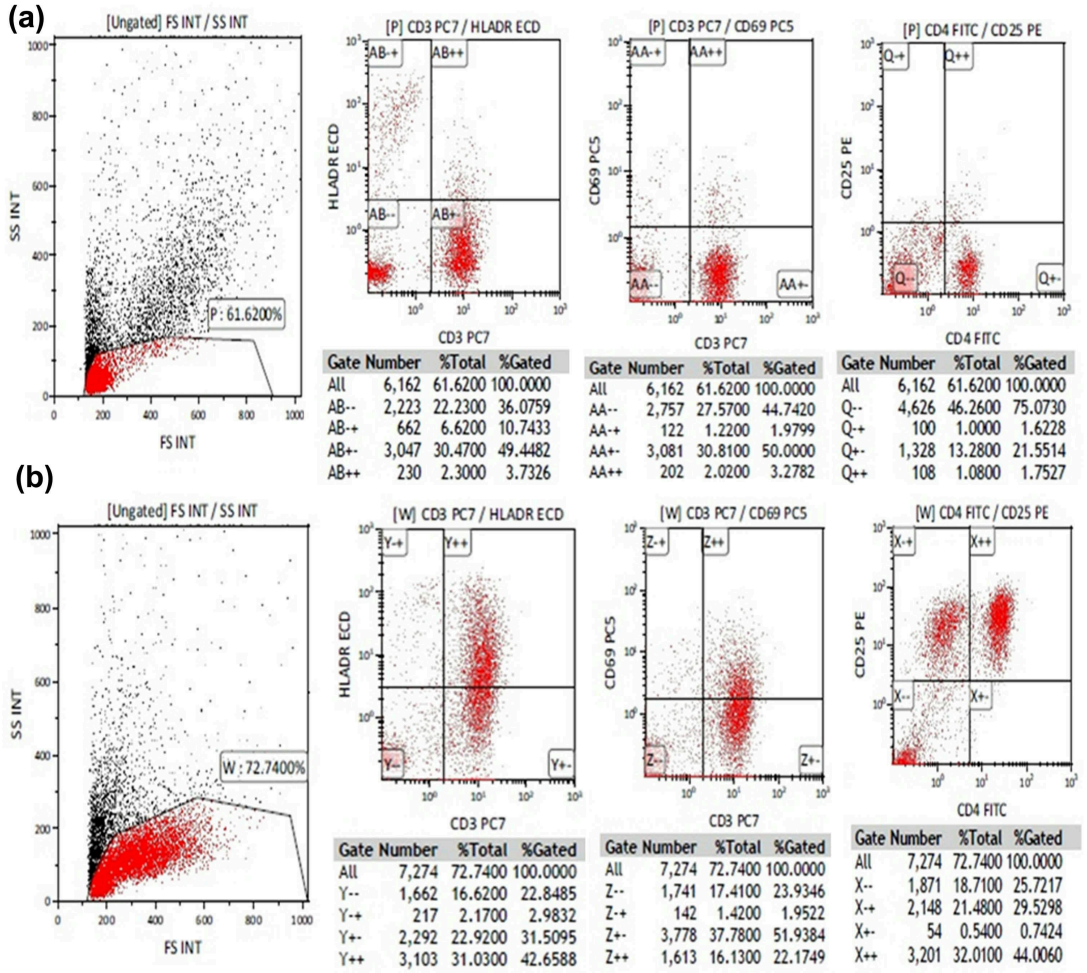

Figure 3. Flow-cytometric analysis of MNCs from induced with and without phytohaemagglutinin of AML group. Induced (a)Non-induced PHA-MNCs isolated from AML and, (b)induced by PHA-MNCs isolated from AML. The positive cells are indicated in the rectangular region.

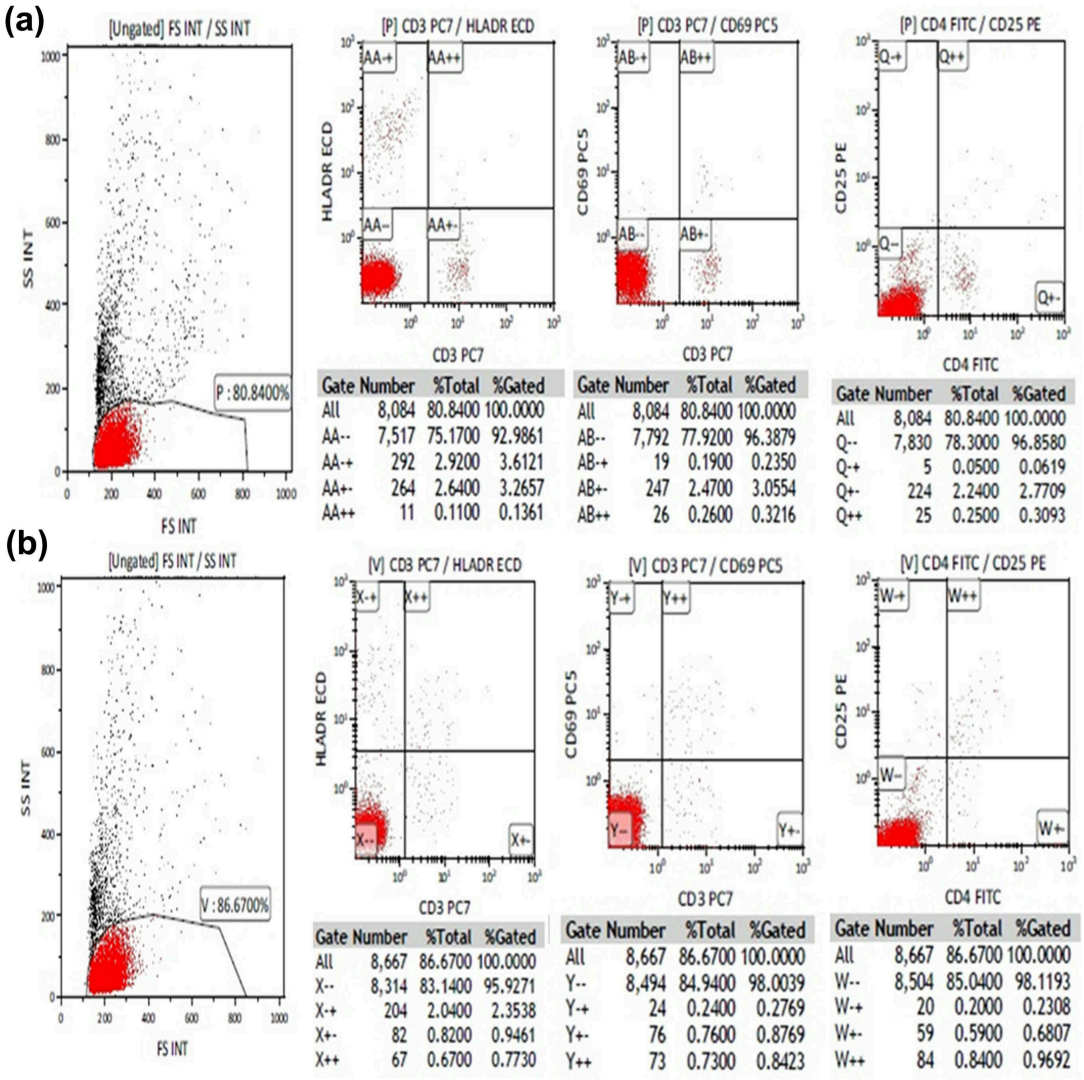

Figure 4. Flow-cytometric analysis of MNCs from induced with and without phytohaemagglutinin of pediatric control group. (a) Non-induced by PHA-MNCs isolated from control and, (b) Induced by PHA-MNCs isolated from control. The positive cells are indicated in the rectangular region.

literature regarding the expression of T-cell surface markers. However, the expression pattern of MNCs of AML patients indicated that they do not exhibit an effective immune response to PHA. The $CD3^+CD69^+$, $CD3^+HLA\text{-}DR^+$, and $CD4^+CD25^+$ MNCs of all groups of AML patients were similar before and after co-culture (Table 4).The mean percentage of $CD3^+CD69^+$ cells ($p=0.015$) were higher in D1 than in C2. After co-culture, the mean percentage of $CD3^+CD69^+$ cells was higher in F1 compared with D1 (Table 4) (Figure 3-5).

DISCUSSION

Pediatric leukemia, a major leukemia, has seen a 70% survival rate in recent years because of improved care, risk stratification, and intensive chemotherapy. MSCs are essential for tissue homeostasis and can differentiate into different cell types. They are found in many tissues like BM, adipose tissue, cord blood, and placenta (14-18).

This study characterized MSCs in children with AML, focusing on hematopoiesis in the BM microenvironment. Results showed morphological similarity between AML patients and healthy individuals, which is consistent with literature findings after standard cell culture applications. A previous study found no morphological difference in bone marrow-derived MSCs between patients with ALL and healthy individuals (12). The suitability of the variables in the study for normal distribution was assessed using the Shapiro-Wilk test. Because the variables did not show normal distribution and the number of subjects was small, median (minimum-maximum) values were used in the display of descriptive statistics. As additional information, mean ± standard deviation values were provided (Table 1).

Adipose tissue (AT)-derived cells, including BM and AT, exhibit diverse morphologies, including elongated, triangular, and discoidal flat shapes. After three passages, these cells

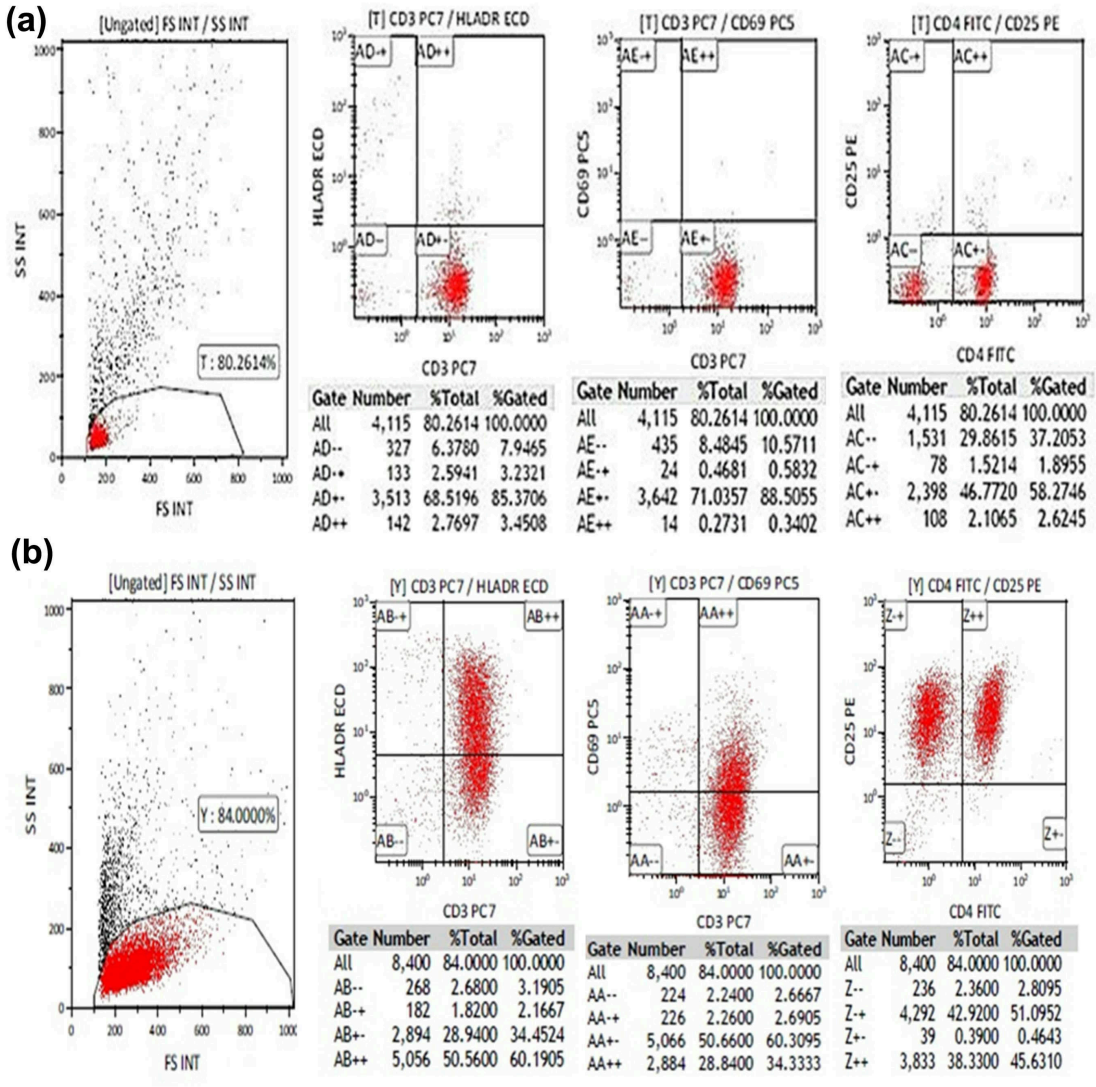

Figure 5. Flow-cytometric analysis of MNCs from induced with and without phytohaemagglutinin of healthy MNC group. (a) Non-induced PHA-MNCs isolated from healthy MNC donor and, (b) induced by PHA-MNCs isolated from healthy MNC donor. The positive cells are indicated in the rectangular region.

exhibit fibroblast-like morphology, abundant cytoplasm, and large nuclei, forming parallel models without morphological differences (19, 20). In 2013, Conforti et al. found that ALL (ALL-MSC=8.89 ± 0.87, p<0.001) had significantly lower proliferation capacity compared with healthy donors, as indicated by the Student's t-test, comparing PD values from passage 1 to passage 5 (HD-MSC=12.12 ± 1.09) (12). Compared with BM-derived MSCs, AT-derived MSCs showed higher proliferative capacity and higher numbers per passage in cumulative PD studies, with CPD values of 13.7 ± 0.5 and 17.2 ± 0.3, respectively (19). In our study, the Mann–Whitney U test was used to compare the values obtained from AML patients and donors in each well and to compare PD2 values for the cell proliferation assay (z=1.074; p=0.394) (Figure 1). According to cell viability analysis, when BM-MSC+Healthy PHA(+) MNCs were cocultured with healthy MSCs, it was found to be statistically significant (z=2.246; p=0.026) (Table 3).

PHA is a member of the lectin family and crosslinks with different cell membrane glycoproteins. PHA is also an inducing agent in polyclonal stimulation of lymphocytes (21). PHA mimics T lymphocyte signaling, but PKC activation persists despite crosslinking with TCR, CD2, and CD3. Calcium levels increase, but IL-2 from T cells is needed for antigen-presenting cell proliferation, and induced T lymphocytes require helper signaling from antigen-presenting cells (22-27). TNF-α transcription and gene expression are regulated by PHA, with CD69 being an early activation marker. After 4 h, transcription increases in T, B, and NK cells, resulting in increased affinity for IL-2 in the plasma membrane. ALL patients and healthy donors exhibited similar anti-inflammatory effects on MSCs, with HLA-DR expression beginning on the T cell surface after 40-60 h. *In vitro* inhibition of polyclonal-induced allogeneic peripheral blood mononuclear cells (PBMCs) in ALL-MSCs and healthy donor MSCs showed equal effects. Anti-inflammatory

Table 3. Comparison of cell viability between the healthy donor and AML groups

	Pediatric AML group		Healthy Group		z	p value
	Median (min-max)	Mean ± SD	Median (min-max)	Mean ± SD		
Control	70.95 (53.30-94.30)	70.98 ± 14.01	70.95 (56.30-79.00)	69.40 ± 8.80	0.161	0.937
BM-MSC+Healthy PHA(+) MNC	65.70 (55.60-80.80)	68.05 ± 10.04	89.05 (61.80-90.50)	84.60 ± 11.27	2.246	0.026
BM-MSC+AML PHA(+) MNC	73.50 (56.40- 92.50)	73.73 ± 13.16	78.85 (76.60-85.40)	76.40 ± 3.31	0.321	0.818
BM-MSC+Newly isolated MNC	73.10 (56.50-87.50)	72.20 ± 13.57	73.70 (51.30-84.40)	72.52 ± 12.49	0.320	0.818
BM-MSC+Healthy PHA(-) MNC	76.30 (64.70-81.80)	74.35 ± 7.23	73.60 (56.50-84.30)	72.45 ± 9.09	0.320	0.818
BM-MSC+AML PHA(+) MNC	78.55 (60.00-86.90)	76.38 ± 9.21	73.95 (63.60-86.90)	73.68 ± 8.51	0.643	0.589
χ^2; p value	2.184; 0.823		10.714; 0.057			

Abbreviations: Min:minimum; max:maximum; SD: Standard deviation; AML: Acute myeloid leukemia; BM: Bone marrow; MNC: Mononuclear cells; MSC:Mesenchymal stromal cells; PHA:Phytohemagglutinin; MNC: Mononuclear cells.

Table 4. Immunological assay determining activation markers of lymphocytes obtained from peripheral blood of AML and healthy groups

Activation markers	Control 1	Before co-culture		After co-culture			
AML Group	C1	B1	B2	E1	E2	E3	E4
$CD3^+CD69^+$	2.155 ± 1.619	5.46 ± 5.857	1.837 ± 2.186	3.77 ± 3.841	1.926 ± 2.238	17.228 ± 14.494	6.426 ± 9.47
$CD3^+HLA\text{-}DR^+$	19.455 ± 26.382	12.453 ± 18.669	5.44 ± 6.689	7.628 ± 10.304	3.302 ± 2.998	31.268 ± 19.212	4.434 ± 2.896
$CD4^+CD25^+$	4.525 ± 4.377	13.18 ± 14.776	10.023 ± 12.972	13.002 ± 7.987	9.35 ± 2.569	20.718 ± 12.179	6.382 ± 1.444
Healthy Group	Control 2	Before co-culture		After co-culture			
	C2	D1	D2	F1	F2	F3	F4
$CD3^+CD69^+$	0.42 ± 0.339	26.7 ± 6.985	16.233 ± 27.485	0	19.775 ± 19.127	17.895 ± 2.977	10.445 ± 8.04
$CD3^+HLA\text{-}DR^+$	2.455 ± 2.581	33.98 ± 23.516	9.353 ± 10.052	0	19.775 ± 19.127	34.525 ± 19.057	14.435 ± 6.951
$CD4^+CD25^+$	0.885 ± 0.587	26.26 ± 16.782	12.423 ± 16.954	32.5 ± 3.536	33.335 ± 47.143	22.745 ± 16.454	26.665 ± 9.426

AML Group (p values)	C1&B	C1&B2	B1&E1	B1&E2	B1&E3	B1&E4	B2&E1	B2&E2	B2&E3	B2&E4
$CD3^+CD69^+$	0.511	0.874	0.634	0.255	0.238	1.00*	0.463	0.958	0.127	0.571*
$CD3^+HLA\text{-}DR^+$	0.745	0.413	1.00*	0.3	0.225	0.358	0.571*	0.546	0.071	0.771
$CD4^+CD25^+$	0.498	0.619	0.983	0.572	0.461	0.321	0.696	0.91	0.284	0.535
Healthy Group (p values)	C2&D1	C2&D2	D1&F1	D1&F2	D1&F3	D1&F4	D2&F1	D2&F2	D2&F3	D2&F4
$CD3^+CD69^+$	0.015	0.496	0.014	0.585	0.204	0.094	0.486	0.887	0.941	0.8
$CD3^+HLA\text{-}DR^+$	0.171	0.432	0.148	0.533	0.98	0.355	0.3	0.468	0.138	0.585
$CD4^+CD25^+$	0.136	0.429	0.656	0.816	0.832	0.978	0.214	0.508	0.549	0.371

Abbreviations: C1 (control 1): AML MNC; B1: AML MNC PHA (+); B2: AML MNC PHA (-); E1: AML MSC+AML MNC PHA (+); E2: AML MSC+AML MNC PHA (-); E3:MSC+ Healthy MNC PHA (+); E4: AML MSC+ Healthy MNC PHA (-). C2 (control 2): Healthy MNC; D1: Healthy MNC PHA (+); D2: Healthy MNC PHA (-); F1: Healthy MSC+ AML MNC PHA (+); F2: Healthy MSC+ AML MNC PHA (-); F3: Healthy MSC+ Healthy MNC PHA (+); F4: Healthy MSC+ Healthy MNC PHA (-). **Note:** Data was presented mean ± standard deviation. Statistical significance was $p<0.05$. * Statistical analysis was performed using the Mann–Whitney U test.

cytokines and growth factors increased in both groups (12, 28). Studies have shown that MSC suppress T-lymphocyte proliferation when co-cultured with mixed lymphocytes. The suppression effects of MSCs are dose-dependent and independent of the MHC complex. Autologous and allogeneic MSCs suppress alloresponsiveness to T cells, but allogeneic

MSCs are not compliant to induce T cell proliferation when transfected with co-stimulatory molecules or IFN-γ. TNF, a cytokine produced by T cells, is highly receptive to allogeneic PBMCs, indicating their ability to respond to these cells (29).

The Mann–Whitney U test was used to examine whether $CD3^+CD69^+$, $CD3^+HLA\text{-}DR^+$, and $CD4^+CD25^+$ values obtained in PHA and non-PHA groups of AML patients differed. A comparison between the healthy MNC and healthy MNC PHA(+) groups revealed statistical significance (p=0.015). There was a statistically significant difference between the healthy MSC+AML MNC PHA(+) and healthy MNC PHA(+) groups (p=0.014). It has been shown that healthy MNCs activated with PHA create an inflammatory microenvironment for MSC, which transform their immunosuppressive properties into pro-inflammatory effects. These MSC-PHA co-cultures have cytotoxic effects against AML *in vitro*. This study aimed to elucidate the potential therapeutic implications of PHA-activated healthy mononuclear cells along with MSC for the treatment of acute myeloid leukemia. Healthy MNCs improve treatment responses against AML by enhancing anti-leukemia reactivity. hMNCs can be activated *ex vivo* using pharmacological agents that target the toll-like receptor (TLR) pathways and/or combine TLR agonists with proinflammatory cytokines. hMNCs activated by this approach elicit a more potent anti-leukemia immune response (30). PHA-induced healthy MNCs (hMNCs) are a promising approach for the treatment of AML patients. However, understanding the interplay between hMNCs and AML cells is crucial for their clinical application. The findings showed that PHA-induced healthy MNCs could effectively improve the transformation of unhealthy MNCs to healthy MNCs from AML patients, which was not observed in the PBMCs of healthy individuals (31).

The proliferative capacity of BM-MSCs from older individuals has been found to be faulty, with lower proliferation and survival compared with young healthy MSCs. Co-cultured with PHA-induced MNCs, these cells suppress B cell development and acquisition (32, 33). MSCs inhibit B cell proliferation, activation, differentiation, and Ig production, blocking B lymphocyte stimulation in the G0/G1 phase, linked to human BM-MSC and p38 mitogen-activated protein kinase (MAPK) and extracellular signal-regulated kinase (ERK) 1/2 phosphorylation (18). The plastic surface of bone marrow from AML patients and donors shows fibroblast-like cells similar in morphology and adhesion to it. The study found no significant differences in PD2 values between the two cell groups. MSCs differentiated into adipocytes and osteocytes, demonstrating their potential for AML treatment. Flow cytometric analysis revealed no significant differences in $CD3^+CD69^+$, $CD3^+HLA\text{-}DR^+$, and $CD4^+CD25^+$ T-cell activation markers between MNC cell cultures from AML patients and healthy donors. AML donor and AML patients' MSCs were obtained, revealing significant differences in interaction between the two groups. No significant difference was found between AML patients or donors. Co-culture of MSCs from AML patients and healthy individuals is expected. The functionalities of MSCs vary with donor age, making it crucial for physicians to define detailed immunological markers considering donor age to understand the effects of MNCs on MSCs in the bone marrow microenvironment.

CONCLUSION

Oncogenic mutations are responsible for the development of AML, a stem cell disease. Despite normal functionality, cell-cell interaction in bone marrow tissue influences disease prognosis, and further immunological analyses are required for a better understanding.

Acknowledgements: We would like to thank all faculty members at Ankara Yildirim Beyazit University, Faculty of Medicine, Department of Biostatistics and Medical Informatics for their statistical analyses.

Ethics Committee Approval: The study protocol was approved by the Clinical Research Ethics Committee of the Ministry of Health Ankara Children's Hematology Oncology Education and Research Hospital (ID:2014062). This study was conducted in accordance with the Declaration of Helsinki and the International Conference on Harmonization guidelines for Good Clinical Practice. All patients provided written informed consent, and an independent ethics committee or institutional review board at each study site approved the study protocol.

Peer Review: Externally peer-reviewed.

Author Contributions: Conception/Design of Study – I.P., T.O.S., Y.K., M.O.; Data Acquisition – I.P., T.O.S., Y.K., H.N.Y., B.T., M.O.; Data Analysis/Interpretation – I.P., T.O.S., Y.K., H.N.Y., F.K., M.O.; Drafting Manuscript – I.P., T.O.S., M.O.; Critical Revision of Manuscript – I.P., T.O.S., Y.K., H.N.Y., B.T., M.O.; Final Approval and Accountability – I.P., T.O.S., Y.K., H.N.Y., F.K., B.T., M.O.

Conflict of Interest: The authors declare no conflict of interest.

Financial Disclosure: The Ankara Yildirim Beyazit University Scientific Research Projects Coordination Unit supported this study (Project Number:1647).

Author Details

Ilkay Piskin

[1] Department of Histology Embryology, Faculty of Medicine, Ankara Yildirim Beyazit University, Ankara, Turkiye

0000-0002-5125-302X ilkaycorumluoglu@aybu.edu.tr

Tuba Ozdemir Sanci

[1] Department of Histology Embryology, Faculty of Medicine, Ankara Yildirim Beyazit University, Ankara, Turkiye

0000-0002-9468-4719

Yasin Koksal
[2] Department of Pediatric Hematology Oncology, Stem Cell Processing Laboratory, Ministry of Health Ankara Bilkent City Hospital, Ankara, Turkiye
0000-0003-0797-9568

H. Nese Yarali
[3] Department of Pediatric Hematology, Ministry of Health Ankara Bilkent City Hospital, Ankara, Turkiye
0000-0001-5488-2385

Fatma Karaca Kara
[4] Department of Medical Biochemistry, Ministry of Health Ankara Kecioren Training and Research Hospital, Ankara, Turkiye
0000-0002-4379-3085

Bahattin Tunc
[5] Ankara Child Health and Diseases Hematology Oncology Training and Research Hospital, Ankara, Turkiye
0000-0003-3800-0519

Meltem Ozguner
[1] Department of Histology Embryology, Faculty of Medicine, Ankara Yildirim Beyazit University, Ankara, Turkiye
0000-0003-0364-5907

REFERENCES

1. Miari KE, Williams MTS. Stromal bone marrow fibroblasts and mesenchymal stem cells support acute myeloid leukaemia cells and promote therapy resistance. Br J Pharmacol 2024; 181(2): 216-37.
2. Umeda M, Ma J, Westover T, Ni Y, Song G, Maciaszek JL, et al. A new genomic framework to categorize pediatric acute myeloid leukemia. Nat Genet 2024; 56(2): 281-93.
3. Elgarten CW, Aplenc R. Pediatric acute myeloid leukemia: Updates on biology, risk stratification, and therapy. Curr Opin Pediatr 2020; 32(1): 57–66.
4. Baker N, Boyette LB, Tuan RS. Characterization of bone marrow-derived mesenchymal stem cells in aging. Bone 2015; 70(1): 37–47.
5. Koung Ngeun S, Shimizu M, Kaneda M. Characterization of rabbit mesenchymal stem/stromal cells after cryopreservation. Biology (Basel) 2023; 12(10): 1312.
6. Sabbah R, Saadi S, Shahar-Gabay T, Gerassy S, Yehudai-Resheff S, Zuckerman T. Abnormal adipogenic signaling in the bone marrow mesenchymal stem cells contributes to supportive microenvironment for leukemia development. Cell Commun Signal 2023; 10; 21(1): 277
7. Lin H, Sohn J, Shen H, Langhans MT, Tuan RS. Bone marrow mesenchymal stem cells: Aging and tissue engineering applications to enhance bone healing. Biomaterials 2019; 203: 96–110.
8. Gulden G, Sert B, Teymur T, Ay Y, Tiryaki NN, Mishra AK, et al. CAR-T Cells with phytohemagglutinin (PHA) provide anti-cancer capacity with better proliferation, rejuvenated effector memory, and reduced exhausted T cell frequencies. Vaccines (Basel) 2023; 31; 11(2): 313.
9. Ok Bozkaya I, Azik F, Tavil B, Koksal Y, Ozguner M, Tunc B, et al. The Effect of granulocyte colony-stimulating factor on immune-modulatory cytokines in the bone marrow microenvironment and mesenchymal stem cells of healthy donors Biol. Blood Marrow Transplant 2015; 21(11): 1888–94.
10. Bennett JM, Catovsky D, Daniel MT, Flandrin G, Galton DA, Gralnick HR, et al. Proposals for the classification of the acute leukaemias. French-American-British (FAB) co-operative group. Br J Haematol 1976; 33(4): 451–8.
11. Vardiman JW, Thiele J, Arber DA, Brunning RD, Borowitz MJ, Porwit A, et al. The 2008 revision of the World Health Organization (WHO) classification of myeloid neoplasms and acute leukemia: Rationale and important changes. Blood 2009; 114(5): 937–51.
12. Conforti A, Biagini S, Del Bufalo F, Sirleto P, Angioni A, Starc N, et al. Biological, functional and genetic characterization of bone marrow-derived mesenchymal stromal cells from pediatric patients affected by acute lymphoblastic leukemia. PLoS One 2013; 7; 8(11): e76989.
13. Barachini S, Trombi L, Danti S, D'Alessandro D, Battolla B, Legitimo A, et al. Morpho-functional characterization of human mesenchymal stem cells from umbilical cord blood for potential uses in regenerative medicine. Stem Cells Dev 2009; 18(2): 293–305.
14. de Rooij JDE, Michel Zwaan C, van den Heuvel-Eibrink M. Pediatric AML: From biology to clinical management. J Clin Med 2015; 4(1): 127–49.
15. Kfoury Y, Scadden DT. Mesenchymal cell contributions to the stem cell niche. Cell Stem Cell 2015; 16(3): 239–53.
16. Caplan AI. Mesenchymal stem cells. J Orthop Res 1991; 9(5): 641–50.
17. Haddad R, Saldanha-Araujo F. Mechanisms of T-cell immunosuppression by mesenchymal stromal cells: What do we know so far? Biomed Res Int 2014; 2014: 216806.
18. Ribeiro A, Laranjeira P, Mendes S, Velada I, Leite C, Andrade P, et al. Mesenchymal stem cells from umbilical cord matrix, adipose tissue and bone marrow exhibit different capability to suppress peripheral blood B, natural killer and T cells. Stem Cell Res Ther 2013; 4(5): 125.
19. Stein PH, Singer A. Similar co-stimulation requirements of $CD4^+$ and $CD8^+$ primary T helper cells: Role of IL-1 and IL-6 in inducing IL-2 secretion and subsequent proliferation. Int Immunol 1992; 4(3): 327–35.
20. Li CY, Wu XY, Tong JB, Yang XX, Zhao JL, Zheng QF, et al. Comparative analysis of human mesenchymal stem cells from bone marrow and adipose tissue under xeno-free conditions for cell therapy. Stem Cell Res Ther 2015; 13; 6(1): 55.
21. Zhang W, Ge W, Li C, You S, Liao L, Han Q, et al. Effects of mesenchymal stem cells on differentiation, maturation, and function of human monocyte-derived dendritic cells. Stem Cells Dev 2004; 13(3): 263-71.
22. Simms PE, Ellis TM. Utility of flow cytometric detection of CD69 expression as a rapid method for determining poly- and oligoclonal lymphocyte activation. Clin Diagn Lab Immunol 1996; 3(3): 301–4.
23. Kuhweide R, Van Damme J, Lorre K, Baroja ML, Tsudo M, Ceuppens JL. Accessory cell-derived helper signals in human T-cell activation with phytohemagglutinin: Induction of interleukin 2, responsiveness of interleukin 6, and production of interleukin 2 by interleukin 1. Cytokine 1990; 2(1): 45–54.
24. Rea IM, McNerlan SE, Alexander HD. CD69, CD25, and HLA-DR activation antigen expression on CD3lymphocytes and relationship to serum TNF-α, IFN-γ, and sIL-2R levels in aging. Exp Gerontol 1999; 34(1): 79–93.
25. Damle RN, Ghiotto F, Valetto A, Albesiano E, Fais F, Yan XJ, et al. B-cell chronic lymphocytic leukemia cells express a surface membrane phenotype of activated, antigen-experienced B lymphocytes. Blood 2002; 99(11): 4087–93.
26. Del Poeta G, Del Principe MI, Zucchetto A, Luciano F, Buccisano F, Rossi FM, et al. CD69 is independently prognostic in chronic lymphocytic leukemia: A comprehensive clinical and biological profiling study. Haematologica 2012; 97(2): 279–87.
27. Dimitriou H, Linardakis E, Martimianaki G, Stiakaki E, Perdikogianni CH, Charbord P, et al. Properties and potential of bone marrow mesenchymal stromal cells from children with hematologic diseases. Cytotherapy 2008; 10(2): 125–33.
28. Stenderup K, Justesen J, Clausen C, Kassem M. Aging is associated with decreased maximal life span and accelerated senescence of bone marrow stromal cells. Bone 2003; 33(6): 919–26.
29. Machado Cde V, Telles PD, Nascimento IL. Immunological characteristics of mesenchymal stem cells. Rev Bras Hematol Hemoter 2013; 35(1): 62–7.
30. Peng Y, Wang Y, Wang M, Lan J, Chen Y. Therapeutic applications of toll-like receptors (TLRs) agonists in AML. Clin Transl Oncol 2022; 24(12): 2319-29.
31. Zeng AGX, Bansal S, Jin L, Mitchell A, Chen WC, Abbas HA, et al. A cellular hierarchy framework for understanding heterogeneity and predicting drug response in acute myeloid leukemia. Nat Med 2022; 28(6): 1212-23.
32. Bochev I, Elmadjian G, Kyurkchiev D, Tzvetanov L, Altankova I, Tivchev P, et al. Mesenchymal stem cells from human bone marrow or adipose tissue differently modulate mitogen-stimulated B-cell immunoglobulin production in vitro. Cell Biol Int 2008; 32(4): 384–93.

33. Tabera S, Pérez-Simón JA, Díez-Campelo M, Sánchez-Abarca LI, Blanco B, López A, et al. The effect of mesenchymal stem cells on the viability, proliferation and differentiation of B-lymphocytes. Haematologica 2008; 93(9): 1301–09.

İSTANBUL UNIVERSITY PRESS

Experimed 2025, 15 (1): 77–85

https://doi.org/10.26650/experimed.1587358

Submitted: 19.11.2024
Revision Requested: 05.02.2025
Last Revision Received: 19.02.2025
Accepted: 04.03.2025
Published Online 20.03.2025

Experimed

Research Article

Open Access

The Evaluation of Serum Total Tau, NFL, Neurogranin, YKL-40, and FABP-3 as Screening Biomarkers for Alzheimer's Disease

Gozde Ceylan [1], Nazan Karagoz Sakalli [2], Hacer Eroglu Icli [3], Canan Basaran Kucukgergin [1], Semra Dogru-Abbasoglu [1] & Pervin Vural [1]

[1] Department of Biochemistry, Istanbul Faculty of Medicine, Istanbul University, Istanbul, Turkiye
[2] Department of Neurology, Bakirkoy Mazhar Osman Mental Health and Neurological Diseases Training and Research Hospital, Istanbul, Turkiye
[3] Department of Biochemistry, Bakirkoy Mazhar Osman Mental Health and Neurological Diseases Training and Research Hospital, Istanbul, Turkiye

Abstract

Objective: Alzheimer's disease (AD) is a neurodegenerative disorder that causes dementia and accounts for 50-75% of all cases. Since cerebrospinal fluid sampling (CSF) is an invasive procedure, there is a need for non- or less invasive alternatives to identify new biomarkers that reflect the underlying AD pathology.
Materials and Methods: Blood samples were obtained from 86 AD patients (33 mild, 29 moderate, and 24 severe AD) and 30 controls. Serum total tau, neurofilament light polypeptide (NFL), neurogranin, chitinase-3-like protein 1 (YKL-40), and fatty acid-binding protein 3 (FABP-3) were measured using enzyme-linked immunosorbent assay (ELISA).
Results: Serum total tau and NFL levels were higher in AD patients compared to controls, whereas neurogranin, YKL-40, and FABP-3 levels remained unchanged. In the receiver operating characteristic (ROC) curve analysis, the sensitivity and specificity for total tau alone (cut-off point: 71.5 pg/mL) were 79.1% and 76.7% (Area under the curve (AUC): 0.865; p<0.001), while the sensitivity and specificity for NFL alone (cut-off point: 1.835 pg/mL) were 66.3% and 66.7% (AUC: 0.693; p=0.002). When total tau and NFL were concomitantly evaluated, the AUC was 0.848 (p<0.001).
Conclusion: Alongside the established core AD biomarkers, serum total tau and NFL are promising biomarkers for AD, reflecting additional pathological changes during the disease.

Keywords Alzheimer's disease · Serum · Biomarker · Tau · NFL · YKL-40 · FABP-3

Citation: Ceylan, G., Karagoz Sakalli, N., Eroglu Icli, H., Basaran Kucukgergin, C., Dogru-Abbasoglu, S. & Vural, P. The evaluation of serum total tau, NFL, neurogranin, YKL-40, and FABP-3 as screening biomarkers for Alzheimer's disease. Experimed 2025; 15(1): 77-85. DOI: 10.26650/experimed.1587358

Corresponding author: Pervin Vural pervinvural@yahoo.com

INTRODUCTION

Dementia is a global health problem and one of the leading causes of death. Alzheimer's disease (AD) is a neurodegenerative disorder that causes dementia, accounting for 50-75% of all cases. With increasing average lifespan and an aging population, AD is expected to become one of the most serious health challenges in the future. Progressive memory loss and other cognitive impairments are the main clinical characteristics of AD. On the other hand, extracellular deposits of β-amyloid (Aβ) plaques and intracellular neurofibrillary tangles, composed of clusters of hyperphosphorylated tau protein, are the primary pathological hallmarks of AD (1). Other pathological changes include microglial activation, neuronal degeneration, neuroinflammation, altered protein clearance, lipid metabolism disturbances, disrupted synaptic function, and impaired blood-brain barrier (BBB) integrity (2). Previously, cerebrospinal fluid (CSF) was the most preferred sample for studying AD biomarkers. However, CSF sampling is an invasive lumbar puncture procedure that carries a risk of infection and headaches. Alternatively, less invasive biological samples include peripheral blood and urine. Recently, new candidate biomarkers in blood samples that reflect the underlying AD pathology have been investigated for early diagnosis. Among these markers, neurofilament light polypeptide (NFL) is the most abundant component of myelinated axons and serves as a marker of axonal degeneration (2). Neurogranin is a postsynaptic protein that plays a crucial role in synaptic activity and plasticity, reflecting synaptic degeneration (2). Chitinase-3-like protein 1 (YKL-40) is synthesized by activated macrophages and microglia and serves as a marker of neuroinflammation. Fatty acid-binding protein 3 (FABP-3) is essential for membrane fluidity, synapse formation, and lipid transport, and it indicates lipid metabolism disorders (2).

Recent studies have clarified that AD neuropathology is associated with metabolic syndrome (MetS) and insulin resistance (IR). Moreover, AD has been classified as "Type 3 Diabetes" (3, 4). Components of MetS and IR, including hyperglycemia, dyslipidemia, and central obesity, adversely affect the pathogenesis of AD through various mechanisms, such as neuroinflammation, brain IR, oxidative stress with increased lipid peroxidation, and synaptic and axonal dysfunction (3, 4).

In the present study, we measured serum total tau, NFL, neurogranin, YKL-40, and FABP-3 levels in patients with mild, moderate, and severe AD, as well as in cognitively healthy controls, to assess whether these biomarkers provide relevant information for AD diagnosis. Additionally, we aimed to evaluate their potential for early diagnosis and disease monitoring. The second objective of this study was to investigate the relationship between these biomarkers and blood glucose and lipid profiles in AD patients.

MATERIALS AND METHODS

Study Population and Sample Collection

Eighty-six AD patients from the Department of Neurology at Bakirkoy Mazhar Osman Mental Health and Neurological Diseases Training and Research Hospital, along with 30 cognitively normal individuals, were included in this case–control study. The characteristics of patients with AD and controls are presented in Table 1. Age and gender distributions were comparable between the patient and control groups.

Each patient underwent a comprehensive clinical evaluation, including medical history, physical and neurological examination, laboratory screening tests, brain magnetic resonance imaging (MRI), and positron emission tomography (PET). All participants completed cognitive assessments, including the Mini-Mental State Examination (MMSE) and the Clinical Dementia Rating Scale-Sum of Boxes (CDR-SB). An MMSE score below 24 and a CDR-SB score above 4 indicated AD severity. Patients with mild cognitive impairment (MCI) were not included in the study. AD diagnosis was made according to the NINCDS-ADRDA criteria (5). The exclusion criteria included a history of neuropsychiatric disorders other than AD, metabolic disorders, cerebral infarction, subdural hematomas, hydrocephalus, intracranial tumors, infections, alcohol abuse, or substance abuse. This study was approved by the Local Ethics Committee at Istanbul Faculty of Medicine (18.01.2023-1582983). Written informed consent was obtained from all participants or their close relatives. Fasting venous blood samples were collected, centrifuged at 2500 rpm for 15 min within 20 to 60 min of collection, aliquoted, and stored at −80°C until use. Glucose and lipid profile parameters were measured using an autoanalyzer (Roche Cobas C6000, Switzerland).

Determining Serum Total Tau, NFL, Neurogranin, YKL-40, and FABP-3 Levels

Serum total tau, NFL, neurogranin, YKL-40, and FABP-3 levels were measured using enzyme-linked immunosorbent assay (ELISA) test kits (TAU, Elabscience E-EL-H0948, Houston, Texas; NFL, Elabscience E-EL-H0741, Houston, Texas, USA; Neurogranin, Mybiosource MBS167225, San Diego, CA, USA; YKL-40, Invitrogen BMS2322, Waltham, MA, USA; and FABP-3, Invitrogen BMS2263, Waltham, MA, USA). All measurements were performed in duplicate within the same run. The inter-run coefficients of variation (CV) for the studied parameters

Table 1. Characteristics of patients with Alzheimer's disease (AD) and controls

	AD (n= 86)	Control (n= 30)	p value
Age	71.73 (48-91)	72.63 (62-87)	0.377
Gender			
Male, n (%)	37 (43)	15 (50)	0.518
Female, n (%)	49 (57)	15 (50)	-
Disease onset		-	-
<65 years, n (%)	28 (32.5)		
>65 years, n (%)	58 (67.5)		
Family history, n (%)	39 (45)	-	-
Clinical dementia staging scale		-	-
Mild, n (%)	33 (38.4)		
Moderate, n (%)	29 (33.7)		
Severe, n (%)	24 (27.9)		
MMSE, median (range)	13.76 (0-24)	-	-
CDR-SB, median (range)	11.31 (4-18)	-	-
Glucose, (mg/dL) median (range)	120.29 (78 - 267)	100.34 (68 - 140)	**0.014**[a]
Total cholesterol, (mg/dL) median (range)	206.10 (96.2 - 292.8)	174 (101.3 - 243.2)	**0.001**[a]
Triglyceride, (mg/dL) median (range)	151.04 (48.3 - 437)	114.65 (50.7 –255.1)	**0.028**[a]
LDL-cholesterol, (mg/dL) median (range)	126.96 (35 - 190)	103.36 (46 - 172)	**0.003**[a]
HDL-cholesterol, (mg/dL) median (range)	50.63 (32.3 - 141.6)	54.52 (26.5 - 86.6)	0.248[a]
Total tau, (pg/mL) median (range)	208.97 (20.2 - 679.62)	48.33 (6.98 - 117.42)	**< 0.001**[a]
NFL, (pg/mL) median (range)	3.67 (0.11 - 13.23)	1.66 (0.32 - 7.08)	**< 0.001**[a]
Neurogranin, (ng/mL) median (range)	232.83 (58.01- 688.34)	216.17 (70 - 635.96)	0.612[a]
YKL-40, (pg/mL) median (range)	56441.1 (21094.22 - 93599.2)	64927.34 (19262.78 - 173242.26)	0.213[a]
FABP-3, (pg/mL) median (range)	2552.41 (1065.63 - 6182.5)	2459.9 (717.75 - 6285.03)	0.608[a]

Mann–Whitney U test, [a] Analysis of covariance and Bonferroni post hoc correction tests

Abbreviations: AD: Alzheimer's disease; MMSE: Mini-Mental State Examination; CDR-SB: Clinical dementia rating scale-sum of boxes; NFL: Neurofilament light polypeptide; YKL-40: chitinase-3-like protein 1; FABP-3: Fatty acid binding protein-3.

were as follows: total tau: 4.8%; NFL: 4.9%; neurogranin: <10%; YKL-40: 7.2% and FABP-3: 6.2%.

Statistical Analyses

Statistical analyses were performed using IBM SPSS Statistics 22.0 (IBM Corp., SPSS Inc., Chicago, IL, USA) and GraphPad Prism 10 (GraphPad Software, La Jolla, CA, USA). Data distribution and homogeneity were assessed using the Kolmogorov-Smirnov and Levene tests. Since obtained data were non-homogeneous and non-normally distributed, Kruskal-Wallis and Mann–Whitney U tests were applied. Serum total tau, NFL, neurogranin, YKL-40, and FABP-3 levels of the mild, moderate, severe AD patients and control groups were compared with the Analysis of covariance (ANCOVA) test. Age, which is thought to affect biochemical parameters, was used as covariate. Bonferroni correction was used as a post hoc test. Gender distribution between the study and control groups was analyzed using the chi-square test. The correlation between continuous variables was assessed using Spearman's rank correlation analysis. Receiver operating characteristic (ROC) curve analysis was performed to evaluate the ability of candidate biomarkers to discriminate between Alzheimer's patients and control groups. For biomarkers with an area under the curve (AUC)>0.6 in ROC analysis, sensitivity and specificity were calculated. Statistical significance was set at $p<0.05$. The study population was determined as 116 with G-power program by taking impact size 0.36 , $\alpha=0.05$, power $(1-\beta)=0.95$ at a confidence level of 95%.

RESULTS

The characteristics of patients with AD and controls are presented in Table 1. AD patients had higher serum glucose, total cholesterol, triglyceride, and low density lipoprotein (LDL) levels compared to controls. As expected, significant correlations were observed between glucose and lipid profile parameters including positive correlations between glucose and triglyceride, total cholesterol and triglyceride, and total cholesterol and LDL. Conversely, a negative correlation was found between glucose and high density lipoprotein (HDL) (data not shown). MMSE scores gradually decreased, while

CDR-SB scores increased across mild, moderate, and severe AD (data not shown).

Serum total tau and NFL levels were significantly higher in AD patients compared to controls (p<0.001), whereas neurogranin, YKL-40, and FABP-3 levels remained unchanged (Figure 1A, B, C, D, E). Total tau levels were elevated in all AD subgroups compared to controls (Figure 1A).

Serum NFL levels were significantly higher in moderate and severe AD patients compared to controls (p<0.001), whereas no significant change was observed in mild AD. Additionally, NFL levels were significantly increased in severe AD compared to mild AD and in moderate AD compared to mild AD (p<0.001, p=0.001, respectively) (Figure 1B).

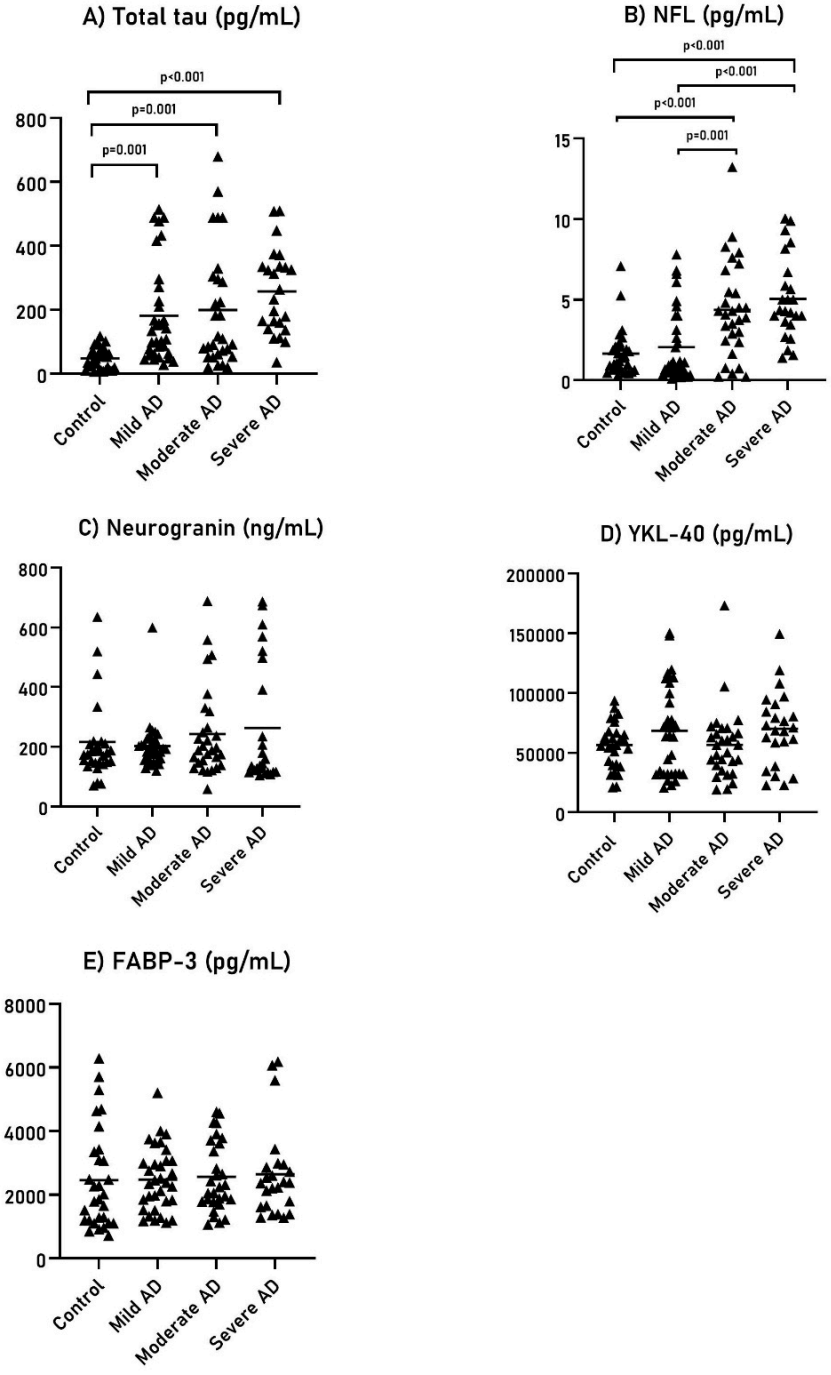

Figure 1. Serum total tau (A), NFL (B), neurogranin (C), YKL-40 (D), and FABP-3 (E) in controls and mild AD, moderate AD, and severe AD. Analysis of covariance and Bonferroni post hoc correction tests. Abbreviations: AD: Alzheimer's disease; NFL: Neurofilament light polypeptide; YKL-40: Chitinase-3-like protein 1; FABP-3: Fatty acid binding protein-3.

In addition, to assess the diagnostic potential of total tau and NFL as biomarkers for AD, ROC curves were generated. With a cut-off point of 71.5 pg/mL for total tau, sensitivity was 79.1% and specificity was 76.7% (AUC: 0.865, p<0.001). For the NFL, with a cut-off point of 1.835 pg/mL, sensitivity was 66.3% and specificity was 66.7% (AUC: 0.693, p=0.002). When total tau and NFL were concomitantly evaluated (total tau*NFL), the AUC was 0.848 (p<0.001; Figure 2).

Serum NFL levels were negatively correlated with the MMSE score (p<0.001; Figure 3A). Both total tau and NFL levels showed a positive correlation with CDR-SB (p=0.017 and p<0.001, respectively; Figure 3B, C). A positive correlation was also observed between total tau and NFL levels (p=0.002; Figure 3D). FABP-3 levels were significantly correlated with age (p=0.006; Figure 3E). Additionally, both NFL and total tau

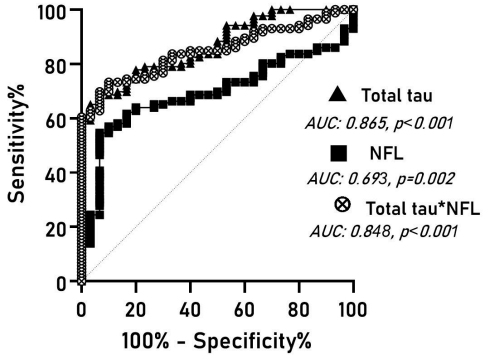

Figure 2. ROC curves for total tau, NFL and total tau * NFL for the discrimination between AD patients and controls. Abbreviations: ROC: Receiver operating characteristics; AUC: Area under the curve; AD: Alzheimer's disease; NFL: Neurofilament light polypeptide.

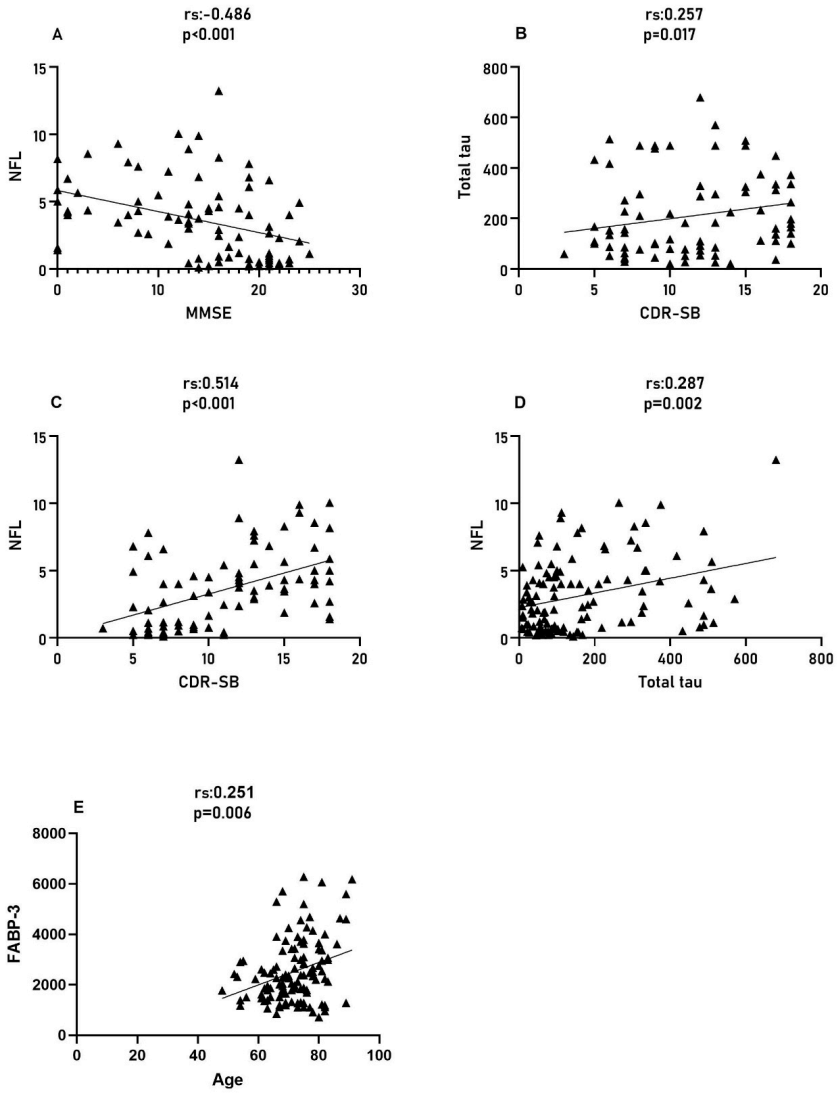

Figure 3. Correlation between NFL – MMSE (A); total tau – CDR-SB (B); NFL – CDR-SB (C); NFL – total tau (D); FABP-3 – age (E). Abbreviations: NFL: Neurofilament light polypeptide; MMSE: Mini-Mental State Examination; CDR-SB Clinical dementia rating scale-sum of boxes; FABP-3: Fatty acid binding protein-3.

showed a strong relationship with lipid profile parameters (Table 2).

Table 2. Correlations between serum total tau, NFL levels with total cholesterol, triglyceride, LDL-cholesterol and glucose levels

	Total tau r (p value)	NFL r (p value)
Total cholesterol	0.299 (**0.001**)	0.247 (**0.008**)
Triglyceride	0.210 (**0.024**)	0.196 (**0.035**)
LDL-cholesterol	0.287 (**0.002**)	0.199 (**0.032**)
Glucose	0.127 (0.175)	0.127 (0.174)

Spearman correlation test was used for analyses. Abbreviations: NFL: Neurofilament light polypeptide; LDL: Low density lipoprotein.

DISCUSSION

In the present study, we aimed to evaluate the relationship between the serum total tau, NFL, neurogranin, YKL-40, and FABP-3 concentrations and cognitive impairment, as well as the diagnostic performance of these potential biomarkers for the early detection of AD.

AD is a neurodegenerative disease and a significant public health concern with an increasing incidence. Laboratory medicine plays a crucial role in the effective monitoring of AD. The primary goal is to improve patients' quality of life while reducing economic costs. Notably, most biomarkers are assessed in CSF, which is the preferred biological sample for reflecting neuropathological alterations. However, obtaining CSF is a challenging procedure because of its invasive nature and the requirement for highly skilled personnel. In contrast, blood collection is far less invasive than lumbar puncture and is routinely performed. Therefore, using serum or plasma for biomarker assessment offers several advantages.

Among the main characteristics of AD are tau and Aβ pathologies (1,6). Tau protein plays a crucial role in maintaining the structural integrity of the neuronal cytoskeleton and regulating axonal transport. Abnormal posttranslational phosphorylation of tau protein disrupts its binding to microtubules, leading to the formation of insoluble double-stranded neurofilaments and intraneuronal tangles, ultimately resulting in neuronal death. Both phosphorylated and total tau are secreted into the CSF and peripheral blood. Several studies have demonstrated a correlation between peripheral blood total tau levels and brain total tau levels, as assessed by PET scan (7, 8). In our study, serum total tau concentrations were significantly elevated in AD patients. Moreover, there was a gradual increase in serum total tau levels from the mild to severe AD. Our findings align with studies that report increasing total tau levels in Alzheimer's patients (9, 10) yet differ from other studies that found no clear relationship between serum total tau and AD (11, 12). Since peripheral blood total tau levels reflect axonal degeneration and neuronal death, they may also serve as an indicator of cognitive decline (13). Therefore, serum total tau measurement could be valuable not only for the early diagnosis of AD but also for monitoring the dynamic process of neurodegeneration as the disease progresses. We observed that with the determined cut-off value, 79.1% sensitivity, 76.7% specificity, and 0.865 AUC value, together with established core AD markers, serum total tau could be a valuable parameter in discriminating between healthy individuals and Alzheimer's patients. Our findings agree with many studies on the same subject (9, 10).

In the spectrum of AD pathologies, neurofilaments are molecules that reflect axonal degeneration and provide prognostic information. Neurofilaments are critical for the growth and stability of axons. NFL is the smallest unit among neurofilaments, consisting of light, medium, and heavy chains, as well as α-internexin and peripherin. In various neurodegenerative, vascular, traumatic, and inflammatory diseases, NFL is secreted in high amounts into the CSF and plasma. Although plasma NFL levels are 50 times lower than in CSF, it has been shown that CSF and plasma concentrations are well correlated (14). In our study, NFL levels were elevated in the AD group compared to the control group. When evaluated according to the CDR, there were significant increases from the mild to the severe stage. However, no significant difference was detected between the control group and the mild AD group. Accordingly, NFL seems to be a suitable parameter for follow-up rather than for the early diagnosis of the disease and may be associated with the progression of cognitive decline. Similar to our findings, various studies have reported increased NFL levels in AD, linked to brain hypometabolism, brain atrophy, and cognitive decline (14, 15). In addition, it is seen from the results that both tau and NFL were correlated with clinical dementia score, reflecting cognitive decline. When total tau and NFL were concomitantly evaluated (total tau*NFL), the accuracy of disease diagnosis increased, with an AUC value of 0.848. A similar correlation was found by Mattsson et al. (14).

It is well known that the degree of cognitive dysfunction is closely related to the number of synapses, and synapse loss in AD is the strongest pathological finding correlated with cognitive decline (16). Therefore, we decided to measure serum neurogranin levels as a marker reflecting synaptic degeneration; however, no significant change was detected. Previous studies have reported elevated CSF neurogranin levels in patients with AD and mild cognitive impairment compared to controls (17). Additionally, it has been shown that the neurogranin 48-76 peptide is dominant in CSF and brain

tissue but is not found in plasma (17). Because neurogranin is enzymatically cleaved, it is expected that neurogranin fragments in brain tissue, CSF, and peripheral blood will vary in length. Another reason for the differing results may be the different sample matrices used in our study.

Neuroinflammation is a prominent feature of AD pathology, and many studies have demonstrated a reduced risk and slower progression of AD following long-term treatment with nonsteroidal anti-inflammatory drugs (18). YKL-40 is a marker of microglial differentiation and activation and is considered an indicator of inflammation (17). Increased CSF levels of YKL-40 have been found in various infectious and non-infectious disorders of the CNS. Additionally, while elevated CSF YKL-40 levels have been reported in AD, conflicting data also exist (19). In our study, although YKL-40 levels showed an increasing pattern, particularly in patients with severe AD, this increase was not statistically significant. This pattern may suggest that the inflammatory process and pro-inflammatory signals are more pronounced in patients with severe AD. Excessive inflammation and microglial activation contribute to the exacerbation of neurodegeneration, impairment of synaptic plasticity, and cognitive decline (20). However, in our study, no correlation was found between YKL-40 levels and clinical dementia score. The most significant limitation of using YKL-40 as a marker appears to be its lack of specificity. Comorbidities such as inflammatory and oncologic diseases, which are highly prevalent among older adults, may lead to increased YKL-40 concentrations. Therefore, when evaluating YKL-40 as a marker, it is essential to take a thorough medical history, considering comorbidities and medications, to avoid misinterpretation.

FABP-3 is a marker reflecting neuronal membrane damage related to lipid metabolism, and its usability for the diagnosis of AD is currently being investigated. FABP-3 was initially isolated from heart muscle and has a widespread tissue distribution. Clinically, FABP-3 may be used as a supplementary serum marker in myocardial infarction. Many studies have suggested that CSF levels of FABP-3 may have diagnostic significance in the early stages of AD (21). It has been reported that high CSF FABP-3 levels positively correlate with brain Aβ burden and are associated with brain atrophy in individuals with Aβ pathology (19). In contrast, Vidal-Pinerio et al. (22) showed that CSF FABP-3 levels predicted brain atrophy in cognitively healthy elderly individuals, independent of amyloidopathy and tauopathy biomarkers. Based on these findings, it is thought that all measured FABP-3 levels originate from the brain rather than from the serum. However, in our study, we did not observe any difference in serum FABP-3 levels between groups. This may be due to the use of serum instead of CSF or the presence of additional diseases, such as cardiovascular disease, in the control group. Our results also revealed a significant correlation between age and FABP-3 concentrations. It is possible that, with aging, the disintegration of lipids and fatty acids in the brain increases, leading to higher serum FABP-3 levels (23).

Recently, many studies have shown that disorders such as diabetes mellitus, obesity, and hypercholesterolemia play an important role in the development of AD (24). Indeed, in our study, serum glucose, total cholesterol, and LDL levels were found to be higher in AD patients. The brain's glucose requirement is met by insulin-independent glucose transporters (GLUT-1, GLUT-3) (25). Increased blood glucose levels lead to causes of abnormally high glucose transfer to neurons, triggering gluconeurotoxicity (26). Glucose exerts neurotoxic effects through various mechanisms, including the polyol pathway, the formation of advanced glycation end products (AGE), and the activation of MAP kinases (27). Studies have reported that high AGE levels induce Aβ accumulation and are associated with cognitive decline in AD (28).

On the other hand, even subtle changes in lipid metabolism can have profound effects on cognitive function. The human brain produces approximately 30% of the body's cholesterol, which plays a crucial role in regulating the membrane fluidity of neurons and astrocytes. Cholesterol is also essential for the formation of myelin, which provides insulation around axons and increases the speed of signal transmission throughout the nervous system. Demyelination is used as a biomarker for dementia pathology. Moreover, cholesterol is a key component of lipid rafts, which are involved in signal transmission, cell-to-cell adhesion, and cell division. Therefore, alterations in cholesterol metabolism may contribute to various diseases, including AD. Another link between cholesterol and AD is 24-hydroxycholesterol, an oxidation product of cholesterol that occurs exclusively in the brain. This oxysterol can cross the blood-brain barrier, and its increased plasma levels in AD likely reflect neuronal death and disrupted membrane cholesterol turnover (29). Additionally, high LDL levels induce vascular changes similar to atherosclerotic inflammatory lesions and impair blood-brain barrier permeability (30). Tau and Aβ pathologies have been observed in patients with metabolic syndrome (3, 4). Since AD shares many biochemical features with insulin resistance and metabolic syndrome, the elevated serum glucose, total cholesterol, and LDL cholesterol levels observed in AD patients in our study are not surprising. Moreover, the strong correlations between both serum total tau and NFL with lipid profile parameters further support the hypothesis that dyslipidemia is likely a predisposing factor for AD.

CONCLUSION

This study demonstrated increased serum total tau and NFL levels in AD. For the first time, we evaluated the concomitantly use of serum total tau and NFL as biomarkers for the early diagnosis of AD and assessed whether the created ROC curves enhanced the predictive power of these parameters.

Our findings showed that serum total tau alone had the highest sensitivity and specificity. Moreover, when NFL and total tau were concomitantly used, both sensitivity and specificity were higher compared to their individual values. This suggests that, alongside the established core AD biomarkers, serum total tau and NFL are promising biomarkers that reflect additional pathological changes in the progression of AD. Additionally, the significant correlations between both total tau and NFL with lipid profile parameters in AD support a possible relationship between AD and metabolic syndrome. Although lifestyle changes such as dietary modifications and increased physical activity cannot fully prevent AD, they may positively influence disease progression by reducing modifiable risk factors.

Ethics Committee Approval	This study was approved by the Local Ethics Committee of Istanbul Faculty of Medicine (18.01.2023-1582983).
Peer Review	Externally peer-reviewed.
Author Contributions	Conception/Design of study: P.V., S.D.A.; Data Acquisition: G.C., N.K.S., H.E.I.; Data Analysis/Interpretation: G.C., C.B.K., P.V.; Drafting Manuscript: P.V., G.C.; Critical Revision of Manuscript: S.D.A.; Final Approval and Accountability: P.V., S.D.A., G.C., N.K.S., H.E.I., C.B.K.
Conflict of Interest	The authors declare no conflict of interest.
Financial Disclosure	This work was financially supported by the Research Fund of Istanbul University (Project No. TTU-2023-39857).

Author Details

Gozde Ceylan
[1] Department of Biochemistry, Istanbul Faculty of Medicine, Istanbul University, Istanbul, Turkiye
0000-0003-3397-9676

Nazan Karagoz Sakalli
[2] Department of Neurology, Bakirkoy Mazhar Osman Mental Health and Neurological Diseases Training and Research Hospital, Istanbul, Turkiye
0000-0002-7172-954X

Hacer Eroglu Icli
[3] Department of Biochemistry, Bakirkoy Mazhar Osman Mental Health and Neurological Diseases Training and Research Hospital, Istanbul, Turkiye
0000-0002-9775-1710

Canan Basaran Kucukgergin
[1] Department of Biochemistry, Istanbul Faculty of Medicine, Istanbul University, Istanbul, Turkiye
0000-0002-1797-5889

Semra Dogru-Abbasoglu
[1] Department of Biochemistry, Istanbul Faculty of Medicine, Istanbul University, Istanbul, Turkiye
0000-0003-3467-9763

Pervin Vural
[1] Department of Biochemistry, Istanbul Faculty of Medicine, Istanbul University, Istanbul, Turkiye
0000-0001-6462-7388 pervinvural@yahoo.com

REFERENCES

1. Guo T, Zhang D, Zeng Y, Huang TY , Xu H , Zhao Y. Molecular and cellular mechanisms underlying the pathogenesis of Alzheimer's disease. Mol Neurodegener 2020; 15: 1-37.
2. Park SA, Han SM, Kim CE. New fluid biomarkers tracking non-amyloid-β and non-tau pathology in Alzheimer's disease. Exp Mol Med 2020; 52: 556-68.
3. Fahed G, Aoun L, Zerdan MB, Allam S, Zerdan MB, Bouferraa Y. Metabolic syndrome: updates on pathophysiology and management in 2021. Y Int J Mol Sci 2022; 23: 786.
4. Al-Kuraishy HM, Majid S. Jabir MS, Albuhadily AK, Al-Gareeb AI, Rafeeq MF. The link between metabolic syndrome and Alzheimer disease: A mutual relationship and long rigorous investigation. Ageing Res Rev 2023; 91: 102084.
5. Jack CR Jr, Bennett DA, Blennow K, Carrillo MC, Dunn B, Haeberlein SB, et.al. NIA-AA Research Framework: Toward a biological definition of Alzheimer's disease. Alzheimers Dement 2018; 14: 535-62.
6. Pais M, Martinez L, Ribeiro O, Loureiro J, Fernandez R, Valiengo L, et al. Early diagnosis and treatment of Alzheimer's disease: new definitions and challenges. Braz J Psychiatry 2020; 42: 431-41.
7. Mielke MM, Hagen CE, Xu J, Chai X, Vemuri P, Lowe VJ, et al. Plasma phospho-tau181 increases with Alzheimer's disease clinical severity and is associated with tau- and amyloid-positron emission tomography. Alzheimers Dement 2018; 14: 989-97.
8. Park JC, Han SH, Yi D, Byun MS, Lee JH, Jang S, et al. Plasma tau/amyloid-β1-42 ratio predicts brain tau deposition and neurodegeneration in Alzheimer's disease. Brain 2019; 142: 771-86.
9. Tsai CL, Liang CS, Lee JT, Su MW, Lin CC, Chu HT, et al. Associations between plasma biomarkers and cognition in patients with Alzheimer's disease and amnestic mild cognitive impairment: a cross-sectional and longitudinal study. J Clin Med 2019; 8: 1893.
10. Jiang T, Gong PY, Tan MS, Xue X, Huang S, Zhou JS, et al. Soluble TREM1 concentrations are increased and positively correlated with total tau levels in the plasma of patients with Alzheimer's disease. Aging Clin Exp Res 2019; 31: 1801-5.
11. Verberk IMW, Slot RE, Verfaillie SCJ, Heijst H, Prins ND, van Berckel BNM, et al. Plasma amyloid as prescreener for the earliest alzheimer pathological changes. Ann Neurol 2018; 84: 648-58.
12. De Wolf F, Ghanbari M, Licher S, McRae-McKee K, Gras L, Weverling GJ, et al. Plasma tau, neurofilament light chain and amyloid-β levels and risk of dementia; a population-based cohort study. Brain 2020; 143: 1220-32.
13. Chiu MJ, Chen YF, Chen TF, Yang SY, Yang FP, Tseng TW, et al. Plasma tau as a window to the brain-negative associations with brain volume and memory function in mild cognitive impairment and early Alzheimer's disease. Hum Brain Mapp 2014; 35: 3132-42.
14. Mattsson N, Andreasson U, Zetterberg H, Blennow K. Association of plasma neurofilament light with neurodegeneration in patients with Alzheimer disease. JAMA Neurol 2017; 74: 557-66.
15. Lewczuk P, Ermann N, Andreasson U, Schultheis C, Podhorna J, Spitzer P, et al. Plasma neurofilament light as a potential biomarker of neurodegeneration in Alzheimer's disease. Alzheimers Res Ther 2018; 10: 71.

16. Jessen F, Amariglio RE, Buckley RF, van der Flier WM, Han Y, Molinuevo JL, et al. The characterisation of subjective cognitive decline. Lancet Neurol 2020; 19: 271-8.
17. Hellwig K, Kvartsberg H, Portelius E, Andreasson U, Oberstein TJ, Lewczuk P, et al. Neurogranin and YKL-40: independent markers of synaptic degeneration and neuroinflammation in Alzheimer's disease. Alzheimers Res Ther 2015; 7: 74.
18. McGeer PL, McGeer EG. The amyloid cascade-inflammatory hypothesis of Alzheimer disease: implications for therapy. Acta Neuropathol 2013; 126: 479-97.
19. Mattsson N, Tabatabaei S, Johansson P, Hansson O, Andreasson U, Månsson JE, et al. Cerebrospinal fluid microglial markers in Alzheimer's disease: elevated chitotriosidase activity but lack of diagnostic utility. Neuromolecular Med 2011; 13: 151-9.
20. Norden DM, Muccigrosso MM, Godbout JP. Microglial priming and enhanced reactivity to secondary insult in aging, and traumatic CNS injury, andneurodegenerative disease Neuropharmacology 2015; 96: 29-41.
21. Chiasserini D, Parnetti L, Andreasson U, Zetterberg H, Giannandrea D, Calabresi P, et al. CSF levels of heart fatty acid binding protein are altered during early phases of Alzheimer's disease. J Alzheimer's Dis 2010; 22: 1281-8.
22. Vidal-Piñeiro D, Sorensen Q, Blennow K, Capogna E, Halaas NB, Idland AV, et al. Relationship between cerebrospinal fluid neurodegeneration biomarkers and temporal brain atrophy in cognitively healthy older adults. Neurobiol Aging 2022; 116: 80-91.
23. Shioda N, Yabuki Y, Kobayashi Y, Onozato M, Owada Y, Fukunaga K. FABP3 protein promotes α-synuclein oligomerization associated with 1-Methyl-1,2,3,6 tetrahydropiridine- induced neurotoxicity. J Biol Chem 2014; 289: 18957-65.
24. Armstrong RA. Risk factors for Alzheimer's disease. Folia Neuropathol 2019; 57:87-105.
25. Simpson IA, Carruthers A, Vannucci SJ. Supply and demand in cerebral energy metabolism: The role of nutrient transporters. J Cereb Blood Flow Meta 2007; 27: 1766-91.
26. Jacob RJ, Fan X, Evans ML, Dziura J, Sherwin RS. Brain glucose levels are elevated in chronically hyperglycemic diabetic rats: No evidence for protective adaptation by the blood brain barrier. Metabolism 2002; 51: 1522-4.
27. Tomlinson DR, Gardiner NJ. Glucose neurotoxicity. Nat Rev Neurosci 2008; 9:36-45.
28. Li S, Jin M, Zhang D, Yang T, Koeglsperger T, Fu H, et al. Environmental novelty activates beta2-adrenergic signaling to prevent the impairment of hippocampal LTP by Abeta oligomers. Neuron 2013; 77: 929-41.
29. Vega GL, Weiner MF, Lipton AM, Von Bergmann K, Lutjohann D, Moore C, et al. Reduction in levels of 24S-hydroxycholesterol by statin treatment in patients with Alzheimer disease. Arch Neurol 2003; 60: 510-5.
30. Chakraborty A, de Wit NM, van der Flier WM, de Vries HE. The blood brain barrier in Alzheimer's disease. Vascul Pharmacol 2017; 89: 12-8.

İSTANBUL UNIVERSITY PRESS

Experimed 2025, 15 (1): 86–92

https://doi.org/10.26650/experimed.1642791

Submitted: 19.02.2025
Revision Requested: 17.03.2025
Last Revision Received: 21.03.2025
Accepted: 21.03.2025
Published Online 28.03.2025

Experimed

Research Article

Open Access

Evaluation of the Effects of Corrective Exercises on the Posture of Ballet Dancers Using the Photogrammetric Measurement Technique

Zekiye Gizem Caner [1] & Bulent Bayraktar [2]

[1] Department of Physiotherapy and Rehabilitation, Faculty of Health Sciences, Istanbul Yeni Yuzyil University, Istanbul, Turkiye
[2] Department of Sports Medicine, Istanbul Faculty of Medicine, Istanbul University, Istanbul, Turkiye

Abstract

Objective: This study investigated the effects of individualized corrective exercises on posture based on postural assessments conducted by a physiotherapist.

Materials and Methods: The study included 47 ballet students (39 females, 8 males) aged 11–19 years. Participants underwent one photogrammetric assessment at the beginning of the study and another after completing an 8-week personalized corrective exercise program. Servidor de Apontadores Portugueses Online (SAPO) postural assessment software was used for postural evaluation.

Results: In the anterior view, when pre- and post-intervention measurements were compared to reference values, statistically significant improvements were observed in the horizontal alignment of the head, acromions, and anterior superior iliac spines, tibial tuberosities ($p<0.05$). Significant improvement was noted in the horizontal asymmetry of the scapula relative to the T3 vertebra. Lateral views and vertical alignment of the head improved significantly. To the best of our knowledge, no studies have assessed the effects of corrective exercises on posture using SAPO software.

Conclusion: This study quantitatively showed that individualized corrective exercise programs by physiotherapists improve posture in ballet students, potentially reducing injury rates and enhancing physical performance. It lays the groundwork for future research on the efficacy of corrective exercises.

Keywords Posture · Corrective exercise · Ballet · Physiotherapist · Injury prevention · Physical performance

Citation: Caner, Z. G. & Bayraktar, B. Evaluation of the Effects of Corrective Exercises on the Posture of Ballet Dancers Using the Photogrammetric Measurement Technique. Experimed 2025; 15(1): 86-92. DOI: 10.26650/experimed.1642791

Corresponding author: Zekiye Gizem Caner gizem-caner@hotmail.com

INTRODUCTION

The American Academy of Orthopaedic Surgeons defines posture as a state of balance in standing, sitting, and lying positions, where muscles and bones have sufficient capacity to protect other body structures from injury (1).

From a biomechanical and physiological perspective, good posture minimizes stress on ligaments, muscles, tendons, and bones (2, 3). Proper posture facilitates bodily functions and reduces the energy expenditure of muscles required to maintain an upright position. In contrast, improper, forced, asymmetric, prolonged, and sustained postures result in excessive loads on tissues, surpassing the tolerable stress threshold, leading to strain or injury, and causing imbalance (4, 5). Improper posture is frequently observed in dancers, particularly ballet performers, and may increase the risk of injuries.

There is no universally accepted standard approach to posture assessment. The use of photography for measuring joint positions was first introduced by Wilson and Strasch in 1964. Compared to radiographic imaging, photography is more practical, non-invasive, and cost-effective, making its clinical and research applications highly valuable (6). Photogrammetric posture analysis provides objective data with high reliability and practical clinical utility. Therefore, its use has been recommended in clinical settings and scientific literature (7).

Various software programs have been developed for postural assessment. Servidor de Apontadores Portugueses Online (SAPO) postural assessment software was used in the present study. Although several studies in the literature have employed different methods for postural analysis, no previous research has objectively evaluated the effects of corrective exercises on posture using an advanced postural analysis technique.

The present study aimed to assess the effectiveness of personalized corrective exercises prescribed by physiotherapists through objective data collection.

MATERIALS AND METHODS

A total of 47 ballet students, including 8 males (17%) and 39 females (83%), aged between 11 and 19 years were enrolled. The study was initiated after the approval of the clinical research ethics committee of Istanbul University, Istanbul Faculty of Medicine (2019/782). For volunteers from participants' families, the consent form was obtained.

Participants underwent two photographic measurement sessions: one at the beginning of the study and another after completion of their personalized corrective exercise program for eight weeks. The photographs were captured at Mimar Sinan Fine Arts University, State Conservatory, Ballet Department. During the sessions, participants wore clothing that did not obstruct the visibility of the designated anatomical landmarks. Male students wore briefs, while female students wore ballet leotards or sports tops.

For posture assessment, 32 anatomical landmarks were marked with round, colored, and easily identifiable markers before imaging. Anatomical reference points were used as specified in the SAPO protocol. These included 32 points: the midpoint of the tragus, acromion, midpoint of the horizontal midline of the knee joint, the midpoint of the patella, tibial tuberosity, greater trochanter, anterior superior iliac spine (ASIS), C7 spinous process, inferior angle of the scapula, T12 spinous process, posterior superior iliac spine, the midpoint of the medial line of the leg, region between the malleolus and calcaneal tendon, midpoint between the second and third metatarsals of the calcaneus, lateral malleolus, and medial malleolus (Figure 1).

Program Development

The most critical factor in designing a corrective exercise program is individualization, in which the exercise prescriptions should be tailored to each person's specific needs. The exercises must be appropriately designed and correctly taught. Initially, the exercises should be performed under the supervision of a physiotherapist. The program should be flexible and progressive. It should be organized in a way that is functional according to the person's lifestyle, occupation, recreational activities, and sports participation, considering the results of the evaluation. The sustainability of the program is essential.

The primary goal of corrective exercise training is to eliminate muscle imbalances. If the program begins before optimal muscle balance is achieved, the exercises may further exacerbate imbalances.

In summary, the four fundamental objectives in the sequence should be:

1. Muscle balance
2. Stability
3. Functional strength
4. Functional power

Selecting the most beneficial exercises for the individual, modifying them when necessary, and properly adjusting the load, repetitions, and rest intervals enhance the effectiveness of the program (8).

The exercise program was individually designed based on the initial postural assessment measurements of each participant. In the development of the program, lateral trunk muscle flexibility was evaluated using side reach tests, core strength was assessed through pre-core exercises, and the functional capacity of the hip abductors was examined using modified side plank tests. The exercises were prescribed to be performed in a symmetrical and correct posture, ensuring postural balance.

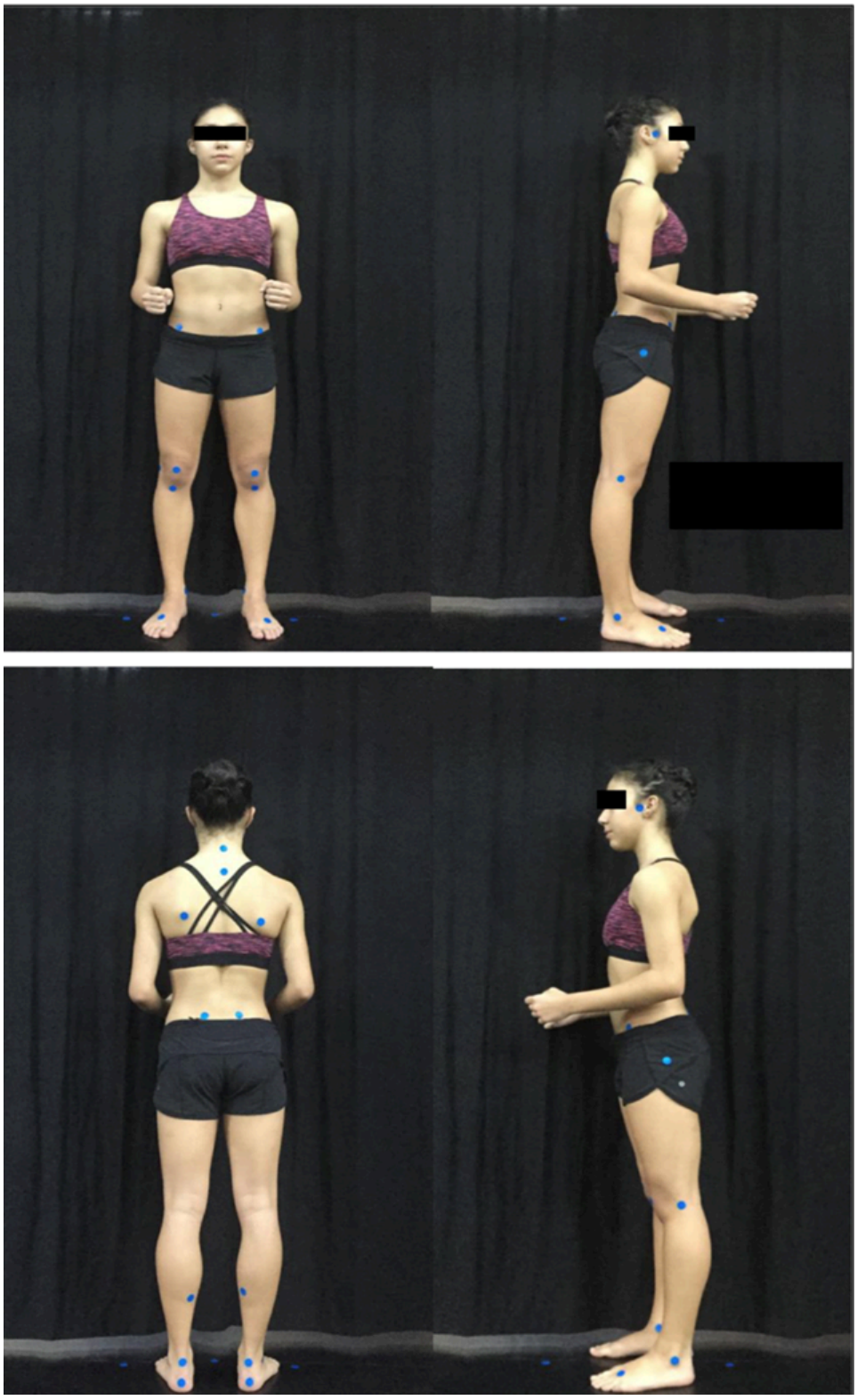

Figure 1. Postural assessment according to photogrammetric measurement method.

The program was designed with beginner-level core strength, stability, functional strength, and mobility exercises. Strength exercises were performed using body weight and resistance bands. After four weeks, the difficulty of exercises using resistance bands was increased by transitioning to a higher-resistance band. The exercises were performed three times per week for eight weeks.

Statistical Analyses

Data analysis was conducted using SPSS v21 software, with statistical significance set at $p<0.05$. Pre- and post-exercise data were analyzed using the paired sample t-test.

RESULTS

Demographic data of 47 ballet students who participated in the study are given in the Table 1 (Table 1). A total of 47 ballet students, including 8 males (17%) and 39 females (83%). Pre and post-test results are shown in the Table 2. Postural assessments conducted before and after the exercise program revealed significant improvements across anterior, lateral, and posterior views. In the second measurements taken following the intervention, most parameters showed a notable shift toward the reference value of 0. This indicates a reduction in postural asymmetry and an overall improvement in body alignment. In the anterior view, changes in the horizontal alignment of the head, acromions, ASIS, the angle between bilateral acromions and ASIS, and the tibial tuberosity angles were all statistically significant ($p<0.05$). These results suggest that the body's frontal symmetry improved, approaching the ideal postural alignment. In both right and left lateral views, significant improvements were observed in head alignment, trunk verticality, pelvic positioning, hip and knee angles ($p<0.05$). While the ankle angle did not show a statistically significant change in some comparisons ($p>0.05$), other parameters indicated a clear postural correction. This suggests that the ankle may respond differently or more slowly to the applied exercise program. In the posterior view, the scapular alignment relative to the T3 vertebra showed a statistically significant improvement toward symmetry ($p<0.05$). Additionally, changes in both right and left rear foot angles were also found to be significant ($p<0.05$), further supporting the positive impact of the exercise regimen. Overall, the findings demonstrate that the exercise program led to improvements in postural alignment by moving measured values closer to their ideal reference points. This indicates a beneficial effect on body symmetry and postural control.

Table 1. Demographic data

	Mean ± SD	Min	Max
Age (years)	13.72 ± 2.23	11	19
Height (cm)	152.55 ± 13.20	129.5	178
Weight (kg)	39.73 ± 11.05	24.3	62.5
BMI	16.72 ± 2.13	13.37	22.17

SD: Standard Deviation; BMI: Body Mass Index

DISCUSSION

The present study objectively and quantitatively demonstrated, for the first time, the effectiveness of individualized corrective exercise programs designed by physiotherapists in improving posture. This study will serve as a foundation for future research on the effectiveness of corrective exercises.

With advancements in technology, posture assessment through photographic analysis has become possible. Although there are studies evaluating posture using technological tools, research focusing on the assessment of whole-body posture remains limited. Studies that simultaneously evaluate all body segments are essential for accurately defining an ideal posture model.

Research examining whole-body posture in healthy individuals is necessary to establish reference values for normal posture. Quantifiable data play a critical role in physical therapy (9). In a study conducted by Robertson et al., symmetrical postural alignment was defined as the standard posture (8). Robertson et al. used reference values recommended by physiotherapy and rehabilitation departments (8). However, some researchers have debated this topic, suggesting that an individual's ideal posture does not necessarily have to conform to the "normal" posture. These researchers emphasize that future studies involving a larger sample of individuals without musculoskeletal disorders and evaluating all body segments could contribute to the ongoing discussion on standardizing reference values for normal posture (10). In the present study, the SAPO postural assessment software was used to evaluate posture through photographic analysis. From the anterior view, the horizontal alignment of the head and acromions and the angle between the two acromions and two ASIS were analyzed. From the posterior view, the reference angle for scapular horizontal asymmetry relative to T3 was set at "0" (11, 12).

There is no universally accepted standard approach for posture assessment (13), and the methods used vary (13). In a study by Roggio et al., which assessed the posture of 200 healthy adult men and women using photogrammetric analysis, a significant difference in shoulder adduction angles

Table 2. Pre- and post-test results

Angles and Distances	Measurement First	Measurement Second	t	p value
ANTERIOR VIEW				
Head Horizontal Alignment (°)	2.30 ± 1.45	0.81 ± 0.66	7.26	*0.001
Horizontal Alignment of Acromions (°)	1.60 ± 0.98	0.72 ± 0.67	7.87	*0.001
Horizontal Alignment of (ASIS) (°)	1.80 ± 1.04	0.80 ± 0.69	6.42	*0.001
Angle Between the Two Acromions and Two ASIS (°)	2.00 ± 1.25	0.87 ± 0.74	7.84	*0.001
Right Upper Extremity Anteversion Angle (°)	−2.56 ± 2.76	−2.045 ± 2.25	−2.27	*0.027
Left Upper Extremity Anteversion Angle (°)	−3.13 ± 3.04	−2.52 ± 2.27	−1.78	0.081
Tibial Tuberosity Horizontal Angle (°)	2.11 ± 1.19	1.11 ± 0.88	5.06	*0.001
Right Q Angle (°)	15.37 ± 6.15	14.46 ± 4.19	0.95	0.347
Left Q Angle (°)	12.42 ± 5.58	12.66 ± 3.21	−0.29	0.768
LATERAL VIEW (RIGHT)				
Head Horizontal Alignment (Side View) (°)	59.59 ± 5.34	57.91 ± 3.48	2.38	*0.021
Head Vertical Alignment (°)	10.76 ± 5.48	6.91 ± 4.38	5.27	*0.001
Trunk Vertical Alignment (°)	−1.48 ± 0.41	−0.76 ± 0.27	−2.53	*0.015
Hip Angle (°)	−10.78 ± 0.83	−8.21 ± 0.86	−3.56	*0.001
Body Vertical Alignment (°)	3.12 ± 0.97	2.38 ± 1.03	5.19	*0.001
Pelvis Horizontal Alignment (°)	−13.60 ± 0.51	−5.33 ± 0.49	−13.38	*0.001
Knee Angle (°)	−8.73 ± 0.68	−5.94 ± 0.61	−4.90	*0.001
Ankle Angle (°)	75.27 ± 45.26	87.48 ± 5.41	−1.81	0.075
LATERAL VIEW (LEFT)				
Head Horizontal Alignment (Side View) (°)	58.30 ± 18.89	58.18 ± 3.36	0.048	0.962
Head Vertical Alignment (°)	11.86 ± 5.70	7.97 ± 5.49	6.44	*0.001
Trunk Vertical Alignment (°)	−0.68 ± 0.48	−0.65 ± 0.26	−0.72	*0.943
Hip Angle (°)	−10.78 ± 0.83	−8.21 ± 0.86	−3.56	*0.001
Body Vertical Alignment (°)	3.12 ± 0.97	2.38 ± 1.03	5.19	*0.001
Pelvis Horizontal Alignment (°)	−13.60 ± 0.51	−5.33 ± 0.49	−13.36	*0.001
Knee Angle (°)	−8.73 ± 0.68	−5.94 ± 0.61	−4.90	*0.001
Ankle Angle (°)	80.59 ± 8.24	89.42 ± 2.28	−1.55	0.127
POSTERIOR VIEW				
Scapular Horizontal Asymmetry Relative to T3 (cm)	17.78 ± 11.89	8.54 ± 7.45	6.83	*0.000
Right Posterior Foot Angle (°)	0.83 ± 3.80	4.18 ± 10.5	−2.13	*0.038
Left Posterior Foot Angle (°)	4.18 ± 1.59	0.65 ± 0.57	2.31	*0.025

Values are presented as mean ± standard deviation. Comparisons were performed using the paired sample t-test. *: $p < 0.05$ was considered statistically significant in all analyses.

was observed between males and females (14). Elpeze et al. investigated the effects of corrective exercises on balance and kyphosis in adolescents diagnosed with kyphosis and concluded that a corrective exercise program resulted in a reduction in kyphotic curvature and improvements in balance (15). Similarly, Kouchi et al. reported that an 8-week corrective dance exercise program in adolescent girls led to a decrease in thoracic hyper-kyphosis and an improvement in scapular positioning (16). Another study examining the impact of corrective and stabilization exercise programs on fundamental movement patterns in dance students reported that these programs led to improvements in basic movement skills, balance, and motor control (17).

In a study involving dancers aged 18–24 years, exercise interventions targeting forward head posture and rounded shoulders resulted in significant postural improvements (18). A systematic review investigated the effects of exercise on postural alignment and categorized studies based on conditions such as forward head and shoulder dysfunction, hyper-kyphosis, and scoliosis. The review concluded that interventions designed to stretch tight muscles and

strengthen weak muscles could effectively improve postural dysfunction (19).

In most studies, posture assessment has been limited to single-segment evaluations, such as the position of the head relative to the shoulders in the sagittal plane (20). The average angular values of each segment have typically been determined using different methods (21). Due to methodological differences among studies and the isolated evaluation of individual segments, comparisons between results have become challenging.

In the present study, post-exercise measurements of parameters with reference values defined by the SAPO software showed a statistically significant improvement toward the reference values. Furthermore, for parameters without predefined reference values, intra-group comparisons revealed statistically significant differences.

In the photogrammetric method used for posture assessment in this study, the accurate localization of anatomical landmarks depends on the examiner's anatomical knowledge and is subject to potential error. Despite the use of the anatomical landmark feature in the SAPO software, markings on the photographs still have a margin of error, which can introduce measurement errors. Moreover, a lack of familiarity with the software may complicate the assessment process. To minimize the likelihood of error, all pre- and post-exercise measurements in the present study, including determination of anatomical landmarks by palpation, marking on photographs, and posture assessment using the software, were conducted by a single physiotherapist with expertise in this area.

Minimizing error is crucial for obtaining objective data in posture assessment, which has clinical significance, as it allows for the evaluation of load distribution across the musculoskeletal system. Our primary goal during corrective exercises was to identify and correct imbalances in load distribution through targeted interventions.

Although previous studies have used the SAPO software for posture assessment, no study has evaluated the effects of corrective exercises on posture using photogrammetric measurement with SAPO.

In conclusion, the data obtained in the present study indicate that individualized corrective exercise programs designed by physiotherapists have positive effects on posture, potentially leading to reduced injury rates and improved performance.

Ethics Committee Approval: The study was initiated after the approval of the clinical research ethics committee of Istanbul University, Istanbul Faculty of Medicine (2019/782).

Informed Consent: For volunteers from participants' families, the consent form was obtained.

Peer Review: Externally peer-reviewed.

Author Contributions: Conception/Design of Study – Z.G.C., B.B.; Data Acquisition – Z.G.C.; Data Analysis/Interpretation – Z.G.C.; Drafting Manuscript – Z.G.C.; Critical Revision of Manuscript – Z.G.C.; Final Approval and Accountability – Z.G.C., B.B.

Conflict of Interest: The authors declare no conflict of interest.

Financial Disclosure: The authors declare that they received no financial support for this study.

Author Details

Zekiye Gizem Caner

[1] Department of Physiotherapy and Rehabilitation, Faculty of Health Sciences, Istanbul Yeni Yuzyil University, Istanbul, Turkiye

0000-0002-1357-5060 gizem-caner@hotmail.com

Bulent Bayraktar

[2] Department of Sports Medicine, Istanbul Faculty of Medicine, Istanbul University, Istanbul, Turkiye

0000-0001-8102-4896

REFERENCES

1. Ye J, Jiang Z, Chen S, Cheng R, Xu L, Tsai TY. Rehabilitation practitioners' perceptions of optimal sitting and standing posture in men with normal weight and obesity. Bioengineering (Basel) 2023; 10(2): 210.
2. Lippert LS. Clinical Kinesiology and Anatomy 5th ed. Oregon: F.A. Davis Company; 2011.
3. Öznur A, Postür Analizinde Symmetrigraf ile Orthoröntgenogram Sonuçlarının Değerlendirilmesi. T.C. Sağlık Bakanlığı Okmeydanı E.H.A. Fizik Tedavi ve Rehabilitasyon. Uzmanlık Tezi, 2006.
4. Vieira ER, Kumar S. Working postures: a literature review. J Occup Rehabil 2004; 14(2): 143-59.
5. Legaye J, Duval-Beaupère G. Sagittal plane alignment of the spine and gravity: a radiological and clinical evaluation. Acta Orthop Belg 2005; 71(2): 213-20.
6. Cromie JE, Robertson VJ, Best MO. Occupational health and safety in physiotherapy: guidelines for practice. Aust J Physiother 2001; 47(1): 43-51.
7. Fortin C, Feldman DE, Cheriet F, Labelle H. Clinical methods for quantifying body segment posture: a literature review. Disabil Rehabil 2011; 33(5): 367-83.
8. Robertson JA, Kendall FP, McCreary EK. Muscles, testing and function" (third edition). Br J Sports Med 1984; 18(1): 25.
9. Macedo Ribeiro AF, Bergmann A, Lemos T, Pacheco AG, Mello Russo M, Santos de Oliveira LA, et al. Reference values for human posture measurements based on computerized photogrammetry: a systematic review. J Manipulative Physiol Ther 2017; 40(3): 156-68.
10. Grimmer K, Dansie B, Milanese S, Pirunsan U, Trott P. Adolescent standing postural response to backpack loads: a randomised controlled experimental study. BMC Musculoskelet Disord 2002; 17: 3-10.
11. Ferreira EA, Duarte M, Maldonado EP, Bersanetti AA, Marques AP. Quantitative assessment of postural alignment in young adults based on photographs of anterior, posterior, and lateral views. J Manipulative Physiol Ther 2011; 34(6): 371-80.
12. Niaradi FDSL, Niaradi MFDSL, Gasparetto MERF. Effect of eutonia, holistic gymnastics, and pilates on body posture for pre-adolescent girls: randomized clinical trial. J Bodyw Mov Ther 2022; 30: 226-36.
13. Harrison AL, Barry-Greb T, Wojtowicz G. Clinical measurement of head and shoulder posture variables. J Orthop Sports Phys Ther 1996; 23(6): 353-61.

14. Roggio F, Di Grande S, Cavalieri S, Falla D, Musumeci G. Biomechanical posture analysis in healthy adults with machine learning: applicability and reliability. Sensors (Basel) 2024; 24(9): 2929.
15. Elpeze G, Usgu G. The effect of a comprehensive corrective exercise program on kyphosis angle and balance in kyphotic adolescents. Healthcare (Basel) 2022; 10(12): 2478.
16. Kouchi D, Sahebozamani M, Daneshjoo A, Amatachaya S, Alimoradi M, Iranmanesh M. Effects of an 8-week corrective dance exercises intervention on thoracic hyperkyphosis, scapular position, respiratory function, and happiness in girls aged 10-12 years. Pediatr Exerc Sci 2024; 22: 1-8.
17. Marta S, Karpowicz K, Bartkowiak S, Strzelczyk R. The impact of the corrective and stability exercises program on the quality of basic movement patterns among dance students. Trends Sports Sci 2017; 24: 31-8.
18. Jordan CL, Sydney DR. Correcting forward head posture and rounded shoulders in collegiate dancers: strengthening versus manual release. Kinesiology, Dance Science, Texas A&M University, Undergraduate Research Scholars Thesis, 2022.
19. Porto AB, Nascimento Guimarães A, Alves Okazaki VH. The effect of exercise on postural alignment: A systematic review. J Bodyw Mov Ther 2024; 40: 99-108.
20. Raine S, Twomey LT. Head and shoulder posture variations in 160 asymptomatic women and men. Arch Phys Med Rehabil 1997; 78(11): 1215-23.
21. Normand MC, Descarreaux M, Harrison DD, Harrison DE, Perron DL, Ferrantelli JR, et al. Three dimensional evaluation of posture in standing with the PosturePrint: an intra- and inter-examiner reliability study. Chiropr Osteopat 2007; 24:15: 15.